JYU DISSERTATIONS 549

Parveen Kumar

Synthesis and Structural Studies on Halogen(I) Complexes

UNIVERSITY OF JYVÄSKYLÄ
FACULTY OF MATHEMATICS
AND SCIENCE

JYU DISSERTATIONS 549

Parveen Kumar

Synthesis and Structural Studies on Halogen(I) Complexes

Esitetään Jyväskylän yliopiston matemaattis-luonnontieteellisen tiedekunnan suostumuksella
julkisesti tarkastettavaksi yliopiston Ylistönrinteen salissa Kem4
elokuun 19. päivänä 2022 kello 12.

Academic dissertation to be publicly discussed, by permission of
the Faculty of Mathematics and Science of the University of Jyväskylä,
in Ylistönrinne, auditorium Kem4, on August 19, 2022 at 12 o'clock noon.

JYVÄSKYLÄN YLIOPISTO
UNIVERSITY OF JYVÄSKYLÄ

JYVÄSKYLÄ 2022

Editors
Kari Rissanen
Department of Chemistry, University of Jyväskylä
Ville Korkiakangas
Open Science Centre, University of Jyväskylä

ISBN 978-951-39-9366-5 (PDF)
URN:ISBN:978-951-39-9366-5
ISSN 2489-9003

Permanent link to this publication: http://urn.fi/URN:ISBN:978-951-39-9366-5

ABSTRACT

Kumar, Parveen
Synthesis and Structural Studies on Halogen(I) Complexes
Jyväskylä: University of Jyväskylä, 2022, 160 p.
(JYU Dissertations
ISSN 2489-9003; 549)
ISBN 978-951-39-9366-5 (PDF)

This thesis work has focused on the preparation and structural analysis of the halogen(I) complexes from mono and multivalent ligands in solution, in gas phase and in the solid state. Single crystal X-ray diffraction (SCXRD), NMR experiments, and mass spectrometry were used to identify the conformations and structures of the halogen(I) complexes. In the literature part, firstly the overview of the halogen bonding and the introduction of the three-center four-electron halogen bond are given. Later the halogen(I) complexes of aromatic and aliphatic ligands in solution and in the solid state are reviewed. The review chapter also presents the recent solid-state study of nucleophilic iodine(I) interactions.

In this thesis, the results and discussion part describes the synthesis and characterization of the silver(I), iodine(I), and bromine(I) complexes of mono and di-substituted pyridine ligands. All $[N\cdots Ag\cdots N]^+$ and $[N\cdots X\cdots N]^+$ complexes were analyzed with ^{1}H-NMR and SCXRD. In addition, some of the complexes were studied by ^{1}H-^{15}N-NMR HMBC spectroscopy. In the second part, silver(I) and iodine(I) complexes of 1-methyl-1H-1,2,3-triazole are synthesized and later used for the synthesis of $[I(mtz)_2]PF_6$*$[Ag(bpy)_2]PF_6$ complex (solid-state NIIs) and have been analyzed by NMR and SCXRD. The third part of the result and discussion outlines the iodine $[N\cdots X\cdots N]^+$ complexes of $NR_1R_2R_3$ amines. This is the first example of $[N\cdots I\cdots N]^+$ iodine(I) complex where the nitrogen of the tertiary amines acts as halogen bond acceptor, derived from their parent $[N\cdots Ag\cdots N]^+$ complexes. Final part reports results from silver(I) complexes of tetra- and hexadentate ligands studied by using SCXRD, NMR, and mass spectrometry.

Keywords: halogen bond, three-center four-electron bond, halogen(I) ions, supramolecular chemistry, nucleophilic iodine(I) interactions, NMR spectroscopy, X-ray crystallography, Mass spectrometry.

TIIVISTELMÄ (ABSTRACT IN FINNISH)

Kumar, Parveen
Halogeeni(I)-kompleksien synteesi- ja rakennetutkimuksia
Jyväskylä: Jyväskylä yliopisto, 2022, 160 s.
(JYU Dissertations
ISSN 2489-9003; 549)
ISBN 978-951-39-9366-5 (PDF)

Väitöskirjatyö raportoi mono- ja multivalenttisten ligandien halogeeni(I)-kompleksien tutkimuksia liuostilassa, kaasufaasissa sekä kiinteässä tilassa. Yksikideröntgendiffraktio-(SCXRD), NMR-spektrokopia- sekä massa-spektrometriamittauksia käytettiin hyväksi tutkittaessa valmistettujen halogeeni(I)-kompleksien konformaatoita ja rakenteita. Kirjallisuusosa käsittelee halogeenisidosta yleisesti ja keskittyy tarkemmin neljän elektronin välittämään kolmikeskus (3c-4e) halogeenisidokseen. Kirjallisuuskatsauksen loppuosassa käsitellään hivenen yksityiskohtaisemmin aromaattisten ja alifaattisten ligandien halogeeni(I)-komplekseja liuoksessa ja kiinteässä tilassa, sekä lisäksi kuvataan lyhyesti nukleofiilisen jodi(I):n vuorovaikutuksia (NII) Ag(I) ionin kanssa. Kokeellisen osan tulokset raportoivat Ag(I), I(I) ja Br(I) kationien sisältävien mono- ja disubstituoitujen pyridiinien synteesi- ja rakennekemiaa. Kaikki $[N\cdots Ag\cdots N]^+$ and $[N\cdots X\cdots N]^+$ rakenneosan sisältävät kompleksit analysoitiin NMR-spektrokopian ja yksikideröntgendiffraktion (SCXRD) avulla. Kokeellisen osan toisessa osiossa syntetisoitiin 1-metyyli-1H-1,2,3-triatsolin Ag(I) ja I(I) kompleksit ja niiden avulla valmistettiin erikoinen, kiinteän tilan NII-vuorovaikuksia sisältävä, $[I(mtz)_2]PF_6$*$[Ag(bpy)_2]PF_6$ kompleksi, joka analysoitiin NMR:n ja SCXRD:n avulla. Kokeellisen osan kolmas osio raportoi jodi(I):n $[N\cdots X\cdots N]^+$ komplekseja tertiaaristen $NR_1R_2R_3$ amiinien kanssa. Työssä saadut tertiaaristen amiinien $[R1R2R3N\cdots I\cdots NR_3R_2R_1]^+$ jodi(I) komplesit on ensimmäiset erimerkit tilanteesta, jossa kolme eri substituenttia sisältävä amiini toimii halogeenisidoksen vastaanottajana ja valmistetaan lähtien vastaavasta $[R1R2R3N\cdots I\cdots NR_3R_2R_1]^+$-kompleksista. Kokeellinen osan viimeisessä osassa tutkitaan tiettyjen 4- ja 6-hampaisten ligandien Ag(I)-komplekseja SCXRD:n, NMR:n ja massaspektrometria avulla.

Avainsanat: Halogeenisidos, 3-keskinen 4-elektronin sidos, halogeeni(I) ionit, supramolekyylikemia, nukleofiilinen jodi(I) vuorovaikutus, NMR-spektroskopia, Röntgenkristallografia, massaspektrometria.

Author

Parveen Kumar
Department of Chemistry
University of Jyväskylä
P.O. Box 35
FI-40014 Finland
parveen.p.kumar@jyu.fi

Supervisors

Professor Kari Rissanen
Department of Chemistry
University of Jyväskylä
P.O. Box 35
FI-40014 Finland

Reviewers

Associate Professor Marijana Dakovic
Division of General and Inorganic Chemistry
Department of Chemistry
University of Zagreb
Croatia

Professor (emer.) Risto Laitinen
Environmental and Chemical Engineering
Inorganic Chemistry
University of Oulu
Finland

Opponent

Docent Anssi Peuronen
Department of Chemistry
University of Turku
Finland

PREFACE

This thesis work was carried out at the Department of Chemistry, University of Jyväskylä, Finland, during years 2018 and 2022. These years have been the most rewarding, exciting, and unforgettable. During this journey, I have met a lot of amazing people, to whom I want to express my sincere gratitude.

First and foremost, I want to express my sincerest gratitude to my supervisor, Professor Kari Rissanen, for letting me work in his group and for continues guidance and supervision. I have learned immensely from you, and the work herein would not have been possible without your support. Thank you for being the coolest supervisor anyone could imagine.

Associate Professor Marijana Dakovic and Professor (emer.) Risto Laitinen are greatly acknowledged for the pre-examination of this thesis. I am honoured to receive such supportive comments on my thesis from such distinguished scientists.

Senior Lecturer Elina Kalenius and Senior Lecturer Elina Sievänen are thanked for helping with the analysis of the results. Also, a huge thanks go to Dr. Rakesh Puttreddy, Dr. Jas Ward, Dr. Khai Truong, and Dr. Shilin Yu for the guidance, encouragement, and endless research ideas. I would like to thank all the staff and co-workers at the Department of Chemistry. Thank you for creating such a positive working environment and assistance during these years.

Special thanks go to the amazing group of people, with whom I have shared great moments both working and non-working. It has been a pleasure to work with all of you. Moreover, working here in Jyväskylä would not have been the same without them. Thanks for the friendship, support, and fun times we have had.

My work would not have been possible without the support of my friends and family. Thanks to my parents and my sisters for all the love and support you have given me. And lastly, a big thank you to my best friend Akshita, for being there for me in every situation.

Jyväskylä

Parveen Kumar

ABBREVIATIONS

CSD	Cambridge Structural Database
X	halogen atom
XB	halogen bond
Y	hydrogen- or halogen-bond acceptor
3c-4e	three-center four-electron
HB	hydrogen bond
L	ligand
R	atom or a molecule
Me	methyl
MeCN	acetonitrile
DCM	dichloromethane
THF	tetrahydrofuran
DMF	dimethylformamide
ESI-MS	electrospray ionization mass spectrometry
Et	ethyl
HMBC	heteronuclear multiple bond correlation
IM-MS	ion mobility mass spectrometry
IUPAC	International Union of Pure and Applied Chemistry
NMR	nuclear magnetic resonance spectroscopy
OTf	trifluoromethanesulfonate

CONTENTS

1. INTRODUCTION

Halogen bonding (XB) is defined as the attractive interaction of covalently bonded halogen atoms towards nucleophiles.[1] Halogen atoms are usually considered as an electron donor in organic compounds because of their high electronegativity. However, when a halogen atom is involved in covalent bond formation, the electron density is anisotropically distributed in halogen atoms and that creates the lower electron density region along with the extension of covalent bond.[2] This lower electron density region (σ-hole) leads to the formation of positive electrostatic potential which can show interaction with electron-rich sites (aka nucleophiles).

The first halogen-bonded complex was reported in the 19th century when I_2 interacted with electron-rich NH_3 molecules containing lone pairs.[3] In 1819 P. Pelletier and J. B. Caventou reported the preparation of strychnine triiodide, in which I_3^- anion was synthesised by the interaction of I^- with I_2.[4] It still took around another 100 years before grounbreaking discoveries on charge-transfer interaction by R. S. Mulliken[5] and O. Hassel[6] (Nobel Prize in chemistry in 1966 and 1969, respectively), probed these interactions which form such donor-acceptor complexes. I. Remsen and J. F. Norris reported the 1:1 dimer synthesized by Br_2 and Cl_2 with several amines in the late 19th century.[7] The first XB adduct (complex) of F_2 was prepared and reported after 80 years[8-10] and the preparation of $F_2\cdots NH_3$ and $F_2\cdots OH_2$ complexes were reported in the 1990s.[11]

1.1 Historical perspective

1.1.1 Background

In 1950 R. S. Mulliken[5,12,13] reported intermolecular donor-acceptor interactions when I_2 was dissolved in a solution of ethers, thioethers, and carbonyl derivatives, where charge-transfer

from the halogen occurs in all these complexes were analysed by UV-VIS spectroscopy. The extensive X- crystallographic analysis by O. Hassel in 1950s provided valuable information about these complexes formed by intermolecular interaction between dihalogens or halocarbons with electron-donor moieties.[14-18] In 1954, Hassel published the first crystal structure of a halogen-bonded complex, a striking crystal structure of a 1-D polymer of alternating 1,4-dioxane and bromine molecules obtained from a 1:1 mixture of bromine and 1,4-dioxane (Figure 1).[14] The Br···O distance was reported to be 2.71 Å, which is smaller than the sum of their respective van der Waals radii confirming the generation of a halogen bond and the noticeable lengthening of the intramolecular bromine - bromine bond, from 2.28 to 2.31 Å, was concluded to result from the charge-transfer interaction of 1,4-dioxane and bromine. The bond angle of Br-Br···O was close to 180°. Later Hassel reported the crystal structure of the complexes $Br_2 \cdots C_6H_6$ and $Cl_2 \cdots C_6H_6$, which showed that π-donating component also form complexes with halocarbons.[16,19]

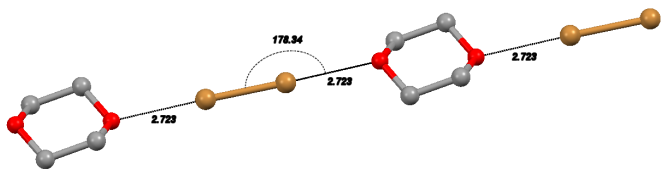

Figure 1. The structure of the polymeric 1:1 XB complex of 1,4-dioxane and bromine (Cambridge Structural Database (CSD), ref. code: DOXABR).[14]

In the following years, more research on such intermolecular interactions involving halogen atoms was conducted[20,21] and a review was published by H. A. Bent about donor-acceptor complexes in 1968.[22] J.-M. Dumas, M. Gomel, and M. Guerin[23] studied the intermolecular interactions in 1983, involving halo-organics in solution and in the solid state.

The real turning point for halogen bonding research was during the 1990's when A. Legon and co-workers started the systematic analysis of a series of halogen-bonded complexes in the gas phase and studied their geometries and charge distribution via microwave spectroscopy.[24,11] Their study shows the similarities between "isolated" complexes and complexes in the condensed phase (solid state), while a minor influence on halogen bond length and angle were noticed just because of lattice effects present in solid state and solvent effect influence bond length and angle in the solution state. Within the same time period Resnati and, Metrangolo and co-workers highlighted the significance of halogen bonding in the self-assembly processes[25-27] and researchers started the "rediscovery" of halogen bonding as a recognition motif in self-assembly processes.

Later on, it became clear one could regulate the structure and function of self-assembled complexes by changing the structure of molecules involved in XB synthesis. At the same time, it took a long time to recognize that halogens are an essential part of the predictable formation of strong, highly directional interactions in solid, liquid, and gas phases.[27,28] The computational analysis by P. Politzer and J. S. Murray showed the anisotropic charge distribution on covalently bonded halogen atoms[29-31] and introduced the concept of "σ-hole", viz. a region where halogen atoms have a positive electrostatic potential.

Halogen bonds in the solid, solution, and gas phases are highly predictable and highly directional, which has attracted the scientific community's attention and more researchers started to notice the potential of halogen bonding as a new recognition motif from the beginning of the 21st century. Over the past few decades, this interaction has evolved into a routinely used tool to direct and control molecular assembly processes.[32] It has found a place in a wide variety of contemporary chemical research fields including, material science, and medicinal chemistry.[63,64,120,121,76]

1.1.2 The halogen bond

In the middle of the 20th century, the term 'halogen bond' began to emerge although it is hard to pinpoint exactly when it was first used. Zingaro and Hedges used the term "halogen bond" in 1961 to describe compounds originating from halogens or interhalogens, in solution, with phosphine oxides and sulfides.[33] In 1976 D. E. Martire and co-workers used this term to describe complexes formed between haloforms with ethers and amines in the gas phase.[34] Then the term began to be used for other related systems.[35,36] Following the publication of the Metrangolo and Resnati report which correlated the structure of XB donors and acceptors and the strength of their interactions, researchers began to use the halogen bond name regularly.[28]

As part of the International Union of Pure and Applied Chemistry's (IUPAC's) 2009-032-1-100 project, halogens as electrophilic species were evaluated for their interactions with other halogens.[8] In 2013, IUPAC proposed a definition that states that **"*A halogen bond occurs when there is evidence of a net attractive interaction between an electrophilic region associated with a halogen atom in a molecular entity and a nucleophilic region in another, or the same, molecular entity*."**[1]

Halogen bond (XB) is commonly defined as follows:

$$R{-}X \cdot \cdot \cdot Y$$

where the three dots represent a halogen bond, and X is any covalently bonded halogen atom to R, and Y is an nucleophilic atom. R-X is referred as a halogen bond donor while Y is halogen bond acceptor (electron donor) and it can be either neutral or an anion. Halogen(I), X^+, (aka halenium ions) can also behave as bis-functional XB donors and form a three-centre four-electron halogen bond. As a result of the R-X···Y system, the interatomic distance between X and Y is smaller than the sum of the van der Waals radii of the X and Y atoms involved and due to this new interaction, concomitant lengthening of the covalent R-X bond is typically observed. There is a directional nature to halogen bonds, with a bond angle of 180° in R-X-Y.

1.2 Nature of halogen bonding

1.2.1 The sigma-hole concept

Understanding the origin and characteristics of halogen bonding has become more important in recent years. Originally, this interaction was described as a charge-transfer interaction,[37] later denoted as the σ-hole interaction. Several theoretical studies have investigated the nature of the halogen bond over the past decade, but recently the σ-hole concept and purely electrostatic interactions have been challenged.[38-49] The true nature of halogen bonding is frequently debated, but it is commonly described as non-covalent interaction. The σ-hole concept was introduced by Politzer and co-worker[50] and elegantly explained the behavior of halogen atoms in halogen bonds as an electrophile. Although, there are few halogen-bonded complexes whose behavior cannot be simply explained based on the σ-hole concept. [42,51] Computational studies focus on the electron density distribution in the ground state and isolated state. The electron density redistribution occurs when halogen atoms form covalent bonds and the electric potential becomes anisotropic as a result of covalent bonds. Initially, P. Murray and colleagues[20,52,53] demonstrated the amphoteric nature of covalently bonded halogen atoms by studying crystal structures and found that they could form interactions with both electrophiles and nucleophiles. While electrophiles interact orthogonally, and nucleophiles prefer elongation of the R-X bond. This phenomenon is called polar flattening and was later proved by computational studied[54] and X-ray structural analysis.[55-57] Halogen atoms become oblate

with shorter radius along with covalent bonds (Figure 2). Computational studies of CF_3X molecules (X = F, Cl, Br, I) show the formation of positive electrostatic potential (the σ-hole) on the outermost portion of the halogen's (Cl, Br, I) surface due to the anisotropic distribution of electrons of covalently bonded halogen atoms. Around X's central part, three unshared electron pairs produce a belt of negative electric potential.[50] This explains the interaction pattern of the covalently bonded halogen atom and shows liner interaction with a nucleophile and lateral interaction with an electrophile. Which explains the synthesis of a linear complex R-X···Y, through the attractive interaction between the σ-hole of a covalently bonded halogen atom X and a negative site of Y.[58] The presence of σ-hole explains the electrophilic nature of halogen atoms and forms close to linear structure with a nucleophile in halogen bond (Figure 2).

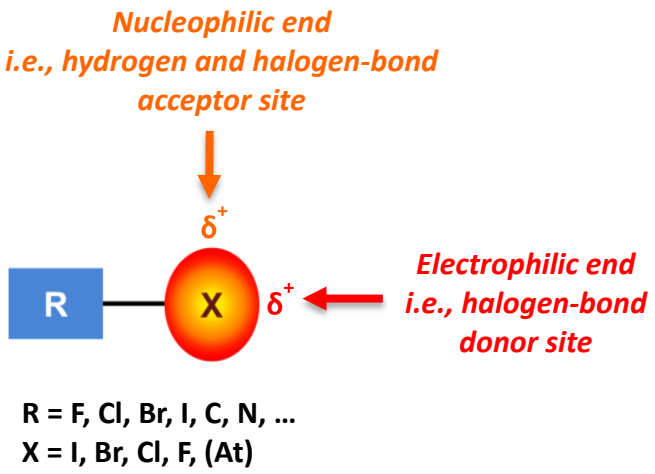

Figure 2. This diagram illustrates the anisotropic distribution of electron density surrounding covalently bound halogen atoms and the pattern of their interactions.[58]

1.2.2 Factors affecting halogen bonding

However, the halogen bonding ability of the molecules would depend on many factors like polarizability, electronegativity of the halogen atom and the electron-withdrawing power of the R-group.[58] Higher the positive charge on σ-hole, stronger the halogen bond, and strong electronegative R-group will enlarge the XB donor potential of the R-X group. While an unexpected trend was recorded in the strength of CY_3I (Y = F, Cl, Br, I) complexes formed through halogen bond with chloride and trimethylamine.[42] Later it has been explained by computational studies and noticed that higher electronegativity of the R-group always doesn't increase the donor strength of the R-X group. It was not fully explained by the electrostatic effects of the σ-hole and therefore, charge-transfer interactions and the Pauli repulsion were suggested to have an impact.[42]

Halogen bonds formed by Lewis bases interacting with halogen σ-hole are typically weak and do not affect interatomic distance much. It is possible to increase the bond strength of the halogen bond by increasing the halogen's positive charge by oxidizing them into halogen(I), X^+.[59,60] There is a preference for simultaneous interactions with two Lewis bases, producing halogen-bonded halogen (a halogen(I)) $[L\cdots X\cdots L]^+$ structures.[61] The central halogen(I) ion X^+ possesses a s^2p^4 electron configuration, and its p-orbital shows spin-paired $p_x^2p_y^2p_z^0$ arrangement, induced by electrostatic fields of the Lewis bases. In this case, halogen bond form when Lewis base trasfer charge to the empty two lobes of the p_z^0 orbital of the halogen atom. Therefore, halogens form a halogen bond to the Lewis base through π -hole interaction rather than σ-hole interaction (Figure 3). A complex formed through this interaction shows a short donor-acceptor distance. This interaction is partly covalent and partly electrostatics, and strongly dependent on the involved halogen atom.[62]

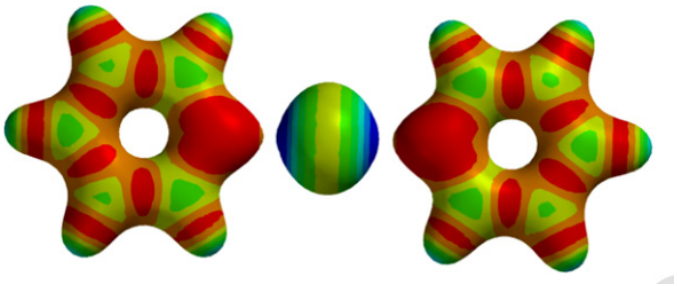

Figure 3. The electrostatic potential at the surface of the [bis(pyridine)iodine(I)]+ complex. Blue is positive and red is negative potential.[62]

1.3 The structural features of halogen bonding

Halogen bond shows unique features like directionality, strength tunability, hydrophobicity, and donor atom dimensions, which allows XB interaction to design and develop self-assembled systems and is regularly used as the non-covalent interaction to synthesize supramolecular complexes. Halogen bond (XB) is very much like the hydrogen bond (HB) and these similarities of the bonding geometries and directionality have been successfully used to influence the self-assembly of host-guest complexes, from porous, magnetic, and phosphorescent materials, liquid-crystals, ion-pair recognition, biomolecules, and chemical separations.[63,64]

In halogen bond, nucleophile interacts with the halogen atom's σ-hole precisely on the prolongation of the covalent bond(s) axis[50] and due to that XB is more directional than HB.[65] The R−X···Y angle is commonly very close to180°.[21,58]

1.3.1 The three-center four-electron (3c-4e) bond

Halogen bond strength is elucidateed by the synthesis of the three-center, four-electron (3c-4e) bond by interaction of two-electron donor Lewis's bases and electron acceptor halogen(I), and when aromatic Lewis bases like pyridine[59,60,66] are involved, the charge transfer process increases this interaction strength. In the process of charge-transfer, halogen(I) loses its positive charge, and this positive charge is distributed over the aromatic ring. This loss of charge and effective charge-transfer process makes the short distance ($R_{XB} < 1.0$) (R_{XB}, is halogen bond interaction ratio, defined as $R_{XB} = d_{XB}/(X_{vdw} + B_{vdw})$, where d_{XB} [Å] is the distance between the donor atom (X) and the acceptor atoms (B), divided by the sum of vdW radii [Å] of X and B, and the XB donor···acceptor (XB···A))[21] of halogen(I) involved into [bis(heteroaryl)halogen(I)]$^+$ component straightforward.[67] In the solid state, coplanar geometry of the ring was observed and that is transition state in solution.[68] There is a rapid association-dissociation equilibrium between bromine(I) and iodine(I) complexes in solution (Scheme 1). It is known that these complexes are stable in solid form, as well as in solution in the absence of nucleophiles, such as moisture, for numerous hours or even days at a time.[69] Lifetime of complexes depends on the electron density of the involved pyridine ring, which is typically < 5s in solution.[69]

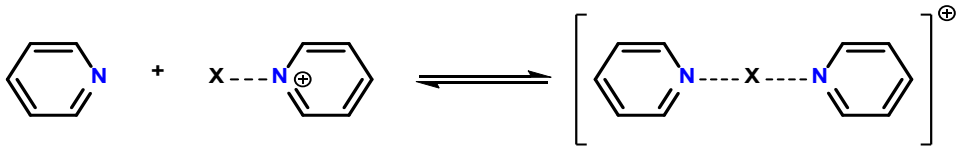

Scheme 1. Solution-based association-dissociation equilibrium of [Bis(pyridine)halogen(I)]+ complexes occurs rapidly.[69]

All four halogens can form a halogen bond and their ability to behave as XB donors is explained by the polarizability of the halogen atoms and generally follows the order F << Cl < Br < I. Fluorine forms halogen bonds only under specific conditions[55,56] and chlorine(I) and fluorine(I) complexes prepared only in solution at low temperature so far,[66] whereas their solid state structures are still not reported. Fluorine shows conventional asymmetric arrangement while forming halogen bond, that is L–X···L, in contrast to the other heavier halogens that form similar long and strong halogen bond with symmetric geometric arrangements.[55,56]

The strongest halogen bond known so far is in I_3^-, between $I^-\cdots I_2$ while the Cl···Cl interactions between chlorocarbons are among the weakest observed halogen bonds.[28] The strength of the halogen bond can be modified by changing the halogen atom involved in bond and the electron-withdrawing power of the R-group covalently attached to the halogen atom.[28] The strength of halogen bond reported to range from 10 kJ/mol to 180 kJ/mol depending on the donor and acceptor used.[28] Molecules that increase the anisotropy of the electron distribution of the X, form stronger XB donors and that makes a strong halogen bond. In halocarbons covalently bonded halogen atom shows different donor strength and this strength increase in the order $C(sp^3) < C(sp^2) < C(sp)$ when there are no other structural differences present.[28]

Halogen bonding is a directional bond, and it prefers linearity in the formed complex. These directionality and geometry of the formed complex not only depend on the donor and the s-hole, but it also affected by the acceptor moieties. For example, an acceptor involving heteroatom Y with a lone electron pair generally forms the halogen bond along the axis of the donated lone pair on Y, and an acceptor with π electrons of an unsaturated system, the donor is perpendicular to the π system. Halide anions have spherical nature and due to that they can adapt a variety of coordination numbers and shows several R-X···X⁻···X-R angles.[70]

1.3.2 Halogen(I) complexes and $[N\cdots X\cdots N]^+$ halogen bond

In contrast to conventional halogen bonding, when an electron is taken from the halogen atom, it form a positively charged halogen(I), or halenium, ion X^+ (X = I, Br, or Cl). This X^+ halenium ion behaves as an immensely polarized halogen atom and acts as a strong XB donor.[59] Halogen(I) ion interact with two suitable Lewis base (XB donor) and forms a three-center four-electron (3c-4e) bond and is stabilized into a $[L\cdots X\cdots L]^+$ (L, Lewis base) complex.[71] In 1960s, Hassel *et al.* have reported the first [*bis*(pyridine)iodine(I)] complex with a $[N\cdots I\cdots N]^+$ 3c-4e bond[72] and later in 1960s, Crichton et al.,[73,74] and Hague et al.[62] have reported also the synthesis or halogen(I) complexes and later it became popular in synthetic chemistry in the form of Barluenga's reagent.[75] Barluenga's reagent, [*bis*(pyridine)iodine(I)]tetrafluoroborate (Figure 4), is a stable white solid powder that function as a iodine atom transfer reagent as well as an oxidant. It is soluble in both organic and aqueous solutions (it quickly decomposes).[76] Jose Barluenga and his coworker did more research about its use as a reagent and published a variety of applications for the bis(pyridine)iodine(I) complex as an oxidating agent and as an iodonating agent for aromatic electrophilic substitutions.[77-80] Halogen(I) ion

based complexes are very stable under suitable conditions and show exceptional strength of the 3c-4e bond and ever since its discovery it became limelight in halogen bonding research with recently published work by Erdelyi *et al.*,[59-61,66,68,71,81-84] and Rissanen *et al.*[85-93]

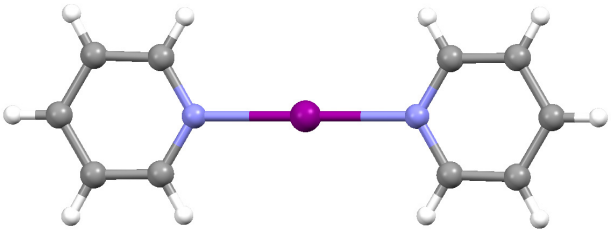

Figure 4. The structure of bis(pyridine)iodonium tetrafluoroborate complex (counter-ion BF_4^- has been omitted for clarity) (CSD ref. code: HUMMAD).[101]

The crystal structure of $[py\cdots I\cdots py]^+$ was reported in 1961, with a centrosymmetric arrangement and I_3^- as a counteranion.[72] At the same time, many crystal structures involving nitrogen and iodine(I) or bromine(I) ions complexes were reported, but mainly they were reported as charge-transfer complexes or reactive intermediates in organic synthesis.[94-100] The $[N\cdots X\cdots N]^+$ systems were found to be fully or close to symmetric and pyridine and pyridine derivatives are commonly used in the formation of linear $[N\cdots X\cdots N]^+$ bonds,[95,96,100] and $[N\cdots X\cdots N]^+$ bonds containing other than aromatic sp^2 nitrogen atoms are also reported.[94,97,101]

The halogen(I) based halogen bonded complexes have been recently reviewed by Erdelyi and Turunen,[59] where nitrogen-based ligand used as lone pair donor and mostly reported complexes show symmetric $[N\cdots X\cdots N]^+$ bonds.[82,89] Very recently, the first-ever asymmetric halogen(I) complex (Figure 5) in a solid-state was reported by Rissanen and coworkers in between pyridine and dimethylaminopyridine (DMAP).[89]

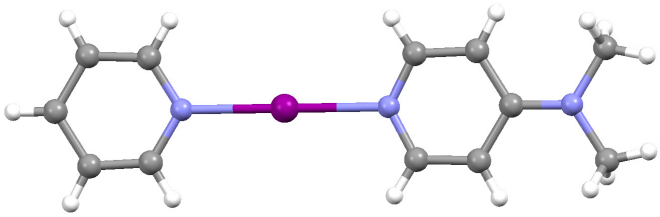

Figure 5. Structure of the asymmetric iodine(I) $[N\cdots I\cdots N]^+$ complex (counter-ion omitted for clarity) (CSD ref. code: SURTIL).[89]

Erdélyi and co-workers were the first research group who studied the halogen(I) ion from the perspective of halogen bonding.[61,66,68,81,83,84] In this three-center four-electron (3*c*4*e*) $[N\cdots X\cdots N]^+$ system, the halenium ion (X^+) is simultaneously stabilized by two identical nitrogen electron donors, pyridine or pyridine derivatives of a clamp ligand (Figure 6). This 3c4e complex system can be symmetric where the halogen(I) is centered between two nitrogen

atoms having equally strong and long N···X bonds, and in another case, it can be asymmetric where the X^+ ion is closer to one donor atom with one shorter and stronger covalent N-X bond and one longer and weaker N···X halogen bond.[60]

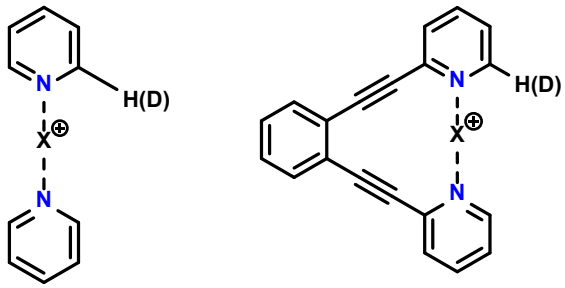

Figure 6. The structures of [bis(pyridine)iodine]$^+$ complexes used to investigate 3c-4e systems in solution and in solid state.[81]

The $[N\cdots X\cdots N]^+$ halogen bond and the $[N\cdots Ag\cdots N]^+$ coordination bond are structurally analogous and both systems result in bis-coordinated complexes with linear geometry.[102] Contrary to the silver(I) complexes, the halogen(I) complexes in solution[68,81] as well in solid-state[87] prefer symmetric bonds. However, based on the Lewis basicity of the XB acceptor, halogen(I) complexes undergo rapid ligand exchange.[82] This ligand exchange occurring for weak Lewis bases, is observed as line broadening in the NMR spectrum.[82] The symmetric nature of the halogen(I) bond has been reported constant even by changing solvent polarity[61] and counterion interaction.[84] The robust nature of the halogen(I) complexes, and the tunability of their strength, together with the possibility of the remoulding of the electron density in the three-centered system, have made them a reliable tool both in the prepration of the large supramolecular structures[91-93] and use in synthetic chemistry.[59]

1.4 Halogen(I) complexes in the solid state

The halogen(I) complexes $[L\cdots X\cdots L]^+$ (X = Cl, Br, I), also known as halogen(I) complexes, are prepared by removing an electron from the halogen atom to its cationic state X^+,[59,90] and then stabilizing it with two Lewis bases (L). In the 1960s, these complexes were the first time reported though they have not been recognized by researchers until the 1990s when Barluenga reagent (bis(pyridine)iodine(I) tetrafluoroborate) shows many applications, including electrophilic iodination of unactivated arenes, promoting the formation of C–C and C–X bonds, and selectively direct iodination of peptides.[77,78,80]

The $[L\cdots I\cdots L]^+$ iodine(I) complex can be directly prepared by using elemental iodine (I_2) with mighty strong Lewis bases such as DMAP (Scheme 2, route A). With other Lewis bases, [*bis*(ligand)halogen(I)]$^+$ complexes can be easily synthesized (Scheme 2) via cation exchange process from their respective 2-coordinate silver(I) complexes $[L\cdots Ag\cdots L]^+$. This process is more reliable due to AgX formation, which is a stable side product and acts as driving force in this reaction.[59]

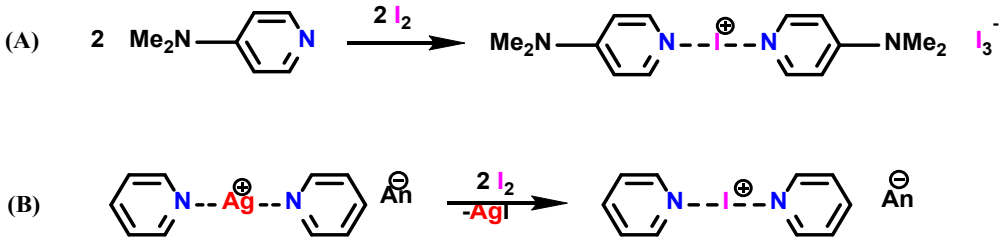

Scheme 2. The synthesis of [*bis*(ligand)halogen(I)]$^+$ complexes, route A shows direct method and route B shows via cation exchange from their respective silver(I) salts (an = anion).[59]

Within the halogen(I) complexes, the most stable complexes is [*bis*(ligand)iodine(I)]$^+$ and the largest sub-group of [*bis*(ligand)halogen(I)]$^+$ complexes, their stability order are : $[L\cdots I\cdots L]^+ >$ $[L\cdots Br\cdots L]^+ >> [L\cdots Cl\cdots L]^+$. The *N*-heterocyclic ligands (mostly pyridine derivatives, Figure 7) are the commonly used Lewis bases in the synthesis of [*bis*(ligand)halogen(I)]$^+$ compounds with a $[N\cdots I\cdots N]^+$ 3c-4e bond. These complexes show decent stability as solids, for example Barluenga's reagent even being available commercially.

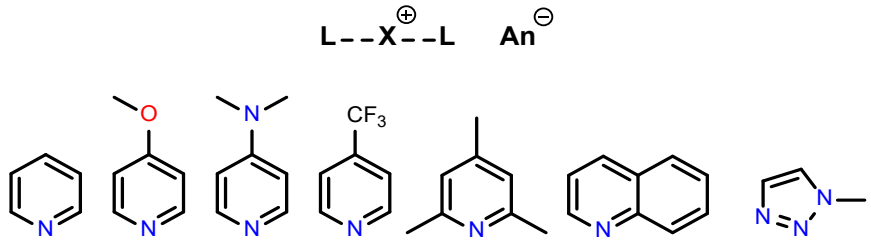

Figure 7. The aromatic N-heterocyclic ligands previously used to synthesize [*bis*(ligand)halogen(I)]$^+$ complexes.

1.4.1 Aromatic $[L\cdots I\cdots L]^+$ iodine(I) complexes

The stability of [*bis*(ligand)iodine(I)]$^+$ complexes have motivated researchers to look upon these complexes and extensive solid state examples have been reported as well as their structural features interrogated by many research groups. From all these studies, the $I^+\cdots N$ bond length of [bis(ligand)iodine(I)]$^+$ complexes lies between 2.23(1)-2.32(1)Å.[103] It has been reported that steric as well as electronic effects do not influence much on the $I^+\cdots N$ bond length[83] in the solid-state but these effects play a major role in electron distribution, $I^+\cdots N$ bond strength and its reactivity (Figure 8). For example, when 4-aminopyridine (4-NH_2py) is

used in place of pyridine (I–N, bond length 2.256 Å, average) as a Lewis base to form $[L\cdots I\cdots L]^+$ complexes, the $I^+\cdots N$ bond length becomes shorter ($I\cdots N$, bond length 2.245 Å, average) as expected and $I^+\cdots N$ bond becomes stronger.[103] Similarly, the predicted trend was observed with sterically bulky group 2,4,6-trimethylpyridine in place of pyridine, in which two ortho methyl groups shows steric hindrance and due to that [*bis*(2,4,6-trimethylpyridine)iodine(I)]$^+$ complex have longer $I^+\cdots N$ bonds ($I^+\cdots N$, bond length 2.288 Å, average).[83] Comprehensively, the $I^+\cdots N$ bond strengths are significantly affected by steric and electronic effects compared to $I^+\cdots N$ bond length, indicating that bond strength should be carefully considered when interpreting interaction strength.[83]

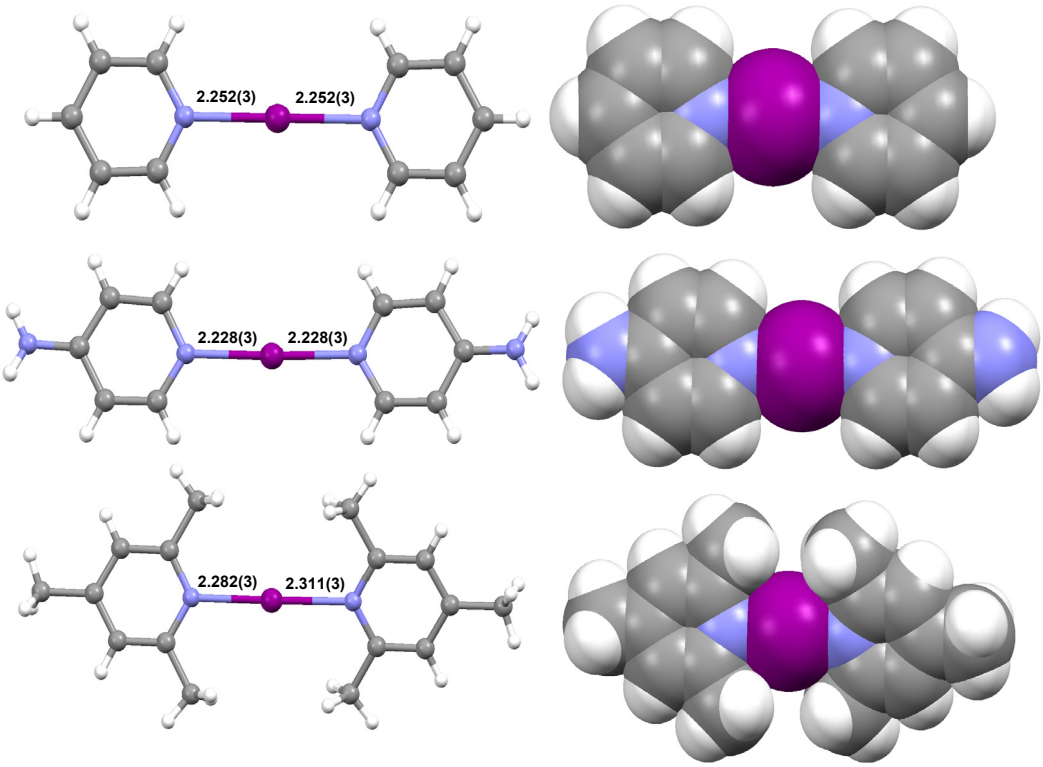

Figure 8. The structure of the three [*bis*(ligand)iodine(I)]$^+$ complexes and their $I^+\cdots N$ bond lengths are shown. (all distances in Å and counter-ions omitted for clarity) (CSD ref. code: CICQIQ03[84], YOFKIQ[104], CICQOW01[105]).

In all published, [*bis*(ligand)iodine(I)]$^+$ complexes, the $[N\cdots I\cdots N]^+$ halogen bond shows almost perfect 2-coordinated linear geometry with a bond angle of 180°. While the [*bis*(4-trifluoromethylpyridine)iodine(I)]$^+$ complexes show the largest deviation from linear geometry reported so far with an $[N\cdots I\cdots N]^+$ bond angle of 175.2(2)°.[83] In all the reported iodine(I) complexes, many anions have been used, no interactions between the anions (being nucleophilic) and halogen(I) ions have been observed, the iodine(I) ions seems to "abhore" anions.[84]

1.4.2 Aromatic [L···Br···L]$^+$ bromine(I) complexes

Bromine(I) ion based complexes are very reactive compared to their iodine(I) analogues and due to their less stability, very few examples of [bis(ligand)bromine(I)]$^+$ complexes appear in the literature. Like the iodine(I) complexes, most of the bromine(I) complexes are reported by using *N*-heterocyclic ligands with Br$^+$···N bond lengths inside the range of 2.049(2)-2.144(6)Å,[103] (Figure 9) and N···Br$^+$···N bond angles within the range 176.2(2)–180°.[103] The [bis(3-methylpyridine)bromine(I)]$^+$ was one of the exceptions reported with an N···Br$^+$···N bond angle of 173.89°.[106] The shortest Br$^+$···N bond length was observed in [bis(pyridine)bromine(I)]$^+$,[107] and the longest for [bis(2,4,6-trimethylpyridine)-bromine(I)]$^+$.[105] The Br$^+$···N bond length can be expected to be longest and weakest in strength in the case of electron-poor Lewis base ligands like in [bis(4-trifluoromethylpyridine)iodine(I)]$^+$ complex.[83] Since, bromine(I) complexes are not much stable, they tend to require strong Lewis base and due to that bromine(I) complexes haven't been reported much with electron-poor ligands.

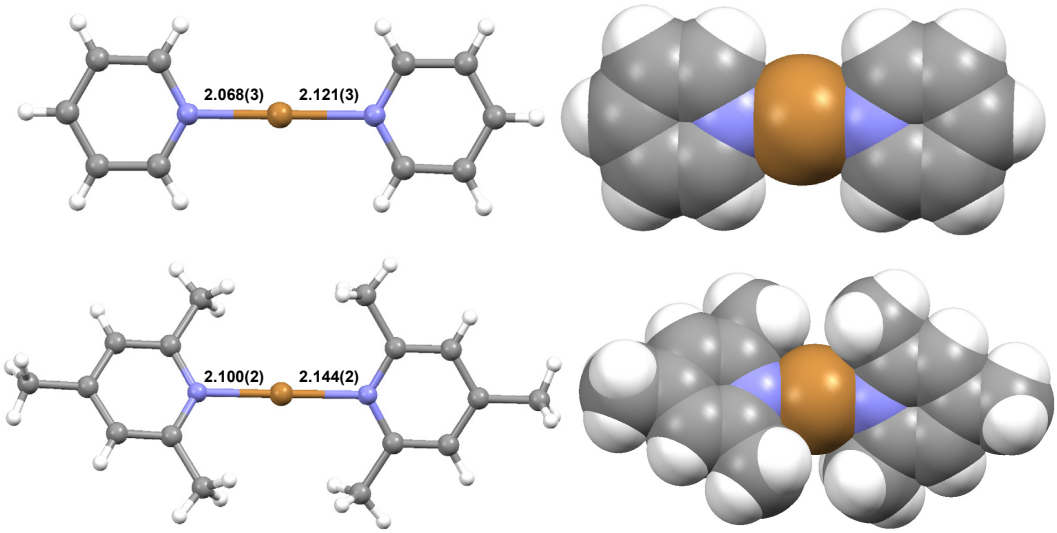

Figure 9. The structures [*bis*(ligand)bromine(I)]$^+$ complexes (left; all distances in Å and counter-ions omitted for clarity) (CSD ref. code: DOWBIC[107] and AKOXON02[105]).

Since the longest Br$^+$···N bond length reported in 1975 (2.1862Å) is from a room temperature data collection.[95] Therefore, it might not be relevant to compare it to modern, low-temperature data collections.

1.4.3 Aliphatic [L···X···L]$^+$ halogen(I) complexes

The halogen(I) complexes containing aliphatic amines as Lewis bases are vastly more rare when compared to [bis(ligand)iodine(I)]$^+$ and [bis(ligand)bromine(I)]$^+$ complexes

incorporating *N*-heterocyclic ligands (e.g., substituted pyridines). So far a limited number of confirmed solid state examples are known and all have one of the three ligand as a coordinating group: quinuclidine,[87,97,98] DABCO(1,4-diazabicyclo[2.2.2]octane),[108,109] or hexamethylenetetramine (Figure 10).[94,110] An absence of potentially favorable π-stabilization is reported in the tertiary amine-based complexes of [bis(ligand)iodine(I)]+ compare to their N-heterocyclic analogs, although the tertiary amine iodine(I) complexes remain stable as their aromatic counterparts.[87] Tertiary amines with structure of $NR_1R_1R_2$ or $NR_1R_2R_3$ based $[bis(ligand)halogen(I)]^+$ complexes are not known in the solid state.

The known $I^+\cdots N$ bond length ranges are 2.268–2.319Å and 2.1202–2.1572Å for $Br^+\cdots N$. [103] The slightly bulkier nature of tertiary amines and absence of halogen(I) π-stabilization affect their bond length and their bond length is a slightly towards the longer side of the ranges above discussed for $[bis(ligand)halogen(I)]^+$ complexes contaning aromatic *N*-heterocyclic ligands.

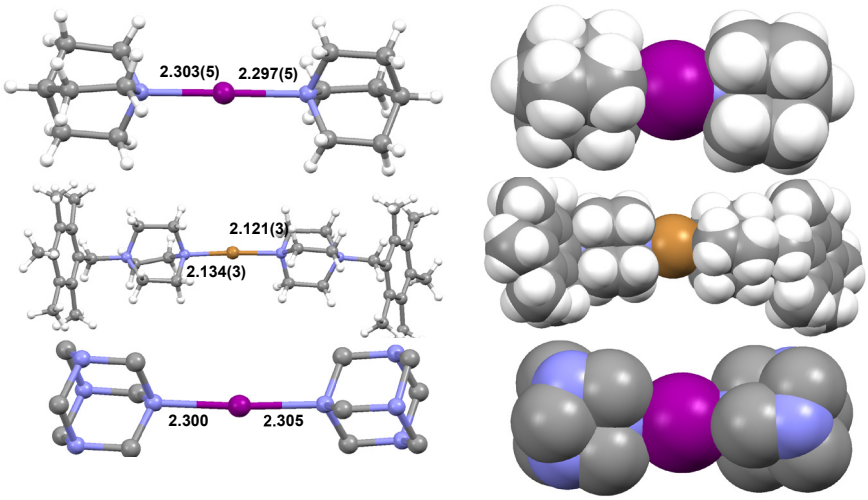

Figure 10. The structure of the the three coordinating motifs that comprise all reported solid-state examples of $[bis(ligand)halogen(I)]^+$ complexes incorporating tertiary amines (all distances in Å and counter-ions omitted for clarity).(CSD ref. code: IWABIU[87], EDANAA[108], HMTITI[94]).

1.4.4 Multi-halogen(I) complexes

The supramolecular complexes based on halogen bonding are known to be constructed through appropriate ligand design. There are not many instances where advanced architectures have been achieved from $[bis(ligand)halogen(I)]^+$ ion complexes formed with aromatic *N*-heterocyclic ligand, from their respective silver(I) complexes. In 2019, the first helix based on iodine(I) ion was reported (Figure 11),[67] with the bond length for $I^+\cdots N$ bond were within the range observed for iodine complexes with pyridine ligands (2.253(4)-2.302(4) Å). The unique helical conformation brings the two iodine(I) centers very close to each other, only 3.887(1)Å

which is lesser than the van der Waals radii of two iodine atoms (3.96Å), but helix structure has no evident effect on the $I^{+}\cdots N$ bond lengths.

The iodine(I) atoms in [bis(pyridine)halogen(I)]+ type complexes have a partial positive charge (partial positive charges are transferred into the aromatic Lewis bases)[66] so there is almost no electrostatic repulsion in between two iodine(I) centers. Thus, the helix was stabilized by strong three-centre four electron halogen bonds in conjunction with the efficient hydrophobic packing of its aromatic rings. There is even smaller $I^{+}\cdots I^{+}$ distance (3.7774(19)Å), in the electron-rich [bis(4-dimethylaminopyridine)iodine(I)]$^{+}$ complex.[89]

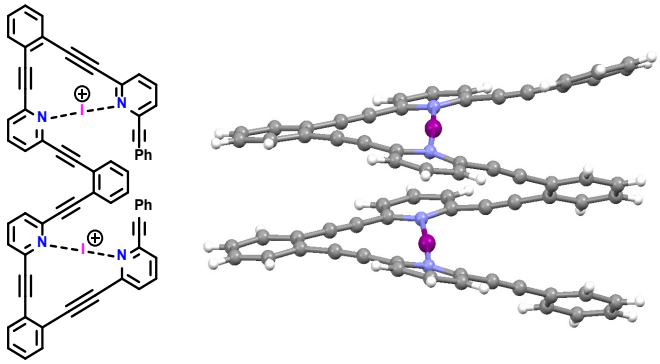

Figure 11. The structure of the first reported helix based on halogen(I) ion, which contains two iodine(I) centers in close proximity (counter-ions omitted for clear view) (CSD ref. code: NOMCAW[67]).

The highly directional nature and reproducible bonding characteristics make [bis(ligand)halogen(I)]$^{+}$ complexes a classic case for the self-assembling process towards supramolecular architectures,[59] even though it was achieved recently. Halogen(I) based supramolecular cages (Figure 12) have been synthesized by using pyridine and DABCO as a rigid molecular backbone.[91,93] Small modifications, like using synthons based upon either meta- or para-attached pyridyl groups, solvent-based rearrangements, and considering factors namely micro-solvation and entropic considerations[111] have even allowed for generating different supramolecular compositions.[112] By using these methodologies, polymeric halogen(I) species have been manufactured, also known as halogen-bonded organic frameworks (XOFs).[113] These polymeric halogen(I) species open up the halogen(I) ion complexes field.

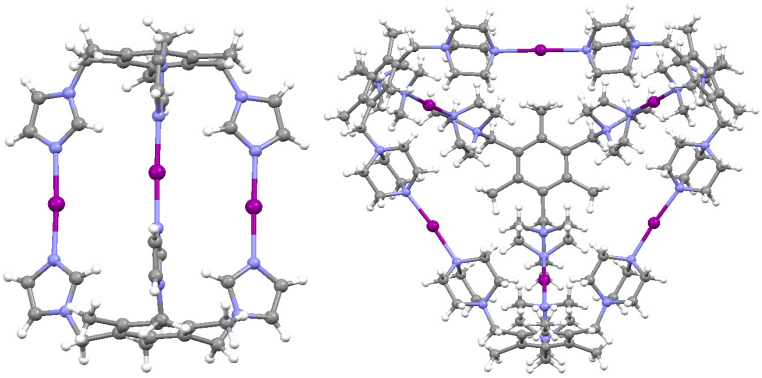

Figure 12. Crsystal structures of the supramolecular architectures constructed from iodine(I) ions (counter-ions omitted for clarity). (CSD ref. code: WEHTEL and WEHSUA). [93]

The first symmetric dimeric capsules stabilised by $[N\cdots I\cdots N]^+$ halogen bonds were reported in 2016 by Rissanen *et al.* These dimeric capsules using tetrakis(3-pyridyl) ethylene cavitands with different lower rim alkyl chains were synthesized and analysed in solution, solid and in the gas phase (Figure 13).[91] More recently, dimeric iodine(I) and silver(I) cages from tripodal N-donor ligands (Figure 14) via the $[N\cdots Ag\cdots N]^+$ to $[N\cdots I\cdots N]^+$ cation exchange reaction were reported by Rissanen *et al.*[118] These reports serve as further proof of the indisputable importance of halogen(I) ions as supramolecular synthons, in simple monodentate ligand- complexes as well as in more sophisticated capsular assemblies.

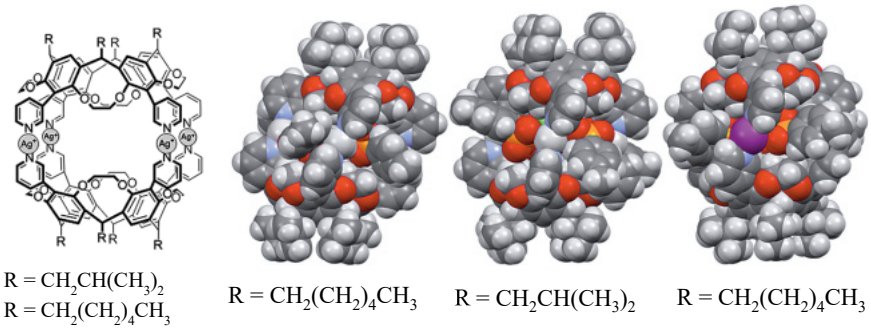

Figure 13. The structure of the first reported symmetric dimeric Ag^+ capsules using tetrakis(3-pyridyl) ethylene cavitands, and the modelled structure of the iodonium capsule. (counter-ions omitted and ligand simplified for clarity) (CSD ref. code: EZACIT).[91]

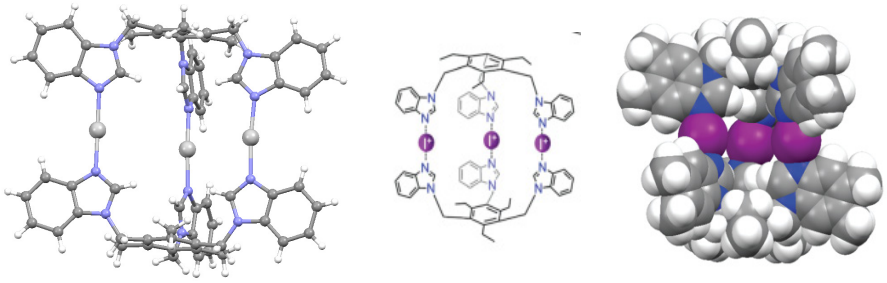

Figure 14. The structure of silver(I) cages from tripodal N-donor ligands(left), and the dimeric iodine(I) cages structure(middle) and spacefill representation of the calculated structure of iodine(I) cage(right). (counter-ions omitted and ligand simplified for clarity). (CSD ref. code: XECJIC).[118]

1.4.5 Solid-state nucleophilic iodine(I) interactions (NIIs)

Nucleophilic iodonium interaction (NII) is a new solid state intermolecular interaction between iodine(I) and silver(I) complexes,[85] where iodine(I) center behave as a nucleophile to a Ag^+ cation of a 4- or 2-coordinate complex. This new short $I^+\cdots Ag^+$ contact was first reported in 2021 by Rissanen *et al*[90] where NII interaction was observed in the solid state [90,85,86] as well as in solution by isothermal microcalorimetry (ITC).[90] To observe and define this interaction is very troublesome due to its apparent similarity to the $Ag^+\cdots Ag^+$ argentophilic interactions which are often observed for the Ag-complex structure in the solid state. Computational studies have shown that no retrodonation of silver(I) metal centers to iodine(I) ions occurs when I^+ and Ag^+ interact strongly.[90]

It is relatively easy to isolate a solid-state compound based on nucleophilic iodonium interaction from the compatible pairs of 2-coordinate $[L\cdots I\cdots L]^+$ and $[L\cdots Ag\cdots L]^+$ complexes, which mix 1:1 ratio even when ligand exchange occurs rapidly in solution.[85] The $[bpy\cdots Ag\cdots L]^+$ complexes (Scheme 3) of bipyridine and substituted pyridine can also be used to create NIIs complexes, where 4-coordinate Ag-complexes $[bpy\cdots Ag\cdots bpy]^+$ interact with a linear 2-coordinate geometry of iodine(I).[90,86] Elusive behavior of this interaction makes it difficult to confirm its existence and due to that reason only three examples have been confirmed so far by using X-ray diffraction in solid state (Figure 15). These include $I^+\cdots Ag^+$ distances, 3.5184(7) Å,[85] 3.4608(3) Å,[90] and 3.4043(4) Å,[86] which are reasonably smaller than the sum of the van der Walls radii of iodine and a silver atoms (3.70 Å).

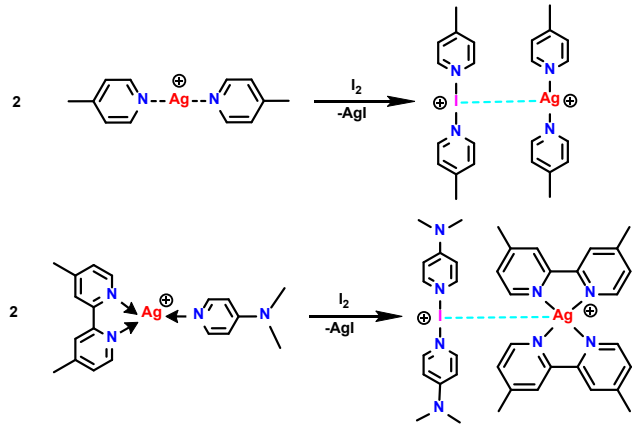

Scheme 3. The synthetic routes to synthesise NIIs complexes from 2- or 3-coordinate silver(I) complexes. [85,86]

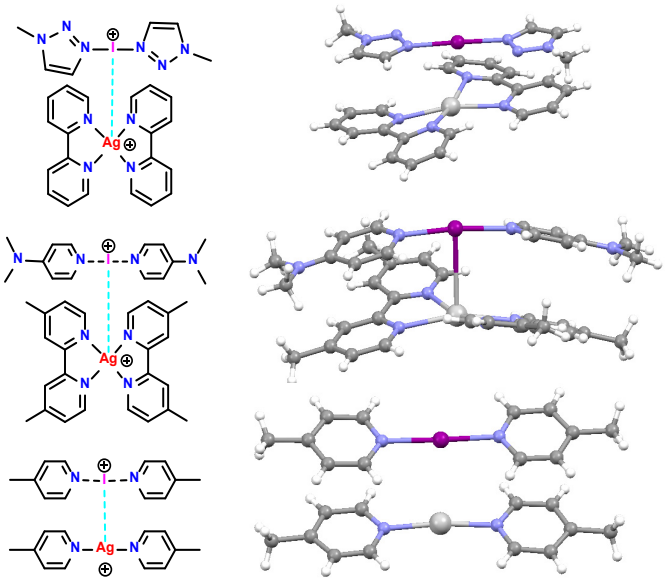

Figure 15. Three examples of Nucleophilic Iodine(I) Interactions (NIIs, shown by dashed lines, counter-ions omitted for clarity) (CSD ref. code: OMIQOT[90], EPEZAD[86], EROGIE[85]).

1.5 Halogen(I) complexes in solution

The strength of halogen bonds and their properties have puzzled researchers, and it triggered the investigations in this field. In 2010, study of their properties has been started and mainly in solution by spectroscopic techniques, later supported by computational calculations. [68,81]

1.5.1 Fluorine(I) complexes

A fluorine(I) atom prefers traditional halogen bonds, L^{+}-F···L, which have one distinct and strong covalent bonds, L-F and a week and long L···F halogen bond.[66] These complexes form halogen bond through a σ hole and ligand(L) contains the positive charge of the complex. There

are very few fluorine-based halogen bonds, which can only be prepared when fluorine is directly connected to a strong electron-withdrawing group, that augments its σ-hole, such as pyridine nitrogen. Fluorine(I) complexes have been studied by diffusion NMR spectroscopy, where the diffusion rate of *N*-fluoropyridinium ion (D = 41 × 10−10 m^2/s), is a bit slower in the presence of pyridine compare to in the absence of it (D = 120 × 10−10 m^2/s).[66] The complex is not stable at ambient temperature, it decomposes quickly, but it is stable at -35°C in solution.[66] Fluorine(I) based complexes, known as 1-fluoropyridinium heptafluorodiborate pyridine, are used as a fluorinating reagent in synthetic chemistry and this complex is stabilized by protonation of non-covalently bonded pyridine ring(otherwise it will be active for electrophilic fluorine(I) approach).

1.5.2 Chlorine(I) complexes

The chlorine-centered halogen bonds are uncommon as well. The [bis(pyridine)chlorine(I)]$^+$ complex is stable in DCM solution at -80°C, and examined by relaxation studies.[66] It has been observed that protons close to halogen bonded chlorine(I) ion, relaxes much faster than the static pyridine and [bis(pyridine)silver(I)] triflate complexes or of the [bis(pyridine)proton]$^+$ complex. Because of the rapid relaxation of proton close to the chlorine(I) ion, only ^1H,^{13}C NMR have been observed for this complex.

1.5.3 Iodine(I) and bromine(I) complexes

Iodine(I) and bromine(I) behave similar to chlorine(I) complexes and form 3c-4e bonds in solution. These [L···X···L]$^+$ complexes are stable at ambient temperature in dichloromethane and acetonitrile solutions, while bromine(I) complexes were more sensitive.[68,81] Further studies like isotropic perturbation of equilibrium observation using NMR,[60,68,81] confirms their centrosymmetric geometry and they maintain their symmetry in the solid state as well.[60] The properties of these complexes are studied initially using monodentate ligands, but later avoided due to the possible misinterpretation of the data resulting from the dynamic equilibrium.[82] Later researchers focused more on preparing entropically favored ligands that are less susceptible to chemical exchange process(Figure 16). [59,81,82] The unstrained bis(pyridine)-type complexes undergo ligand scrambling by involving into dynamic association-dissociation equilibrium, while complexes with 1,2-diethynylbenzene backbone (middle, Figure 16) does not agonize from ligand scrambling and also entropically favored. Although the flexible

analogue (right, figure 16) is not prone to strain, it does retain an entropic advantage that prevents the scrambling of ligands.[81,82]

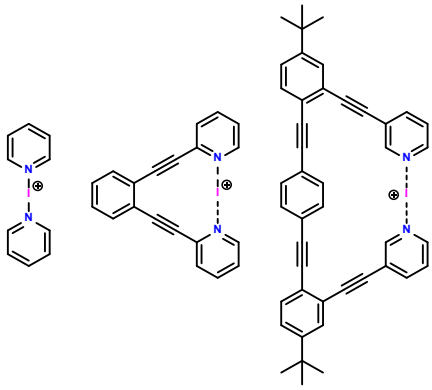

Figure 16. Three examples of $[N\cdots I\cdots N]^+$ halogen bonds of different nature and geometry.[81,82]

The centrosymmetry of these complexes have not been affected by the different polarity of the solvent, though it does influence counter-ion coordination, and somewhat explain the solvent-dependent reactivity of Barluenga's reagent.[114] The major differences have been observed between the behavior of silver(I) complex and halogen(I) complexes where silver(I) coordinates to anion through available empty orbitals in silver(I) and form argentophilic interactions, however, due to the lack of empty orbitals, $[N\cdots X\cdots N]^+$ complexes cannot form Lewis acids. In solids, counter ions pack asymmetrically, but have no effect on the $[N\cdots X\cdots N]^+$ bond's symmetry.[84] These differences have been confirmed by studies of bidentate ligands using diffusion NMR analysis and later by computational studies and SCXRD, results specify that silver(I) forms dimers or polymer complexes with the 3,3′-di(pyridin-2-yl)-1,1′-binaphthalene ligand, whereas iodine(I) stabilized into monomeric form.[115]

It has been reported that the electron density of the Lewis base has a major influence on the strength of the bonds, however, the electron density changes on both coordinating Lewis bases in a symmetrical manner does not affect the geometry of $[N\cdots I\cdots N]^+$ complexes (Figure 17).[79] The electron-deficient Lewis base forms a weaker halogen bond and correspondingly shows higher reactivity in halogen(I) transfer reactions. On the other hand, an asymmetric Lewis base causes asymmetry in the halogen bonds between $[N\cdots I\cdots N]^+$.[116]

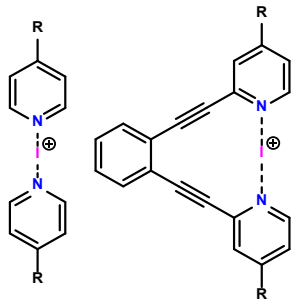

Figure 17. A systematic change in the electron density of the iodine(I) was achieved by variation of the substituents of pyridines (R = H, Me, OMe, NMe_2, F, CF_3, NO_2), which resulted in complexes that possess increasing electron density as follows: $NO_2 < CF_3 < H < F < Me < OMe < NMe_2$.[79]

The NMR spectroscopy in solution[116] and X-ray crystallography in solid state[89] confirms the asymmetric electron density produces asymmetric halogen bonds. The asymmetry of the halogen bond was measured by the change in coordination shift of the halogen bonded nitrogen atoms (Table 1). Thus, the $\Delta\delta^{15}$Ncoord of the nitrogen atoms of the asymmetric systems possessing methyl and trifluoromethyl substituted pyridine, are ~ 10 ppm greater and smaller than those in the systems with two CH_3 or two CF_3 groups. Which tells us about the change in δ^{15}N of the nitrogen atoms of the asymmetric complexes differs due to the formation of different strengths and lengths of N···I bonds as well, along with the distinct electron densities on ligands. The $\Delta\delta^{15}$Ncoords indicate that the iodine(I) in the halogen bonded complex is much more close to the nitrogen of the 4-CH_3 substituted pyridine ring than the less electron-rich, 4-CF_3 substituted pyridine. The computational calculation also confirms these analyses and recently reported X-ray crystallographic studies of the asymmetric bis(pyridine) iodine(I) complexes authenticate these results (Figure 5).[89]

Table 1. The ^{15}N NMR chemical shifts and coordination shifts (ppm) of the ligand, symmetric and asymmetric Iodine(I) complexes.[116]

Structure	R/R′	$\delta^{15}N_{complex}$	$\delta^{15}N_{ligand}$	$\Delta\delta^{15}N_{coord}$
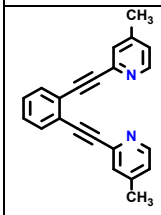	CH_3/CH_3	-170.3	-69.2	-101.1
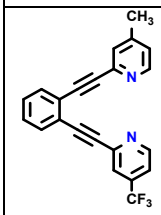	CH_3 CF_3	-183.1 -145.1	-71.8 -53.7	-111.3 -91.4
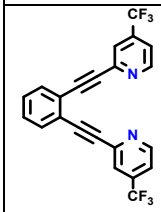	CF_3/CF_3	-156.7	-53.4	-103.3

The backbone and N-N distance play a vital role in the geometry and stability of the bidentate ligand-based halogen bonded complexes.[81] The optimal value for $[N\cdots I\cdots N]^+$ bonds is 4.5 Å, where ligands imposing a N-N bond distance larger than 4.8 Å are anticipated to show asymmetric geometry.[116]

2 RESULT AND DISCUSSION

Aim of the work

The primary aim of this work was to synthesize $[N\cdots X\cdots N]^+$ (X = Ag, I, Br) complexes by using different nucleophilic ligands, like 2-halo- and 2,6-dihalopyridines and analyzing their halogen bond formation behavior. In the second part of the work, a new interaction between halogen(I) ions and Ag(I) ions has been previously published[90], and report the candidate's work in that publication.[90] In addition, $NR_1R_2R_3$ tertiary amines were used to synthesize new chiral $[N\cdots I\cdots N]^+$ complexes to probe halogen bond formation using tertiary amines. The last step of this thesis work was to investigate the silver(I), iodine(I), and bromine(I) complexes of tetra- and hexavalent ligands.

The halogen(I) complexes are most frequently been prepared through the $[N\cdots Ag\cdots N]^+ \rightarrow [N\cdots I\cdots N]^+$ cation exchange reaction. New 2-coordinate and 3-coordinate silver complexes were utilized to further collect knowledge that they undergo the cation exchange with the treatment of the silver complex with elemental iodine, while the now used 4- and 6-coordinate Ag-complexes have not been tested for similar reactions to yield halogen(I) complexes.[86,90,102]

The ^{1}H-NMR spectroscopy and HMBC spectroscopy in solution were the main characteriszation techniques to be used. Mass spectrometry and single-crystal X-ray diffraction studies were done by the collaborators and analyzed by the candidate. The silver(I) complexes of tetra- and hexavalent ligands were studied in different solvents and solvent mixtures.

2.1 Silver(I), iodine(I) and bromine(I) complexes of 2-halo- and 2,6-di-halopyridines

2.1.1 Synthesis of the [N···X···N]⁺ complexes

The halogen(I) complexes are prepared through the $[N\cdots Ag\cdots N]^+ \rightarrow [N\cdots X\cdots N]^+$ cation exchange reaction from the analogous silver(I) complexes, which is ubiquitous for 2-coordinate silver(I) precursors. The 2-coordinate[67,71,82,84,89,91-93,102,117,118] and 3-coordinate [86,90,102] silver complexes are shown to readily to undergo the cation exchange with the treatment of the silver complex with elemental iodine and bromine. The synthesis of the halogen(I) complexes, named here as [**L**-X-**L**]Y (L = ligand, X = I or Br, Y = PF_6^-, TfO^-, BF_4 or Br_3^-, - = ···) proceeds smoothly from the corresponding [**L**-Ag-**L**]Y (Y = PF_6^-, BF_4 or TfO^-) silver complexes of commercially available pyridine derivatives upon treatment with elemental iodine (I_2) or bromine (Br_2) (Scheme 4).[66]

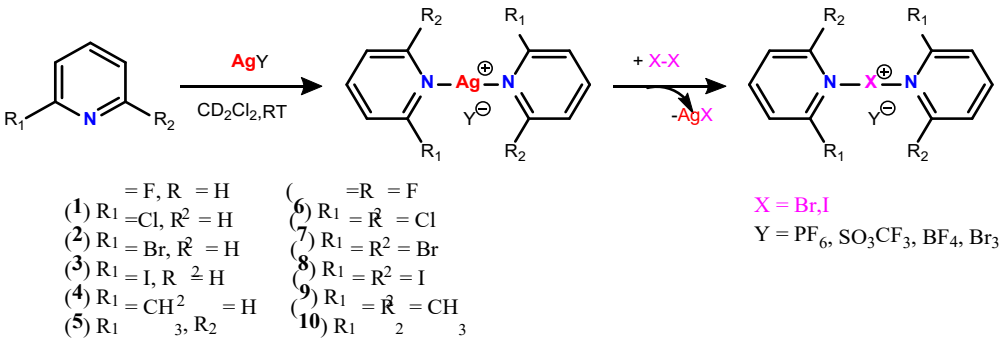

Scheme 4. General synthesis of [**N**–X–**N**]⁺ complexes using mono- and di-substituted pyridines, 2-fluoro-pyridine (**1**), 2-chloropyridine (**2**), 2-bromopyridine (**3**), 2-iodopyridine (**4**), 2-methylpyridine (**5**), 2,6-difluoropyridine (**6**), 2,6-dichloropyridine (**7**), 2,6-dibromopyridine (**8**), 2,6-diiodopyridine (**9**), and 2,6-dimethylpyridine (**10**).

The silver complexes were synthesized by mixing 2.0 eq of halopyridines (**1** - **10**, Scheme 4) with 1.0 eq silver(I) salts ($AgPF_6$, $AgSO_3CF_3$ and $AgBF_4$) in a DCM solvent. To obtain the $[\mathbf{L}\cdots Ag\cdots \mathbf{L}]^+$ silver(I) complexes, solution was stirred for 10 min at room temperature. The conversion from the free ligand to the silver(I) complexes were followed with ^1H NMR spectroscopy by using CD_2Cl_2 solvent. The corresponding $[\mathbf{L}\cdots I\cdots \mathbf{L}]^+$ and $[\mathbf{L}\cdots Br\cdots \mathbf{L}]^+$ halogen(I) complexes were obtained through the $[\mathbf{L}\cdots Ag\cdots \mathbf{L}]^+ \rightarrow [\mathbf{L}\cdots X\cdots \mathbf{L}]^+$ (X = I or Br) cation exchange reaction (Scheme 4) by the addition of 1.1 eq of elemental iodine(I_2) and bromine(Br_2) respectively to a solution of the silver(I) complexes,[66] which concomitantly resulted in the immediate precipitation of AgI. The solution was filtered, and the filtrate transferred into two portions. The bromine (I) and iodine(I) complexes $[\mathbf{L}\cdots X\cdots \mathbf{L}]^+$

(X = I or Br) were not isolated and the first portion was used as such for the ^{1}H and ^{1}H-^{15}N HMBC NMR experiments and second portion were used as such for the crystallization.

2.1.2 NMR studies of the Ag(I), I(I) and Br(I) complexes

The complexation of the ligands (**1** - **10**, Scheme 4) to the silver(I) and iodine(I) complexes were studied with ^{1}H NMR spectroscopy (Figure 18-23) in a non-coordinating CD_2Cl_2 solvent as hexafluorophosphate as the counter ion. The ^{1}H-^{15}N HMBC correlation measurements were done only to ligands **4**, **5** and **9**, their silver(I), iodine(I), bromine(I) complexes and protonated ligands as their trifluoroacetate salts ([**4**H]TFA, [**5**H]TFA and [**9**H]TFA) (Figure 24-38). The ^{1}H NMR analyses of the silver complexes [**L**-Ag-**L**]PF_6 (Scheme 4) for ligand **1**–**5** and **10** indicated conversion from the ligands to the silver(I) complexes and demonstrated clear complexation-induced changes in the chemical shifts for the silver(I) complexes of the 2-halo ligands **1**–**4**, 2-methylpyridine (**5**) and 2,6-dimethylpyridine (**10)** (Figure 18-23). The 2,6-dihalo ligands **6**–**9** showed ambiguous coordination shifts ($D\delta^{1}Hcoord = \delta^{1}Hcomplex - \delta^{1}Hligand$ and $D\delta^{15}Ncoord = \delta^{15}Ncomplex - \delta^{15}Nligand$), yet the 2,6-dimethylpyridine (**10**) showed similar behaviour as **1-5**. The ^{1}H NMR spectra of ligands **1-5** and their silver(I), iodine(I) and bromine(I) complexes, and the protonated ligands **1**H^+, **2**H^+, **3**H^+, **4**H^+, and **5**H^+ are given in figure 18-22.

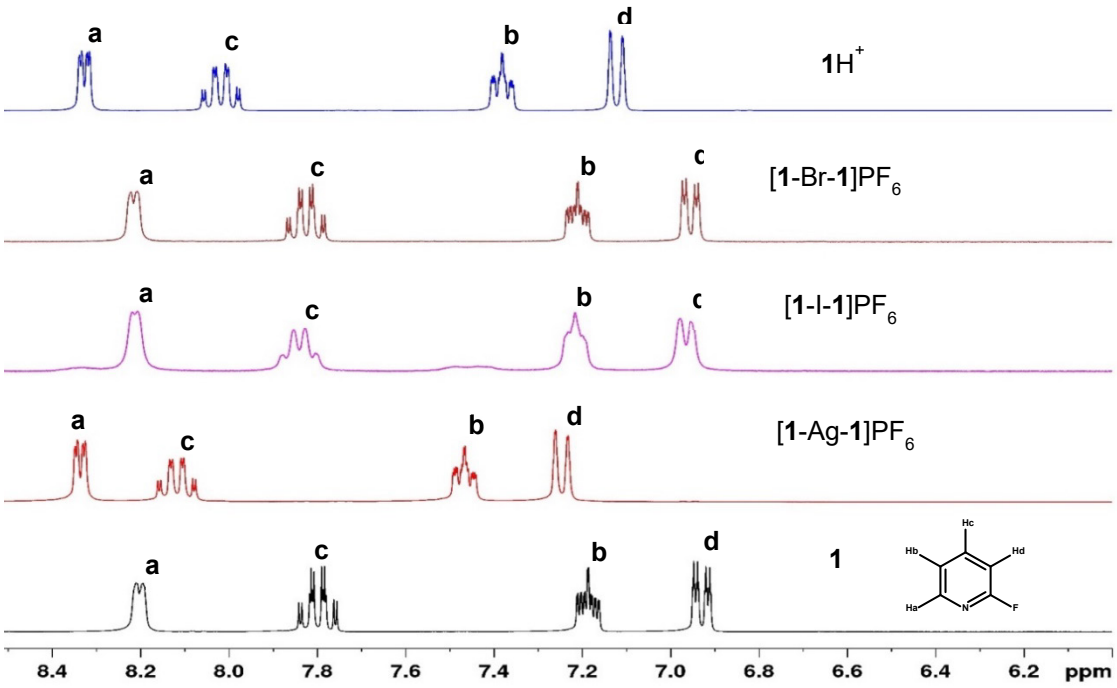

Figure 18. The ^{1}H NMR chemical shifts for **1** (black), [**1**-Ag-**1**]$^{+}$ (red), [**1**-I-**1**]$^{+}$ (pink), [**1**-Br-**1**]$^{+}$ (brown), and **1**H^+ (blue) in CD_2Cl_2 at 300 MHz.

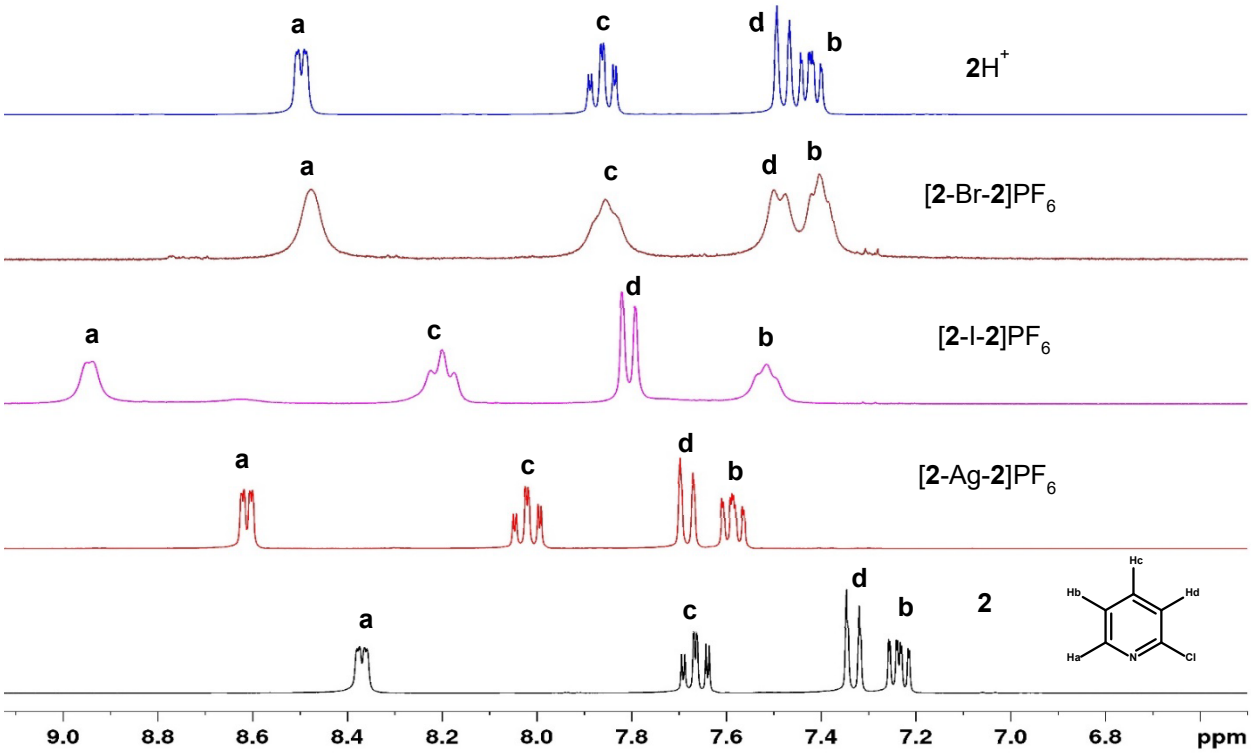

Figure 19. The ^{1}H NMR chemical shifts for **2** (black), [**2**-Ag-**2**]PF_6 (red), [**2**-I-**2**]PF_6 (pink), [**2**-Br-**2**]PF_6 (brown), and **2**H$^+$ (blue) in CD_2Cl_2 at 300 MHz.

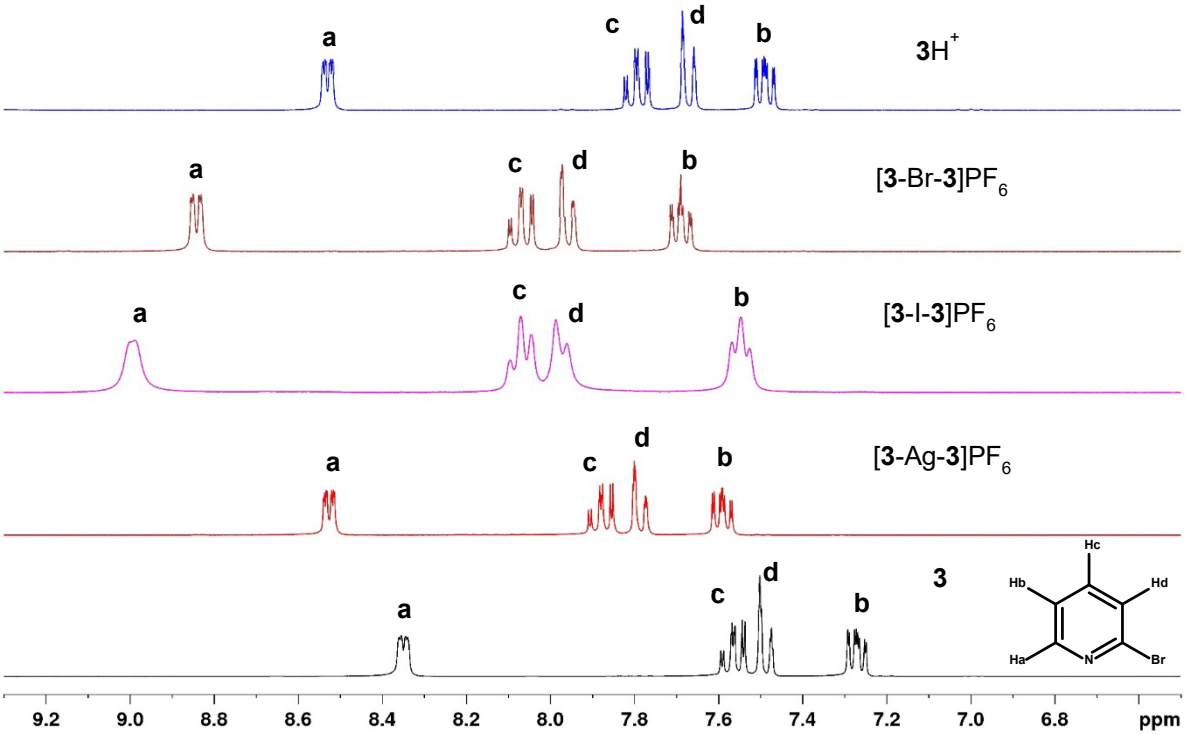

Figure 20. The ^{1}H NMR chemical shifts for **3** (black), [**3**-Ag-**3**]PF_6 (red), [**3**-I-**3**]PF_6 (pink), [**3**-Br-**3**]PF_6 (brown), and **3**H$^+$ (blue) in CD_2Cl_2 at 300 MHz.

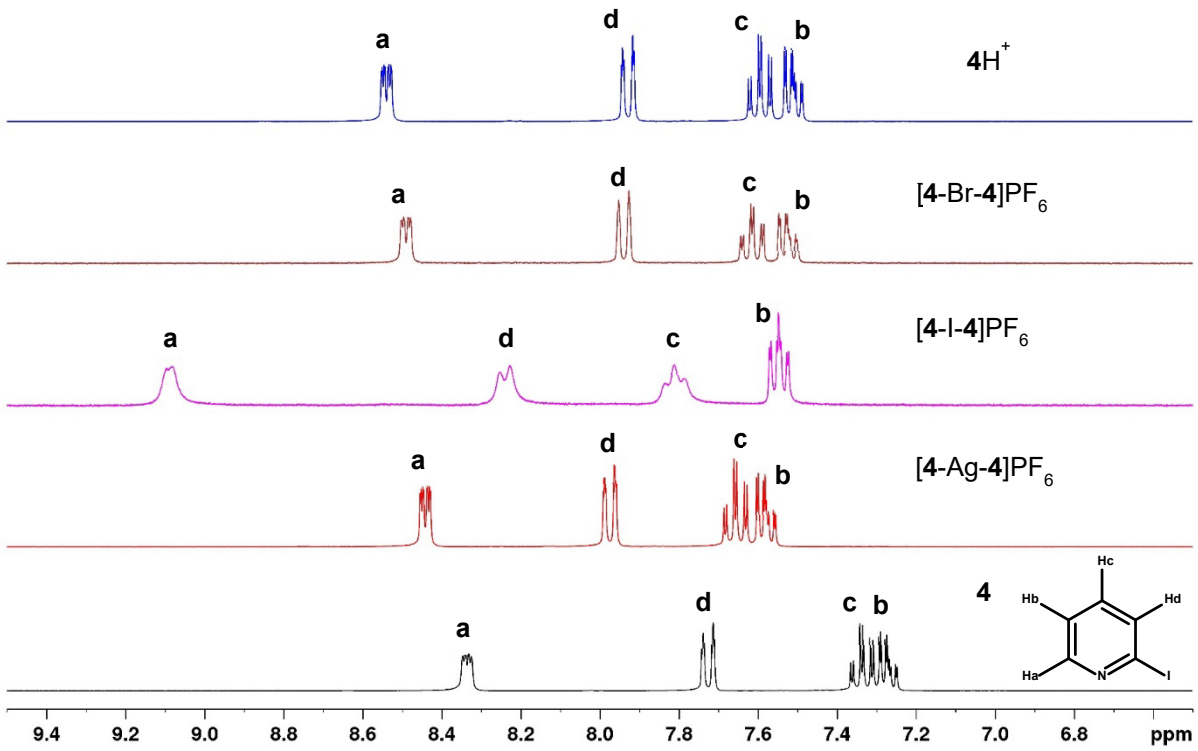

Figure 21. The ^{1}H NMR chemical shifts for **4** (black), [**4**-Ag-**4**]$^+$ (red), [**4**-I-**4**]$^+$ (pink), [**4**-Br-**4**]$^+$ (brown), and **4**H$^+$ (blue) in CD_2Cl_2 at 300 MHz with hexafluorophosphate as counterion.

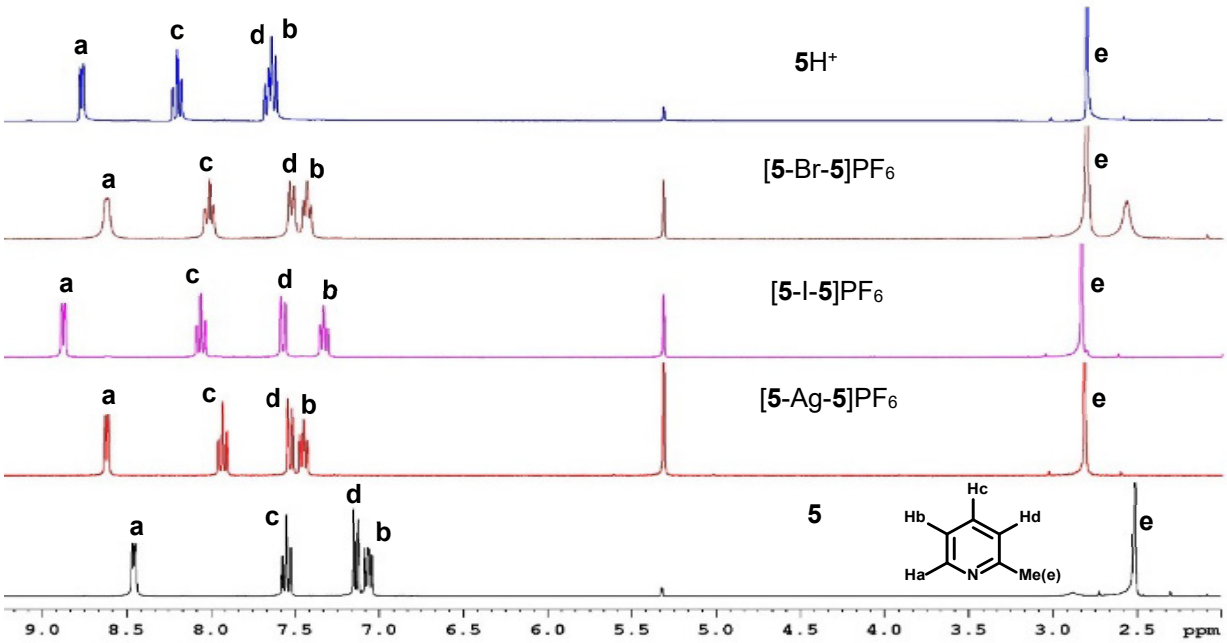

Figure 22. The ^{1}H NMR chemical shifts for **5** (black), [**5**-Ag-**5**]$^+$ (red), [**5**-I-**5**]$^+$ (pink), [**5**-Br-**5**]$^+$ (brown), and **5**H$^+$ (blue) in CD_2Cl_2 at 300 MHz with hexafluorophosphate as counterion.

The ^{1}H NMR coordination shifts from the free ligand to the silver(I) complexes are all down-field (+, less shielded) varying from 0.10 to 0.41 ppm for all silver(I) complexes with very similar trends. For [**4**-Ag-**4**]$^+$ (Figure 21) they are +0.10 (proton a), +0.31 (proton b), +0.32

(proton c) and + 0.24 (proton d) ppm, the corresponding values for [**5**-Ag-**5**]$^+$ (Figure 22) are +0.18, +0.40, +0.39, + 0.41 ppm. The protonated ligands (**1**H$^+$-**10**H$^+$) are frequent side products of the Ag(I) -> I(I)/Br(I) cation exchange reaction and often give very similar ^{1}H NMR spectrum as the corresponding silver(I) complex. [67,71,82,84,89,91-93,102,117,118] Thus the ^{1}H NMR of the protonated ligands were measured under same conditions to distinguish them from each other and from the iodine(I) and bromine(I) complexes. The chemical shift changes from the free ligand for **4**H$^+$ (Figure 21) are +0.20 (a), +0.24 (b), +0.26 (c) and +0.20 (d) ppm, **5**H$^+$ (Figure 22) +0.32 (a), +0.57 (b), +0.66 (c), + 0.53 (d) ppm. Small but definitive differences in the ^{1}H NMR spectra of the silver(I) complexes and protonated ligand allows unambiguous distinction between these two species.

The iodine(I) and bromine(I) complexes of the 2-halo ligands **1**-**4** and 2-methylpyridine (**5**) show a very similar ^{1}H NMR coordination shift trends as the previously published pyridine derivative iodine(I) and bromine(I) complexes.[67,71,82,84,89,91-93,102,117,118] The iodine(I) complexes show larger downfield shifts than the corresponding bromine(I) complexes, varying from 0.01 to 0.75 ppm for the iodine(I) and 0.01 to 0.50 ppm for the bromine(I) complexes of the monohalo ligands (Figure 18-22). For [**4**-I-**4**]$^+$ and [**4**-Br-**4**]$^+$ (Figure 21) the shifts are +0.75 (a), +0.28 (b), +0.47 (c) and + 0.51 (d) and +0.15 (a), +0.25 (b), +0.28 (c) and + 0.21 (d) ppm, respectively. Analogously the corresponding values for [**5**-I-**5**]$^+$ are +0.43, +0.28, +0.52 and +0.45, and for [**5**-Br-**5**]$^+$ +0.18, +0.38, +0.47 and + 0.40 ppm (Figure 22).

The ^{1}H NMR spectra 2,6-dihalo ligands **6**-**9** show completely different, unpresentended, behaviour while the 2,6-dimethylpyridine (**10**) behaves as the previously reported halogen(I) pyridine[67,71,82,84,89,91-93,102,117,118] and 2-halosubstituted pyridine (**1**-**5**) complexes (Figure 18-23). The figure 23 depict an overlay of the aromatic region (8.1-6.6 ppm) of 25 ^{1}H NMR spectra of **L**, [**L**-Ag-**L**]$^+$, [**L**-I-**L**]$^+$, [**L**-Br-**L**]$^+$ and **L**H$^+$ (**L** = **6**, **7**, **8**, **9**, and **10**). The ^{1}H NMR spectra of **10**, [**10**-Ag-**10**]$^+$, [**10**-I-**10**]$^+$, [**10**-Br-**10**]$^+$ and **10**H$^+$ reveals the "expected" downfield coordination shifts upon Ag(I), I(I) and Br(I) complexation.

The 2,6-disubstituted pyridines have only two protons (*a*, a doublet and *b*, a triplet, Figure 23), which in the case of ligand **10** manifest very clear downfield shifts from the free ligand **10**, viz. +0.35 (*a*) and +0.33 (*b*) ([**L**-Ag-**L**]$^+$), +0.28, +0.32 ([**L**-I-**L**]$^+$) , +0.35, +0.37 ([**L**-Br-**L**]$^+$), +0.47, +0.59 (**L**H$^+$) (Figure 23, thick blue spectra). The chemical shifts of the *a* and *b* protons on the free 2,6-dihalo ligands **6**-**9** show a rather peculiar behavior of signal position exchange. For the 2,6-difluoropyridine (**6**, red spectrum, Figure 23) the proton *a* resonates at 6.85 ppm and the *b* at 7.92 ppm with a separation of 1.07 ppm. For 2,6-dichloropyridine (**7**, black spectrum) the *a* signal moves down-field and the *b* up-field, approaching each other with separation

of 0.35 ppm. In 2,6-dibromopyridine the same movement continues so that the *a* and *b* signal overlap at 7.46 ppm (**8**, magenta spectrum). Finally, the signal movement reaches its peak with 2,6-diiodopyridine (**9**, green spectrum, Figure 23), where the *a* and *b* signals exchange position so that *a* resonates at 7.71 and *b* at 6.97 ppm (with separation of 0.74 ppm).

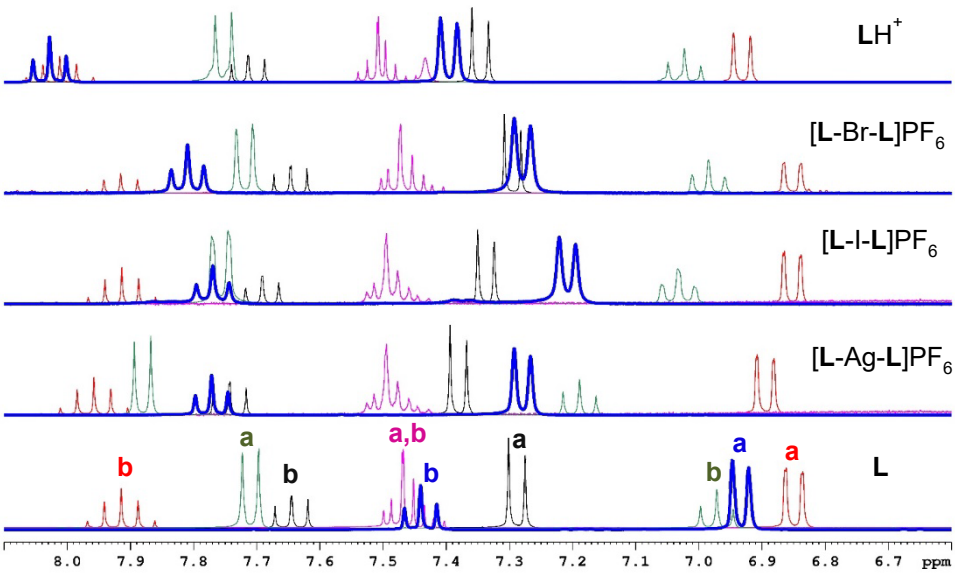

Figure 23. The ^{1}H NMR chemical shifts for **L**, [**L**-Ag-**L**]$^+$, [**L**-I-**L**]$^+$, [**L**-Br-**L**]$^+$ and **L**H$^+$ from bottom to top, **6** (red), **7** (black), **8** (magenta), **9** (green) and **10** (blue) in CD_2Cl_2 at 300 MHz with hexafluorophosphate as counterion.

The coordination shifts in the ^{1}H NMR spectra of the 2,6-dihalo ligand Ag(I), I(I) and Br(I) complexes [**L**-Ag-**L**]$^+$, [**L**-I-**L**]$^+$, [**L**-Br-**L**]$^+$ (**L** = **6**, **7**, **8** and **9)** are markedly different from the previously published corresponding unsubstituted,[82] para-,[83] and 2-halo (**1-4** above) pyridine complexes. Most remarkably the 2,6-dibromopyridine **8** seems to be surprisingly persistent to the coordinative interaction with the silver(I) and halogen(I) cations, the overlapping *a* and *b* signals are hardly shifting at all, only the [**8**-Ag-**8**]$^+$ and **8**H$^+$ manifest a slight (< 0.05 ppm) downfield shift (Figure 23, magenta spectra) and the [**8**-I-**8**]$^+$ and [**8**-Br-**8**]$^+$, ^{1}H NMR spectra being virtually identical with the free ligand **8**. Within experimental error such a small coordination shift will render the identification of each species of **8** ambiguous. The 2,6-difluoro- (**6**, red spectra) and 2,6-dichloropyridine (**7**, black spectra) behave similarly, both showing very small (< 0.1 ppm) downfield coordination shift upon silver(I) complexation, while the iodine(I) and bromine(I) complexation indices no shift for **6**, and only very minute for the **7**. Slightly larger, yet analoguous coordination shifts as for **6** and **7** occur for the 2,6-diiodopyridine (**9**, green spectra) observable downfield shifts from the free ligand **9**, viz. +0.19 (*a*) and +0.22 (*b*) ([**9**-Ag-**9**]$^+$), +0.05, +0.08 ([**9**-I-**9**]$^+$), +0.02, +0.03 ([**9**-Br-**9**]$^+$), +0.03, +0.03

(**L**H$^+$) (Figure 20, green spectra). The most feasible explanation about the ambiguous ^{1}H NMR behaviour of the 2,6-dihalopyridines and their complexes is the very weak nucleophilicity/nucleophilic character of the ligands that renders the formation of the I$^+$ and Br$^+$ complexes during the [**N**-Ag-**N**]$^+$ → [**N**-X-**N**]$^+$ (X = I or Br). The trifluoroacatic acid (TFA) is not strong enough to protonate the ligands **6-9** failing to form the pyridinium cation. Only the Ag$^+$ cation is able to coordinate to the less nucleophilic nitrogen of **6-9**. This is also supported by the fact that no solid state I$^+$, Br$^+$ and H$^+$ complexes could be isolated, yet all except the 2,6-difluoropyridine (**6**) afforded the Ag$^+$ complex X-ray structure (see below XRD part).

The above observation about the different complexation behaviour of the 2-halo- *vs.* 2,6-dihalopyridiens was verified by the use of ^{1}H-^{15}N HMBC NMR spectroscopy, which has proven to be much more powerful tool for the study of the complex formation compared to the small or negligible coordination shifts observed in the ^{1}H NMR spectra (Figure 23). The chemical shift range of the ^{15}N nuclei is much wider (5-150 ppm) and the direct coordination of the nitrogen nuclei to the cation in the complexation makes ^{15}N NMR, especially the ^{1}H-^{15}N HMBC NMR a convenient technique for monitoring the cation exchange reaction.[61,66,68,83,84,91,119]

For successful complex formation large and consistent ^{15}N NMR coordination shift (Dδ^{15}Ncoord) to lower frequencies (downfield) are observed for the pyridinic N-atom upon silver(I) and halogen(I) complex due to the coordination of silver(I) to the N-atoms of the pyridine ([**N**-Ag-**N**]$^+$) bonds and subsequent [**N**-X-**N**]$^+$ three-center four-electron (3c-4e) bond formation. The unsubstituted uncomplexed pyridine has a ^{15}N chemical shift (δ^{15}N) of -67.7ppm[89] (^{1}H-^{15}N HMBC NMR, *d*-DCM), increasing nucleophility by an electron-releasing ethyl substituent in the para-position results in δ^{15}N of -75.6 ppm under the same conditions.[89] Very strongly electron-withdrawing CF_3-substituent at the 4-position of pyridine have been shown to cause a shift by +17ppm to -51 ppm[83] reflecting the diminished nucleophilic character of the N-atom.

The δ^{15}N of ligands 2-iodo- (**4**) and 2-methylpyridine (**5**), and 2,6-diiodopyridine (**9**) and their complexes were measured in CD_2Cl_2 using ^{1}H-^{15}N HMBC experiments (Figure 24-38). Formation of the [**N**-I-**N**]$^+$ halogen bond has been observed to result in downfield Dδ^{15}Ncoord ≥ 100 ppm.[59] The N-atom in 2-iodopyridine **4** is less nucleophilic with δ^{15}N of -50ppm due to the iodine atom at the 2-position(Figure 24). In 2-methylpyridine **5** the situation is reversed leading to a δ^{15}N of -68 ppm, very similar to that of pyridine (Figure 29). A dramatic change in δ^{15}N occurs with the 2,6-diiodopyridine **9**, where the nucleophilicity is lowered even more giving δ^{15}N of -36.8 ppm

(Figure 34). Both **4** and **5** manifest the expected Dδ^{15}Ncoord behavior upon the Ag(I), I(I) and Br(I) complexation and increases in the order of Ag(I) < Br(I) < I(I) (Figure 25-27 for **4** and Figure 30-32 for ligand **5**). The Dδ^{15}Ncoord for **4** are smaller, -104, -57 and -32 ppm for I^+, Br^+ and Ag^+ complexes, respectively, while for **5** they are -99, -75 and -58ppm. The most drastic difference between **4** and **5** occurs in their H^+ complexes ppm (Figure 28 and 33). For **5**H^+ it has the expected value, -164ppm, very close to that if the I^+ complex[59], while **4**H^+ δ^{15}N is -74ppm, with only Dδ^{15}Ncoord of -24ppm., a very unusually small Dδ^{15}Ncoord value. This very likely is a result of formation of a "normal" R-COOH···N hydrogen bond which has much lesser effect on the chemical environment of the N-atoms. However, the nucleophilicity of **4** is not reduced so much that the I^+ and Br^+ complexes would not form, this is evidenced by the isolation the I^+ and Br^+ complexes in the solid state (see XRD below).

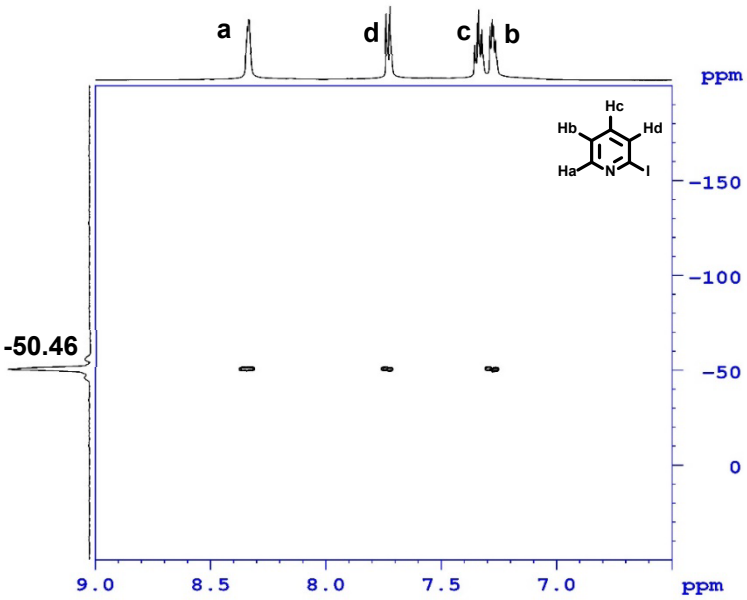

Figure 24. ^{1}H,^{15}N HMBC spectra of **4** in CD_2Cl_2.

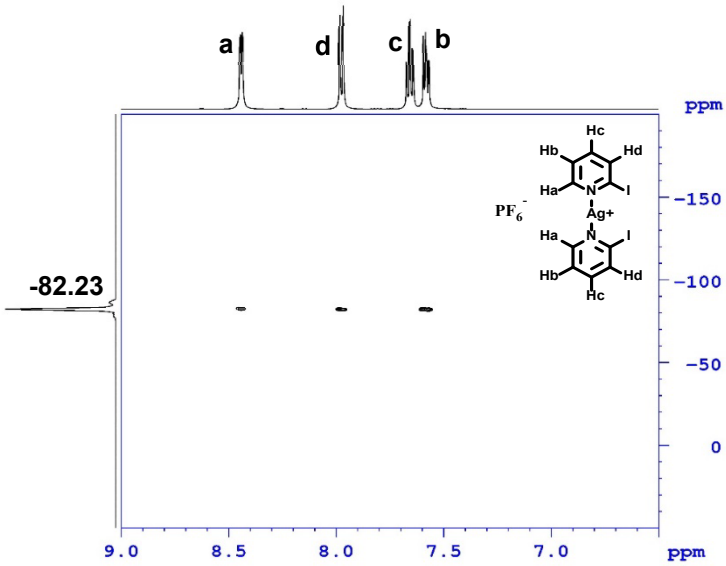

Figure 25. $^{1}H,^{15}N$ HMBC spectra of [**4**-Ag-**4**]PF_6 in CD_2Cl_2.

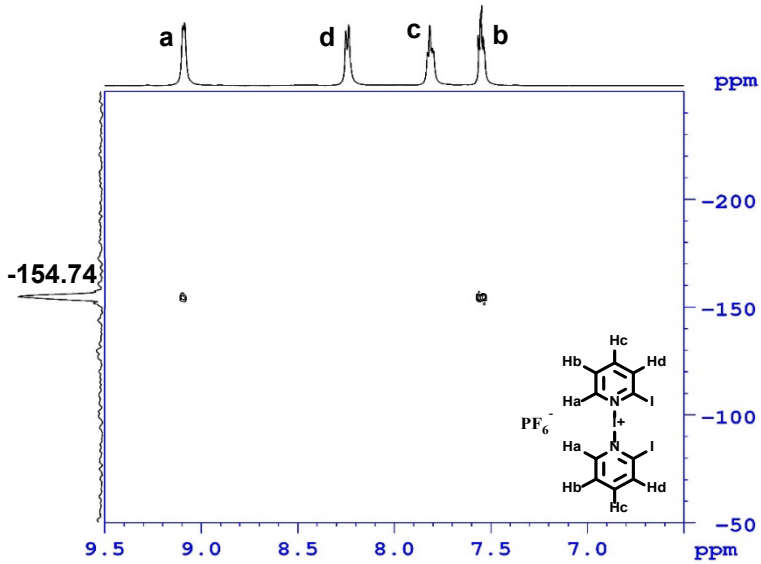

Figure 26. $^{1}H,^{15}N$ HMBC spectra of [**4**-I-**4**]PF_6 in CD_2Cl_2.

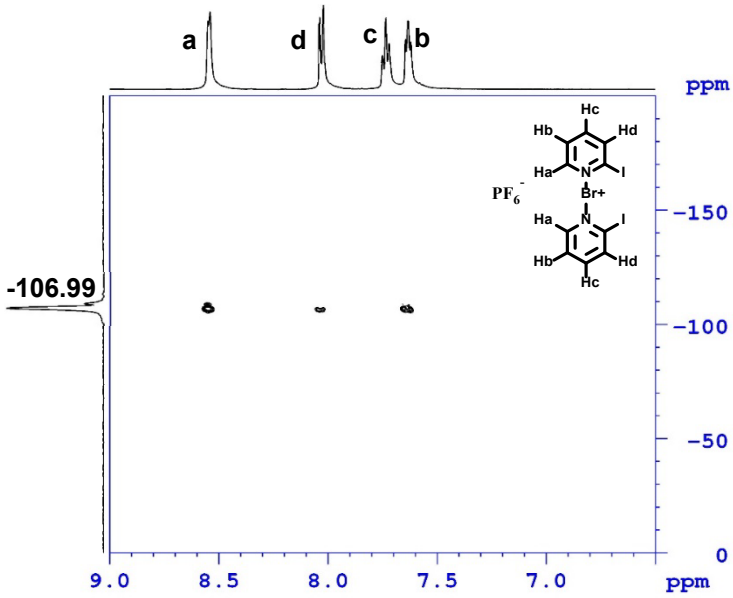

Figure 27. $^{1}H,^{15}N$ HMBC spectra of [**4**-Br-**4**]PF_6 in CD_2Cl_2.

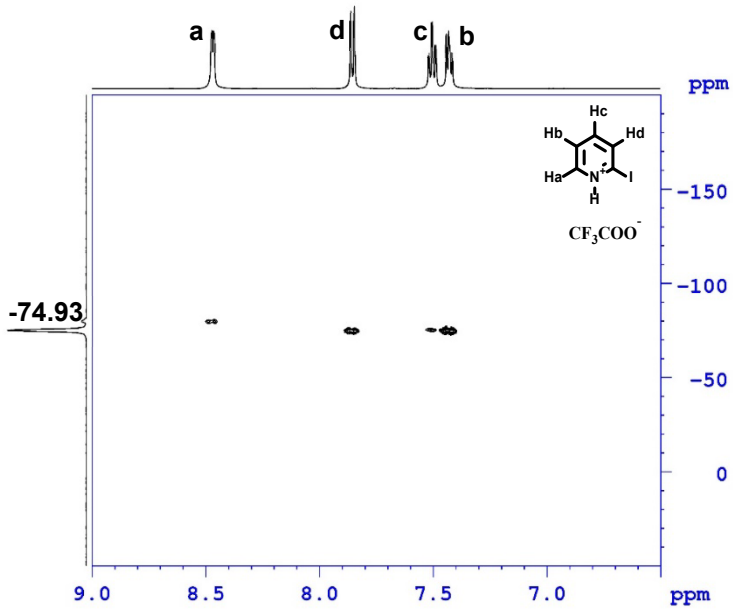

Figure 28. $^{1}H,^{15}N$ HMBC spectra of [**4**H] CF_3COO in CD_2Cl_2.

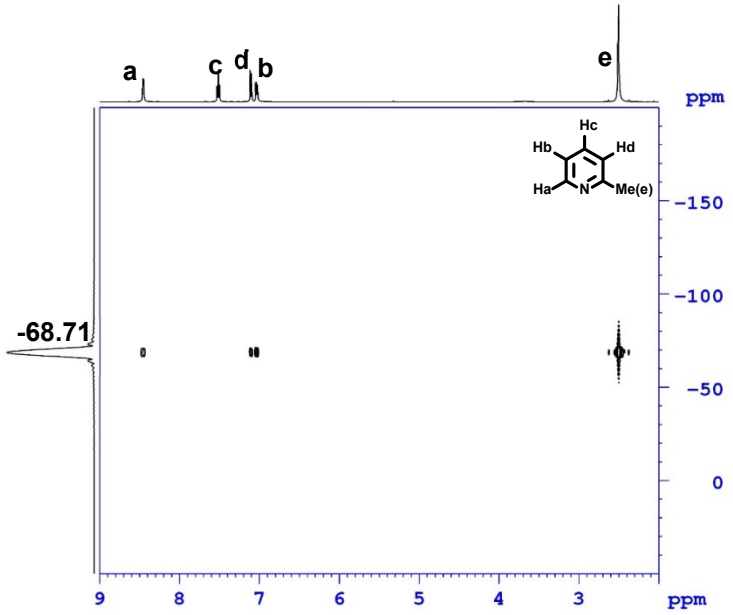

Figure 29. $^{1}H,^{15}N$ HMBC spectra of **5** in CD_2Cl_2.

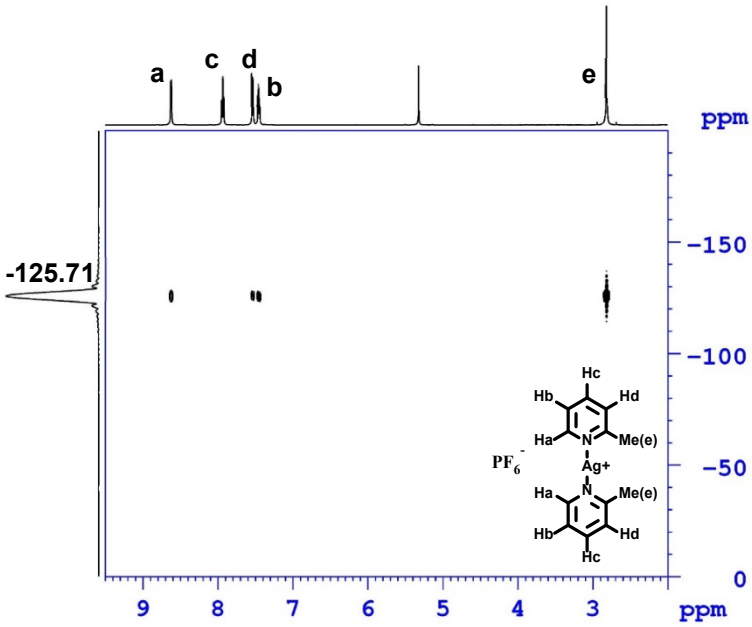

Figure 30. $^{1}H,^{15}N$ HMBC spectra of [**5**-Ag-**5**]PF_6 in CD_2Cl_2.

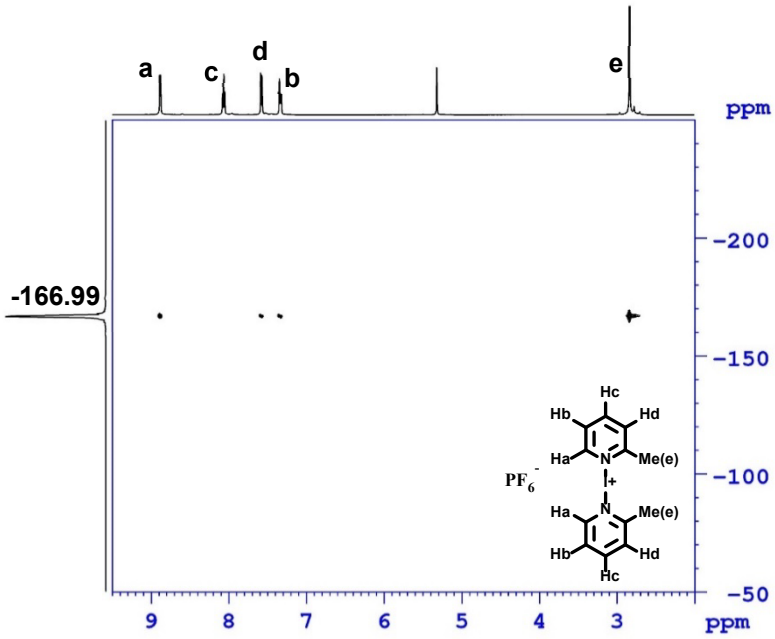

Figure 31. $^{1}H,^{15}N$ HMBC spectra of [**5**-I-**5**]PF_6 in CD_2Cl_2.

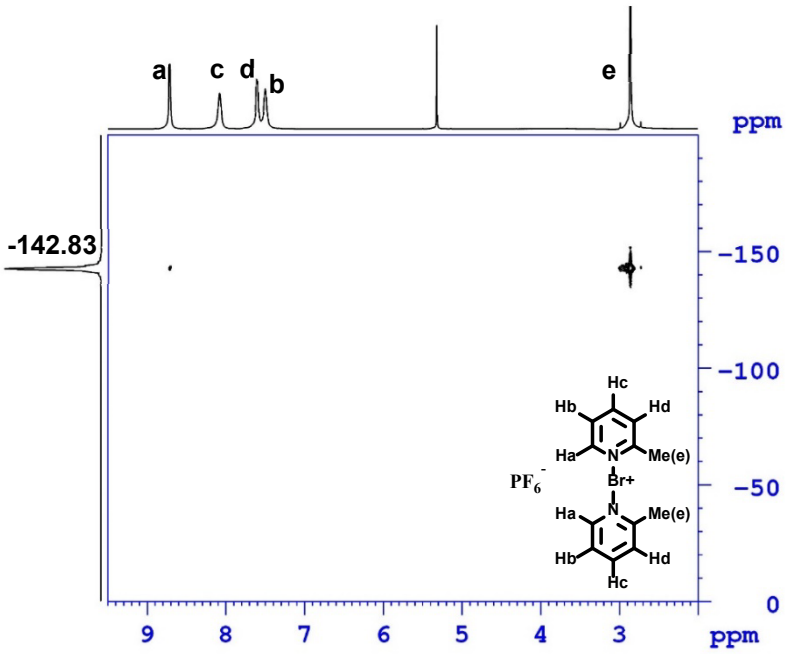

Figure 32. $^{1}H,^{15}N$ HMBC spectra of [**5**-Br-**5**]PF_6 in CD_2Cl_2.

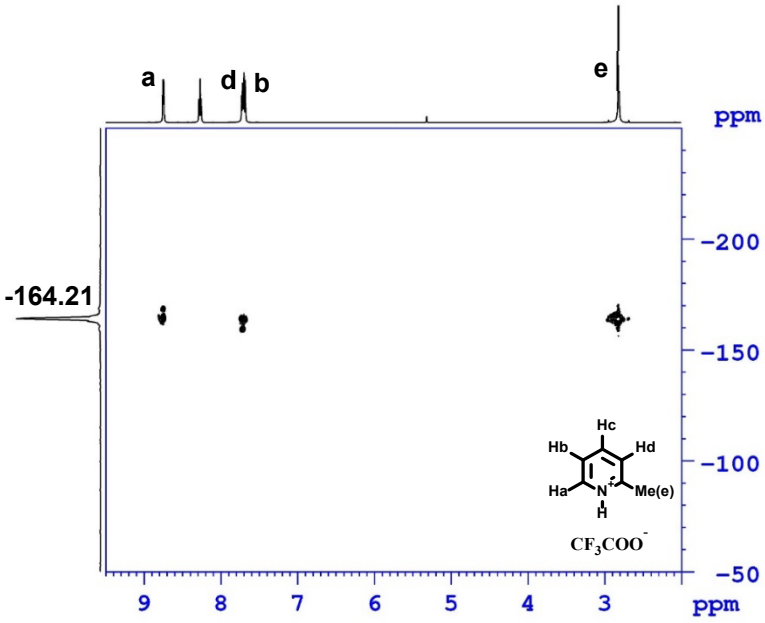

Figure 33. $^{1}H,^{15}N$ HMBC spectra of [**5**H] CF_3COO in CD_2Cl_2.

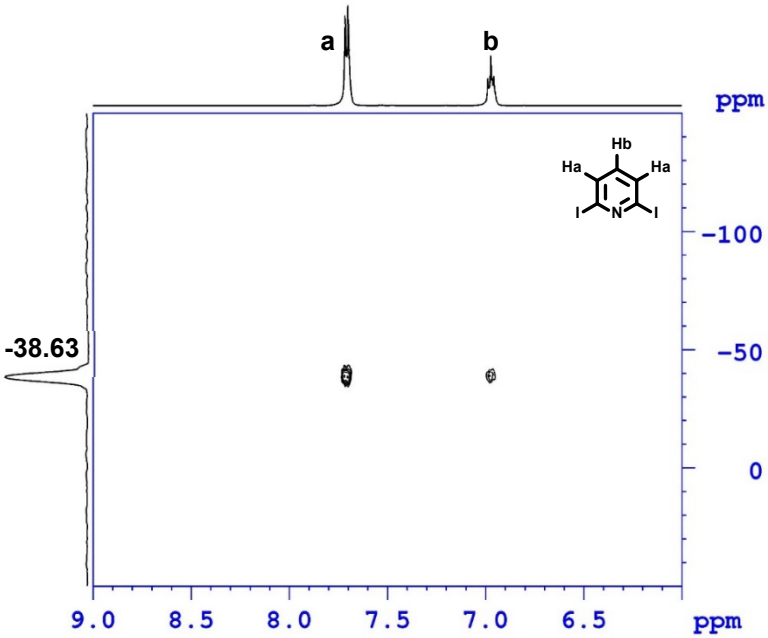

Figure 34. $^{1}H,^{15}N$ HMBC spectra of **9** in CD_2Cl_2.

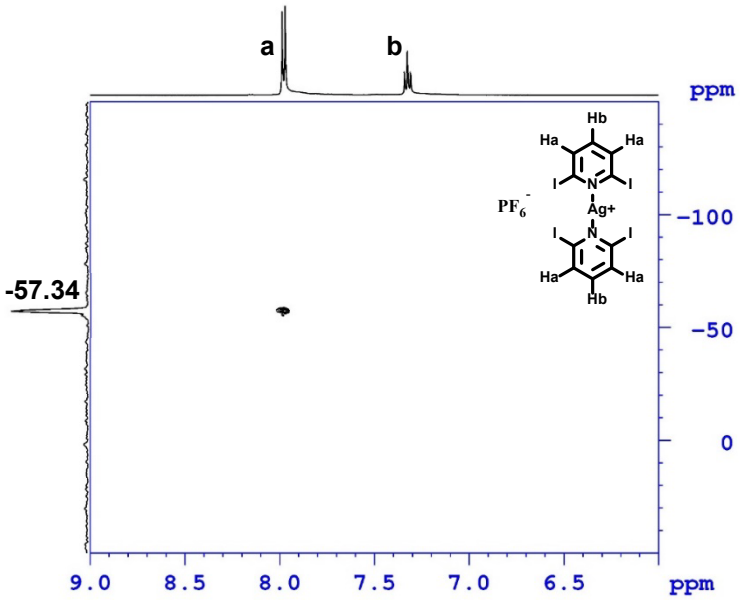

Figure 35. $^{1}H,^{15}N$ HMBC spectra of [**9**-Ag- **9**]PF_6 in CD_2Cl_2.

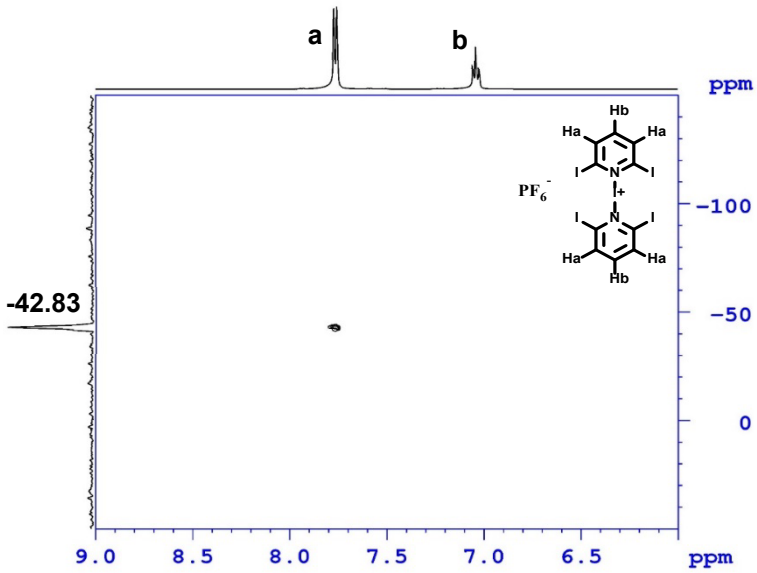

Figure 36. $^{1}H,^{15}N$ HMBC spectra of [**9**-I-**9**]PF_6 in CD_2Cl_2.

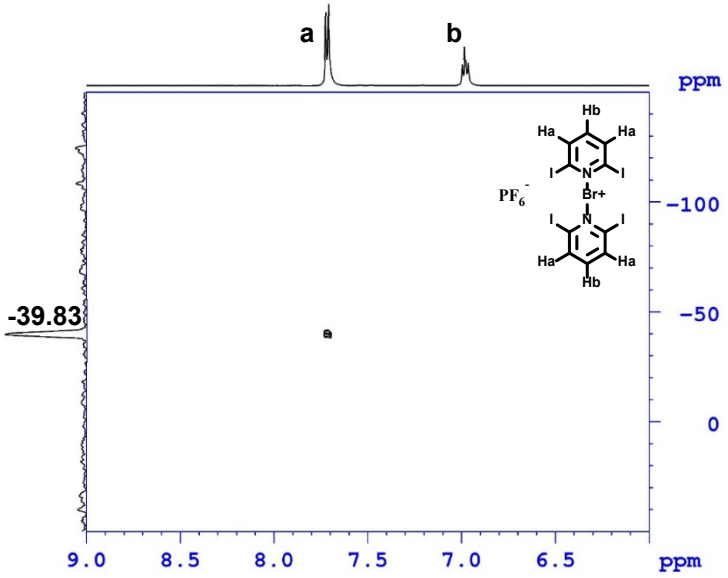

Figure 37. $^{1}H,^{15}N$ HMBC spectra of [**9**-Br-**9**]PF_6 in CD_2Cl_2.

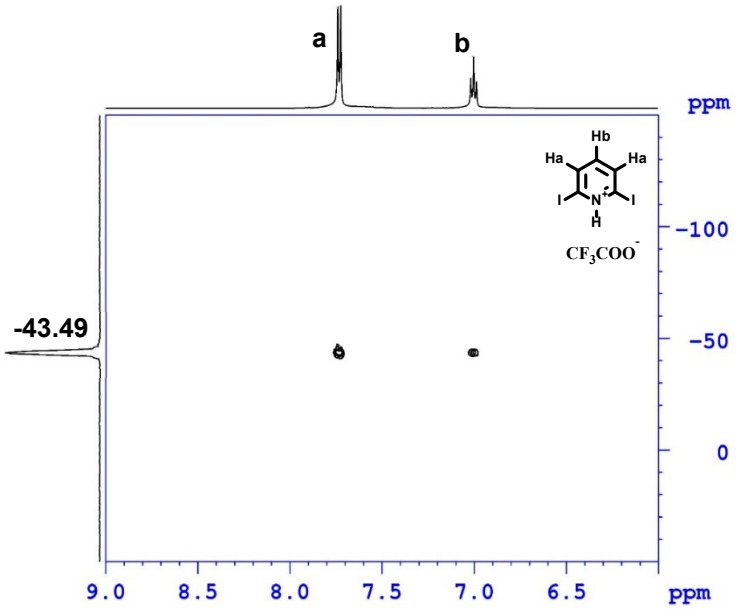

Figure 38. $^{1}H,^{15}N$ HMBC spectra of [**9**H] CF_3COO in CD_2Cl_2.

The ^{1}H NMR of the 2,6-dihalopyridines evidenced that the nucleophilicity is reduced so much that the I^+ and Br^+ complexes are no longer stable. The ^{1}H-^{15}N HMBC NMR of **9** is very clear evidence in this situation (Figure 34-38). The $D\delta^{15}$ of **9** is -39ppm (Figure 34), a much lower value that for **4** (-50 ppm) and **5** (-68 ppm) indicating severely reduced nucleophilicity. Due to the stronger complexation ability of the Ag^+ cation, the complex is formed in solution and also verified by X-ray structure (see XRD part below)

in the solid state. The $D\delta^{15}$Ncoord of -19ppm for the [**9**-Ag-**9**]$^+$ complex is small, yet in relatively terms (49%) the same as for [**4**-Ag-**4**]$^+$ (39%) and [**5**-Ag-**5**]$^+$ (46%). The **9**H$^+$ δ^{15}N of -44ppm, with $D\delta^{15}$Ncoord of only -5ppm, indicates a really weak "normal" hydrogen bonding between TFA and **9**. The $D\delta^{15}$ values -43ppm ("[**9**-I-**9**]$^+$") and -40ppm ("[**9**-Br-**9**]$^+$") for complexes of **9** after the [N-Ag-N]$^+$ → [N-X-N]$^+$ (X = I or Br) cation exchange reaction shows that the I$^+$ and Br$^+$ complexes are not formed, and a mixture of free **9** and **9**H$^+$ explains the observed δ^{15}N values. This is also supported by the fact that no I$^+$ and Br$^+$ complexes from **6-9** could be isolated in the solid state.

2.1.3 Crystallographic studies of the Ag(I), I(I) and Br(I) complexes

Single crystal was grown by the slow evaporation process (see details section 3.2). This synthesis procedure successfully leads us to obtain twenty-six crystal structures (Table 2, see crystal data in appendix 1-26) for the present study, and their structural bond parameters are given in Table 3.

Table 2. Crystallization experiments data for the Ag$^+$, I$^+$, Br$^+$ and the H$^+$ complexes.

Ligand	Ag(I) complex	I(I) complex	Br(I) complex	H$^+$ complex
1	-	[**1**-I-**1**]PF_6	[**1**-Br-**1**]PF_6	-
2	[**2**-Ag-**2**]PF_6 [**2**-Ag-**2**]OTf	-	-	[**2**-H-**2**]PF_6
3	[**3**-Ag-**3**]PF_6	[**3**-I-**3**]PF_6	[**3**-Br-**3**]PF_6	-
4	[**4**-Ag-**4**]PF_6	[**4**-I-**4**]PF_6	[**4**-Br-**4**]PF_6	-
5	[**5**-Ag-**5**]PF_6	[**5**-I-**5**]PF_6	[**5**-Br-**5**]PF_6 [**5**-Br-**5**]Br_3	-
6	-	-	-	-
7	[**7**-Ag-**7**]OTf	-	-	-
8	[**8**-Ag-**8**]OTf [**8**-Ag-**8**]BF_4	-	-	-
9	[**9**-Ag-**9**]PF_6 [**9**-Ag-**9**]OTf	-	-	-
10	[**10**-Ag**10**]PF_6 [**10**-Ag**10**]OTf	[**10**-I-**10**]PF_6	[**10**-Br-**10**]PF_6 [**10**-Br-**10**]OTf [**10**-Br-**10**]]Br_3	-

Table 3. Crystallographic parameters for $[N\cdots Ag\cdots N]^+$ and $[N\cdots X\cdots N]^+$ complexes.

	(N···Ag/X···N) Å	**(N···N) Å**	**(N···Ag/X···N) deg**	**R_{XB}**	**Torsion angle (planes)**
[**1**-I-**1**]PF_6	2.263(2) *2	4.549(3)	175.69(8)	0.641	37.91(8)
[**1**-Br-**1**]PF_6	2.098(4)*2	4.195(6)	176.3(2)	0.617	38.69(2)
[**2**-Ag-**2**]PF_6	2.150(4)*2	4.300(6)	178.0(2)		0.00
[**2**-Ag-**2**]OTf	2.210(3), 2.224(3)	4.350(5)	157.7(1)		60.8(1)
[**3**-Ag-**3**]PF_6	2.151(4)*2	4.299(6)	176.0(1)		33.5(1)
[**3**-I-**3**]PF_6	2.265(3)*2	4.530(6)	180.0(2)	0.642	0.00
[**3**-I-**3**]PF_6	2.265(3), 2.288(4)	4.551(5)	176.9(1)	0.642, (X−B=2.26) 0.648, (X−B=2.29)	52.8(1)
[**3**-Br-**3**]PF_6	2.097(3)*2	4.192(5)	177.3(2)	0.617	0.00
[**4**-Ag-**4**]PF_6	2.162(3), 2.161(3)	4.321(5)	176.5(1)		45.1(1)
[**4**-I-**4**]PF_6	2.261(2), 2.297(2)	4.557(4)	176.99(9)	0.640, (X−B=2.26) 0.651, (X−B=2.30)	9.54(9)
[**4**-Br-**4**]PF_6	2.113(5), 2.094(5)	4.204(8)	175.6(2)	0.621, (X−B=2.11) 0.616, (X−B=2.09)	18.34(2)
[**4**-Br-**4**]PF_6	2.081(3)*2	4.144(8)	169.5(2)	0.621	7.73(2)
[**5**-Ag-**5**]PF_6	2.129(3), 2.124(3)	4.250(5)	178.2(1)		5.4(1)
[**5**-I-**5**]PF_6	2.262(8)*2	4.52(1)	180	0.641	0.00
[**5**-Br-**5**]PF_6	2.095(2)*2	4.189(3)	180	0.616	0.00
[**5**-Br-**5**]Br_3	2.095(5)*2	4.190(8)	180	0.616	0.00
[**7**-Ag-**7**]OTf	2.210(3), 2.217(3)	4.422(5)	174.7(1)		41.4(1)
[**8**-Ag-**8**]OTf	2.223(4), 2.212(4)	4.426(6)	171.4(1)		45.6(1)
[**8**-Ag-**8**]BF_4	2.170(3)*2	4.340(4)	179.0(2)		42.6(2)
[**9**-Ag-**9**]OTf	2.247(7), 2.246(7)	4.47(2)	171.2(3)		46.71(3)
[**9**-Ag-**9**]PF_6	2.207(5), 2.218(5)	4.423	176.2(2)		43.40
[**10**-Ag-**10**]PF_6	2.139(3)*2	4.277(4)	178.8(1)		51.9(1)
[**10**-Ag-**10**]OTf	2.153(2), 2.152(2)	4.297(3)	173.6(6)		10.94(6)
[**10**-I-**10**]PF_6	2.29(1)*2	4.59(2)	180.0(6)	0.649	0.14(6)
[**10**-Br-**10**]PF_6	2.120(4)*2	4.240(7)	180.0(2)	0.623	0.00
[**10**-Br-**10**]OTf	2.08(1), 2.17(1)	4.25(2)	178.3(4)	0.612, (X−B=2.08) 0.639, (X−B=2.17)	16.91(1)
[**10**-Br-**10**]Br_3	2.121(4)*2	4.241(6)	180	0.624	0.00

The N-Ag, Ag-O, and N-N bond lengths, and angles around the linear and T-shape silver(I) are comparable to those observed in related silver(I) complexes. The 2:1 ligand: I^+/Br^+ complexes are typical for 3-*centered*-4-*electron* complexes formed between *n*-donor halopyridines and accepting p_z-orbitals of halogen(I) ion. As shown in Table 3, for I^+/ Br^+-complexes the central cation ion lies on a crystallographic inversion center the N···X···N bond angles are essentially 180°, otherwise, with an exception for [**4**-Br-**4**]PF_6 the overall N···X···N bond angles are more linear [175.69(8)–180°] when compared to Ag^+-complexes. Considering the high directional nature of p_z-orbital of the halogen(I) ion, small deviations from linearity for bond angles are probably caused by close packing of the ion-pair units. Iodine cation is larger than Ag^+ and Br^+, consequently, the N-N decreases as the atom size decreases, I^+ (4.51 - 4.59 Å) > Ag^+(4.25 - 4.48 Å) > Br^+ (4.14 - 4.25 Å). The two pyridine rings across the N···X···N motifs are not coplanar, the interplanar angles between two pyridine rings, defined as θ, are larger in Ag^+ - complexes (0 - 64.0°) and reduced for I^+- (0 - 52.1°) and Br^+- complexes (0 - 38.3°). The N-I bond distances in [**1**-I-**1**]PF_6 - [**5**-I-**5**]PF_6 are longer only by ~0.012 Å compared to unsubstituted pyridine complex, [**Py**···I···**Py**]$^+$ PF_6^-, regardless of the 2-*ortho* substituent type. The N–I bonds of [**10**-I-**10**]PF_6, where two electron-donating methyl groups installed at C2- and C6-positions, does not differ substantially (0.04 Å) either relative to the [**Py**···I···**Py**]$^+$ PF_6^-. In [**1**-I-**1**]PF_6 and [**4**-I-**4**]PF_6 a *cis*- disposition of 2-substituents was observed (Figure 39 and 42, respectively), while for [**3**-I-**3**]PF_6 and [**5**-I-**5**]PF_6 the substituents are in *trans*-position (Figure 41 and 43, respectively).

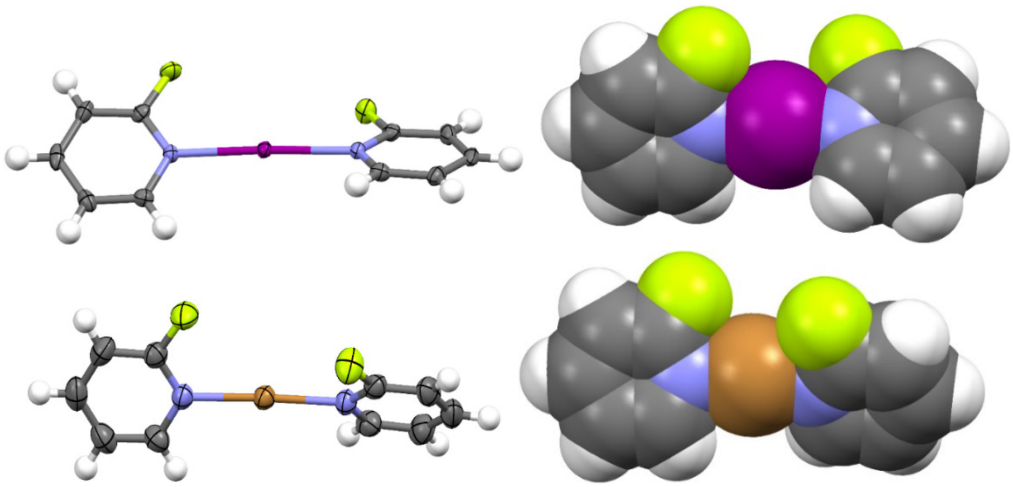

Figure 39. The structure of [**1**-I-**1**]PF_6(top) and [**1**-Br-**1**]PF_6(bottom). Anions and solvent molecules omitted for clarity.

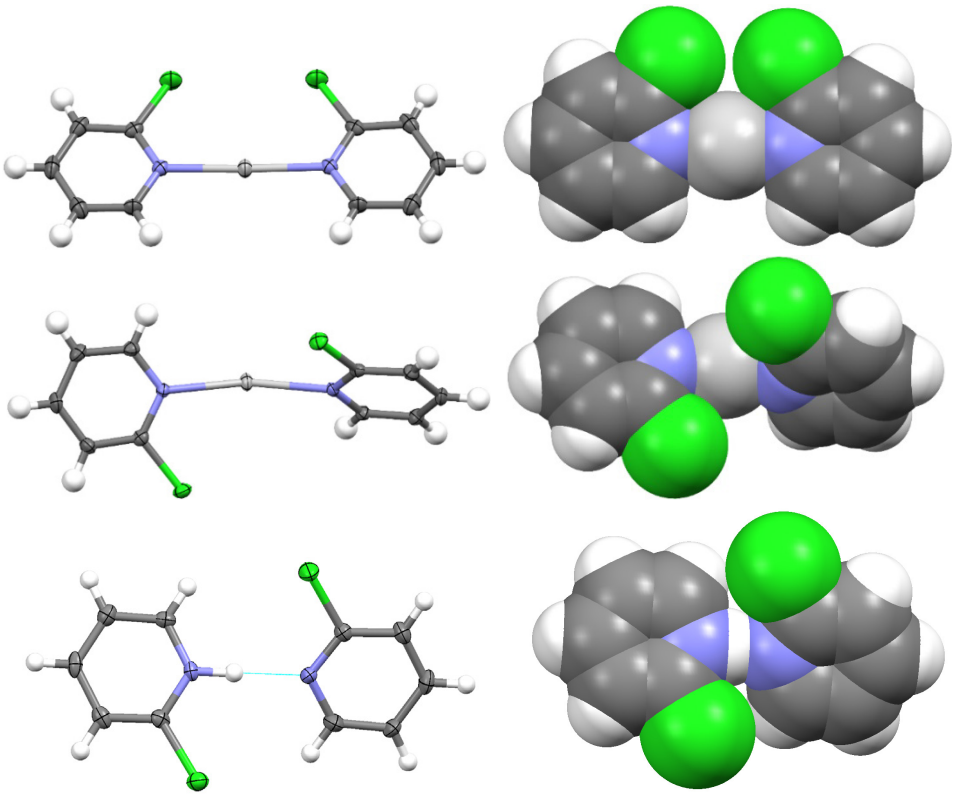

Figure 40. The structure of [**2**-Ag-**2**]PF_6(top), [**2**-Ag-**2**]OTf (middle) and [**2**-H-**2**]PF_6(bottom). Anions and solvent molecules omitted for clarity.

Comparison of [**Py**···Br···**Py**]$^+$Y$^-$ with structures, [**1**-Br-**1**]PF_6 - [**5**-Br-**5**]PF_6, including complexes of **10**, highlights the N-Br bonds lengthened maximum by 0.025Å(Table 3). In solid-state crystals, considering the N-X bond distances, the N-I^+/Br^+ bond shortening is entirely based on the overlap efficiency of N-atom lone-pair and p_z-orbital and the role halogen and their electronic effects on halogen(I) ion formation is passive.

In [**3**-I-**3**]PF_6 and [**4**-Br-**4**]PF_6 two types of crystal structure were observed from the same sample, one with the crystallographic inversion centre and other with two different N-Ag bond length (Table 3). The N-N bond length is longer in case of [**4**-I-**4**]PF_6 compared to [**3**-I-**3**]PF_6 and [**5**-I-**5**]PF_6, due to which [**4**-I-**4**]PF_6 prefer cis position. However [**3**-I-**3**]PF_6 and [**5**-I-**5**]PF_6 form single-crystal where 2-substituents are in *trans* position to avoid steric hindrance.

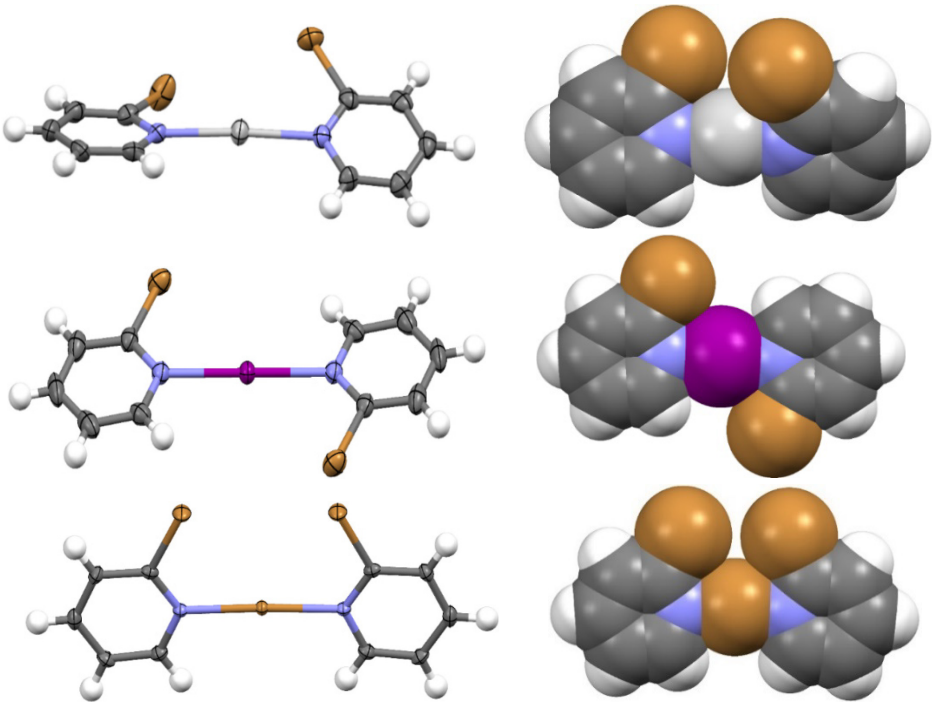

Figure 41. The structure of [**3**-Ag-**3**]PF_6(top), [**3**-I-**3**]PF_6 (middle) and [**3**-Br-**3**]PF_6(bottom). Anions and solvent molecules omitted for clarity.

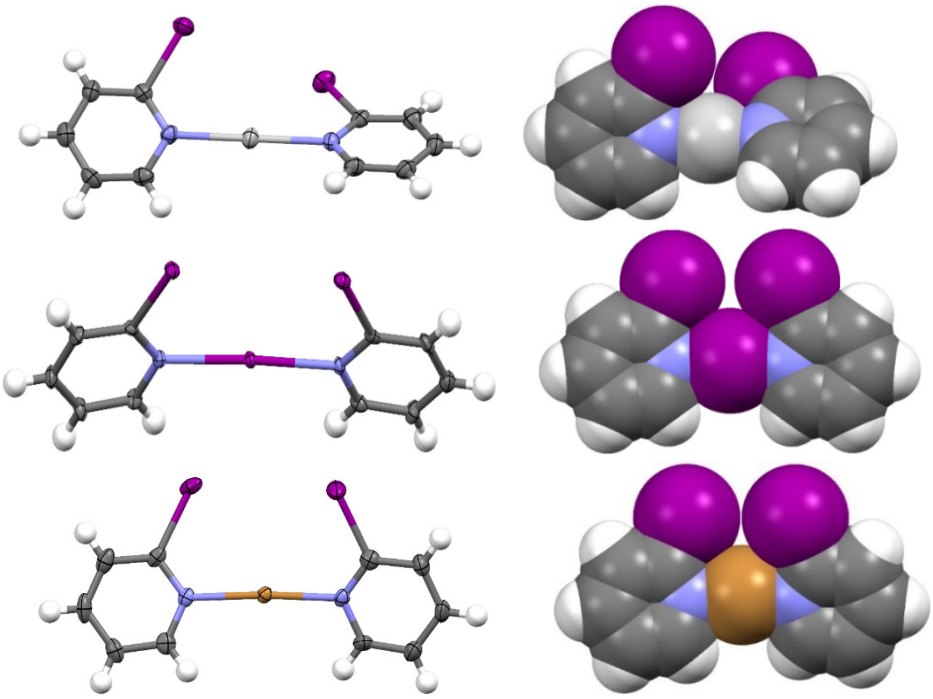

Figure 42. The structure of [**4**-Ag-**4**]PF_6(top), [**4**-I-**4**]PF_6 (middle) and [**4**-Br-**4**]PF_6(bottom). Anions and solvent molecules omitted for clarity.

In [**3**-Br-**3**]PF_6 and [**4**-Br-**4**]PF_6 a cis position of 2-substituents was observed, while for [**5**-Br-**5**]PF_6 the substituents occupied trans-position to stabilise the bulky methyl group.

The 2-substituted pyridine rings across the N···X···N motifs are planar in case of [**3**-I-**3**]PF_6, [**3**-Br-**3**]PF_6, [**5**-I-**5**]PF_6 and [**5**-Br-**5**]PF_6. Silver complexes of **3** and **4** are less planer compared to [**5**-Ag-**5**]PF_6, this non-planarity is attributed when the empty orbitals of silver interact with 2-substituted bromine and iodine in [**3**-Ag-**3**]PF_6 and [**4**-Ag-**4**]PF_6 respectively.

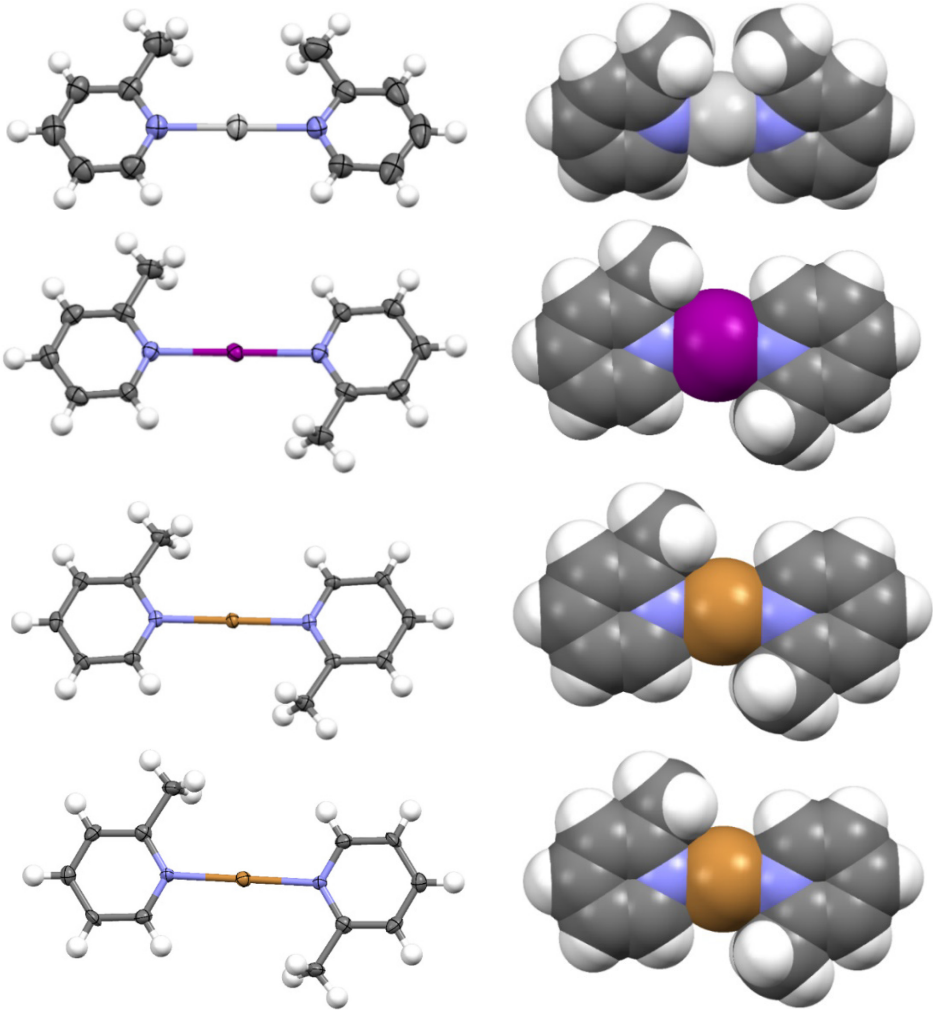

Figure 43. The structure of [**5**-Ag-**5**]PF_6(top), [**5**-I-**5**]PF_6 (second from top), [**5**-Br-**5**]PF_6(second from bottom) and [**5**-Br-**5**]Br_3(bottom). Anions and solvent molecules omitted for clarity.

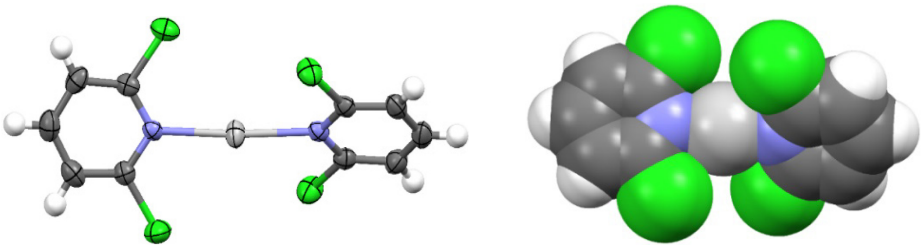

Figure 44. The structure of [**7**-Ag-**7**]OTf. Anions and solvent molecules omitted for clarity.

The [**7**-Ag-**7**]OTf and [**8**-Ag-**8**]OTf complexes are less planner compare to [**8**-Ag-**8**]BF_4 with N···Ag···N bond angle 174.7(1), 171.4(1) and 179.0(2) respectively (Table 3, Figure 44, 45). The [**8**-Ag-**8**]BF_4 complex shows center of symmetry with same N-Ag bond length. Silver complexes of **7** and **8** with OTf^- counter ion are less planar, and this non-planarity is due to the interaction between the empty orbitals of silver metal and counter anion.

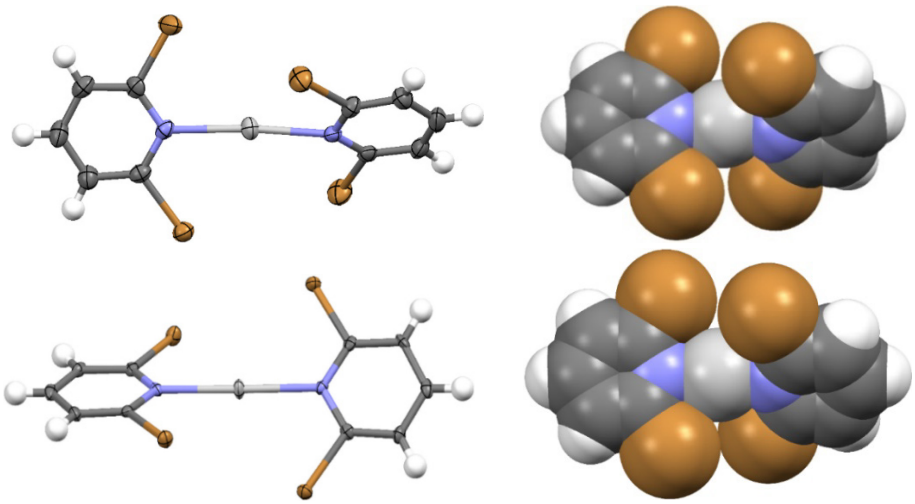

Figure 45. The structure of [**8**-Ag-**8**]OTf(top) and [**8**-Ag-**8**]BF_4(bottom). Anions and solvent molecules omitted for clarity.

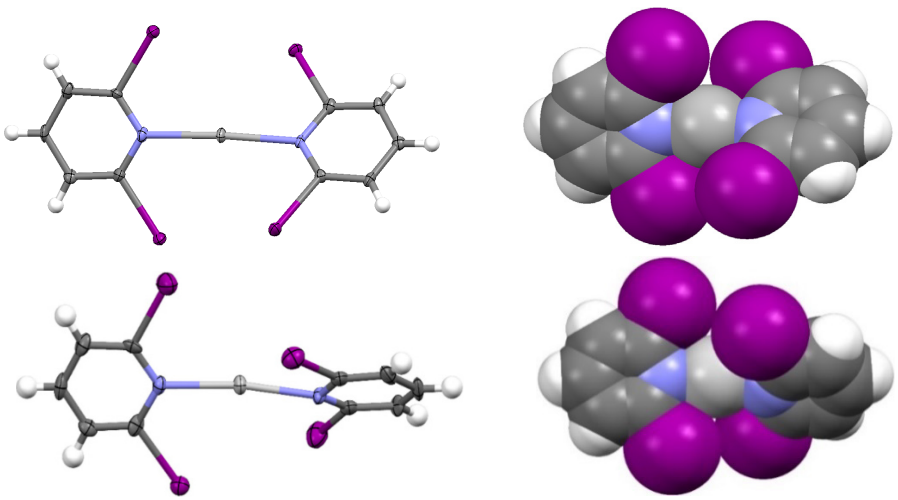

Figure 46. The structure of [**9**-Ag-**9**]PF_6(top) and [**9**-Ag-**9**]OTf (bottom). Anions and solvent molecules omitted for clarity.

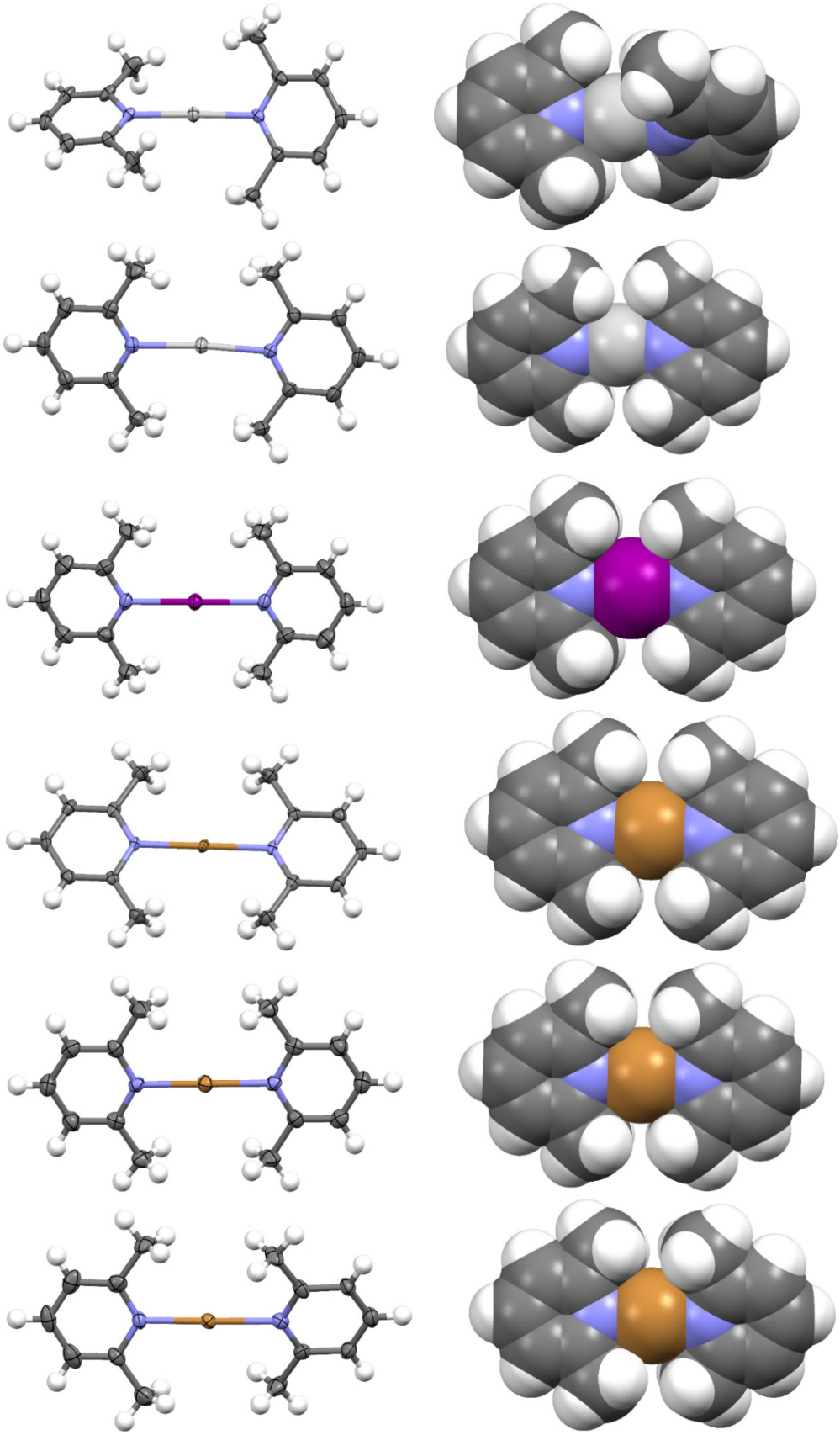

Figure 47. The structure of [**10**-Ag-**10**]PF_6(top), [**10**-Ag-**10**]OTf (second from top), [**10**-I-**10**]PF_6(third from top), [**10**-Br-**10**]PF_6(third from bottom), [**10**-Br-**10**]Br_3(second from bottom) and [**10**-Br-**10**]OTf(bottom). Anions and solvent molecules omitted for clarity.

In ligand **9** two crystal structure of silver complexes, [**9**-Ag-**9**]PF_6 and [**9**-Ag-**9**]OTf were observed with N···Ag···N bond angle 176.2(2) and 171.2(3) respectively(Table 3, Figure 46). In [**9**-Ag-**9**]OTf complex, counter anion interact with empty orbital of silver and make complex crystal less liner. The 2,6-dimethyl substituted pyridine rings across the N···X···N motifs are symmetric in case of [**10**-Ag-**10**]PF_6, [**10**-I-**10**]PF_6, [**10**-Br-**10**]PF_6 and [**10**-Br-**5**]Br_3(Figure 47). However in [**10**-Ag-**10**]OTf and [**10**-Br-**10**]OTf counter anion interact with silver and disturb the linearity of complex. The [**10**-I-**10**]PF_6 complex have largest N-N bond distance in all observed crystal structure for **1-10** (Table 3).

As a summary of the NMR and solid state studies only the 2-halo-, 2-methyl and 2,6-dimethylpyridine behave as previously reported halogen(I) pyridine complexes[67,71,82,84,89,91-93,102,117,118] manifesting unambiguous downfield coordination shifts in the order Ag(I) < Br(I) < I(I) upon complexation in ^{1}H NMR spectra and which is supported by crystal studies. The 2,6-dihalopyridines **6-9**, due to their insufficient nucleophilicity, and contrary to the Ag^+ cation, do not form I^+, Br^+ and H^+ complexes in solution or in the solid state.

2.2 Silver and iodonium complexes for solid state NII's

It has been established that halogen-halogen bonding occurs when electrophilic halogens interact with atoms that are nucleophilic, yet perhaps the most intriguing example would be the three-centre four-electron bond (3c-4e) between the two nitrogens and an iodine atom in Barluenga's reagent $[py\cdots I\cdots py]^+$ (a halogen(I) ion). A new interaction between halogen(I) ions and Ag(I) ions has been reported, providing a new aspect to halogen-bonded complexes, allowing for stable or active halogen(I) ions in a new way, allowing them to be used as new, active, or selective reagents. This nucleophilic iodonium interaction (NII) occurs between molecules containing a nucleophilic iodine(I) center and a silver(I) center.[85] The nucleophilic center functions as the nucleophile for an electrophilic Ag^+ metal center of a 4- or 2-coordinate complex. The $[I(mtz)_2]PF_6$*$[Ag(bpy)_2]PF_6$ complex, which exhibits the unprecedented $I^+\cdots Ag^+$ interaction, hereafter referred to as I*Ag, is obtained straightforwardly via the combination of silver(I) and iodine(I) complexes in a 1:1 ratio in CH_2Cl_2, followed by slow evaporation (Scheme 5).

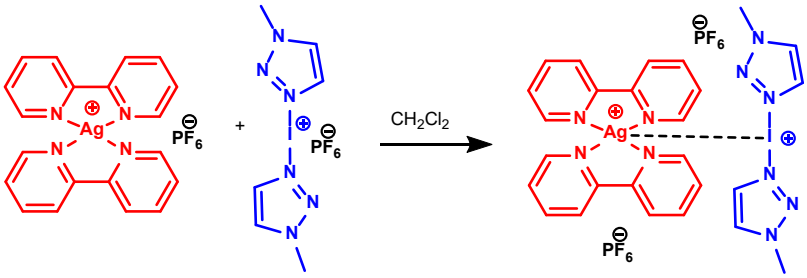

Scheme 5. Synthesis of $[I(mtz)_2]PF_6$*$[Ag(bpy)_2]PF_6$ complex.

2.2.1 Synthesis of [bis(1-methyl-1H-1,2,3-triazole) iodonium hexafluorophosphate

The addition of 1-methyl-1*H*-1,2,3-triazole (**11**, mtz) and $AgPF_6$ in a 2:1 ratio in CH_2Cl_2 yields the linear silver complex $[Ag(mtz)_2]PF_6$ ([**11**-Ag-**11**]PF_6), which, after addition of elemental I_2, affords the corresponding linear iodonium complex $[I(mtz)_2]PF_6$, ([**11**-I-**11**]PF_6) via the selective $[\mathbf{N}\cdots Ag\cdots \mathbf{N}]^+ \rightarrow [\mathbf{N}\cdots I\cdots \mathbf{N}]^+$ cation-exchange.[1,120-126]

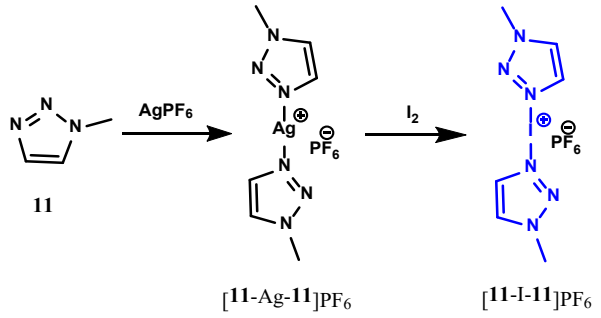

Scheme 6. Synthesis of Complex [**11**-Ag-**11**]PF_6 and [**11**-I-**11**]PF_6.

To a solution of 1-methyl-1*H*-1,2,3-triazole (**11**) (8.2 mg, 0.099 mmol, 2.0 eq) in 0.5 mL of CD_2Cl_2 was added silver hexafluorophosphate (12.4 mg, 0.049 mmol, 1.0 eq). The mixture in an NMR tube was stirred for 10 mins to give a silver complex [bis(1-methyl-1*H*-1,2,3-triazole) silver] hexafluorophosphate [**11**-Ag-**11**]PF_6 (Figure 48).

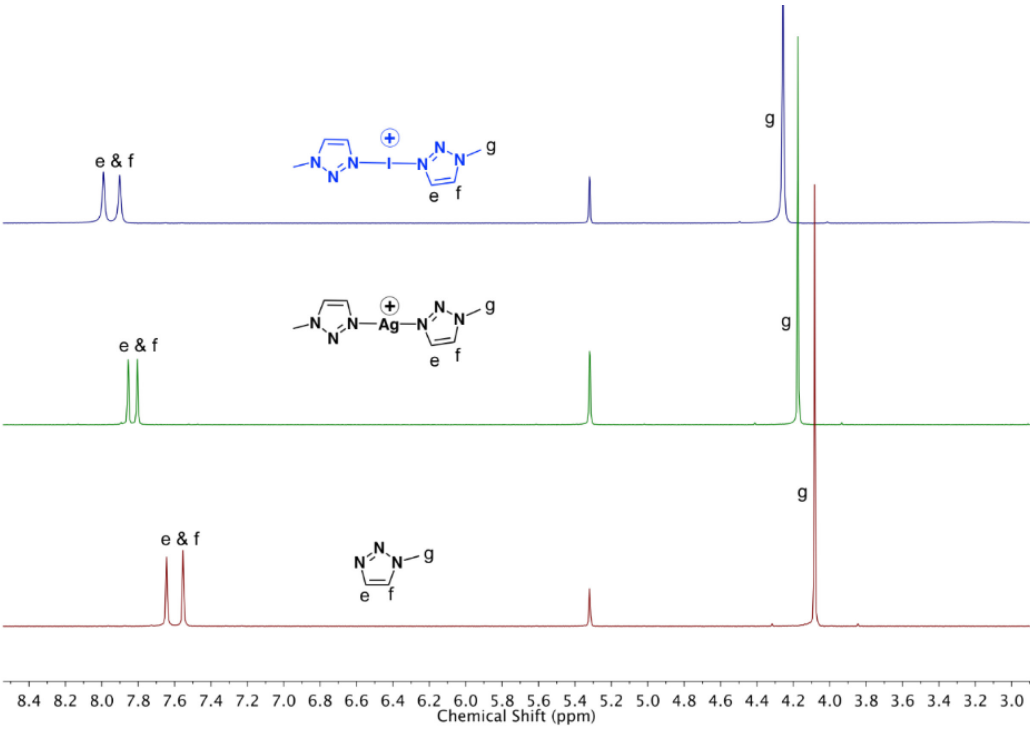

Figure 48. ^{1}H NMR spectra in CD_2Cl_2 at 303 K of compounds **11** (red), [**11**-Ag-**11**]PF_6 (green), and [**11**-I-**11**]PF_6 (blue).

To the solution of [bis(1-methyl-1*H*-1,2,3-triazole) silver] hexafluorophosphate [**11**-Ag-**11**]PF_6, the elementary I_2 (12.5 mg, 0.049 mmol, 1.0 eq) was added. The NMR tube was centrifuged for 5 mins, an iodonium complex [bis(1-methyl-1*H*-1,2,3-triazole) iodonium] hexafluorophosphate [**11**-I-**11**]PF_6 was obtained.

The ^{1}H NMR spectra of ligand **11**, silver complex [**11**-Ag-**11**]PF_6, and iodonium complex [**11**-I-**11**]PF_6 demonstrated significant complexation-induced shifts (Figures 48). The addition of $AgPF_6$ into ligand **11** in a CD_2Cl_2 solution led to a noticeable downfield shift of the ligand proton signals of **11**, confirming the formation of the silver complex [**11**-Ag-**11**]PF_6. A further downfield chemical shift was noticed for the silver complex [**11**-Ag-**11**]PF_6 after the addition of I_2. The ^{1}H-^{15}N HMBC measurements (Figures 49-51) of **11**, [**11**-Ag-**11**]PF_6, and [**11**-I-**11**]PF_6 were also performed, in which the nitrogen nuclei showed large changes in their chemical shifts after addition to the $AgPF_6$, and more so upon the subsequent addition of I_2, which confirms the formation of the silver and iodonium complexes in solution.

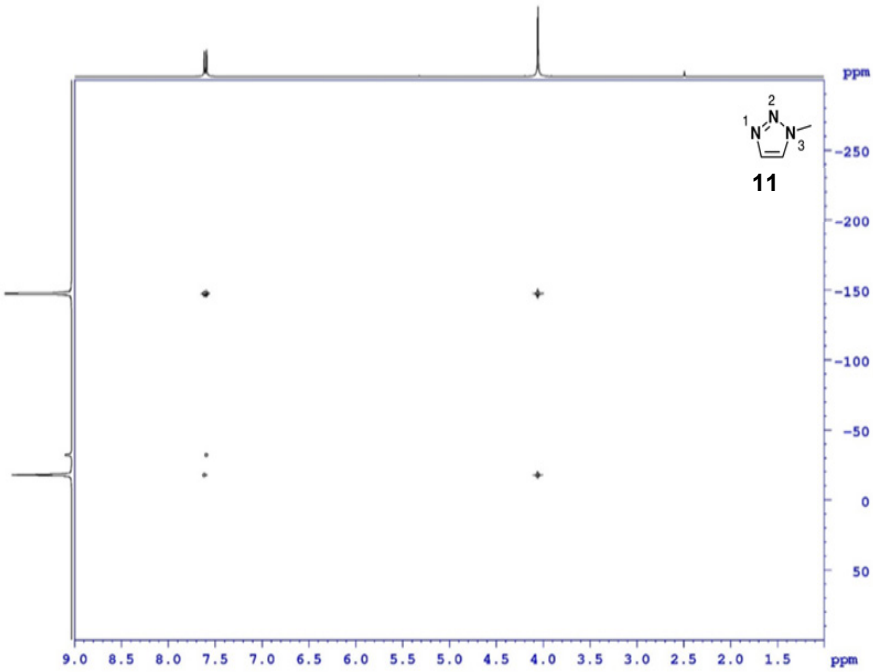

Figure 49. ^{1}H-^{15}N-HMBC spectra in CD_2Cl_2 at 303 K of compound **11**. δ (^{15}N) = -146.26 (N_3), -31.07 (N_1), -16.74 (N_2) ppm.

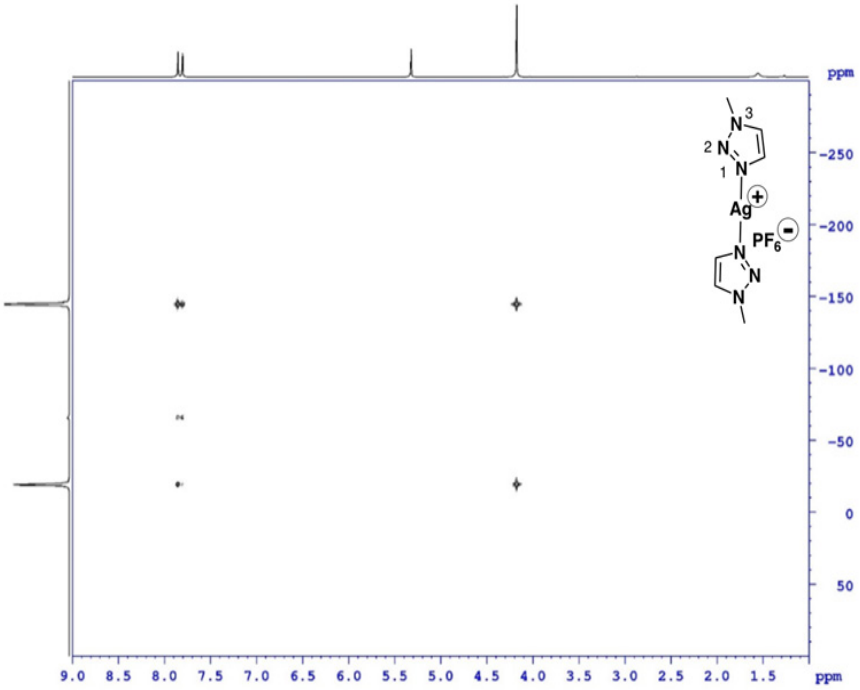

Figure 50. ^{1}H-^{15}N-HMBC spectra in CD_2Cl_2 at 303 K of compound [**11**-Ag-**11**]PF_6. δ (^{15}N) = -144.50 (N_3), -65.44 (N_1), -19.06(N_2) ppm.

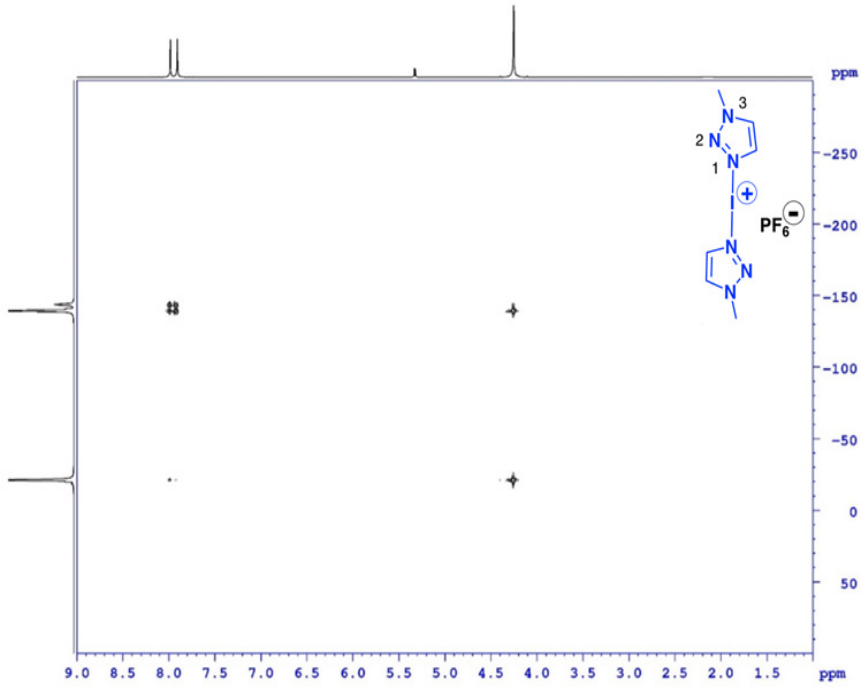

Figure 51. ^{1}H-^{15}N-HMBC spectra in CD_2Cl_2 at 303 K of compound [**11**-I-**11**]PF_6. δ (^{15}N) = -142.45 (N_1), -138.13 (N_3), -20.02 (N_2) ppm.

2.2.2 X-ray Crystallographic studies

The single crystals of [**11**-Ag-**11**]PF_6 shows symmetry around N···Ag···N with N···Ag bond length 2.137(4)A˚ and N···Ag···N bond angle 179.9(3) (Figure 52). The symmetric N···I···N bond lengths in the iodonium complex [**11**-I-**11**]PF_6 are 2.238(2)A˚ (Figure 53). The two triazole rings across the N···Ag···N motifs are not coplanar, the interplanar angles between two triazole rings, defined as θ, are 50.01°. While in [**11**-I-**11**]PF_6, angle between two triazole rings are 0.0° across N···I···N.

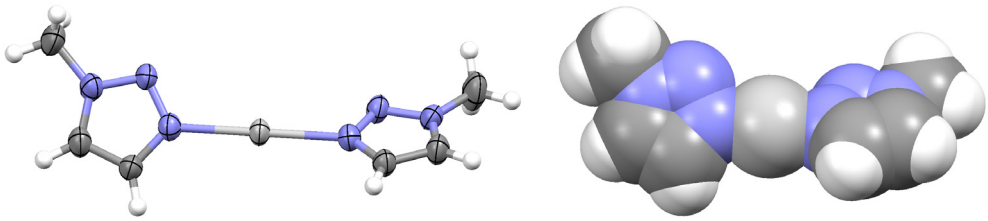

Figure 52. The structure of [**11**-Ag-**11**]PF_6. Anions and solvent molecules omitted for clarity.

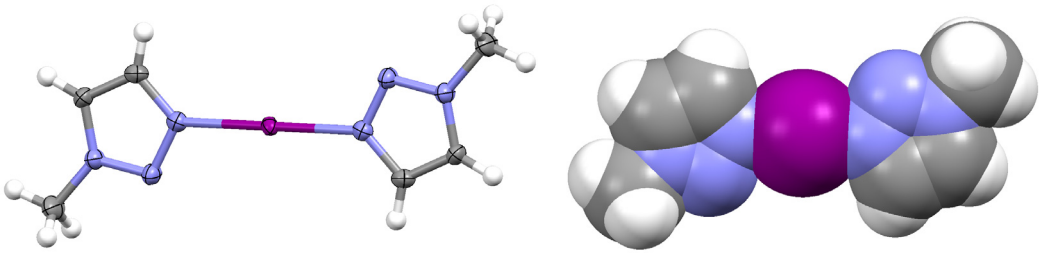

Figure 53. The structure of [**11**-I-**11**]PF_6. Anions and solvent molecules omitted for clarity.

In summary, by using these triazole iodine(I) complexes{[**11**-I-**11**]PF_6} with bis-bipyridine silver {[Ag(bpy)$_2$]PF_6} complexes, an extraordinary and attractive I^+···Ag^+ interaction denoted as I*Ag has been observed.[90] This I^+···Ag^+ interaction between iodonium and silver cations in a complex of complexes have been studied by 1H NMR and 1H-15N HMBC spectroscopy in solution and in the solid state by single-crystal X-ray crystallography. In this iodonium acts as the electron rich part(due to available lone pairs) and the Ag^+ behave as Lewis acid. This new I*Ag interaction is significantly stronger than previously reported argentophilic interactions.

2.3 Iodine(I) [N···I···N]$^+$ complexes of tertiary $NR_1R_2R_3$ amines

This is the first examples of [N···I···N]$^+$ iodonium ions where the nitrogen of the tertiary amines acts as halogen bond acceptor, derived from their parent [N···Ag···N]$^+$ complexes. ^{1}H and ^{15}N NMR studies unambiguously reveal differences between the $^+$Ag···N and $^+$I···N complexations in solution. Furthermore, X-ray crystallography of parent silver(I) complexes further supports the [N···I···N]$^+$ bonding model in the liquid state.

As a result of this work, we observed that meso chiral-at-nitrogen [N···X···N]$^+$ halogen(I) complexes can be synthesised and that *N*-stereocenters is stable enough to survive both in solid-state and solution (Figure 54). This study describes the synthesis and characterization of [N···Ag/I···N]$^+$ complexes based on six tertiary amines. The herein presented data expands the scope of halogen(I) complexes, and due to the electrophilic character of halogen and dissimilar conformational rigidity of the two different N-stereocenters various follow-up asymmetric chemistry applications can be expected. Amine ligands (**L**=**12**–**17**) are synthesised following the literature.[127-131] (Figure 55)

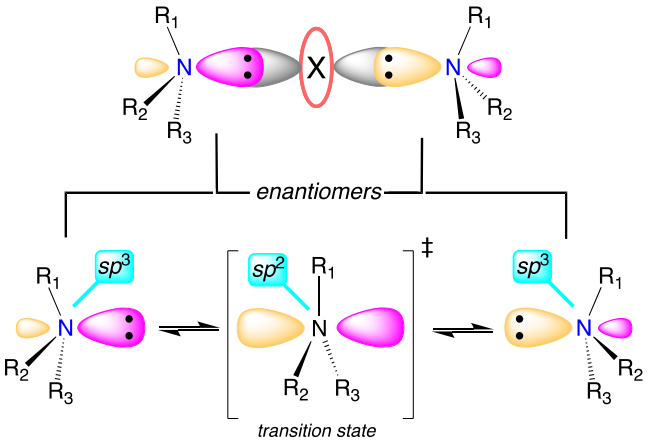

Figure 54. Schematic representation of meso halogen(I) ion complexes (above) and pyramidal inversion via trigonal planar transition state (below) of chiral tertiary amines (when R1≠R2≠R3 = alkyl/arylakyl).

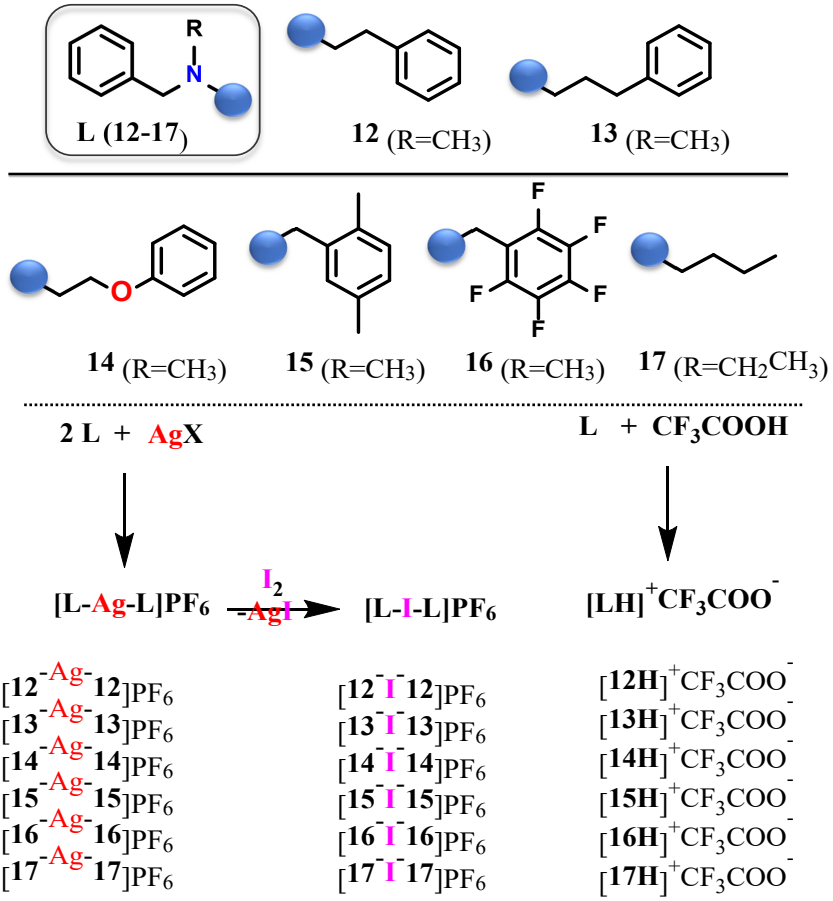

Figure 55. List of chiral tertiary amine ligands, **L**(**12**–**17**), their corresponding $Ag^+/I^+/H^+$ complexes, [**L**–Ag–**L**]PF_6 , [**L**–I–**L**]PF_6 , and [LH]CF_3COO (**L** = **12-17**).

2.3.1 Synthesis and NMR studies of $[N\cdots X\cdots N]^+$ complexes of tertiary $NR_1R_2R_3$ amines

Solution synthesis of iodonium ion complexes is a two-step process, firstly, the pre-dissolved 2 eq. of ligand and 1 eq. of $AgPF_6$ CD_3CN solutions are mixed in an NMR tube at room temperature. Monitoring the mixture by ^1H NMR revealed, in each case, one set of ligand signals different from the uncomplexed ligand confirming the [**L**···Ag···**L**]PF_6 (**L**= **12-17**) symmetric complexation. Secondly, 1.1 eq iodine is added to Ag^+-complexes, subsequently filtered the AgI precipitates and re-measured the ^1H NMR. A new set of proton signals, in each case, different from ligand **12-17** and [**L**···Ag···**L**]PF_6 (**L**= **12-17**) confirm the formation of [**L**···I···**L**]PF_6 (L= **12-17**). A strong clue of I^+-complexation is provided by N–methylene/methyl chemical shifts, which rest at considerably downfield compared to Ag^+ and ligand spectra (Figure 56-61). Unlike $^+Ag\cdots N$ complexation, the $^+I\cdots N$ strong halogen bonding tends to introduce a larger positive charge into the ligand significantly altering the chemical shifts of organic moieties.

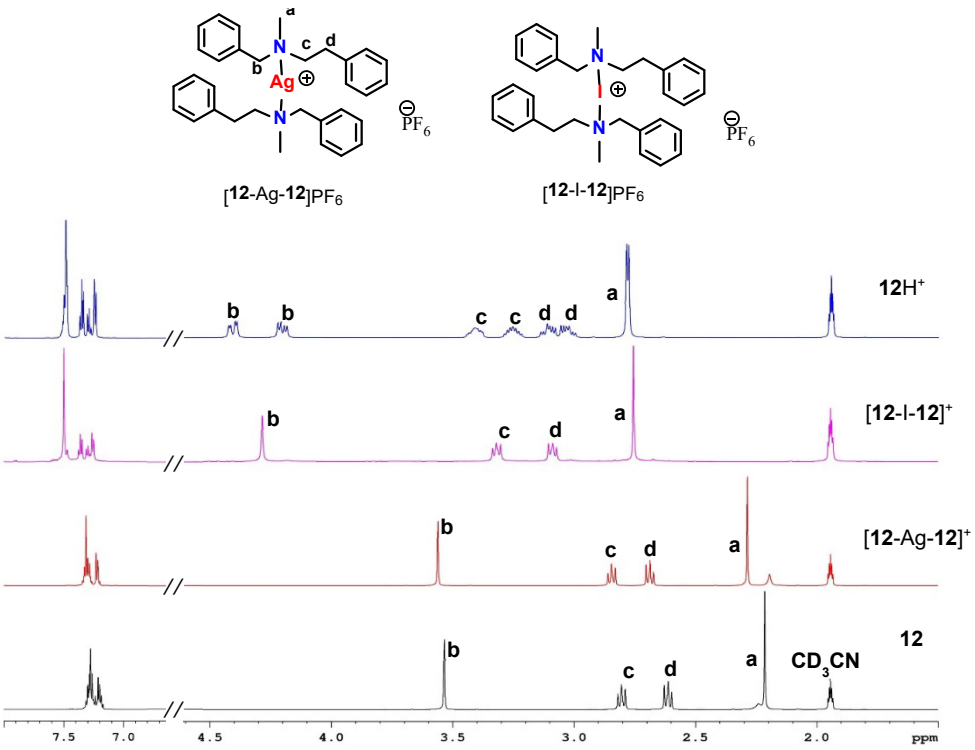

Figure 56. ^{1}H NMR chemical shifts for **12** (black), [**12**-Ag-**12**]$^+$ (red), [**12**-I-**12**]$^+$ (pink), and **12**H$^+$ (blue) in CD_3CN at 500 MHz with hexafluorophosphate as counterion.

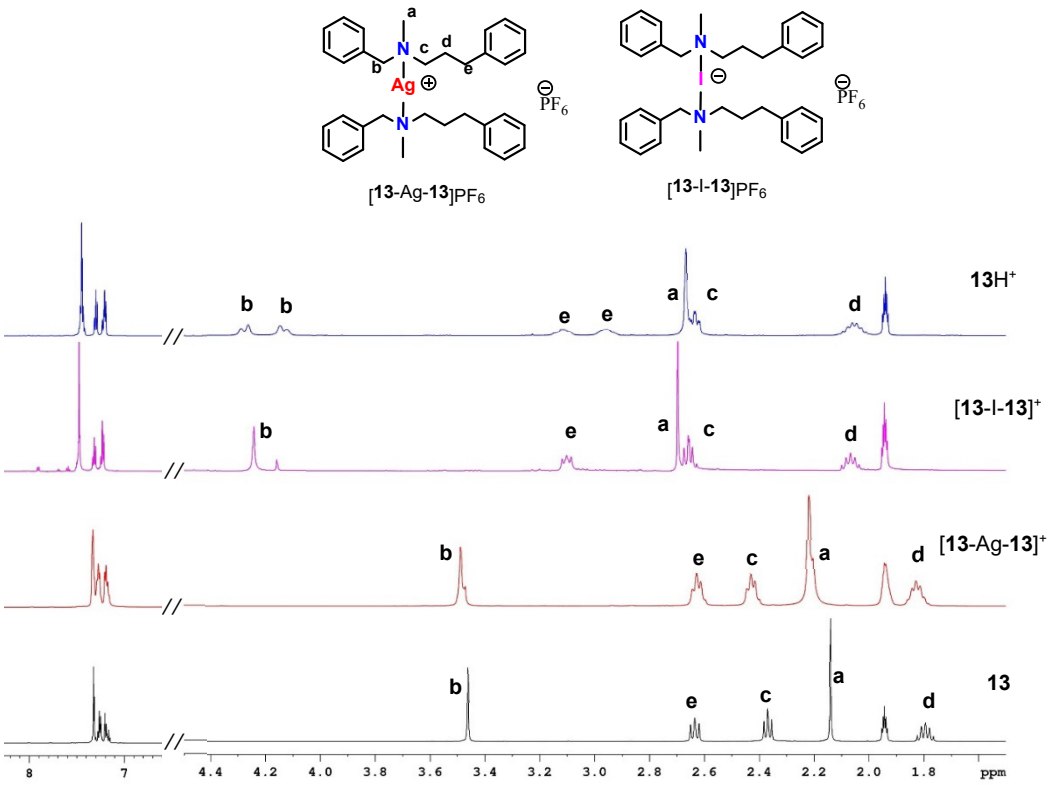

Figure 57. ^{1}H NMR chemical shifts for **13** (black), [**13**-Ag-**13**]$^+$ (red), [**13**-I-**13**]$^+$ (pink), and **13**H$^+$ (blue) in CD_3CN at 500 MHz with hexafluorophosphate as counterion.

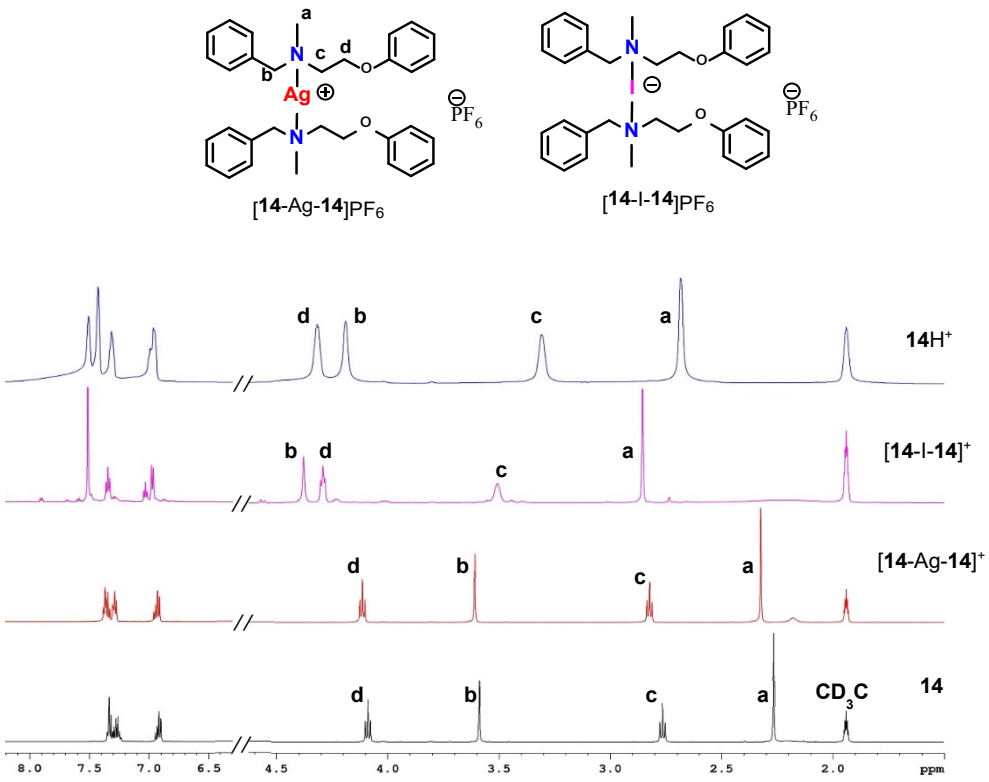

Figure 58. ^{1}H NMR chemical shifts for **14** (black), [**14**-Ag-**14**]$^+$ (red), [**14**-I-**14**]$^+$ (pink), and **14**H$^+$ (blue) in CD_3CN at 500 MHz with hexafluorophosphate as counterion.

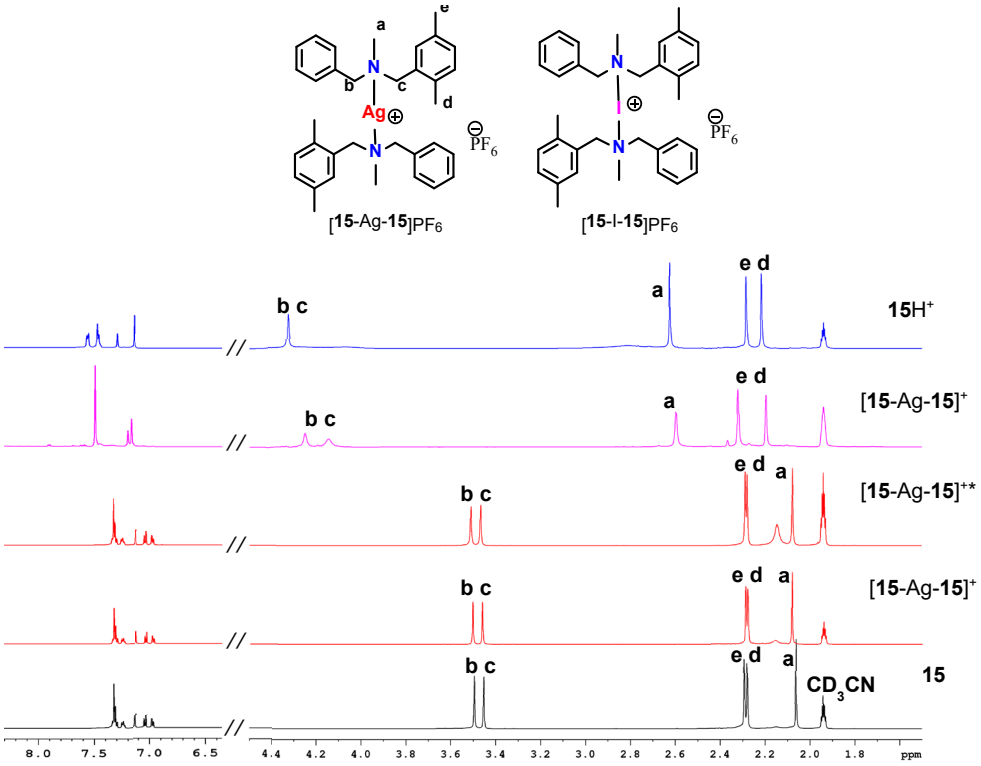

Figure 59. ^{1}H NMR chemical shifts for **15** (black), [**15**-Ag-**15**]$^+$ (red), [**15**-I-**15**]$^+$ (pink), and **15**H$^+$ (blue) in CD_3CN at 500 MHz with hexafluorophosphate as counterion. [**15**-Ag-**15**]* denotes ^{1}H NMR of silver(I) complex crystals.

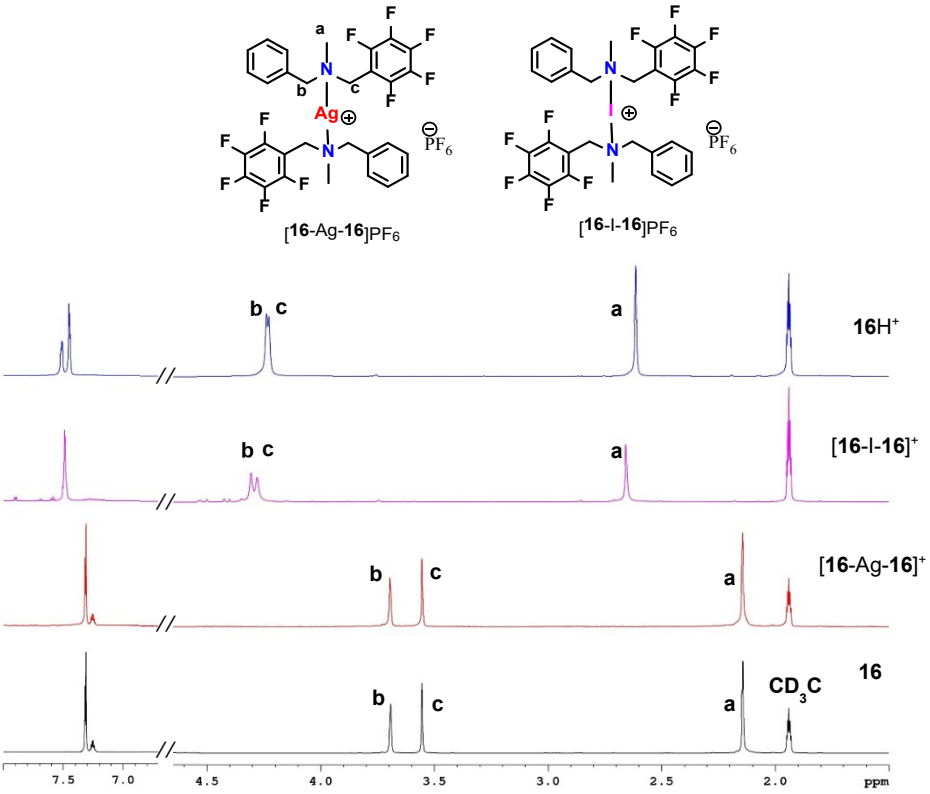

Figure 60. ^{1}H NMR chemical shifts for **16** (black), [**16**-Ag-**16**]$^+$ (red), [**16**-I-**16**]$^+$ (pink), and **16**H$^+$ (blue) in CD_3CN at 500 MHz with hexafluorophosphate as counterion.

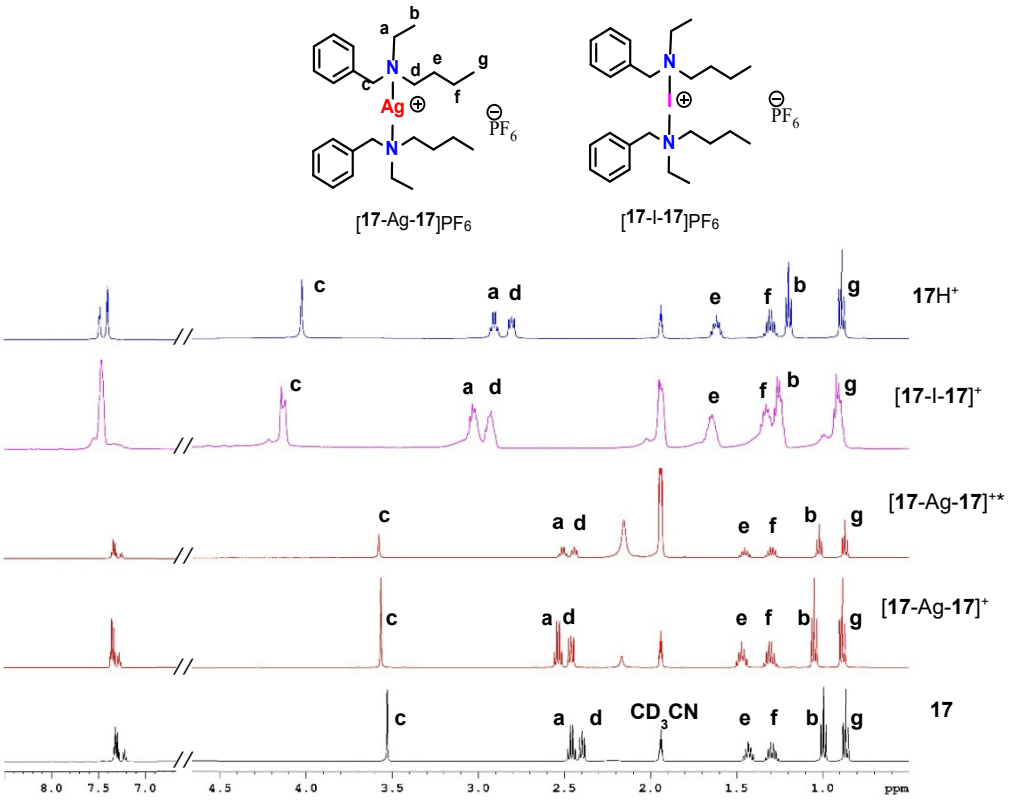

Figure 61. ^{1}H NMR chemical shifts for **17** (black), [**17**-Ag-**17**]$^+$ (red), [**17**-I-**17**]$^+$ (pink), and **17**H$^+$ (blue) in CD_3CN at 500 MHz with hexafluorophosphate as counterion. [**17**-Ag-**17**]* denotes ^{1}H NMR of silver(I) complex crystals.

^{15}N NMR coordination shift ($\Delta\delta^{15}N_{coord}$), described as the ^{15}N chemical shift difference between the complexed ligand ($\delta^{15}N_{compl}$) and its corresponding uncomplexed ligand ($\delta^{15}N_L$), is a sensitive tool to monitor the electronic changes of the N-atom involved in N-protonation[132], N-alkylation[133,134], N-oxidation[135], and N-metal coordination.[136] The $\Delta\delta^{15}N_{coord}$ values of [**L**···Ag···**L**]PF_6, (**L**= **12-17**) are 3-5 times smaller than [**L**···I···**L**]PF_6 , (**L**= **12-17**), suggesting the complete exchange Ag^+ by I^+ and the latter comprises a stronger interaction(Table 4). Further corroboration comes from ^{1}H NMR, the proton chemical shifts of silver complexes are shielded than iodonium complexes involved in $^+$I–N coordination (Figure 56-61). The virtually zero $\Delta\delta^{15}N_{coord}$ of [**16**-Ag-**16**]PF_6 and large $\Delta\delta^{15}N_{coord}$ values of [**16**-Ag-**16**]PF_6 (15.5 ppm) and [**16**-I-**16**]PF_6 (12.4 ppm) warrant a comment (Table 4). We speculate the 2:1 molar ratio of **16**:$AgPF_6$ demands a [N···Ag···N]$^+$ linear arrangement between Ag^+ and **16**'s nitrogen and favours I^+-substitution. The electron-withdrawing $C_6F_5CH_2^-$ decreases the electron density on **16**'s nitrogen, causing weak Ag^+···N bonding and near-zero $\Delta\delta^{15}N_{coord}$. While the stronger $^+$I···N and $^+$H···N interactions install a high amount of positive charge onto **16**'s molecular framework, causing 15.4 ppm and 12.4 $\Delta\delta^{15}N_{coord}$ shifts, respectively (Table 4).

The [**L**H]$^+CF_3COO^-$ (**L**= **12-17**) are prepared by mixing a 1:1 molar ratio of ligands and CF_3COOH in CD_3CN for comparison to eliminate the possibility that the [**L**···Ag···**L**]PF_6, (**L**= **12-17**) and [**L**···I···**L**]PF_6, (**L**= **12-17**) chemical shifts are not due to [**L**H]$^+$ salts formation. The ^{1}H NMR spectra of [**L**H]$^+CF_3COO^-$ (**L**= **12-17**) and their corresponding **L**'s, silver and iodine complexes, are not superimposable suggesting solely Ag^+/I^+-complexations (Figure 55-61). It should be noted that the [**L**H]$^+CF_3COO^-$ (**L**= **12-17**) are chiral and their tetrahedral nitrogen encompasses four different substituents. The presence of two sets of non-equivalent aromatics and N–CH_2/CH_3 signals validates the [**L**H]$^+$ tetrahedral structure. The [**L**H]$^+CF_3COO^-$ (**L**= **12-17**) $\Delta\delta^{15}N_{coord}$ values are ∼3-5 times larger than [**L**···Ag···**L**]PF_6, (**L**= **12-17**) and are comparable to [**L**···I···**L**]PF_6, (**L**= **12-17**) and to those reported N-protonated tertiary amines, both in sign and magnitude.[132]

Table 4. ^{15}N NMR Chemical shifts (CD_3CN, 298.0 K) of amines **12-17** and corresponding Ag^+-, I^+-, and H^+-complexes.

Code[a]	$\Delta\delta^{15}N_{coord}$[a]	Code	$\Delta\delta^{15}N_{coord}$ [a]	Code	$\Delta\delta^{15}N_{coord}$[a]
[12-Ag-**12]**$^+$	3.9	**[12**-I-**12]**$^+$	15.6	**[12H]**$^+$	15.2
[13-Ag-**13]**$^+$	5.2	**[13**-I-**13]**$^+$	16.6	**[13H]**$^+$	16.6
[14-Ag-**14]**$^+$	3.6	**[14**-I-**14]**$^+$	15.7	**[14H]**$^+$	12.6
[15-Ag-**15]**$^+$	4.0	**[15**-I-**15]**$^+$	19.2	**[15H]**$^+$	15.0
[16-Ag-**16]**$^+$	0.1	**[16**-I-**16]**$^+$	15.5	**[16H]**$^+$	12.4
[17-Ag-**17]**$^+$	6.1	**[17**-I-**17]**$^+$	13.1	**[17H]**$^+$	8.6

[a] $\Delta\delta^{15}N_{coord} = \delta^{15}N_{compl} - \delta^{15}N_L$.

2.3.1 X-ray crystallographic studies of [N···Ag···N]$^+$ complexes of tertiary amines

Complexes [**15**-Ag-**15**] and [**17**-Ag-**17**] are characterised by X-ray crystallography (Figure 62, a and b). The Ag···N {[**15**-Ag-**15**]: 2.1927(16) Å; 2.191(7) Å} and N-N {[**15**-Ag-**15**]: 4.385 Å; [**17**-Ag-**17**]: 4.336 Å} distances are like those in the reported [N···Ag···N]$^+$ pyridine systems.[137] The [**15**-Ag-**15**] has a N···Ag···N linear geometry, whilst the [**17**-Ag-**17**] N···Ag···N bent geometry [163.3(4)°] is similar to [N···Ag···N]$^+$Y$^-$ pyridine systems wherein the coordinating Y counter anions alter the N···Ag···N geometry from linearity. In [**15**-Ag-**15**] and [**17**-Ag-**17**], the aryl/alkyl groups are flanking around the linear silver(I) in a ''*trans*'' manner to avoid the steric clash. In this setting, the silver(I) and aryl/alkyl groups stabilise via $^+$Ag···π [*ca*. 2.9-3.2 Å] and Ag···H-C [*ca*. 2.5-3.1 Å] interactions. Remarkably, the ^{1}H NMR spectra of [**15**-Ag-**15**]/[**17**-Ag-**17**] single crystals and of their as-prepared solution silver(I) complexes are superimposable (Figure 58 and 60). This result confirms the [**L**···Ag···**L**]PF_6, (**L**= **12-17**) solution structures and $^+$Ag···N complexations not necessarily should produce large ^{1}H NMR chemical shifts when compared to uncomplexed ligands, as in cases of reported [N···Ag···N]$^+$ pyridine systems. We are unable to isolate single crystals of other Ag^+-complexes and [**L**···I···**L**]PF_6, (**L** = **12-17**) for X-ray crystallography.

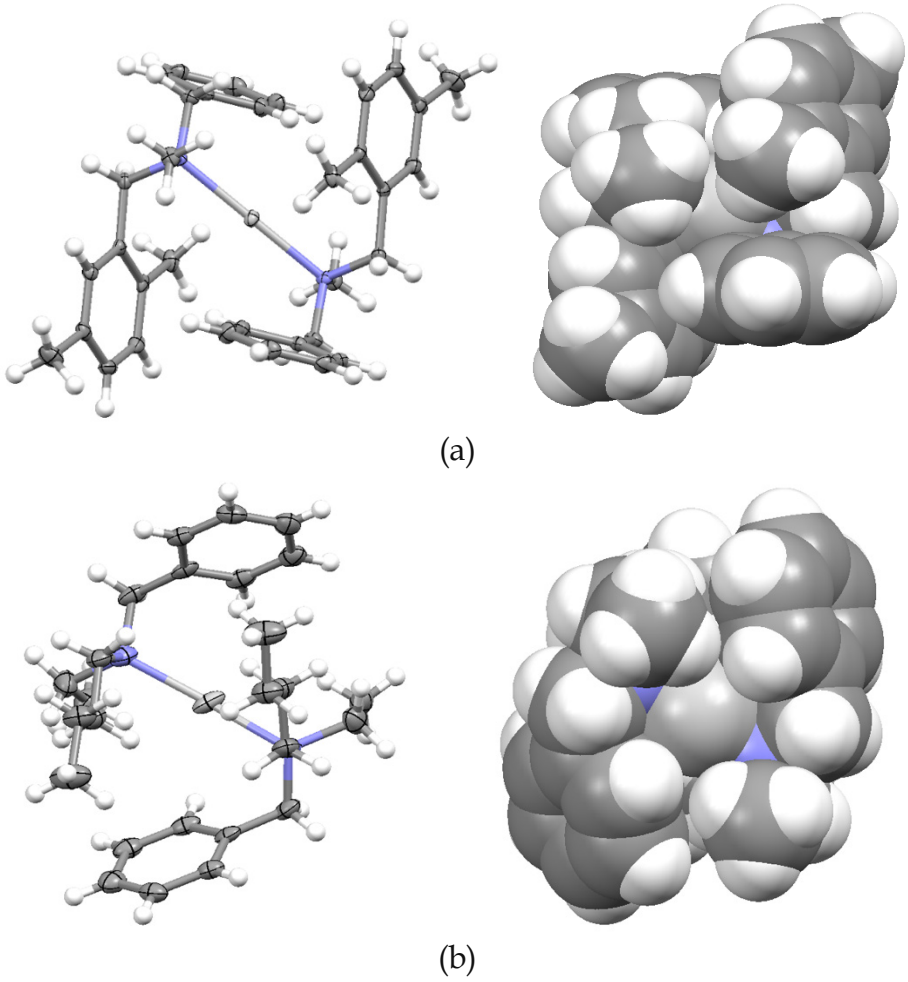

Figure 62. The structure of [**15**-Ag-**15**]PF_6(a) and [**17**-Ag-**17**]PF_6(b). Anions and solvent molecules omitted for clarity. Ellipsoid are drawn at the 50% probability for Complex of [**15**-Ag-**15**]PF_6(a) and 25% for [**17**-Ag-**17**]PF_6(b).

In conclusion, $[N\cdots Ag/I\cdots N]^+$ ions of chiral tertiary amines bearing sp^3 nitrogen are prepared and characterised as their PF_6 salts using solution NMR. The ^1H NMR spectra of $[L\cdots I\cdots L]^+$ and LH^+ for ligand **15** and **16** are very similar which stipulate that it might be tough to replace silver from the $[L\cdots Ag\cdots L]^+$ complexes, which also favoured by solid state studies and slight difference in ^1H NMR peaks is might be because of different counterion in $[L\cdots I\cdots L]^+$ and LH^+ complexes. X-Ray crystallography reveals severe crowding around the silver(I) ion by amines' alkyl and aryl groups and an intimate Ag···H-C and Ag···π interactions. This new strategy provides a starting point to the stabilisation of I^+ ions of the $[N\cdots I\cdots N]^+$ locality by weak non-covalent bonds, and is an important step towards our future endeavours in this research line of halogen(I) ion supramolecular chemistry.

2.4 Tetra- and hexadentate ligand silver(I) complexes

2.4.1 Synthesis, solution and solid-state studies of [(1,10-phenanthroline)$_2$ silver] hexafluorophosphate

The complex $[Ag(phen)_2]PF_6$, [**18**-Ag-**18**]PF_6 (phen = 1,10-phenanthroline) was obtained by following the reported procedure for the $[Ag(phen)_2]NO_3$ from 1,10-phenanthroline (**18**) and $AgNO_3$.[138]

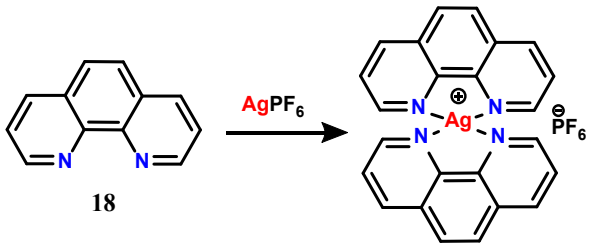

Scheme 7. Synthesis of Complex [**18**-Ag-**18**]PF_6.

To a solution of 1,10-phenanthroline **18** (10 mg, 0.056 mmol, 2.0 eq) in 5 mL of CH_2Cl_2 was added silver hexafluorophosphate (7.01 mg, 0.028 mmol, 1.0 eq). The solution was stirred for 30 mins at room temperature. The reaction mixture was dried under vacuum to give the pale-yellow solid [(1,10-phenanthroline)$_2$ silver] hexafluorophosphate [**18**-Ag-**18**]PF_6 (18.0 g, 99%). A [**18**-I-**18**]PF_6 complex was synthesized from [**18**-Ag-**18**]PF_6 complexes by exchange reaction and analyzed in solution and solid-state. However, the results confirm that Ag-complexes are too stable and cannot be converted into halogen(I) compounds.

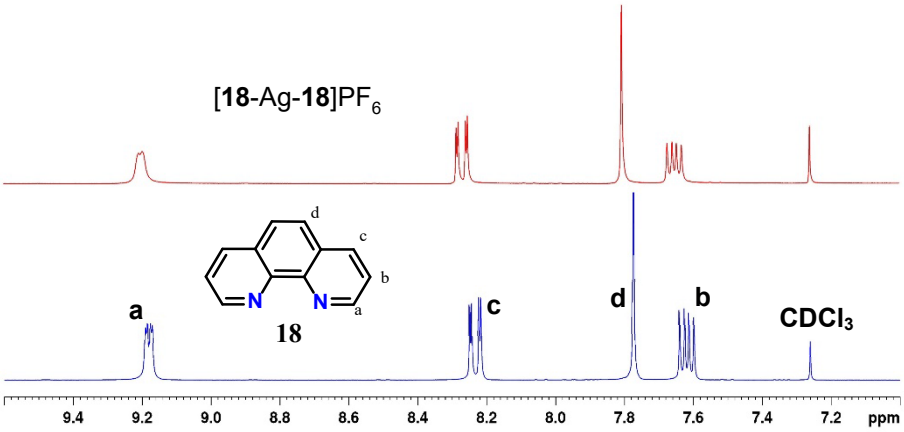

Figure 63. ^{1}H NMR spectra in $CDCl_3$ at 303 K of 1,10-phenanthroline (**18**) and [**18**-Ag-**18**]PF_6.

The ^{1}H NMR spectra of ligand **18** and their silver complex [**18**-Ag-**18**]PF_6, demonstrated significant complexation-induced shifts (Figures 63). The addition of $AgPF_6$ into ligand **18** in

a $CDCl_3$ solution led to a noticeable downfield shift of the ligand proton signals of **18**, confirming the formation of the silver complex [**18**-Ag-**18**]PF_6.

The single crystal of [**18**-Ag-**18**]PF_6 was grown by vapor diffusion process in MeCN/THF solvent (Figure 64). In which two type of Ag-N bond length were observed, Ag-N1 and Ag-N21; 2.332(9) and 2.339(10) respectively. The two 1,10-phenanthroline rings across the N···Ag···N motifs are not coplanar, the interplanar angles between two 1,10-phenanthroline rings (defined as θ) are 40.86°.

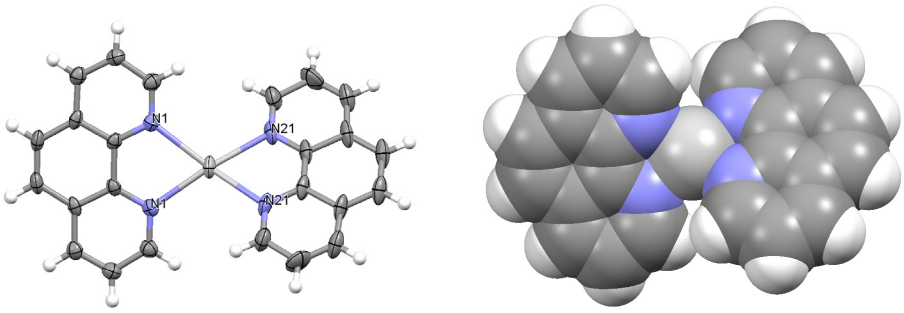

Figure 64. The structure of [**18**-Ag-**18**]PF_6. Anions and solvent molecules omitted for clarity.

2.4.2 Synthesis and solution studies of silver terpyridine complexes

Silver(I) ions react with terpyridine-type ligands in a 1:2 M ratio, which results in the formation of mono- or multi-nuclear species, in particular helical structures.[139] The ^{1}H-NMR (Figure 65) spectra of 1:2 (**19** : $AgPF_6$), gave only one set of NMR signals, different from the uncomplexed ligand (**19**) confirming the symmetric silver complexation.

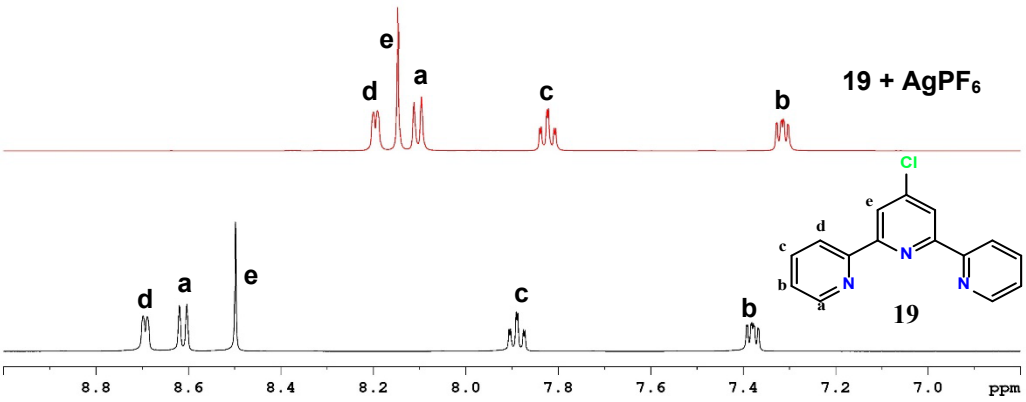

Figure 65. ^{1}H NMR spectra (only aromatic region) of Ligand (black), Silver complex (red) in CD_2Cl_2 solvent.

2.4.3 Crystallographic studies of silver terpyridine complexes

A single crystal was grown by the vapor diffusion process. The complexes were synthesized by mixing 2.0 eq of 4'-Chloro-2,2:6',2''-terpyridine (**19**) and 1.0 eq silver salt ($AgPF_6$, AgOTf) into DCM/THF at room temperature. The mixture was stirred for 10 mins to form a silver complex and left to grow single crystals suitable for X-ray diffraction analysis. We were able to crystalised multi-nuclear silver complexes as shown in the figure 66-69. The structures and numbering scheme for the cation part of silver complexes are shown in Scheme 8 (to understand silver nitrogen bond in multi-nuclear complexes) and bond lengths for these complexes are summarized in Table 5. By following the procedure four multi-nuclear silver complexes $[Ag_3\mathbf{19}_4][PF_6]_3 \cdot C_4H_8O$, $[Ag_3\mathbf{19}_4][PF_6]_3$, $[Ag_2\mathbf{19}_2][OTf]_2 \cdot CH_2Cl_2$ and $[Ag_3\mathbf{19}_4][PF_6]_3 \cdot CH_2Cl_2$ were studies by X-ray crystallography and later analyzed by ^1H, ^1H-^{15}NMR and mass spectroscopy(ESI).

Although terpyridine usually functions as a chelating tetradentate ligand, this bonding mode is not possible with metal ions which have a tendency towards four-coordinate tetrahedral coordination. In these cases, it is possible to anticipate double-helical structures in which two quasi-four-coordinate metal centers are coupled by a bridging nitrogen of the central pyridine ring. Such structures are formed with copper(I)[140-142] and other low-charged metal ions such as silver(I) were expected to behave in a similar manner to copper(I) as we have seen in the case of 2,2' : 6',2"-quaterpyridine ligands[143,144]. As we can clearly see from there crystals, the weakly coordinating anions are not directly coordinated to the metal center.

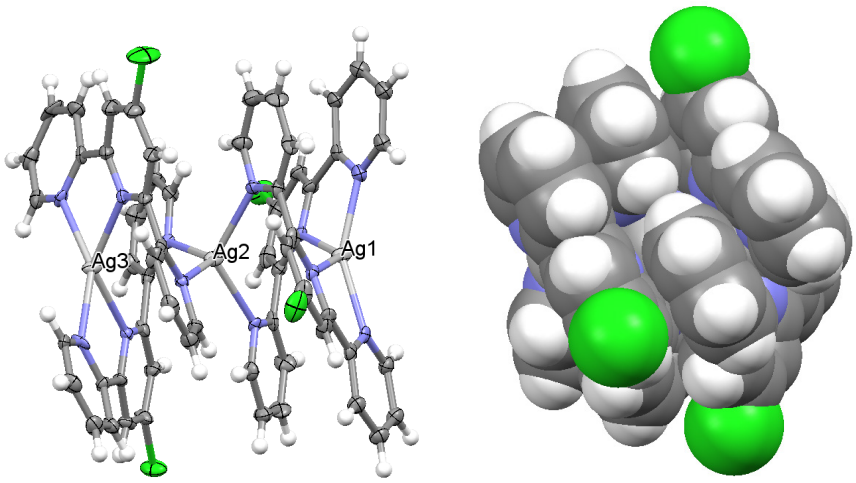

Figure 66. The structure of $[Ag_3\mathbf{19}_4][PF_6]_3 \cdot C_4H_8O$. Anions and solvent molecules omitted for clarity. Ellipsoid are drawn at the 50% probability.

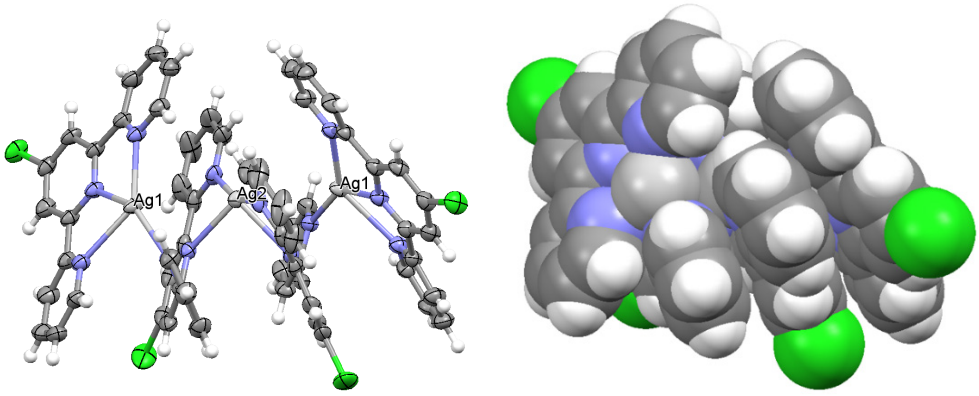

Figure 67. The structure of $[Ag_3\mathbf{19}_4][PF_6]_3$. Anions and solvent molecules omitted for clarity. Ellipsoid are drawn at the 50% probability.

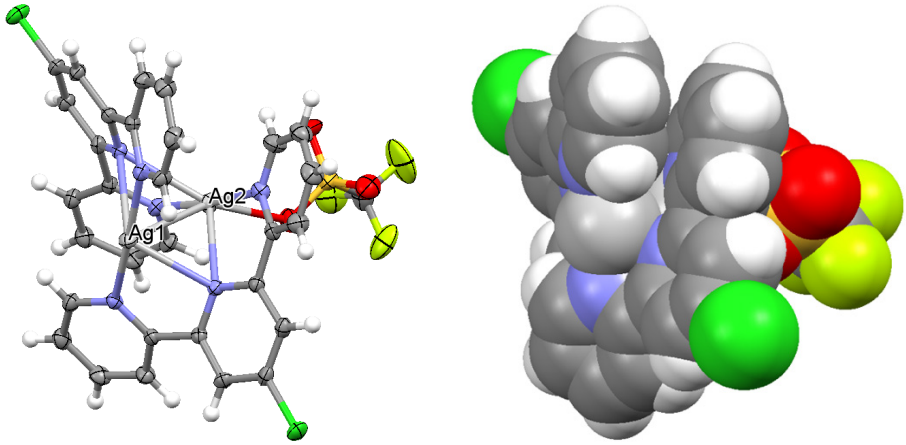

Figure 68. The structure of $[Ag_2\mathbf{19}_2][OTf]_2 \cdot CH_2Cl_2$. Anions and solvent molecules omitted for clarity. Ellipsoid are drawn at the 50% probability.

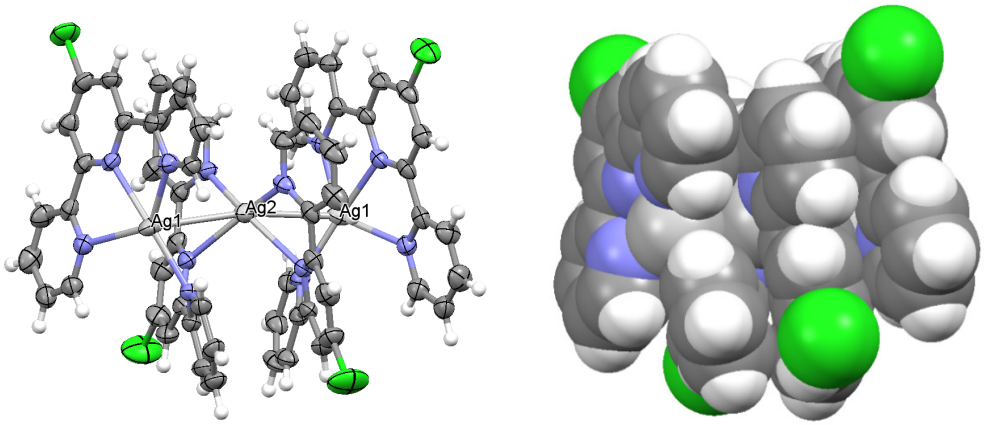

Figure 69. The structure of $[Ag_3\mathbf{19}_4][PF_6]_3 \cdot CH_2Cl_2$. Anions and solvent molecules omitted for clarity. Ellipsoid are drawn at the 25% probability.

The crystal structures of $AgPF_6$ silver salt (Figure 66,67,69) are differ only in terms of the solvent molecule and the amount of solvent in the crystal structure. The two complexes (Figure 67 and 69) mainly differ by the coordination number of the central silver metal. In complex

$[Ag_3\mathbf{19}_4][PF_6]_3 \cdot CH_2Cl_2$ (Figure 69) central Ag formed six bonds with two extra Ag-Ag bonds with bond length of 3.153Å. While in Complex $[Ag_3\mathbf{19}_4][PF_6]_3$ (Figure 67), Ag-Ag bond length is slightly longer, 3.323Å. Complex of AgOTf silver salt have a dimeric structure with a different counterion, OTf^-, in its crystal structure (Figure 68). These differences in the counter ion and solvent molecule affect the crystal packing of the complexes and thus have an impact on the final geometries. The intramolecular Ag-Ag distances are 3.239(5), 3.323(3), 2.960(2), and 3.153 Å, respectively in complexes figure 66-69. The sum of the van der Waals radii of the two silver atoms is 3.44Å, and thus the argentophilic interaction between the silver atoms can be assumed in all cases.

Again, the metals give rise to metal-metal interactions and, according to the Ag-Ag distances, these are likely to be of different strengths of Ag-Ag interaction within Complex $[Ag_3\mathbf{19}_4][PF_6]_3 \cdot C_4H_8O$ molecules: d[Ag(1)-Ag(2)] = 3.392(3)Å and d[Ag(2)-Ag(3)] = 3.2392(10)Å. Many factors (molar ratio of the reagents, solvent, experimental conditions, etc) coupled with the versatile coordination requirements of silver(I) and the wide donor capability of the ligands could heavily affect the obtained products.[145,146] The complex $[Ag_2\mathbf{19}_2][OTf]_2 \cdot CH_2Cl_2$ is a dimer in which the silver atoms are bridged by the tridentate terpyridine ligands, each silver centre is bound to four nitrogen atoms with dissimilar distances, the shortest ones are those of the outside nitrogen atoms, 2.200(4)Å and 2.210(4)Å, and there are two long ones corresponding to the central nitrogen atom, 2.691(4)Å, 2.571(4)Å to the other central nitrogen. Additionally, the silver centres make weak bonds to the oxygen of the triflate anion, 2.649Å. Consequently, the silver atoms have a very irregular molecular geometry with an Ag-Ag bonding interaction of 2.9600(6)Å (Table 5).

Terpyridine ligand self-assembles around metal ions in an identical manner as $[Ag_2\mathbf{19}_2]^{2+}$ motif in $[Ag_2\mathbf{19}_2](OTf)_2$ with OTf^- counterions and central pyridine atom present bridging mode to argentophilic Ag(I) ions (Figure 68). Since even poorly coordinating $CF_3SO_3^-$ ions are involved in interaction with Ag(I), without disrupting the structure into monomeric systems, and form $[Ag_2\mathbf{19}_2][OTf] \cdot CH_2Cl_2$. Such a bridging mode of pyridine moiety is quite unusual. Terpyridine ligand form trinuclear species with PF_6^- counterions, in the form of $[Ag_3\mathbf{19}_3][PF_6]_3$ (Figure 66,67,69).

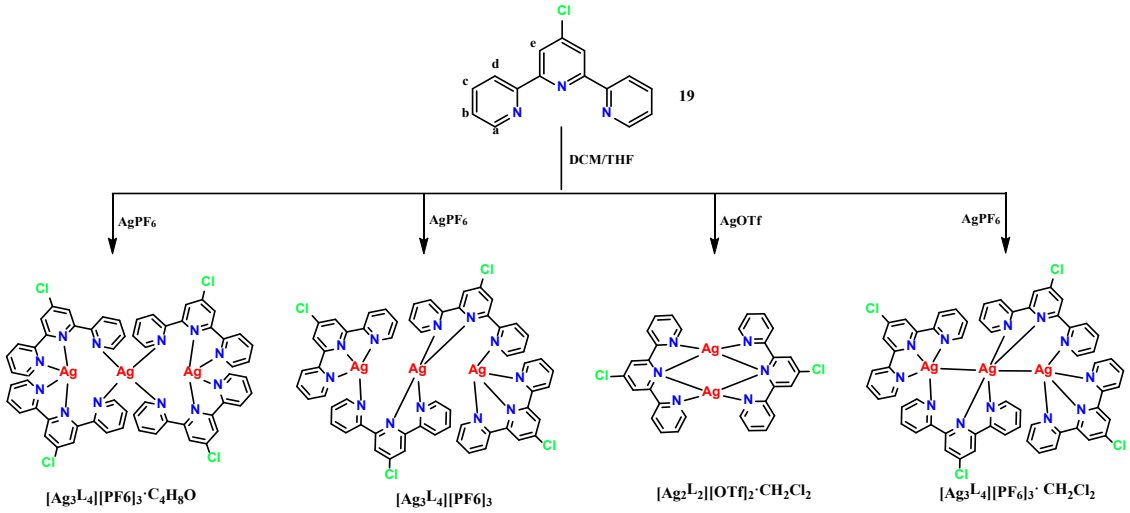

Scheme 8. Reactions of the 4′-Chloro-2,2′:6′,2″-terpyridine (**19**) ligands with silver salts.

Table 5. Selected bond distances (A˚) for silver complexes.

$[Ag_3\mathbf{19}_4][PF_6]_3\cdot C_4H_8O$		$[Ag_3\mathbf{19}_4][PF_6]_3$	
Ag1-N1	2.333(8)	Ag1 Ag2	3.323(3)
Ag1-N8	2.265(8)	Ag1 N1	2.406(3)
Ag1-N21	2.355(8)	Ag1 N8	2.313(3)
Ag1-N28	2.263(8)	Ag1 N15	2.556(3)
Ag2-Ag3	3.239(10)	Ag1 N35	2.284(3)
Ag2-N15	2.388(7)	Ag2 Ag1	3.323(3)
Ag2-N35	2.411(7)	Ag2 N21	2.467(3)
Ag2-N48	2.443(7)	Ag2 N21	2.467(3)
Ag2-N68	2.432(8)	Ag2 N28	2.238(3)
Ag3-N41	2.366(7)	Ag2 N28	2.238(3)
Ag3-N55	2.281(7)		
Ag3-N61	2.370(7)		
Ag3-N75	2.271(7)		
Ag1-Ag2	3.392(3)		
$[Ag_2\mathbf{19}_2][OTf]_2 \cdot CH_2Cl_2$		$[Ag_3\mathbf{19}_4][PF_6]_3\cdot CH_2Cl_2$	
Ag1 Ag2	2.960(6)	Ag1 Ag2	3.097(5)
Ag1 N8	2.200(4)	Ag1 N1	2.354(4)
Ag1 N21	2.619(4)	Ag1 N8	2.375(5)
Ag1 N28	2.210(4)	Ag1 N15	2.537(5)
Ag2 N15	2.219(4)	Ag1 N35	2.263(5)
Ag2 N21	2.571(4)	Ag2 Ag1	3.097(5)
Ag2 N35	2.229(4)	Ag2 N21	2.483(5)
		Ag2 N21	2.483(5)
		Ag2 N28	2.258(5)
		Ag2 N28	2.258(5)

2.4.4 NMR studies

To finally evaluate the complex formed in solution, ^{1}H NMR spectra of each crystal were acquired in CD_2Cl_2 solvent (Figure 66-69) and compared with the ^{1}H -NMR spectra shown in figure 70. ^{1}H NMR spectra of four multi-nuclear silver complexes $[Ag_3\mathbf{19}_4][PF_6]_3 \cdot C_4H_8O$, $[Ag_3\mathbf{19}_4][PF_6]_3$, $[Ag_2\mathbf{19}_2][OTf]_2 \cdot CH_2Cl_2$ and $[Ag_3\mathbf{19}_4][PF_6]_3 \cdot CH_2Cl_2$ are practically identical in a given solvent and this indicates that one type of complex is more stable in solution and corroborated that only one kind of species in solution exists. ^{1}H–^{15}N NMR was successfully used to evaluate which nitrogen is involved in the complex formation (Figure 72-76).[147]

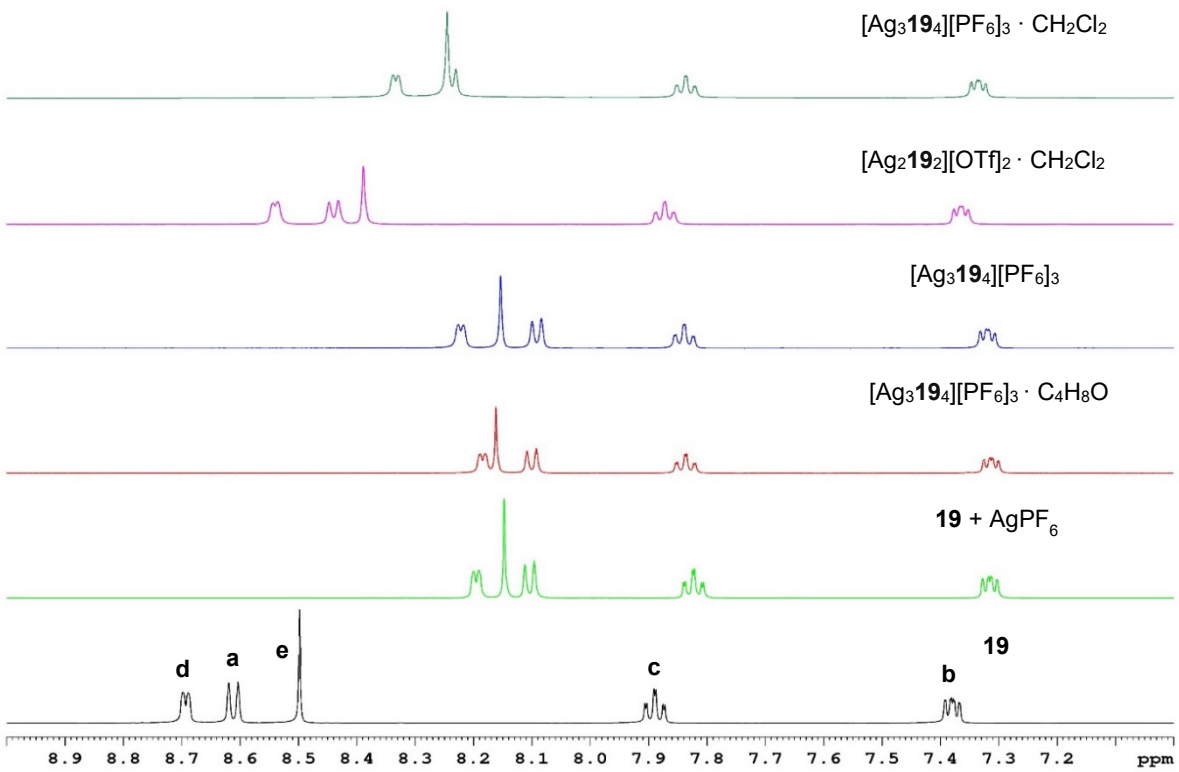

Figure 70. ^{1}H NMR spectra (only aromatic region) of **19** (black), Silver complex (light green), $[Ag_3\mathbf{19}_4][PF_6]_3 \cdot C_4H_8O$ (red), $[Ag_3\mathbf{19}_4][PF_6]_3$ (blue), $[Ag_2\mathbf{19}_2][OTf]_2 \cdot CH_2Cl_2$ (pink) and $[Ag_3\mathbf{19}_4][PF_6]_3 \cdot CH_2Cl_2$ (green), in CD_2Cl_2 solvent.

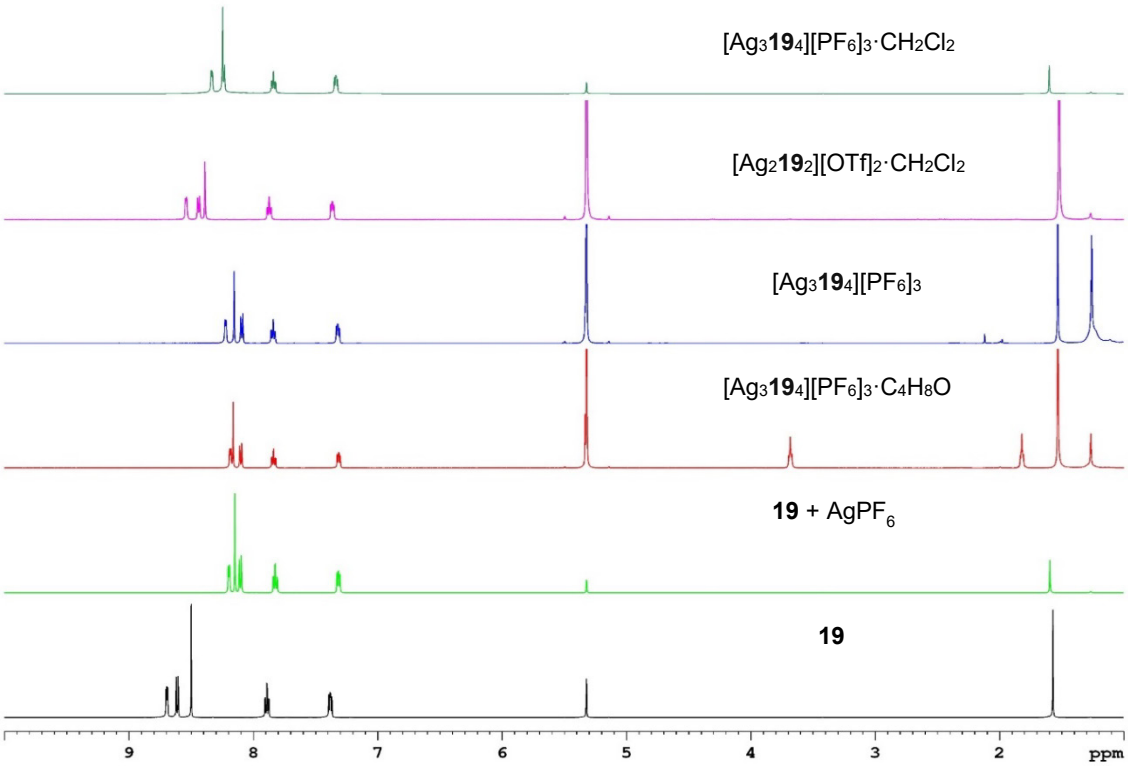

Figure 71. ^{1}H NMR spectra of **19** (black), Silver complex (light green), $[Ag_3\mathbf{19}_4][PF_6]_3\cdot C_4H_8O$ (red), $[Ag_3\mathbf{19}_4][PF_6]_3$ (blue), $[Ag_2\mathbf{19}_2][OTf]_2\cdot CH_2Cl_2$ (pink) and $[Ag_3\mathbf{19}_4][PF_6]_3\cdot CH_2Cl_2$ (green), in CD_2Cl_2 solvent. Peak at δ ≈ 1.56ppm is from water.

The signals attributed to the presence of the terpyridine ligand bonded to the Ag(I) centre, appear to shift concerning those of the free ligand, confirming the coordination of the N-donor ligand to the metal centres. ^{1}H NMR spectrum of $[Ag_3\mathbf{19}_4][PF_6]_3\cdot C_4H_8O$ in CD_2Cl_2 showed five signals (red, Figure 70 and 71). The singlet signal at δ = 8.16 ppm, with the integration of one, is assigned to the protons of the central pyridine ring (H_e) (Labelling of atoms is shown in Scheme 7). Observation of a singlet ^{1}H NMR signal for H_e may be taken as a sign that the ligand is in symmetric mode and absence of incommensurate binuclear double helicates Ag(I) structure.[148] The ^{1}H NMR of each complex has the same pattern of signal, which indicate that only one type of form is more stable in solution irrespective of the counter anion. In $[Ag_2\mathbf{19}_2][OTf]_2\cdot CH_2Cl_2$, counter anion might interact with silver complex and due to that, there is a slight shift in NMR signal and shows a different pattern of signal (Pink, Figure 70 and 71). Complexes $[Ag_3\mathbf{19}_4][PF_6]_3\cdot C_4H_8O$ and $[Ag_3\mathbf{19}_4][PF_6]_2$ (red and blue in Figure 70 and 71) have very much similar ^{1}H NMR, except peak at δ = 3.68ppm and δ = 1.81ppm in complex $[Ag_3\mathbf{19}_4][PF_6]_3\cdot C_4H_8O$ crystal NMR (Figure. 71). These peaks come from THF present in the crystal structure. Solvent molecules present in Complex $[Ag_3\mathbf{19}_4][PF_6]_3\cdot CH_2Cl_2$ crystal, influence the peaks and we noticed a slight shift in doublet and singlet peaks, meanwhile, it shows the same patterns of the signal as complex $[Ag_3\mathbf{19}_4][PF_6]_3\cdot C_4H_8O$ and $[Ag_3\mathbf{19}_4][PF_6]_3$.

The $^{1}H–^{15}N$ NMR was successfully used to evaluate which nitrogen is involved in the complex formation. The Δ^{15N}_{coord} parameter reflects the real effect of heteroatom coordination, i.e. the difference between the chemical shifts of free N and Ag–N (Table 6). However, the $\Delta^{15}N_{coord}$ parameter is temperature, ligand exchange, and solvent dependent. [$^{1}H–^{15}N$] heteronuclear multiple bond coherence (HMBC) NMR spectra of ligand and from crystal sample were recorded in the CD_2Cl_2 solvent.

The ^{15}N chemical shifts of the terminal pyridyl nitrogen and the central pyridine nitrogen atom for free ligand are observed at δ = -89.052 and -74.570 ppm, respectively (Figure 72). Upon complex formation, these signals are observed at δ = -104.248 and -87.126ppm respectively (complex formed after mixing ligand and $AgPF_6$ salt in NMR solvent, Figure 73). In comparison with the ^{15}N chemical shifts of complex $[Ag_3\mathbf{19}_4][PF_6]_3\cdot C_4H_8O$ observed at δ = -107.108 and -91.290 ppm (Figure 74), the corresponding signals are shown at δ = -108.813 and 92.827 ppm in the spectrum of complex $[Ag_3\mathbf{19}_4][PF_6]_3$ (Figure 75). Similar behavior was observed even after changing the counter anion of silver salt (complex $[Ag_2\mathbf{19}_2][OTf]_2\cdot CH_2Cl_2$). The ^{15}N signals of complex $[Ag_2\mathbf{19}_2][OTf]_2\cdot CH_2Cl_2$ (in CD_2Cl_2) are observed at δ = -110.187 and -99.66 ppm (Figure 76).

Table 6. Experimental $\delta^{15}N$ and $\Delta\delta^{15}N_{coord}$ NMR Chemical Shifts in CD_2Cl_2.

Complex	$\delta^{15}N_{Complex}$	$\delta^{15}N_{Ligand}$	$\Delta\delta^{15}N_{coord}$
19 + $AgPF_6$	-104.25 -87.13	-89.05 -74.57	-15.20 -12.56
$[Ag_3\mathbf{19}_4][PF_6]_3\cdot C_4H_8O$	-107.11 -91.29	-89.05 -74.57	-18.06 -16.72
$[Ag_3\mathbf{19}_4][PF_6]_3$	-108.81 -92.83	-89.05 -74.57	-19.76 -18.26
$[Ag_2\mathbf{19}_2][OTf]_2\cdot CH_2Cl_2$	-110.19 -99.66	-89.05 -74.57	-21.14 -25.09

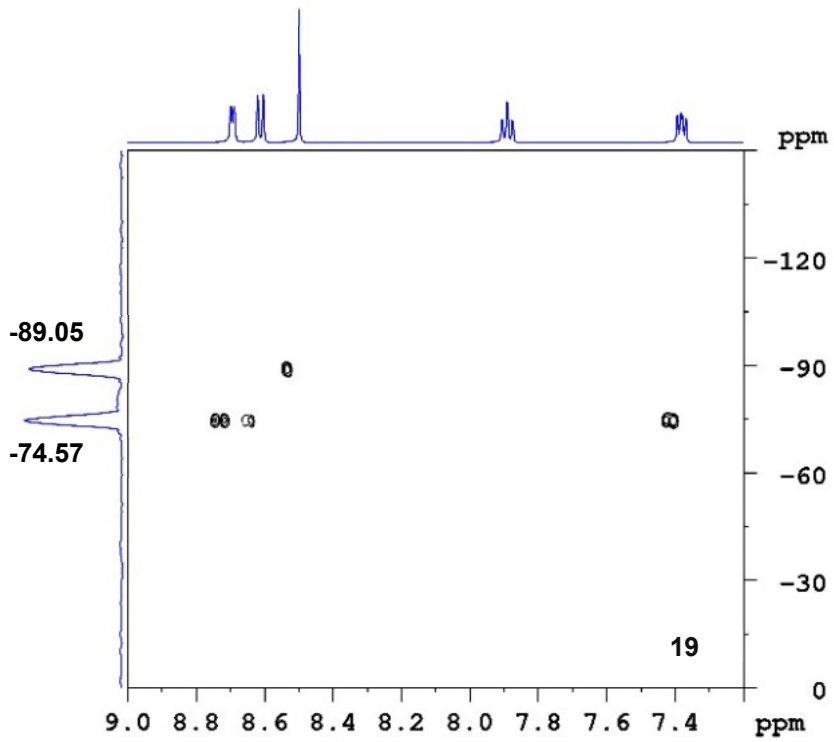

Figure 72. ^{1}H-^{15}N NMR spectra of **19** in CD_2Cl_2 solvent.

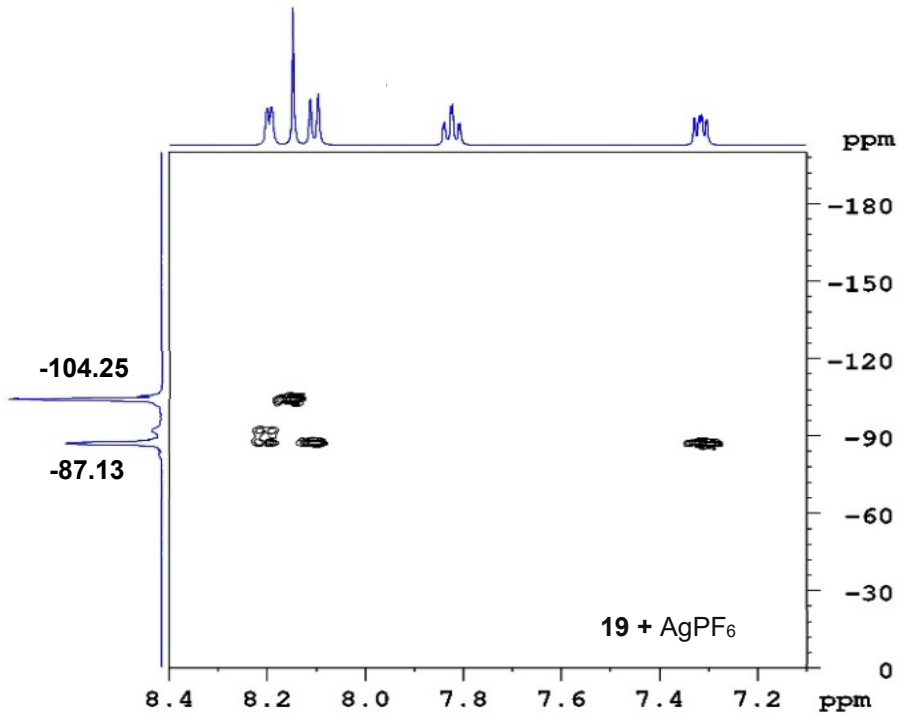

Figure 73. ^{1}H-^{15}N NMR spectra of **19** and silver hexafluorophosphate solution in CD_2Cl_2 solvent.

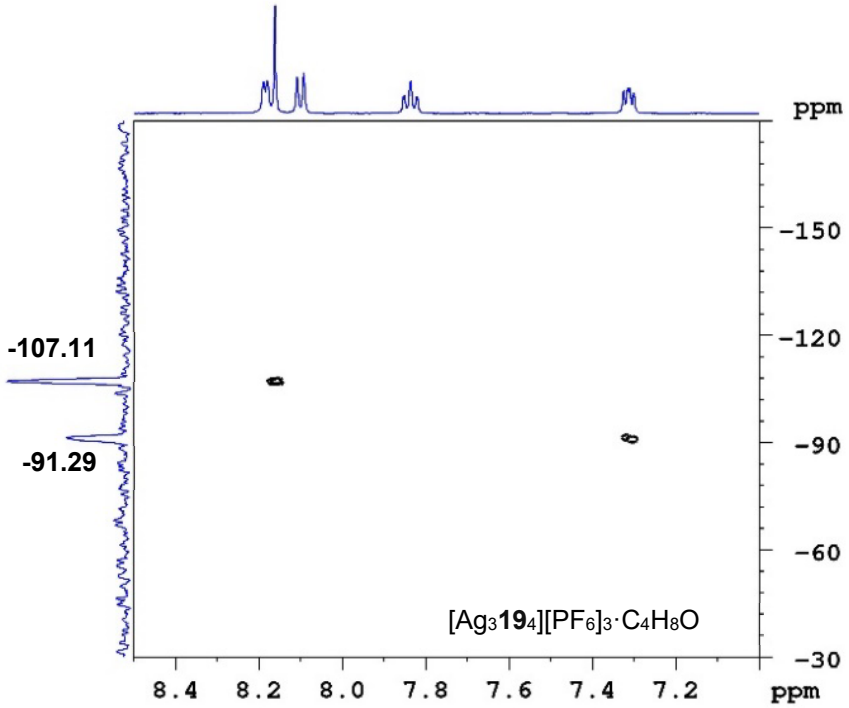

Figure 74. ^{1}H-^{15}N NMR spectra of complex $[Ag_3\mathbf{19}_4][PF_6]_3 \cdot C_4H_8O$ in CD_2Cl_2 solvent.

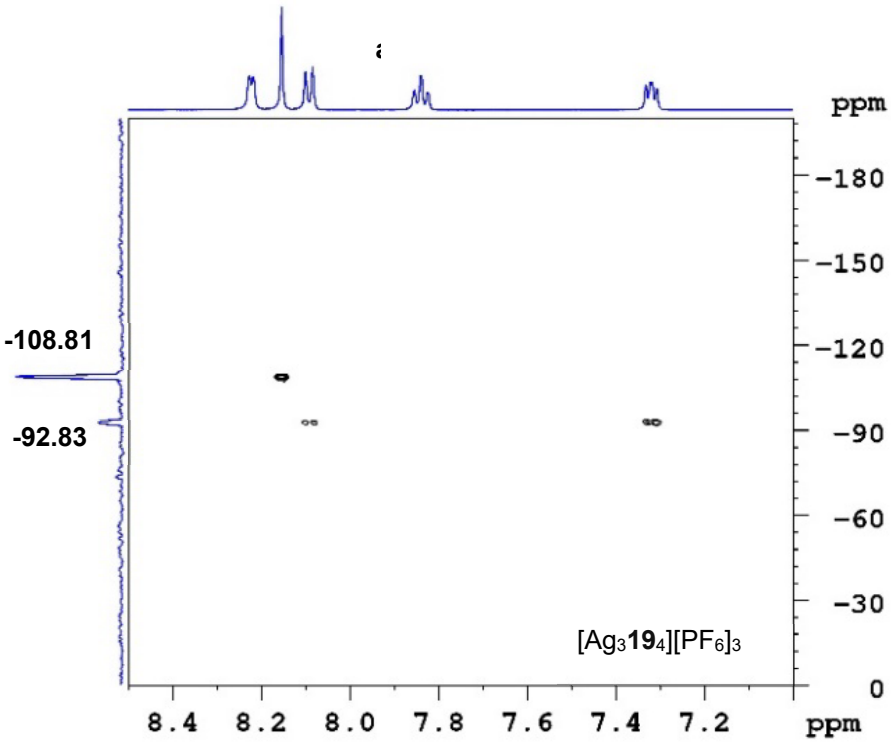

Figure 75. ^{1}H-^{15}N NMR spectra of complex $[Ag_3\mathbf{19}_4][PF_6]_2$ in CD_2Cl_2 solvent.

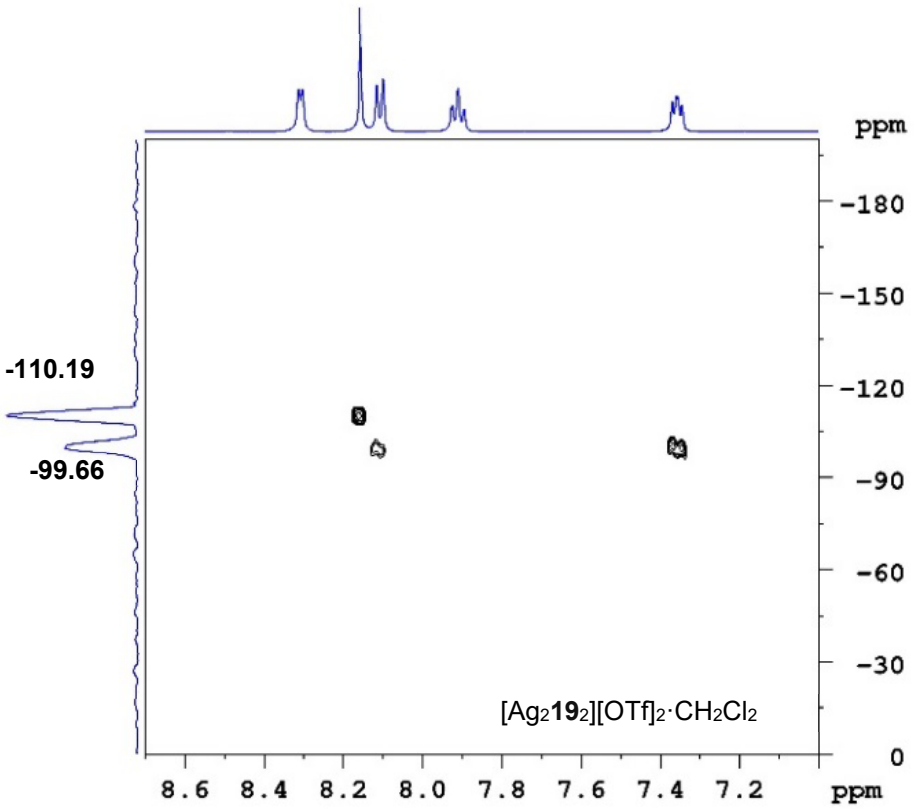

Figure 76. ^{1}H-^{15}N NMR spectra of complex $[Ag_2L_2][OTf]_2 \cdot CH_2Cl_2$ in CD_2Cl_2 solvent.

2.4.5 MS studies

Later to confirm helical silver(I) complexes into a solid state, ESI-MS has been performed for complexes. Electrospray ionization mass spectra are represented by three main sets of silver(I) terpyridine species: $[AgL]^+$, $[AgL_2]^+$ and $[Ag_2L_2](X)^+$ (where X is counterion). (Figure 77-79). The mass spectra of complexes were measured by Agilent 6560 ESI-IMTOF mode(+). Their MALDI-TOF(+) mass spectra display a base peak corresponding to the fragment $[Ag(L)]^+$ at ca. m/z = 375.9599, confirming the presence of the silver derivative. In the ESI(+), the experiment of exact mass for complex $[Ag_3\mathbf{19}_4][PF_6]_3 \cdot C_4H_8O$ and $[Ag_3\mathbf{19}_4][PF_6]_3$ shows the peaks corresponding to $[Ag(L)]^+$ at m/z = 375.9599 and $[Ag_2(L)_2]^+$ at m/z = 643.0161, respectively. Complex $[Ag_2\mathbf{19}_2][OTf]_2 \cdot CH_2Cl_2$ presents a peak at m/z = 898.8734 associated with the $[Ag_2\mathbf{19}_2OTf]^+$ fragment.

The ESI-MS spectra of complex $[Ag_3\mathbf{19}_4][PF_6]_3 \cdot C_4H_8O$, in CH_3CN solvent, show peaks at m/z 375.9628, 643.0166, 786.8896, 268,0642 and 290.0464 assigned to $\{LAg\}^+$, $\{L_2Ag\}^+$, $\{L_2Ag_2Cl\}^+$, $\{L+H\}^+$, and $\{L+Na\}^+$ respectively (Figure 77). The ESI-MS spectra of complex $[Ag_3\mathbf{19}_4][PF_6]_2$, in ACN solvent, show peaks at m/z 375.9605, 643.017, 290.046 and 268,0642 assigned to $\{LAg\}^+$, $\{L_2Ag\}^+$, $\{L+Na\}^+$, and $\{L+H\}^+$ respectively (Figure 78). The ESI-MS

spectra of complex $[Ag_2\mathbf{19}_2][OTf]_2 \cdot CH_2Cl_2$, in ACN solvent, show peaks at m/z 375.9672, 643.018, 786.8887, 898.8734, 517.8354, 517.8354 and 268,0647 assigned to $\{LAg\}^+$, $\{L_2Ag\}^+$, $\{L_2Ag_2Cl\}^+$, $\{L_2Ag_2OTf\}^+$ $\{LAg_2Cl\}^+$, and $\{L+H\}^+$ respectively (Figure 79).

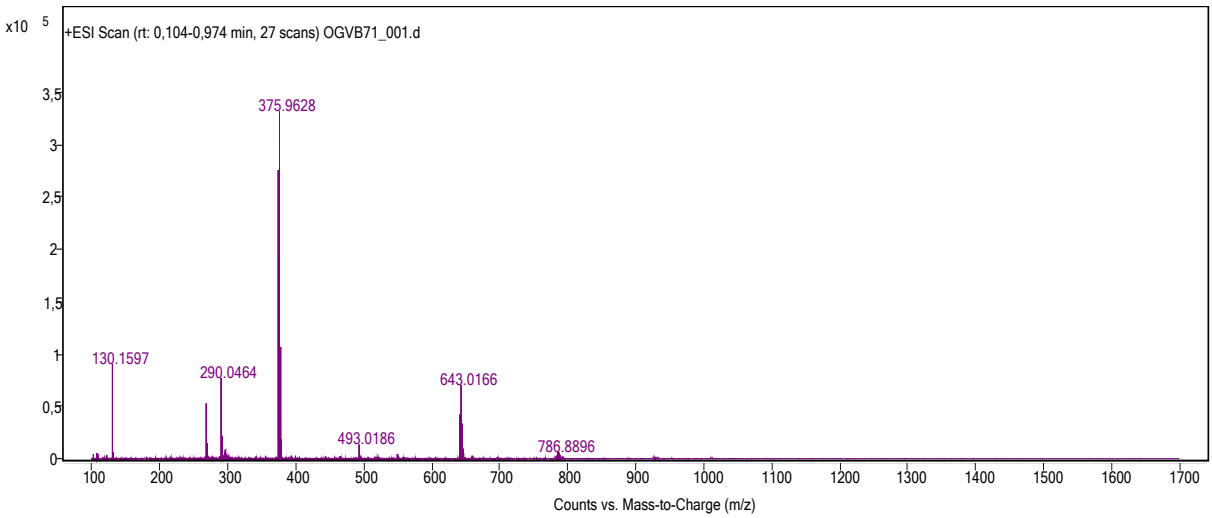

Figure 77. ESI-MS spectra of complex $[Ag_3\mathbf{19}_4][PF_6]_3 \cdot C_4H_8O$ in CH_3CN solvent.

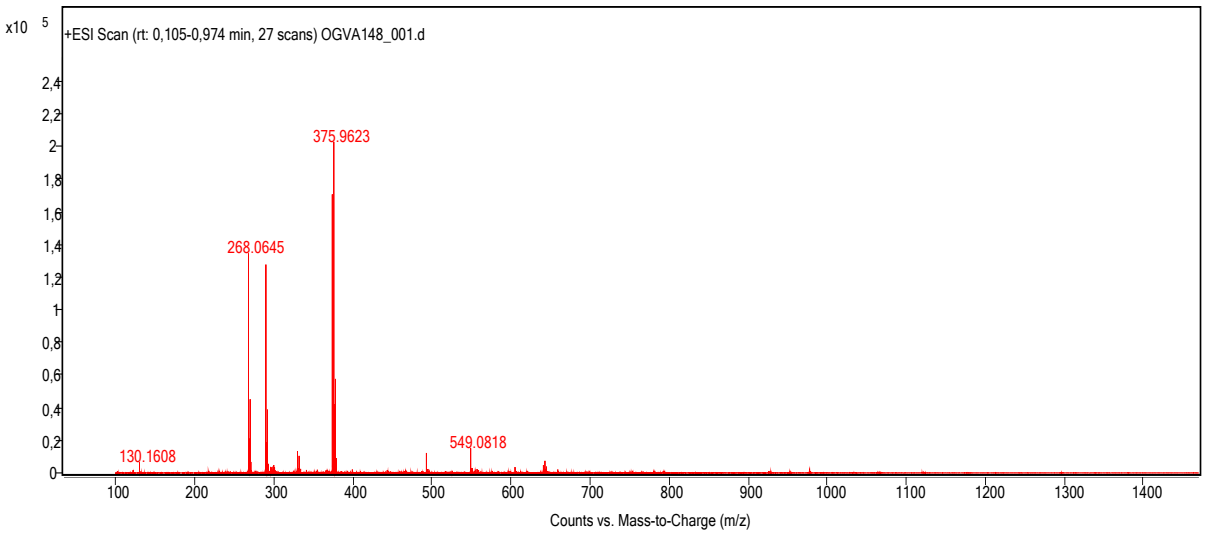

Figure 78. ESI-MS spectra of complex $[Ag_3\mathbf{19}_4][PF_6]_2$ in CH_3CN solvent.

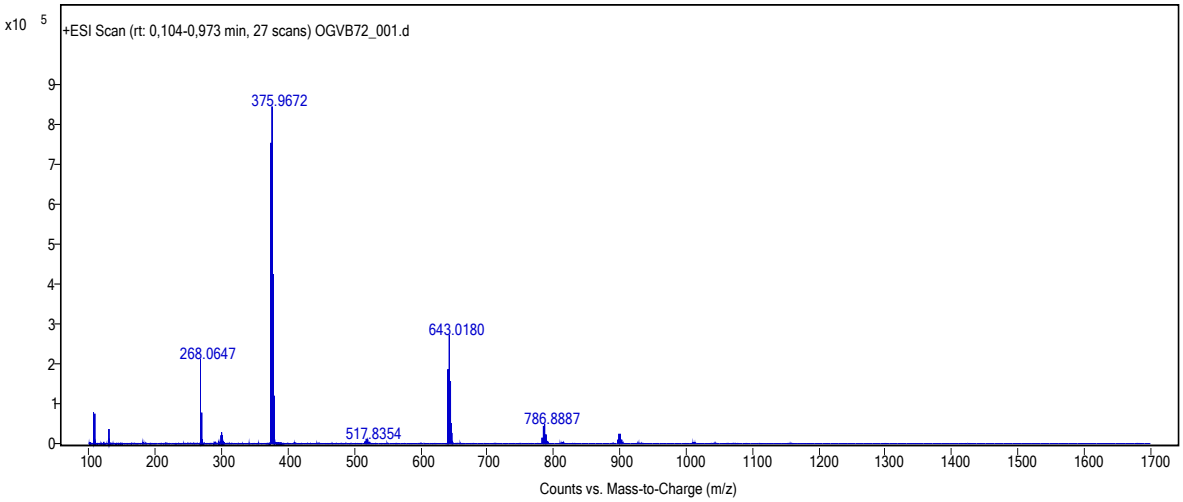

Figure 79. ESI-MS spectra of complex $[Ag_2\mathbf{19}_2][OTf]_2 \cdot CH_2Cl_2$ in CH_3CN solvent.

2.4.6 Halogen bonded and other complexes of terpyridine

Later we have tried to synthesize the halogen(I) ion complexes of terpyridine-based ligands and examined them by using ^{1}H-NMR and X-ray crystallographic techniques. A single crystal was grown by the slow evaporation process in an NMR tube. The complex was synthesized by mixing 1.0eq of 4′-Chloro-2,2′:6′,2″-terpyridine and 0.5 eq $AgPF_6$ into $CD_3CN\backslash CD_3Cl$ (9:1). The mixture was stirred at room temperature for 10 minutes. When all solids have dissolved and the mixture turned clear and colorless, 0.6 eq iodine (I_2) was added, and light-yellow silver iodide precipitates were filtered out from the solution, and the sample was used for NMR analysis and later left for slow evaporation process to grow a crystal (Scheme 9, Figure 80).

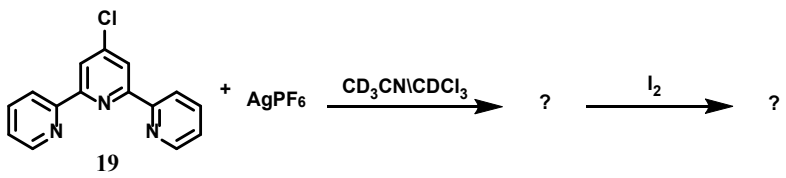

Scheme 9. Synthesis of iodonium complex of **19** in $CD_3CN\backslash CDCl_3$ solvent.

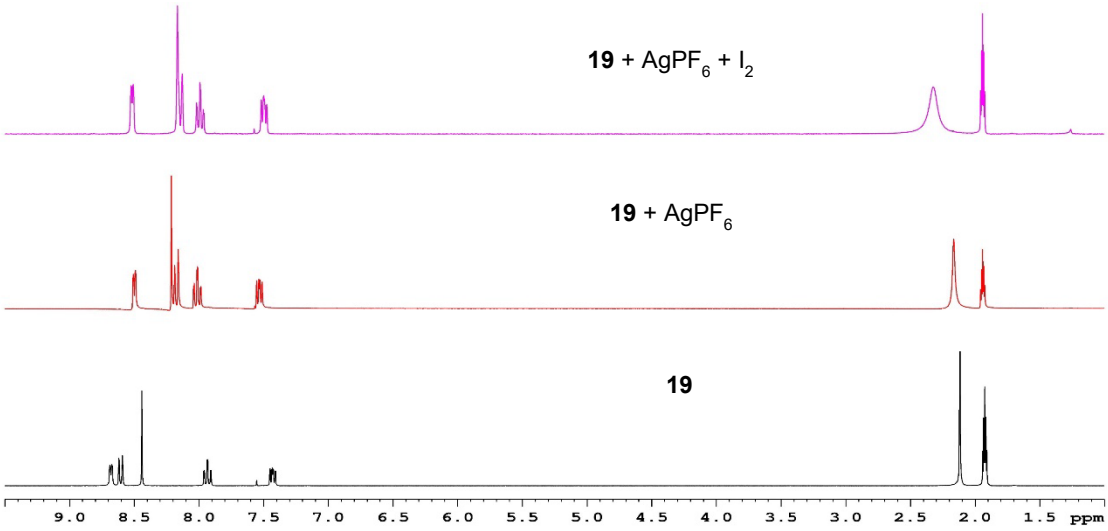

Figure 80. ^{1}H NMR spectra of **19** (black), silver complex (red) and Iodine(I) complex (pink), in $CD_3CN\backslash CD_3Cl$ (9:1) solvent.

Monitoring the ^{1}H NMR of Ligand and $AgPF_6$ mixture revealed the formation of silver complex of terpyridine ligand in solution. There is a shift in peaks in ^{1}H NMR if we compare free ligand with silver complex (Figure 80) however there is no convincing shift in iodine(I) complex when we compare silver and iodine(I) complexes NMR spectra in Figure 80. Alongside, we observed crystal structure (Figure 81) from the iodine(I) sample, and it came out as iodine interacts with silver, and it is hard to break multi-coordinated Ag-N bond by iodine.

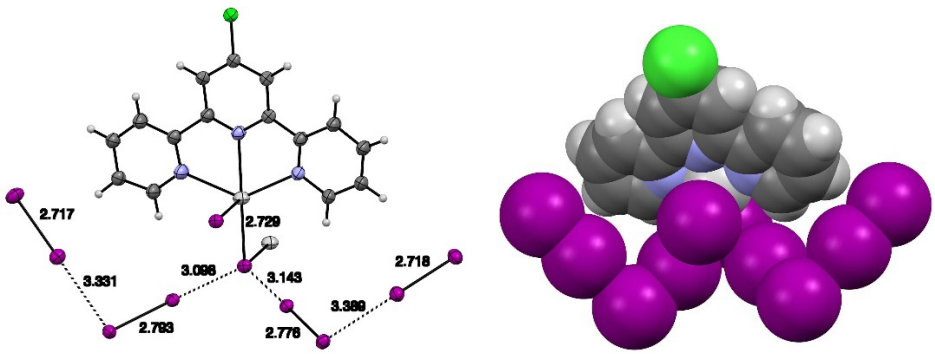

Figure 81. The structure of $[Ag\mathbf{19I}]_n[I]_n$. Anions and solvent molecules omitted for clarity. Ellipsoid are drawn at the 50% probability.

A similar analysis we have observed when we tried to form a bromonium ion complex of 4′-Chloro-2,2′:6′,2″-terpyridine. A single crystal was grown by the vapor diffusion process. The complex was synthesized by mixing 1.0eq of 4′-Chloro-2,2′:6′,2″-terpyridine, and 0.5eq $AgPF_6$ into DCM\THF. The mixture was stirred at room temperature for 10 minutes. When all solids have dissolved and the mixture turned clear and colourless, 0.6eq bromine (Br_2) was added,

and light-yellow silver bromide precipitates were filtered out from the solution and the sample was left to grow a crystal. (Scheme 10, Figure 82)

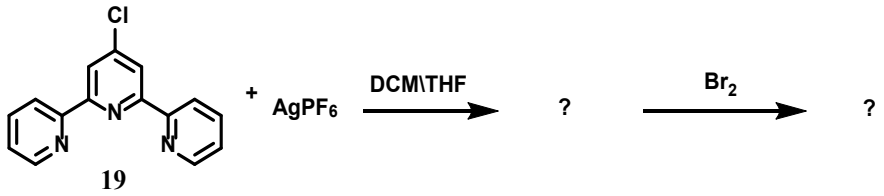

Scheme 10. Synthesis of bromonium complex of **19** in DCM\THF solvent.

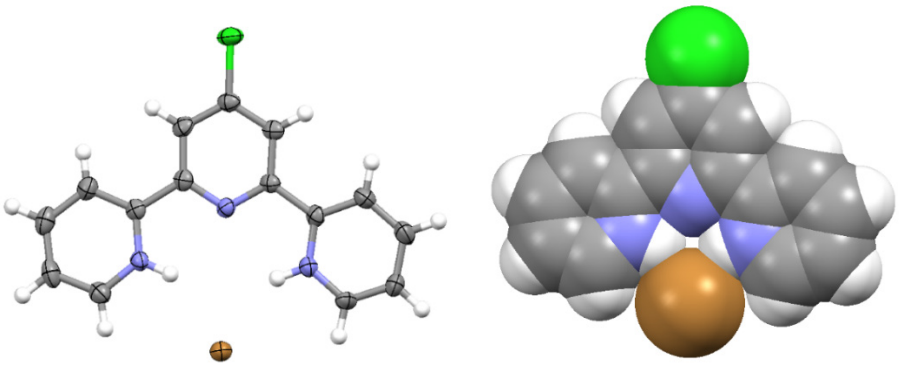

Figure 82. The Structure of protonated form of ligand **19**, the Br_3 and PF_6^- anions omitted for clarity.

The X-ray structural analysis of these complexes revealed several interesting features. Based on these we have tried other coordinating solvents and silver salt. First of all, we used $CHCl_3$:CH_3CN (3:1)/THF solvent to grow crystal by the vapor diffusion process and a single crystal from this sample have a binuclear [Ag**19**]$_2$[OTf]$_2$·MeCN)] unit (Figure 83) with a short silver-silver contact of 2.980Å and nitrogen from solvent form a bond with one of silver metal (2.555Å). Later we used $AgNO_3$ silver salt in DCM/THF, and a mononuclear complex crystal was observed where coordinating anions directly coordinated to the metal center (Figure 84). With $AgClO_4$ silver salt complex crystal, two binuclear metal complexes were in contact through argentophilic interaction with 3.008Å (Ag-Ag) bond length (Figure 85).

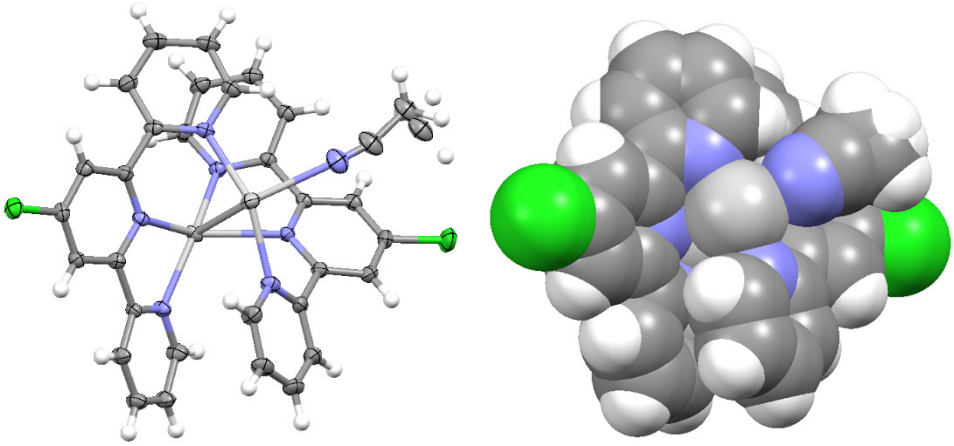

Figure 83. The structure of ligand **19** with AgOTf silver salt in $CHCl_3$:CH_3CN (3:1)/THF solvent. Anions and solvent molecules omitted for clarity. Ellipsoid are drawn at the 50% probability.

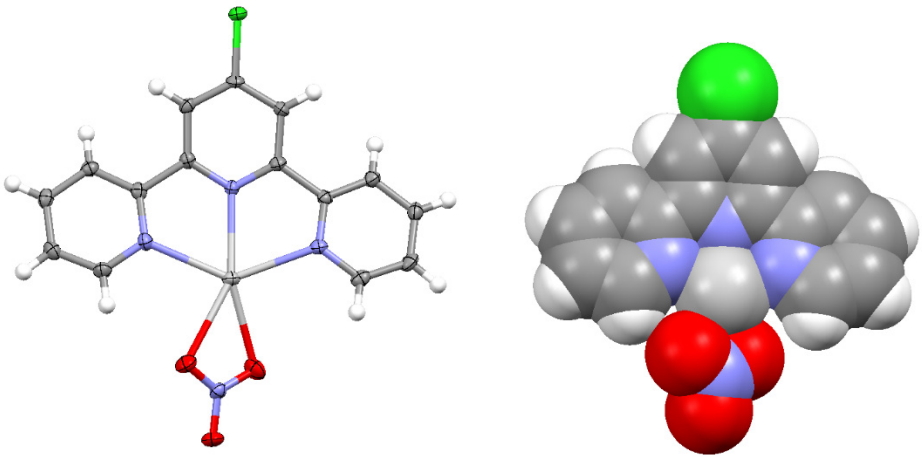

Figure 84. The structure of ligand **19** with $AgNO_3$ silver salt in DCM/THF solvent. Anions nd solvent molecules omitted for clarity. Ellipsoid are drawn at the 50% probability.

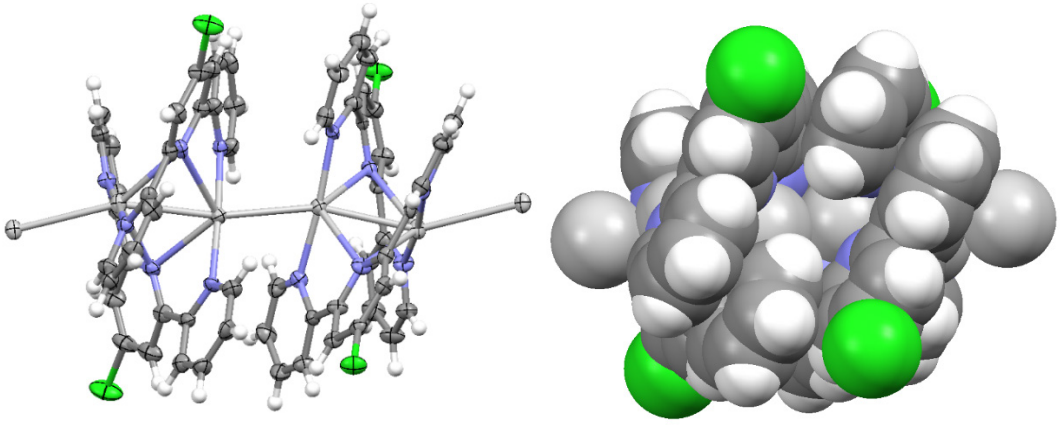

Figure 85. The structure of ligand **19** with $AgClO_4$ silver salt. In DCM/THF solvent. Anions and solvent molecules omitted for clarity. Ellipsoid are drawn at the 50% probability.

In conclusion we noticed from ^{1}H NMR analysis that hexadentate ligand form dimer in solution state and behave differently in solid state, depending on solvent and counterions, terpyridine

stabilized in different structural form. Silver(I) complexes are stable and multidirectional bonding of silver with ligand nitrogen makes hard for iodine and bromine to form $[L\cdots I\cdots L]^{+}$ and $[L\cdots I\cdots L]^{+}$ complexes, respectively.

CONCLUSIONS

The work within this thesis focused on the synthesis and characterization of the halogen(I) complexes from mono and multivalent ligands in solution, in the solid state and in the gas phase. Herein, the resulted structures were analyzed by single crystal X-ray diffraction (SCXRD), NMR experiments, and mass spectrometry. From NMR and solid state studies only the 2-halo-, 2-methyl, and 2,6-dimethylpyridine behave as previously reported halogen(I) pyridine complexes and shows downfield coordination shifts in the order Ag(I) < Br(I) < I(I) upon complexation in ^{1}H NMR spectra and which is supported by crystal studies. While the 2,6-dihalopyridines **6-9**, do not form I^{+}, Br^{+} and H^{+} complexes in solution or the solid state due to their insufficient nucleophilicity. Later from triazole, iodine(I) complexes have been synthesized and used as electron-rich parts to form $I^{+}\cdots Ag^{+}$ interaction with bis-bipyridine silver $\{[Ag(bpy)_2]PF_6\}$ complexes. This new I*Ag interaction is significantly stronger than previously reported argentophilic interactions.

Furthermore, new $[N\cdots Ag/I\cdots N]^{+}$ complexes were synthesized from tertiary $NR_1R_2R_3$ amines. The studies on these complexes give further insight into the effect of bulky groups on the ligand, making it hard to form iodine(I) complex from silver(I) complex and this result is confirmed by NMR and X-ray crystallography.

X-ray crystallography reveals severe crowding around the silver(I) ion by amines' alkyl and aryl groups and an intimate Ag···H-C and Ag···π interactions. This new strategy provides a starting point for the stabilization of I^{+} ions of the $[N\cdots I\cdots N]^{+}$ locality by weak non-covalent bonds and is an important step toward our future endeavors in this research line of halogen(I) ion supramolecular chemistry.

The thesis work also demonstrated the formation of different coordination structures with silver metal and multivalent ligands. Tridentate ligands form dimeric complexes which can further expand to multinuclear complexes in the solid state. For terpyridine silver(I) complexes the solvent molecules and counter ions play an important role. Hexadentate ligand stabilized in dimer form with silver metal and forms different coordination bonds in solid state. Depending on solvent and counterions, terpyridine is stabilized in different structural forms. In certain cases adding iodine(I2) into the terpyridine silver(I) complex lead to complex halogen-bonded structures with Ag-I···I-I halogen bonds.

3 EXPERIMENTAL

3.1 Synthesis, NMR and MS

Reagents were purchased from commercial suppliers and used without further purification. NMR spectra were recorded on a Bruker Avance 300 spectrometers. All signals are given as δ values in ppm using residual solvent signals as the internal standard. The ^{1}H,^{15}N HMBC spectra were measured with Bruker AVIII 500 MHz FT NMR spectrometer equipped with a CryoProbe Prodigy TCI in CD_2Cl_2, ppm scale referenced to external $\delta(CH_3{}^{15}NO_2) = 0.0$ ppm.
The mass spectra of complexes were measured by Agilent 6560 ESI-IMTOF mode (+).

3.2 X-ray crystallography

Single crystal was grown by the slow evaporation process. The solutions were subjected to slow evaporation to give single crystals suitable for X-ray diffraction analysis. The experimental and refinement details were measured using a Rigaku SuperNova dual-source Oxford diffractometer equipped with an Eos detector using mirror-monochromated Mo-Kα (λ = 0.71073 Å) radiation. The data collection and reduction were performed using the program CrysAlisPro,[149] with either an Empirical or Gaussian face index absorption correction method applied. Data collection was performed using the program *COLLECT,*[150] with data reduction performed using *HKL DENZO* and *SCALEPACK*,[151] with intensities absorption corrected using *SADABS.*[152] All structures were solved using ShelXT,[153] and refined by full-matrix least squares on F^2 using SHELXL [154] in the OLEX2 program package.[155]

Single crystal of [**1**-I-**1**]PF_6 was grown by the slow evaporation process. The complex was synthesized by mixing 2.0eq of 2-fluoropyridine and 1.0eq $AgPF_6$ into DCM. The mixture was stirred at room temperature for 10 minutes. When all solids have dissolved and the mixture

turned clear and colorless, 1.1 eq Iodine (I_2) was added and immediately light yellow silver iodide precipitates were filtered out from the solution and sample was left for slow evaporation process to grow the [bis(2-fluoropyridine)iodonium] complex crystal. Single crystal of [**4**-I-**4**]PF_6, [**5**-I-**5**]PF_6 and [**10**-I-**10**]PF_6 were grown by same process.

Single crystal of [**2**-Ag-**2**]PF_6 was grown by the slow evaporation process. The complex was synthesized by mixing 2.0eq of 2-chloropyridine and 1.0eq $AgPF_6$ into DCM. The mixture was stirred at room temperature for 10 minutes. When all solids have dissolved and the mixture turned clear and colorless, the solution was left for slow evaporation process to grow the [bis(2-chloropyridine)silver] complex crystal. Single crystal of [**4**-Ag-**4**]PF_6, [**5**-Ag-**5**]PF_6, [**9**-Ag-**9**]PF_6 and [**10**-Ag-**10**]PF_6 were grown by same synthesis procedure.

The single crystal of [**2**-Ag-**2**]OTf was grown by the slow evaporation process. The complex was synthesized by mixing 2.0eq of 2-chloropyridine and 1.0eq AgOTf into DCM. The mixture was stirred at room temperature for 10 minutes. When all solids have dissolved and the mixture turned clear and colorless, the solution was left for slow evaporation process to grow the [bis(2-chloropyridine)silver] complex crystal. Single crystal of [**7**-Ag-**7**]OTf, [**8**-Ag-**8**]OTf, [**9**-Ag-**9**]OTf and [**10**-Ag-**10**]OTf were grown by same synthesis procedure.

Single crystal of [**3**-Ag-**3**]PF_6 was grown by the slow evaporation process. The complex was synthesized by mixing 2.0eq of 2-bromopyridine and 1.0eq AgPF6 into DCM/ACN (8:2). The mixture was stirred at room temperature for 10 minutes. When all solids have dissolved and the mixture turned clear and colorless, the solution was left for slow evaporation process to grow the [bis(2-bromopyridine)silver] complex crystal. Later by following same procedure the single crystal of [**3**-I-**3**]PF_6 was grown, 1.1 eq Iodine (I_2) was added into the mixture of 2.0eq 2-bromopyridine and 1.0eq $AgPF_6$ into DCM/ACN (8:2), and immediately light yellow silver iodide precipitates were filtered out from the solution and sample was left for slow evaporation process to grow the [bis(2-bromopyridine)iodonium] complex crystal.

Single crystal of [**1**-Br-**1**]PF_6 was grown by the slow evaporation process. The complex was synthesized by mixing 2.0eq of 2-fluoropyridine and 1.0eq $AgPF_6$ into DCM. The mixture was stirred at room temperature for 10 minutes. When all solids have dissolved and the mixture turned clear and colorless, 1.1 eq bromine (Br_2) was added and immediately light yellow silver bromide precipitates were filtered out from the solution and sample was left for slow evaporation process to grow the [bis(2-fluoropyridine)bromonium] complex crystal. Single crystal of [**3**-Br-**3**]PF_6, [**4**-Br-**4**]PF_6, [**5**-Br-**5**]PF_6 and [**10**-Br-**10**]PF_6 were grown by same method.

Single crystal of [**5**-Br-**5**]Br_3 was grown by the slow evaporation process. The complex was synthesized by mixing 2.0eq of 2-methylpyridine and 1.0eq $AgPF_6$ into DCM. The mixture

was stirred at room temperature for 10 minutes. When all solids have dissolved and the mixture turned clear and colorless, 1.1 eq bromine (Br_2) was added and immediately light yellow silver bromide precipitates were filtered out from the solution and sample was left for slow evaporation process to grow the [bis(2-methylpyridine)bromonium] complex crystal. Single crystal of [**10**-Br-**10**]Br_3 was grown by the same way.

Single crystal of [**8**-Ag-**8**]BF_4 was grown by the slow evaporation process. The complex was synthesized by mixing 2.0eq of 2,6-Dibromopyridine and 1.0eq AgBF4 into DCM/ACN (8:2). The mixture was stirred at room temperature for 10 minutes. When all solids have dissolved and the mixture turned clear and colorless, the solution was left for slow evaporation process to grow the [bis(2,6-Dibromopyridine)silver] complex crystal.

Single crystal of [**10**-Br-**10**]OTf was grown by the slow evaporation process. The complex was synthesized by mixing 2.0eq of 2,6-Dimethylpyridine and 1.0eq AgOTf into DCM. The mixture was stirred at room temperature for 10 minutes. When all solids have dissolved and the mixture turned clear and colorless, 1.1 eq bromine (Br_2) was added and immediately light yellow silver bromide precipitates were filtered out from the solution and sample was left for slow evaporation process to grow the [bis(2,6-Dimethylpyridine)bromonium] complex crystal.

Synthesis and characterization of [**1**-Ag-**1**]PF_6, [**1**-I-**1**]PF_6, [**1**-Br-**1**]PF_6

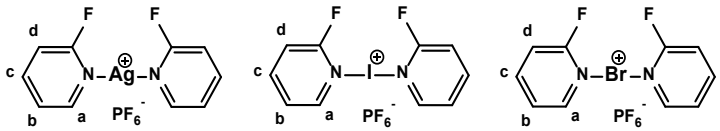

[**1**-Ag-**1**]PF_6 [**1**-I-**1**]PF_6 [**1**-Br-**1**]PF_6

To a solution of 2-fluoropyridine (40 mg, 0.412 mmol, 2.0 eq) in 1 mL of CD_2Cl_2 silver hexafluorophosphate (52.08mg, 0.206 mmol, 1.0 eq) was added. The mixture was stirred for 10 mins at room temperature. When all solids have dissolved and the mixture turned clear and colorless, the solution was divided into two equal portions. Iodine (I_2) (28.754 mg, 0.113 mmol, 1.1 eq) was added to the first portion and immediately light-yellow silver iodide precipitates and was filtered out from the solution leaving the [bis(2-fluoropyridine) iodonium] complex in the solution. Procedure with bromine (Br_2) (18.14 mg, 0.113 mmol, 1.1 eq) was done with the second portion for the [bis(2-fluoropyridine) bromonium] complex. The I^+ and Br^+ complexes were not isolated but used as such for the NMR experiments or crystallized as single crystal for the X-ray diffraction analysis.

[**1**-Ag-**1**]PF_6. ^{1}H NMR (300 MHz, CD_2Cl_2, [δ = ppm]) δ 8.33 (dd, ^2J = 5.31Hz, 1.50Hz, 2H, Ha), 7.79 (m, 2H, Hc), 7.18 (m, 2H, Hb), 6.92 (dd, ^{2}J = 8.39Hz, 0.56Hz, 2H, Hd).

[**1**-I-**1**]PF_6. ^{1}H NMR (300 MHz, CD_2Cl_2, [δ = ppm]) δ 8.21 (dd, ^{2}J = 3.71Hz, 2H, Ha), 7.84 (m, 2H, Hc), 7.21 (t, ^{3}J = 4.74Hz, 2H, Hb), 6.96 (d, ^{2}J = 7.51Hz, 2H, Hd).

[**1**-Br-**1**]PF_6. ^{1}H NMR (300 MHz, CD_2Cl_2, [δ = ppm]) δ 8.21 (d, ^2J = 3.88Hz, 2H, Ha), 7.82 (m, 2H, Hc), 7.21 (m, 1H, Hb), 6.95 (dd, ^2J = 8.28Hz, 2.52Hz, 2H, Hd).

[**1**H]$^+CF_3COO^-$. ^{1}H NMR (300 MHz, CD_2Cl_2, [δ = ppm]) δ 8.31 (dd, ^2J = 1.78Hz, 1.57Hz, 1H, Ha), 7.99 (m, 1H, Hc), 7.36 (m, 1H, Hb), 6.95 (d, ^2J = 8.29Hz, 1H, Hd).

Synthesis and characterization of [2-Ag-2]PF_6, [2-I-2]PF_6, [2-Br-2]PF_6

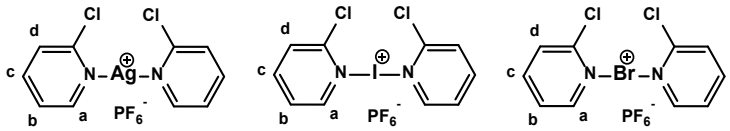

[2-Ag-2]PF_6 [2-I-2]PF_6 [2-Br-2]PF_6

To a solution of 2-chloropyridine (40 mg, 0.352 mmol, 2.0 eq) in 1 mL of CD_2Cl_2 silver hexafluorophosphate (44.50mg, 0.176 mmol, 1.0 eq) was added. The mixture was stirred for 10 mins at room temperature. When all solids have dissolved and the mixture turned clear and colorless, the solution was divided into two equal portions. Iodine (I_2) (24.61 mg, 0.097 mmol, 1.1 eq) was added to the first portion and immediately light-yellow silver iodide precipitates and was filtered out from the solution leaving the [bis(2-chloropyridine) iodonium] complex in the solution. Procedure with bromine (Br_2) (15.50 mg, 0.097 mmol, 1.1 eq) was done with the second portion for the [bis(2-chloropyridine) bromonium] complex. The I^+ and Br^+ complexes were not isolated but used as such for the NMR experiments or crystallized as single crystal for the X-ray diffraction analysis.

[**2**-Ag-**2**]PF_6. ^{1}H NMR (300 MHz, CD_2Cl_2, [δ = ppm]) δ 8.61 (dd, ^2J = 5.32Hz, 1.75Hz, 2H, Ha), 8.02 (dt, ^3J = 11.70Hz, ^2J = 1.88Hz 2H, Hc), 7.68 (d, ^2J = 8.25Hz, 2H, Hd), 7.58 (m, 1H, Hb).

[**2**-I-**2**]PF_6. ^{1}H NMR (300 MHz, CD_2Cl_2, [δ = ppm]) δ 8.94 (d, 2H, Ha), 8.38 (t, 2H, Hc), 7.70 (d, 2H, Hd), 7.35 (t, 2H, Hb).

[**2**-Br-**2**]PF_6. ^{1}H NMR (300 MHz, CD_2Cl_2, [δ = ppm]) δ 8.47 (d, 2H, Ha), 7.85 (t, 2H, Hc), 7.48 (d, 2H, Hd), 7.40 (t, 2H, Hb).

[**2**H]$^+CF_3COO^-$. ^{1}H NMR (300 MHz, CD_2Cl_2, [δ = ppm]) δ 8.49 (dd, ^2J = 5.03, ^2J = 1.28, 1H, Ha), 7.86 (dt, 1H, Hc), 7.47 (d, 1H, Hd), 7.42 (m, 1H, Hb).

Synthesis and characterization of [**3**-Ag-**3**]PF_6, [**3**-I-**3**]PF_6, [**3**-Br-**3**]PF_6

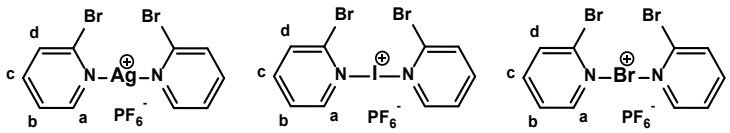

[**3**-Ag-**3**]PF_6 [**3**-I-**3**]PF_6 [**3**-Br-**3**]PF_6

To a solution of 2-bromopyridine (40 mg, 0.253 mmol, 2.0 eq) in 1 mL of CD_2Cl_2 silver hexafluorophosphate (32.11mg, 0.127 mmol, 1.0 eq) was added. The mixture was stirred for 10 mins at room temperature. When all solids have dissolved and the mixture turned clear and colorless, the solution was divided into two equal portions. Iodine (I_2) (17.64 mg, 0.069 mmol, 1.1 eq) was added to the first portion and immediately light-yellow silver iodide precipitates and was filtered out from the solution leaving the [bis(2-bromopyridine) iodonium] complex in the solution. Procedure with bromine (Br_2) (11.10 mg, 0.069 mmol, 1.1 eq) was done with the second portion for the [bis(2-bromopyridine) bromonium] complex. The I^+ and Br^+ complexes were not isolated but used as such for the NMR experiments or crystallized as single crystal for the X-ray diffraction analysis.

[**3**-Ag-**3**]PF_6. ^{1}H NMR (300 MHz, CD_2Cl_2, [δ = ppm]) δ 8.55 (ddd, 2H, Ha), 7.90 (dt, 2H, Hc), 7.81 (d, 2H, Hd), 7.61 (m, 2H, Hb).

[**3**-I-**3**]PF_6. ^{1}H NMR (300 MHz, CD_2Cl_2, [δ = ppm]) δ 8.99 (d, 2H, Ha), 8.07 (t, ^3J = 7.49Hz, 2H, Hc), 7.97 (d, ^{2}J = 7.43Hz, 2H, Hd), 7.54 (t, ^{3}J = 6.30Hz, 2H, Hb).

[**3**-Br-**3**]PF_6. ^{1}H NMR (300 MHz, CD_2Cl_2, [δ = ppm]) δ 8.78 (dd, ^{2}J = 5.70Hz, 1.54Hz, 2H, Ha), 8.05 (dt, ^3J = 11.81Hz, ^{2}J = 1.78Hz, 2H, Hc), 7.92 (dd, ^{2}J = 8.09Hz, 0.90Hz, 2H, Hd), 7.67 (m, 2H, Hb).

[**3**H]$^+CF_3COO^-$. ^{1}H NMR (300 MHz, CD_2Cl_2, [δ = ppm]) δ 8.53 (ddd, ^{2}J = 5.07Hz, J = 0.88Hz, 1H, Ha), 8.05 (dt, ^3J = 11.80Hz, ^{2}J = 2.04, 1H, Hc), 7.66 (td, ^{3}J = 0.88Hz, ^{2}J = 8.08Hz, 1H, Hd), 7.48 (m, 1H, Hb).

Synthesis and characterization of [4-Ag-4]PF_6, [4-I-4]PF_6, [4-Br-4]PF_6

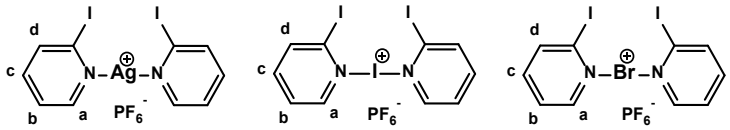

[4-Ag-4]PF_6 [4-I-4]PF_6 [4-Br-4]PF_6

To a solution of 2-iodopyridine (40 mg, 0.195 mmol, 2.0 eq) in 1 mL of CD_2Cl_2 silver hexafluorophosphate (24.78mg, 0.098 mmol, 1.0 eq) was added. The mixture was stirred for 10 mins at room temperature. When all solids have dissolved and the mixture turned clear and colorless, the solution was divided into two equal portions. Iodine (I_2) (13.58 mg, 0.053 mmol, 1.1 eq) was added to the first portion and immediately light-yellow silver iodide precipitates and was filtered out from the solution leaving the [bis(2-iodopyridine) iodonium] complex in the solution. Procedure with bromine (Br_2) (8.55 mg, 0.053 mmol, 1.1 eq) was done with the second portion for the [bis(2-iodopyridine) bromonium] complex. The I^+ and Br^+ complexes were not isolated but used as such for the NMR experiments or crystallized as single crystal for the X-ray diffraction analysis.

[**4**-Ag-**4**]PF_6. ^{1}H NMR (300 MHz, CD_2Cl_2, [δ = ppm]) δ 8.43 (m, 2H, Ha), 7.96 (m, 2H, Hd), 7.64 (dt, ^3J = 11.53Hz, ^2J = 2.06Hz, 2H, Hc), 7.57 (m, 2H, Hb).

[**4**-I-**4**]PF_6. ^{1}H NMR (300 MHz, CD_2Cl_2, [δ = ppm]) δ 9.08 (d, ^2J = 5.08Hz, 2H, Ha), 8.23 (d, ^2J = 7.88Hz, 2H, Hd), 7.81 (dt, ^3J = 7.34MHz, 2H, Hc), 7.54 (m, 2H, Hb).

[**4**-Br-**4**]PF_6. ^{1}H NMR (300 MHz, CD_2Cl_2, [δ = ppm]) δ 8.73 (d, 2H, Ha), 8.09 (d, 2H, Hd), 7.73 (dt, ^3J = 11.54, ^2J = 2.00, 2H, Hc), 7.62 (m, 2H, Hb).

[**4**H]$^+CF_3COO^-$. ^{1}H NMR (300 MHz, CD_2Cl_2, [δ = ppm]) δ 8.53 (d, 1H, Ha), 8.09 (m, 1H, Hd), 7.59 (dt, ^3J = 11.54, ^2J = 2.10, 1H, Hc), 7.51 (m, 1H, Hb).

Synthesis and characterization of [**5**-Ag-**5**]PF_6, [**5**-I-**5**]PF_6, [**5**-Br-**5**]PF_6

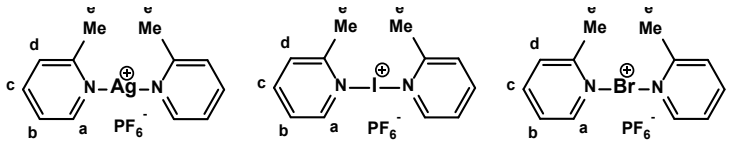

[**5**-Ag-**5**]PF_6 [**5**-I-**5**]PF_6 [**5**-Br-**5**]PF_6

To a solution of 2-methylpyridine (40 mg, 0.430 mmol, 2.0 eq) in 1 mL of CD_2Cl_2 silver hexafluorophosphate (54.36mg, 0.215 mmol, 1.0 eq) was added. The mixture was stirred for 10 mins at room temperature. When all solids have dissolved and the mixture turned clear and colorless, the solution was divided into two equal portions. Iodine (I_2) (29.95 mg, 0.118 mmol, 1.1 eq) was added to the first portion and immediately light-yellow silver iodide precipitates and was filtered out from the solution leaving the [bis(2-methylpyridine) iodonium] complex in the solution. Procedure with bromine (Br_2) (18.85 mg, 0.118 mmol, 1.1 eq) was done with the second portion for the [bis(2-methylpyridine) bromonium] complex. The I^+ and Br^+ complexes were not isolated but used as such for the NMR experiments or crystallized as single crystal for the X-ray diffraction analysis.

[**5**-Ag-**5**]PF_6. ^{1}H NMR (300 MHz, CD_2Cl_2, [δ = ppm]) δ 8.53 (d, 2H, Ha), 7.88 (dt, ^3J = 7.73Hz, 1.76Hz, 2H, Hc), 7.49 (d, ^{2}J = 7.88Hz, 2H, Hd), 7.37 (m, 2H, Hb), 2.75 (s, 6H, He).

[**5**-I-**5**]PF_6. ^{1}H NMR (300 MHz, CD_2Cl_2, [δ = ppm]) δ 8.88 (dd, ^{2}J = 5.75Hz, 1.08Hz, 2H, Ha), 8.06 (dt, ^3J = 11.59Hz, ^{2}J = 1.58Hz, 2H, Hc), 7.57 (d, ^{2}J = 7.73Hz, 2H, Hd), 7.33 (t, 2H, Hb), 2.83 (s, 3H, He).

[**5**-Br-**5**]PF_6. ^{1}H NMR (300 MHz, CD_2Cl_2, [δ = ppm]) δ 8.62 (d, ^{2}J = 4.34Hz, 2H, Ha), 8.01 (t, ^3J = 7.52Hz, 2H, Hc), 7.52 (d, ^{2}J = 7.88Hz, 2H, Hd), 7.43 (t, ^{3}J = 6.57Hz, 2H, Hb), 2.80 (s, 3H, He).

[**5**H]$^+CF_3COO^-$. ^{1}H NMR (300 MHz, CD_2Cl_2, [δ = ppm]) δ 8.77 (dd, ^{2}J = 5.73Hz, 6.84Hz, 1H, Ha), 8.20 (dt, 1H, Hc), 7.67 (m, 1H, Hd), 7.64 (m, 1H, Hb), 2.80 (s, 3H, He).

Synthesis and characterization of [6-Ag-6]PF_6, [6-I-6]PF_6, [6-Br-6]PF_6

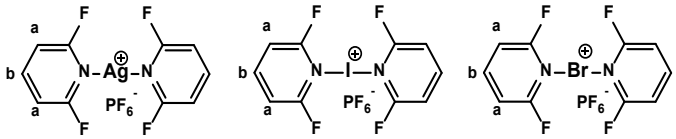

[**6**-Ag-**6**]PF_6 [**6**-I-**6**]PF_6 [**6**-Br-**6**]PF_6

To a solution of 2,6-Difluoropyridine (40 mg, 0.348 mmol, 2.0 eq) in 1 mL of CD_2Cl_2 silver hexafluorophosphate (44.00mg, 0.174 mmol, 1.0 eq) was added. The mixture was stirred for 10 mins at room temperature. When all solids have dissolved and the mixture turned clear and colorless, the solution was divided into two equal portions. Iodine (I_2) (24.24 mg, 0.095 mmol, 1.1 eq) was added to the first portion and immediately light-yellow silver iodide precipitates and was filtered out from the solution leaving the [bis(2,6-Difluoropyridine) iodonium] complex in the solution. Procedure with bromine (Br_2) (15.26 mg, 0.095 mmol, 1.1 eq) was done with the second portion for the [bis(2,6-Difluoropyridine) bromonium] complex. The I^+ and Br^+ complexes were not isolated but used as such for the NMR experiments or crystallized as single crystal for the X-ray diffraction analysis.

[**6**-Ag-**6**]PF_6. ^{1}H NMR (300 MHz, CD_2Cl_2, [δ = ppm]) δ 7.95 (m, 2H, Hb), 6.89 (d, ^2J = 8.02Hz, 4H, Ha).

[**6**-I-**6**]PF_6. ^{1}H NMR (300 MHz, CD_2Cl_2, [δ = ppm]) δ 7.913 (t, 2H, Hb), 6.851 (dd, ^2J = 8.02Hz, 0.59Hz, 4H, Ha).

[**6**-Br-**6**]PF_6. ^{1}H NMR (300 MHz, CD_2Cl_2, [δ = ppm]) δ 7.915 (t, 2H, Hb), 6.851 (dd, ^2J = 8.14Hz, 0.59Hz, 4H, Ha).

[**6**H]$^+CF_3COO^-$. ^{1}H NMR (300 MHz, CD_2Cl_2, [δ = ppm]) δ 8.01 (t, 1H, Hb), 6.93 (d, ^2J = 8.11Hz, 2H, Ha).

Synthesis and characterization of [**7**-Ag-**7**]PF_6, [**7**-I-**7**]PF_6, [**7**-Br-**7**]PF_6

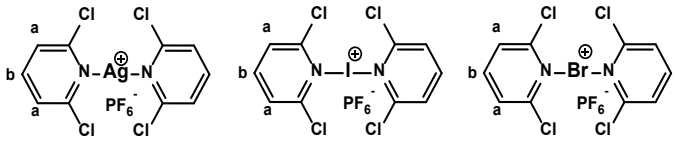

[**7**-Ag-**7**]PF_6 [**7**-I-**7**]PF_6 [**7**-Br-**7**]PF_6

To a solution of 2,6-Dichloropyridine (40 mg, 0.270 mmol, 2.0 eq) in 1 mL of CD_2Cl_2 silver hexafluorophosphate (34.13mg, 0.135 mmol, 1.0 eq) was added. The mixture was stirred for 10 mins at room temperature. When all solids have dissolved and the mixture turned clear and colorless, the solution was divided into two equal portions. Iodine (I_2) (18.91 mg, 0.074 mmol, 1.1 eq) was added to the first portion and immediately light-yellow silver iodide precipitates and was filtered out from the solution leaving the [bis(2,6-Dichloropyridine) iodonium] complex in the solution. Procedure with bromine (Br_2) (11.90 mg, 0.074 mmol, 1.1 eq) was done with the second portion for the [bis(2,6-Dichloropyridine) bromonium] complex. The I^+ and Br^+ complexes were not isolated but used as such for the NMR experiments or crystallized as single crystal for the X-ray diffraction analysis.

[**7**-Ag-**7**]PF_6. ^{1}H NMR (300 MHz, CD_2Cl_2, [δ = ppm]) δ 7.74 (t, ^3J = 7.87, 6H, Ha, Hb), 7.37 (d, ^2J = 7.80Hz, 4H, Ha).

[**7**-I-**7**]PF_6. ^{1}H NMR (300 MHz, CD_2Cl_2, [δ = ppm]) δ 7.67 (t, ^3J = 7.86, 6H, Ha, Hb), 7.31 (d, ^2J = 7.77Hz, 4H, Ha).

[**7**-Br-**7**]PF_6. ^{1}H NMR (300 MHz, CD_2Cl_2, [δ = ppm]) δ 7.64 (t, ^3J = 7.83Hz, 6H, Ha, Hb), 7.29 (d, ^2J = 7.92Hz, 4H, Ha).

[**7**H]$^+CF_3COO^-$. ^{1}H NMR (300 MHz, CD_2Cl_2, [δ = ppm]) δ 7.71 (t, ^3J = 7.80Hz, 1H, Hb), 7.34 (d, ^2J = 7.80Hz, 2H, Ha).

Synthesis and characterization of [**8**-Ag-**8**]PF_6, [**8**-I-**8**]PF_6, [**8**-Br-**8**]PF_6

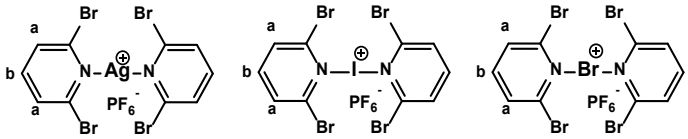

[**8**-Ag-**8**]PF_6 [**8**-I-**8**]PF_6 [**8**-Br-**8**]PF_6

To a solution of 2,6-Dibromopyridine (40 mg, 0.169 mmol, 2.0 eq) in 1 mL of CD_2Cl_2 silver hexafluorophosphate (21.49mg, 0.085 mmol, 1.0 eq) was added. The mixture was stirred for 10 mins at room temperature. When all solids have dissolved and the mixture turned clear and colorless, the solution was divided into two equal portions. Iodine (I_2) (11.80 mg, 0.046 mmol, 1.1 eq) was added to the first portion and immediately light-yellow silver iodide precipitates and was filtered out from the solution leaving the [bis(2,6-Dibromopyridine) iodonium] complex in the solution. Procedure with bromine (Br_2) (7.43 mg, 0.046 mmol, 1.1 eq) was done with the second portion for the [bis(2,6-Dibromopyridine) bromonium] complex. The I^+ and Br^+ complexes were not isolated but used as such for the NMR experiments or crystallized as single crystal for the X-ray diffraction analysis.

[**8**-Ag-**8**]PF_6. ^{1}H NMR (300 MHz, CD_2Cl_2, [δ = ppm]) δ 7.478 (m, 6H, Ha, Hb).

[**8**-I-**8**]PF_6. ^{1}H NMR (300 MHz, CD_2Cl_2, [δ = ppm]) δ 7.475 (m, 6H, Ha, Hb).

[**8**-Br-**8**]PF_6. ^{1}H NMR (300 MHz, CD_2Cl_2, [δ = ppm]) δ 7.472 (m, 6H, Ha, Hb).

[**8**H]$^+CF_3COO^-$. ^{1}H NMR (300 MHz, CD_2Cl_2, [δ = ppm]) δ 7.508 (m, 3H, Ha, Hb).

Synthesis and characterization of [**9**-Ag-**9**]PF_6, [**9**-I-**9**]PF_6, [**9**-Br-**9**]PF_6

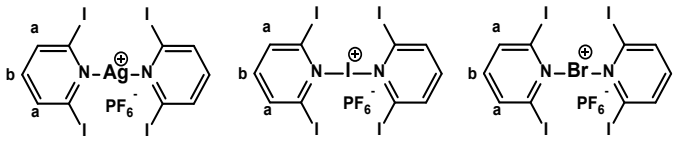

[**9**-Ag-**9**]PF_6 [**9**-I-**9**]PF_6 [**9**-Br-**9**]PF_6

To a solution of 2,6-Diiodopyridine (40 mg, 0.120 mmol, 2.0 eq) in 1 mL of CD_2Cl_2 silver hexafluorophosphate (15.28mg, 0.0604 mmol, 1.0 eq) was added. The mixture was stirred for 10 mins at room temperature. When all solids have dissolved and the mixture turned clear and colorless, the solution was divided into two equal portions. Iodine (I_2) (8.43mg, 0.0332 mmol, 1.1 eq) was added to the first portion and immediately light-yellow silver iodide precipitates and was filtered out from the solution leaving the [bis(2,6-Dibromopyridine) iodonium] complex in the solution. Procedure with bromine (Br_2) (5.30 mg, 0.0332 mmol, 1.1 eq) was done with the second portion for the [bis(2,6-Dibromopyridine) bromonium] complex. The I^+ and Br^+ complexes were not isolated but used as such for the NMR experiments or crystallized as single crystal for the X-ray diffraction analysis.

[**9**-Ag-**9**]PF_6. ^{1}H NMR (300 MHz, CD_2Cl_2, [δ = ppm]) δ 7.882 (d, ^2J = 7.83Hz 4H, Ha), δ 7.190 (t, ^3J = 7.85Hz, 2H, Hb).

[**9**-I-**9**]PF_6. ^{1}H NMR (300 MHz, CD_2Cl_2, [δ = ppm]) δ 7.766 (d, ^2J = 7.75Hz, 4H, Ha), δ 7.039 (t, ^2J = 7.75Hz, 2H, Hb).

[**9**-Br-**9**]PF_6. ^{1}H NMR (300 MHz, CD_2Cl_2, [δ = ppm]) δ 7.725 (d, ^2J = 7.82Hz, 4H, Ha), δ 6.989 (t, ^3J = 7.78Hz, 2H, Hb).

[**9**H]$^+CF_3COO^-$. ^{1}H NMR (300 MHz, CD_2Cl_2, [δ = ppm]) δ 7.756 (d, ^2J = 7.76Hz, 2H, Ha), δ 7.024 (t, ^3J = 7.74Hz, 1H, Hb).

Synthesis and characterization of [10-Ag-10]PF_6, [10-I-10]PF_6, [10-Br-10]PF_6

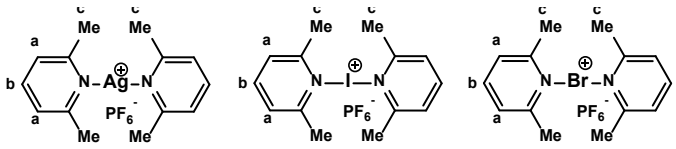

[**10**-Ag-**10**]PF_6 [**10**-I-**10**]PF_6 [**10**-Br-**10**]PF_6

To a solution of 2,6-Dimethylpyridine (40 mg, 0.373 mmol, 2.0 eq) in 1 mL of CD_2Cl_2 silver hexafluorophosphate (47.28mg, 0.187 mmol, 1.0 eq) was added. The mixture was stirred for 10 mins at room temperature. When all solids have dissolved and the mixture turned clear and colorless, the solution was divided into two equal portions. Iodine (I_2) (26.14 mg, 0.103 mmol, 1.1 eq) was added to the first portion and immediately light-yellow silver iodide precipitates and was filtered out from the solution leaving the [bis(2,6-Dimethylpyridine) iodonium] complex in the solution. Procedure with bromine (Br_2) (16.46 mg, 0.103 mmol, 1.1 eq) was done with the second portion for the [bis(2,6-Dimethylpyridine) bromonium] complex. The I^+ and Br^+ complexes were not isolated but used as such for the NMR experiments or crystallized as single crystal for the X-ray diffraction analysis.

[**10**-Ag-**10**]PF_6. ^{1}H NMR (300 MHz, CD_2Cl_2, [δ = ppm]) δ 7.77 (t, ^3J = 7.65Hz, 4H, Hb), 7.27 (d, ^2J = 7.58 Hz, 4H, Ha), 2.73 (s, 6H, Hc).

[**10**-I-**10**]PF_6. ^{1}H NMR (300 MHz, CD_2Cl_2, [δ = ppm]) δ 7.76 (t, ^3J = 7.77Hz, 4H, Hb), 7.20 (d, ^2J = 7.73Hz, 2H, Ha), 2.69 (s, 6H, Hc).

[**10**-Br-**10**]PF_6. ^{1}H NMR (300 MHz, CD_2Cl_2, [δ = ppm]) δ 7.80 (t, ^3J = 7.71Hz, 4H, Hb), 7.79 (d, ^2J = 7.61Hz, 2H, Ha), 2.74 (s, 6H, Hc).

[**10**H]$^+CF_3COO^-$. ^{1}H NMR (300 MHz, CD_2Cl_2, [δ = ppm]) δ 8.02 (t, ^3J = 7.86Hz, 1H, Hb), 7.39 (d, ^2J = 7.91Hz, 2H, Ha), 2.74 (s, 3H, Hc).

Synthesis and characterization of [**11**-Ag-**11**]PF_6

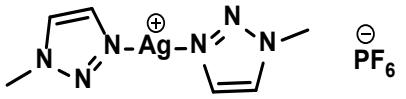

To a solution of 1-methyl-1*H*-1,2,3-triazole (**11**) (8.2 mg, 0.099 mmol, 2.0 eq) in 0.5 mL of CD_2Cl_2 was added silver hexafluorophosphate (12.4 mg, 0.049 mmol, 1.0 eq). The mixture in an NMR tube was stirred for 10 mins to give a silver complex [bis(1-methyl-1*H*-1,2,3-triazole) silver] hexafluorophosphate.

^{1}H NMR (300 MHz, CD_2Cl_2, [δ = ppm]): δ 7.85 (s, 1H), 7.80 (s, 1H), 4.17 (s, 3H).

Synthesis and characterization of [**11**-I-**11**]PF_6

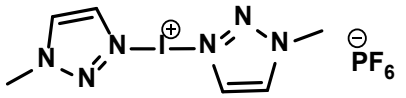

To the solution of [bis(1-methyl-1*H*-1,2,3-triazole)silver] hexafluorophosphate [**11**-Ag-**11**]PF_6, the elementary I_2 (12.5 mg, 0.049 mmol, 1.0 eq) was added. The NMR tube was centrifuged for 5 mins, an iodonium complex [bis(1-methyl-1*H*-1,2,3-triazole) iodonium] hexafluorophosphate was obtained.

^{1}H NMR (300 MHz, CD_2Cl_2 [δ = ppm]): δ 7.98 (s, 1H), 7.90 (s, 1H), 4.25 (s, 3H).

Synthesis and characterization of [**12**-Ag-**12**]PF_6, [**12**-I-**12**]PF_6

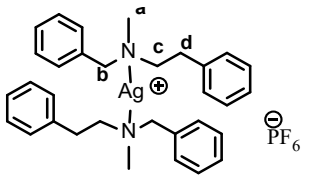

[**12**-Ag-**12**]PF_6

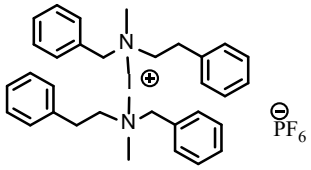

[**12**-I-**12**]PF_6

To a solution of **12** (10mg, 0.0444 mmol, 2.0 eq) in 1ml of CD_2Cl_2 silver hexafluorophosphate (5.61mg, 0.0222 mmol, 1.0 eq) was added. The mixture was stirred for 5 mins at room temperature. When all solids have dissolved and the

mixture turned clear and colorless, the solution were directly used to measure NMR without isolation. Iodine (I_2) (6.20mg, 0.0244 mmol, 1.1 eq) was added to the same solution and immediately light yellow silver iodide precipitates and was filtered out from the solution leaving the [**12**-I-**12**]$^+PF_6^-$ complex in the solution and used as such for the NMR experiments. The [**12**H]$^+CF_3COO^-$ complex was synthesized by mixing **12** (10mg, 0.0444 mmol,1.0eq) and CF_3COOH (5.06mg, 0.0444 mmol, 1.0eq) in 600µl of CD_2Cl_2.

[**12**-Ag-**12**]PF_6. ^{1}H NMR (300 MHz, CD_2Cl_2 [δ = ppm]): δ 3.58 (s, 4H, H_b), 2.51 (t, 4H, H_c), 2.47 (t, 4H, H_d), 2.16 (s, 6H, H_a).

[**12**-I-**12**]PF_6. ^{1}H NMR (300 MHz, CD_2Cl_2 [δ = ppm]): δ 4.31 (s, 4H, H_b), 3.35 (t, 4H, H_c), 3.09 (t, 4H, H_d), 2.76 (s, 6H, H_a).

Synthesis and characterization of [**13**-Ag-**13**]PF_6, [**13**-I-**13**]PF_6

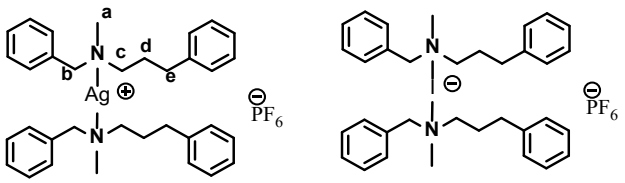

[**13**-Ag-**13**]PF_6 [**13**-I-**13**]PF_6

To a solution of **13** (10mg, 0.0418 mmol, 2.0 eq) in 1ml of CD_2Cl_2 silver hexafluorophosphate (5.28mg, 0.0209 mmol, 1.0 eq) was added. The mixture was stirred for 5 mins at room temperature. When all solids have dissolved and the mixture turned clear and colorless, the solution were directly used to measure NMR without isolation. Iodine (I_2) (5.83mg, 0.0230 mmol, 1.1 eq) was added to the same solution and immediately light yellow silver iodide precipitates and was filtered out from the solution leaving the [**13**-I-**13**]$^+PF_6^-$ complex in the solution and used as such for the NMR experiments. The [**13**H]$^+CF_3COO^-$ complex was synthesized by mixing **13** (10mg, 0.0418 mmol,1.0eq) and CF_3COOH (4.77mg, 0.0418 mmol, 1.0eq) in 600µl of CD_2Cl_2.

[**13**-Ag-**13**]PF_6. ^{1}H NMR (300 MHz, CD_2Cl_2 [δ = ppm]): δ 3.51 (s, 4H, H_b), 2.60 (t, 4H, H_e), 2.41 (t, 4H, H_c), 2.23 (s, 6H, H_a), 1.83 (m, 4H, H_d).

[**13**-I-**13**]PF_6. ^{1}H NMR (300 MHz, CD_2Cl_2 [δ = ppm]): δ 4.23 (s, 4H, H_b), 3.14 (t, 4H, H_e), 2.70 (s, 6H, H_a), 2.68 (t, 4H, H_c), 2.07 (m, 4H, H_d).

Synthesis and characterization of [14-Ag-14]PF_6, [14-I-14]PF_6

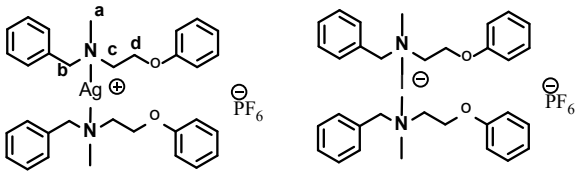

[**14**-Ag-**14**]PF_6

[**14**-I-**14**]PF_6

To a solution of **14** (10mg, 0.0414 mmol, 2.0 eq) in 1ml of CD_2Cl_2 silver hexafluorophosphate (5.24mg, 0.0207 mmol, 1.0 eq) was added. The mixture was stirred for 5 mins at room temperature. When all solids have dissolved and the mixture turned clear and colorless, the solution were directly used to measure NMR without isolation. Iodine (I_2) (5.78mg, 0.0228 mmol, 1.1 eq) was added to the same solution and immediately light yellow silver iodide precipitates and was filtered out from the solution leaving the [**14**-I-**14**]$^+PF_6^-$ complex in the solution and used as such for the NMR experiments. The [**14**H]$^+CF_3COO^-$ complex was synthesized by mixing **14** (10mg, 0.0414 mmol,1.0eq) and CF_3COOH (4.72mg, 0.0414 mmol, 1.0eq) in 600µl of CD_2Cl_2.

[**14**-Ag-**14**]PF_6. ^{1}H NMR (300 MHz, CD_2Cl_2 [δ = ppm]): δ 4.13 (t, 4H, H_d), 3.62 (s, 4H, H_b), 2.80 (t, 4H, H_c), 2.31 (s, 6H, H_a).

[**14**-I-**14**]PF_6. ^{1}H NMR (300 MHz, CD_2Cl_2 [δ = ppm]): δ 4.38 (t, 4H, H_b), 4.30 (s, 4H, H_d), 3.48 (t, 4H, H_c), 2.83 (s, 6H, H_a).

Synthesis and characterization of [15-Ag-15]PF_6, [15-I-15]PF_6

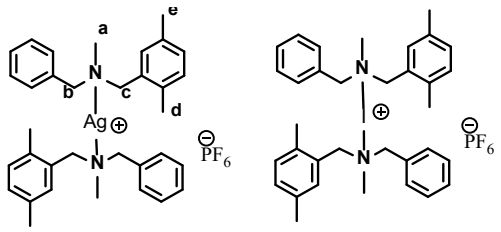

[**15**-Ag-**15**]PF_6 [**15**-I-**15**]PF_6

To a solution of **15** (10mg, 0.0418 mmol, 2.0 eq) in 1ml of CD_2Cl_2 silver hexafluorophosphate (5.29mg, 0.0209 mmol, 1.0 eq) was added. The mixture was stirred for 5 mins at room temperature. When all solids have dissolved and the mixture turned clear and colorless, the solution were directly used to measure NMR without isolation. Iodine (I_2) (5.84mg, 0.0230 mmol, 1.1 eq) was added to the same solution and immediately light yellow silver iodide precipitates and was filtered out from the solution leaving the [**15**-I-**15**]$^+PF_6^-$ complex in the solution and used as such for the NMR experiments. The [**15**H]$^+CF_3COO^-$ complex was synthesized by mixing **15** (10mg, 0.0418 mmol,1.0eq) and CF_3COOH (4.76mg, 0.0418 mmol, 1.0eq) in 600µl of CD_2Cl_2.

[**15**-Ag-**15**]PF_6. ^{1}H NMR (300 MHz, CD_2Cl_2 [δ = ppm]): δ 3.50 (s, 4H, H_b), 3.46 (s, 4H, H_c), 2.29 (s, 6H, H_e), 2.28 (s, 6H, H_d), 2.08 (s, 6H, H_a).

[**15**-I-**15**]PF_6. ^{1}H NMR (300 MHz, CD_2Cl_2 [δ = ppm]): δ 4.23 (s, 4H, H_b), 4.10 (s, 4H, H_c), 2.54 (s, 6H, H_a), 2.30 (s, 6H, H_e), 2.18 (s, 4H, H_d).

Synthesis and characterization of [16-Ag-16]PF_6, [16-I-16]PF_6

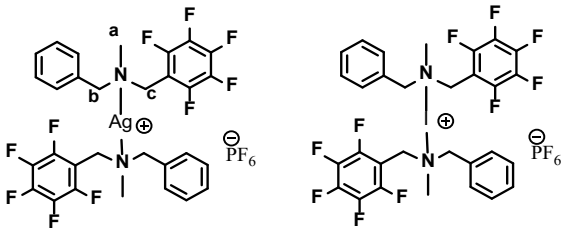

[**16**-Ag-**16**]PF_6 [**16**-I-**16**]PF_6

To a solution of **16** (10mg, 0.0332 mmol, 2.0 eq) in 1ml of CD_2Cl_2 silver hexafluorophosphate (4.20mg, 0.0166 mmol, 1.0 eq) was added. The mixture was stirred for 5 mins at room temperature. When all solids have dissolved and the mixture turned clear and colorless, the solution were directly used to measure NMR without isolation. Iodine (I_2) (4.63mg, 0.0183 mmol, 1.1 eq) was added to the same solution and immediately light yellow silver iodide precipitates and was filtered out from the solution leaving the [**16**-I-**16**]$^+PF_6^-$ complex in the solution and used as such for the NMR experiments. The [**16**H]$^+CF_3COO^-$ complex was synthesized by mixing **16** (10mg, 0.0332 mmol,1.0eq) and CF_3COOH (3.79mg, 0.0332 mmol, 1.0eq) in 600µl of CD_2Cl_2.

[**16**-Ag-**16**]PF_6. ^{1}H NMR (300 MHz, CD_2Cl_2 [δ = ppm]): δ 3.70 (s, 4H, H_b), 3.56 (s, 4H, H_c), 2.13 (s, 6H, H_a).

[**16**-I-**16**]PF_6. ^{1}H NMR (300 MHz, CD_2Cl_2 [δ = ppm]): δ 4.33 (s, 4H, H_b), 4.30 (s, 4H, H_c), 2.67 (s, 6H, H_a).

Synthesis and characterization of [17-Ag-17]PF_6, [17-I-17]PF_6

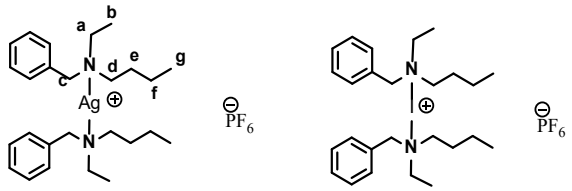

[17-Ag-17]PF_6 [17-I-17]PF_6

To a solution of **17** (10mg, 0.0520 mmol, 2.0 eq) in 1ml of CD_2Cl_2 silver hexafluorophosphate (6.58mg, 0.0260 mmol, 1.0 eq) was added. The mixture was stirred for 5 mins at room temperature. When all solids have dissolved and the mixture turned clear and colorless, the solution were directly used to measure NMR without isolation. Iodine (I_2) (7.26mg, 0.0286 mmol, 1.1 eq) was added to the same solution and immediately light yellow silver iodide precipitates and was filtered out from the solution leaving the [**17**-I-**17**]$^+PF_6^-$ complex in the solution and used as such for the NMR experiments. The [**17**H]$^+CF_3COO^-$ complex was synthesized by mixing **17** (10mg, 0.0520 mmol,1.0eq) and CF_3COOH (5.93mg, 0.0520 mmol, 1.0eq) in 600µl of CD_2Cl_2.

[**17**-Ag-**17**]PF_6. ^{1}H NMR (300 MHz, CD_2Cl_2 [δ = ppm]): δ 3.53 (s, 4H, H_c), 2.50 (q, 4H, H_a), 2.42 (t, 4H, H_d), 1.48 (m, 4H, H_e), 1.30 (m, 4H, H_f), 1.02 (t, 6H, H_b), 0.86 (t, 6H, H_g).

[**17**-I-**17**]PF_6. ^{1}H NMR (300 MHz, CD_2Cl_2 [δ = ppm]): δ 4.18 (s, 4H, H_c), 2.94 (q, 4H, H_a), 2.90 (t, 4H, H_d), 1.63 (m, 4H, H_e), 1.31 (m, 4H, H_f), 1.24 (t, 6H, H_b), 0.89 (t, 6H, H_g).

Synthesis and characterization of [**18**-Ag-**18**]PF_6

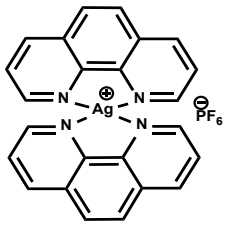

To a solution of 1,10-phenanthroline **18** (10 mg, 0.056 mmol, 2.0 eq) in 5 mL of CH_2Cl_2 was added silver hexafluorophosphate (7.01 mg, 0.028 mmol, 1.0 eq). The solution was stirred for 30 mins at room temperature. The reaction mixture was dried under vacuum to give the pale-yellow solid [(1,10-phenanthroline)$_2$ silver] hexafluorophosphate [**18**-Ag-**18**]PF_6 (18.0 g, 99%).
^{1}H NMR (Figure 63)

<u>^{1}H NMR</u> (300 MHz, $CDCl_3$): δ 9.18 (dd, *J* = 4.48, 1.6 Hz, 4H), 8.23 (dd, *J* = 1.72, 8.10 Hz, 4H), 7.77 (s, 4H), 7.62(dt, *J* = 12.52, 6.19 Hz, 4H).

Synthesis and characterization of [Ag_3**19**$_4$][PF_6]$_3$.C_4H_8O

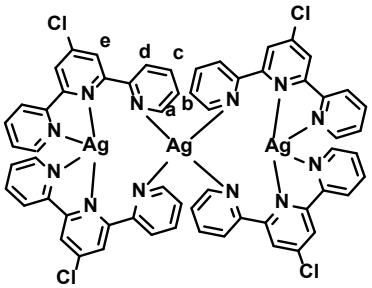

[Ag_3(4′-Chloro-2,2′:6′,2″-terpyridine)$_4$][PF_6]$_3$·C_4H_8O

To the clear solution of Ligand (30 mg, 0.112057 mmol) in CH_2Cl_2 (10 mL) $AgPF_6$ (14.165 mg, 0.056028 mmol) was added, white solution slowly forming. Reaction mixture was stirred for 10 min at room temperature, providing protection from direct sunlight. Crystals suitable for X-ray analysis were obtained by slow diffusion of THF solvent into DCM solution at room temperature.

^{1}H NMR (CD_2Cl_2, 500 MHz, [δ = ppm]): δ (ppm) = 8.260 (d, 4H, J = 4.19 Hz, H_d), 8.198 (s, 4H, H_e), 8.161 (d, 4H, J = 7.92 Hz, H_a), 7.821 (dt, 4H, J = 7.582 Hz, H_c), 7.323 (dt, 4H, J = 6.01Hz, H_b), 3.68 (t, H, THF), 1.82(m, H, THF), 1.53(s, H, water).

ESI-MS(+) (%): 375.9628 $[AgL]^+$, 643.0166 $[AgL_2]^+$, 786.8896 $[Ag_2L_2Cl]^+$ 268,0642 $[L+H]^+$ and 290.0464 $[L+ Na]^+$.

Synthesis and characterization of $[Ag_3\mathbf{19}_4][PF_6]_3$

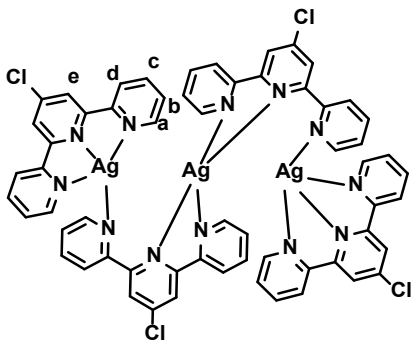

$[Ag_3(4'\text{-Chloro-2,2}':6',2''\text{-terpyridine})_4][PF_6]_3$

To the clear solution of Ligand (30 mg, 0.112057 mmol) in CH_2Cl_2 (10 mL) $AgPF_6$ (14.165 mg, 0.056028 mmol) was added, white solution slowly forming. Reaction mixture was stirred for 10 min at room temperature, providing protection from direct sunlight. Crystals suitable for X-ray analysis were obtained by slow diffusion of THF solvent into DCM solution at room temperature.

^{1}H NMR (CD_2Cl_2, 500 MHz, [δ = ppm]): δ (ppm) = 8.222 (d, 4H, J = 4.65 Hz, H_d), 8.153 (s, 4H, H_e), 8.092 (d, 4H, J = 7.97 Hz, H_a), 7.839 (dt, 4H, J = 7.65 Hz, H_c), 7.319 (dt, 4H, J = 6.19Hz, H_b), 1.53(s, H, water).

ESI-MS(+) (%): 375.9605 $[AgL]^+$, 643.017 $[AgL_2]^+$, 290.046 $[L+Na]^+$ and 268,0642 $[L+H]^+$.

Synthesis and characterization of $[Ag_2\mathbf{19}_2][OTf]_2.CH_2Cl_2$

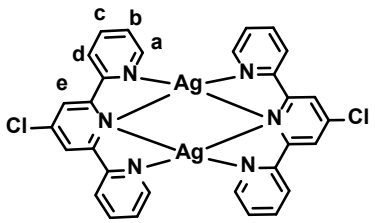

$[Ag_2(4'\text{-Chloro-2,2}':6',2''\text{-terpyridine})_2][OTf]_2 \cdot CH_2Cl_2$

To the clear solution of Ligand (10 mg, 0.0373 mmol) in CH_2Cl_2 (10 mL) AgOTf (4.798 mg, 0.01867 mmol) was added, white solution slowly forming. Reaction mixture was stirred for 10 min at room temperature, providing protection from direct sunlight. Crystals suitable for X-ray analysis were obtained by slow diffusion of THF solvent into DCM solution at room temperature.

<u>^{1}H NMR</u> (CD_2Cl_2, 500 MHz, [δ = ppm]): δ (ppm) = 8.540 (d, 4H, J = 4.21 Hz, H_d), 8.439 (d, 4H, J = 7.90 Hz, H_a), 8.389 (s, 4H, H_e), 7.873 (dt, 4H, J = 7.81 Hz H_c), 7.364 (dt, 4H, J = 6.04Hz, H_b), 1.52(s, H, water).

<u>ESI-MS(+) (%):</u> 375.9672 $[AgL]^+$, 643.018 $[AgL_2]^+$, 786.8887 $[Ag_2L_2Cl]^+$, 898.8734 $[Ag_2L_2OTf]^+$, 517.8354 $[Ag_2LCl]^+$ and 268,0647 $[L+H]^+$.

Synthesis and characterization of $[Ag_3\mathbf{19}_4][PF_6]_3.CH_2Cl_2$

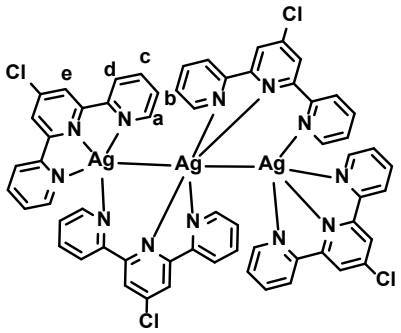

$[Ag_3(4'\text{-Chloro-2,2}':6',2''\text{-terpyridine})_4][PF_6]_3 \cdot CH_2Cl_2$

To the clear solution of Ligand (10 mg, 0.0373 mmol) in CH_2Cl_2 (10 mL) $AgPF_6$ (3.87 mg, 0.0186 mmol) was added, white solution slowly forming. Reaction mixture was stirred for 10 min at room temperature, providing protection from direct sunlight. Crystals suitable for X-ray analysis were obtained by slow diffusion of THF solvent into DCM solution at room temperature.

^{1}H NMR (CD_2Cl_2, 500 MHz, [δ = ppm]): δ (ppm) = 8.335 (d, 4H, J = 4.55 Hz, H_d), 8.237 (s, 4H, H_e), 8.237 (d, 4H, H_a) 7.837 (dt, 4H, J = 7.81 Hz, H_c), 7.335 (dt, 4H, J = 6.02Hz, H_b), 1.59(s, H, water).

Appendix 1. Crystal data and structure refinement for [1-Br-1]PF_6

Identification code	[**1**-Br-**1**]PF_6
Empirical formula	$C_{10}H_8BrF_8N_2P$
Formula weight	419.06
Temperature/K	170.0(1)
Crystal system	monoclinic
Space group	P2/c
a/Å	8.2062(16)
b/Å	6.3110(13)
c/Å	13.467(3)
α/°	90
β/°	90.19(3)
γ/°	90
Volume/$Å^3$	697.4(2)
Z	2
ρ_{calc}g/cm^3	1.996
μ/mm^{-1}	3.149
F(000)	408.0
Crystal size/mm^3	0.14 × 0.09 × 0.09
Radiation	MoKα (λ = 0.71073)
2Θ range for data collection/°	4.964 to 50.454
Index ranges	$-9 \leq h \leq 9$, $-6 \leq k \leq 7$, $-14 \leq l \leq 16$
Reflections collected	5116
Independent reflections	1269 [R_{int} = 0.0759, R_{sigma} = 0.0655]
Data/restraints/parameters	1269/0/102
Goodness-of-fit on F^2	1.057
Final R indexes [I>=2σ (I)]	R_1 = 0.0443, wR_2 = 0.0977
Final R indexes [all data]	R_1 = 0.0521, wR_2 = 0.1016
Largest diff. peak/hole / e $Å^{-3}$	0.39/-0.54

Appendix 2. Crystal data and structure refinement for [**2**-Ag-**2**]OTf

Identification code	[**2**-Ag-**2**]OTf
Empirical formula	$C_{11}H_8AgCl_2F_3N_2O_3S$
Formula weight	484.02
Temperature/K	120.0(1)
Crystal system	triclinic
Space group	P-1
a/Å	5.8623(3)
b/Å	11.3148(7)
c/Å	12.1378(9)
α/°	86.079(6)
β/°	76.576(6)
γ/°	78.384(5)
Volume/Å^3	766.88(9)
Z	2
ρ_{calc}g/cm^3	2.096
μ/mm^{-1}	1.844
F(000)	472.0
Crystal size/mm^3	0.316 × 0.27 × 0.181
Radiation	MoKα (λ = 0.71073)
2Θ range for data collection/°	6.904 to 50.488
Index ranges	$-7 \leq h \leq 7$, $-13 \leq k \leq 13$, $-14 \leq l \leq 14$
Reflections collected	8797
Independent reflections	2770 [R_{int} = 0.0299, R_{sigma} = 0.0295]
Data/restraints/parameters	2770/0/208
Goodness-of-fit on F^2	1.151
Final R indexes [I>=2σ (I)]	R_1 = 0.0288, wR_2 = 0.0722
Final R indexes [all data]	R_1 = 0.0301, wR_2 = 0.0729
Largest diff. peak/hole / e Å^{-3}	1.08/-0.72

Appendix 3 Crystal data and structure refinement for [2-Ag-2]PF_6

Identification code	[**2**-Ag-**2**]PF_6
Empirical formula	$C_{10}H_8AgCl_2F_6N_2P$
Formula weight	479.92
Temperature/K	120.01(10)
Crystal system	orthorhombic
Space group	Pmmn
a/Å	6.6257(3)
b/Å	15.1930(6)
c/Å	7.4063(3)
α/°	90
β/°	90
γ/°	90
Volume/$Å^3$	745.55(5)
Z	2
ρ_{calc}g/cm^3	2.138
μ/mm^{-1}	1.876
F(000)	464.0
Crystal size/mm^3	0.136 × 0.13 × 0.082
Radiation	MoKα (λ = 0.71073)
2Θ range for data collection/°	5.362 to 52.744
Index ranges	$-8 \leq h \leq 4$, $-15 \leq k \leq 18$, $-5 \leq l \leq 9$
Reflections collected	1874
Independent reflections	864 [R_{int} = 0.0351, R_{sigma} = 0.0457]
Data/restraints/parameters	864/27/77
Goodness-of-fit on F^2	1.081
Final R indexes [I>=2σ (I)]	R_1 = 0.0358, wR_2 = 0.0851
Final R indexes [all data]	R_1 = 0.0396, wR_2 = 0.0885
Largest diff. peak/hole / e $Å^{-3}$	0.83/-0.59

Appendix 4 Crystal data and structure refinement for [2-H-2]PF_6

Identification code	[**2**-H-**2**]PF_6
Empirical formula	$C_{10}H_9Cl_2F_6N_2P$
Formula weight	373.06
Temperature/K	120.00(10)
Crystal system	triclinic
Space group	P-1
a/Å	7.0392(15)
b/Å	7.5634(16)
c/Å	13.786(3)
α/°	92.706(18)
β/°	91.360(18)
γ/°	110.60(2)
Volume/Å^3	685.6(3)
Z	2
ρ_{calc}g/cm^3	1.807
μ/mm^{-1}	0.652
F(000)	372.0
Crystal size/mm^3	0.13 × 0.1 × 0.07
Radiation	MoKα (λ = 0.71073)
2Θ range for data collection/°	6.746 to 50.496
Index ranges	$-8 \leq h \leq 8$, $-9 \leq k \leq 8$, $-15 \leq l \leq 16$
Reflections collected	4203
Independent reflections	2463 [R_{int} = 0.0300, R_{sigma} = 0.0643]
Data/restraints/parameters	2463/0/190
Goodness-of-fit on F^2	1.044
Final R indexes [I>=2σ (I)]	R_1 = 0.0433, wR_2 = 0.0773
Final R indexes [all data]	R_1 = 0.0644, wR_2 = 0.0866
Largest diff. peak/hole / e Å^{-3}	0.30/-0.32

Appendix 5 Crystal data and structure refinement for [3-Ag-3]PF_6

Identification code	[**3**-Ag-**3**]PF_6
Empirical formula	$C_{10}H_8AgBr_2F_6N_2P$
Formula weight	568.84
Temperature/K	170
Crystal system	monoclinic
Space group	$P2_1/n$
a/Å	9.9427(5)
b/Å	10.4795(7)
c/Å	15.1278(5)
α/°	90
β/°	103.640(3)
γ/°	90
Volume/Å^3	1531.78(14)
Z	4
ρ_{calc}g/cm^3	2.467
μ/mm^{-1}	6.695
F(000)	1072.0
Crystal size/mm^3	0.36 × 0.2 × 0.16
Radiation	MoKα (λ = 0.71073)
2Θ range for data collection/°	4.466 to 52.734
Index ranges	$-8 \leq h \leq 12$, $-12 \leq k \leq 13$, $-18 \leq l \leq 18$
Reflections collected	8920
Independent reflections	3115 [R_{int} = 0.0429, R_{sigma} = 0.0577]
Data/restraints/parameters	3115/0/199
Goodness-of-fit on F^2	1.026
Final R indexes [I>=2σ (I)]	R_1 = 0.0378, wR_2 = 0.0698
Final R indexes [all data]	R_1 = 0.0595, wR_2 = 0.0767
Largest diff. peak/hole / e Å^{-3}	0.60/-0.77

Appendix 6 Crystal data and structure refinement for [3-Br-3]PF_6

Identification code	[**3**-Br-**3**]PF_6
Empirical formula	$C_{10}H_8Br_3F_6N_2P$
Formula weight	540.88
Temperature/K	120.01(10)
Crystal system	orthorhombic
Space group	Pmmn
a/Å	6.8150(5)
b/Å	14.5541(9)
c/Å	7.8136(5)
α/°	90
β/°	90
γ/°	90
Volume/$Å^3$	775.00(9)
Z	2
ρ_{calc}g/cm^3	2.318
μ/mm^{-1}	7.969
F(000)	512.0
Crystal size/mm^3	0.215 × 0.152 × 0.142
Radiation	MoKα (λ = 0.71073)
2Θ range for data collection/°	5.214 to 50.49
Index ranges	$-8 \leq h \leq 8$, $-17 \leq k \leq 12$, $-8 \leq l \leq 9$
Reflections collected	5010
Independent reflections	802 [R_{int} = 0.0425, R_{sigma} = 0.0275]
Data/restraints/parameters	802/0/68
Goodness-of-fit on F^2	1.149
Final R indexes [I>=2σ (I)]	R_1 = 0.0225, wR_2 = 0.0543
Final R indexes [all data]	R_1 = 0.0268, wR_2 = 0.0565
Largest diff. peak/hole / e $Å^{-3}$	0.55/-0.67

Appendix 7 Crystal data and structure refinement for [3-I-3]PF_6

Identification code	[**3**-I-**3**]PF_6
Empirical formula	$C_{10}H_8Br_2F_6IN_2P$
Formula weight	587.87
Temperature/K	170
Crystal system	monoclinic
Space group	C2/c
a/Å	23.7587(7)
b/Å	6.3272(2)
c/Å	31.6507(9)
α/°	90
β/°	90.9720(10)
γ/°	90
Volume/Å^3	4757.2(2)
Z	12
ρ_{calc}g/cm^3	2.462
μ/mm^{-1}	7.216
F(000)	3288.0
Crystal size/mm^3	0.24 × 0.18 × 0.1
Radiation	MoKα (λ = 0.71073)
2Θ range for data collection/°	2.574 to 52.744
Index ranges	$-29 \leq h \leq 29$, $-7 \leq k \leq 7$, $-39 \leq l \leq 39$
Reflections collected	8868
Independent reflections	4859 [R_{int} = 0.0310, R_{sigma} = 0.0355]
Data/restraints/parameters	4859/0/301
Goodness-of-fit on F^2	1.028
Final R indexes [I>=2σ (I)]	R_1 = 0.0320, wR_2 = 0.0687
Final R indexes [all data]	R_1 = 0.0433, wR_2 = 0.0736
Largest diff. peak/hole / e Å^{-3}	0.55/-0.89

Appendix 8 Crystal data and structure refinement for [4-Ag-4]PF_6

Identification code	[**4**-Ag-**4**]PF_6
Empirical formula	$C_{10}H_8AgF_6I_2N_2P$
Formula weight	662.82
Temperature/K	170
Crystal system	monoclinic
Space group	$P2_1/n$
a/Å	10.0847(4)
b/Å	10.5982(4)
c/Å	15.6011(5)
α/°	90
β/°	104.895(2)
γ/°	90
Volume/$Å^3$	1611.41(10)
Z	4
ρ_{calc}g/cm^3	2.732
μ/mm^{-1}	5.237
F(000)	1216.0
Crystal size/mm^3	0.16 × 0.16 × 0.08
Radiation	MoKα (λ = 0.71073)
2Θ range for data collection/°	4.354 to 61.696
Index ranges	$-14 \leq h \leq 13$, $-13 \leq k \leq 15$, $-21 \leq l \leq 22$
Reflections collected	17316
Independent reflections	4980 [R_{int} = 0.0391, R_{sigma} = 0.0429]
Data/restraints/parameters	4980/0/199
Goodness-of-fit on F^2	1.115
Final R indexes [I>=2σ (I)]	R_1 = 0.0346, wR_2 = 0.0804
Final R indexes [all data]	R_1 = 0.0503, wR_2 = 0.0852
Largest diff. peak/hole / e $Å^{-3}$	0.91/-0.98

Appendix 9 Crystal data and structure refinement for [4-Br-4]PF_6

Identification code	[**4**-Br-**4**]PF_6
Empirical formula	$C_{10}H_8BrF_6I_2N_2P$
Formula weight	634.86
Temperature/K	120.00(10)
Crystal system	monoclinic
Space group	C2/c
a/Å	11.7677(3)
b/Å	27.9608(6)
c/Å	15.8191(4)
α/°	90
β/°	106.296(3)
γ/°	90
Volume/$Å^3$	4995.9(2)
Z	12
ρ_{calc}g/cm^3	2.532
μ/mm^{-1}	6.326
F(000)	3504.0
Crystal size/mm^3	0.109 × 0.1 × 0.062
Radiation	MoKα (λ = 0.71073)
2Θ range for data collection/°	3.89 to 50.5
Index ranges	$-14 \leq h \leq 13$, $-33 \leq k \leq 33$, $-18 \leq l \leq 17$
Reflections collected	16339
Independent reflections	4527 [R_{int} = 0.0344, R_{sigma} = 0.0338]
Data/restraints/parameters	4527/0/271
Goodness-of-fit on F^2	1.035
Final R indexes [I>=2σ (I)]	R_1 = 0.0359, wR_2 = 0.0822
Final R indexes [all data]	R_1 = 0.0428, wR_2 = 0.0868
Largest diff. peak/hole / e $Å^{-3}$	4.44/-1.01

Appendix 10 Crystal data and structure refinement for [4-I-4]PF6

Identification code	[**4**-I-**4**]PF_6
Empirical formula	$C_{10}H_8F_6I_3N_2P$
Formula weight	681.85
Temperature/K	120.01(10)
Crystal system	monoclinic
Space group	$P2_1/c$
a/Å	7.7630(2)
b/Å	13.7428(3)
c/Å	15.8870(3)
α/°	90
β/°	97.510(2)
γ/°	90
Volume/$Å^3$	1680.37(7)
Z	4
ρ_{calc}g/cm^3	2.695
μ/mm^{-1}	5.729
F(000)	1240.0
Crystal size/mm^3	0.198 × 0.15 × 0.099
Radiation	MoKα (λ = 0.71073)
2Θ range for data collection/°	3.934 to 50.5
Index ranges	$-9 \leq h \leq 9$, $-16 \leq k \leq 16$, $-19 \leq l \leq 19$
Reflections collected	11627
Independent reflections	3044 [R_{int} = 0.0307, R_{sigma} = 0.0257]
Data/restraints/parameters	3044/0/199
Goodness-of-fit on F^2	1.056
Final R indexes [I>=2σ (I)]	R_1 = 0.0181, wR_2 = 0.0389
Final R indexes [all data]	R_1 = 0.0210, wR_2 = 0.0400
Largest diff. peak/hole / e $Å^{-3}$	0.39/-0.61

Appendix 11 Crystal data and structure refinement for [**5**-Ag-**5**]PF_6

Identification code	[**5**-Ag-**5**]PF_6
Empirical formula	$C_{12}H_{14}AgF_6N_2P$
Formula weight	439.09
Temperature/K	170.0(1)
Crystal system	triclinic
Space group	P-1
a/Å	8.7457(17)
b/Å	10.008(2)
c/Å	10.385(2)
α/°	70.98(3)
β/°	65.85(3)
γ/°	70.56(3)
Volume/Å^3	762.9(4)
Z	2
ρ_{calc}g/cm^3	1.912
μ/mm^{-1}	1.485
F(000)	432.0
Crystal size/mm^3	0.08 × 0.08 × 0.08
Radiation	MoKα (λ = 0.71073)
2Θ range for data collection/°	5.622 to 50.5
Index ranges	$-9 \leq h \leq 10$, $-11 \leq k \leq 11$, $-12 \leq l \leq 12$
Reflections collected	5337
Independent reflections	2738 [R_{int} = 0.0205, R_{sigma} = 0.0312]
Data/restraints/parameters	2738/25/237
Goodness-of-fit on F^2	1.050
Final R indexes [I>=2σ (I)]	R_1 = 0.0230, wR_2 = 0.0552
Final R indexes [all data]	R_1 = 0.0247, wR_2 = 0.0561
Largest diff. peak/hole / e Å^{-3}	0.41/-0.34

Appendix 12 Crystal data and structure refinement for [5-I-5]PF_6

Identification code	[**5**-I-**5**]PF_6
Empirical formula	$C_{12}H_{14}F_6IN_2P$
Formula weight	458.12
Temperature/K	293(2)
Crystal system	triclinic
Space group	P-1
a/Å	6.906(2)
b/Å	7.721(3)
c/Å	7.868(3)
α/°	82.82(3)
β/°	71.91(3)
γ/°	85.79(3)
Volume/Å^3	395.4(2)
Z	1
ρ_{calc}g/cm^3	1.924
μ/mm^{-1}	2.184
F(000)	222.0
Crystal size/mm^3	0.09 × 0.09 × 0.09
Radiation	MoKα (λ = 0.71073)
2Θ range for data collection/°	6.92 to 50.488
Index ranges	$-7 \leq h \leq 8$, $-9 \leq k \leq 9$, $-9 \leq l \leq 9$
Reflections collected	2508
Independent reflections	1430 [R_{int} = 0.0384, R_{sigma} = 0.0762]
Data/restraints/parameters	1430/0/104
Goodness-of-fit on F^2	1.052
Final R indexes [I>=2σ (I)]	R_1 = 0.0661, wR_2 = 0.1679
Final R indexes [all data]	R_1 = 0.0670, wR_2 = 0.1706
Largest diff. peak/hole / e Å^{-3}	3.66/-0.94

Appendix 13 Crystal data and structure refinement for [**5**-Br-**5**]Br_3

Identification code	[**5**-Br-**5**]Br_3
Empirical formula	$C_{12}H_{14}Br_4N_2$
Formula weight	505.89
Temperature/K	170.0(1)
Crystal system	triclinic
Space group	P-1
a/Å	6.7988(14)
b/Å	7.6795(15)
c/Å	9.0694(18)
α/°	102.10(3)
β/°	107.88(3)
γ/°	106.94(3)
Volume/$Å^3$	407.15(17)
Z	1
ρ_{calc}g/cm^3	2.063
μ/mm^{-1}	9.870
F(000)	240.0
Crystal size/mm^3	0.11 × 0.1 × 0.09
Radiation	MoKα (λ = 0.71073)
2Θ range for data collection/°	4.996 to 50.498
Index ranges	$-8 \leq h \leq 8$, $-9 \leq k \leq 7$, $-10 \leq l \leq 10$
Reflections collected	2899
Independent reflections	1474 [R_{int} = 0.0563, R_{sigma} = 0.0805]
Data/restraints/parameters	1474/0/86
Goodness-of-fit on F^2	1.055
Final R indexes [I>=2σ (I)]	R_1 = 0.0464, wR_2 = 0.1093
Final R indexes [all data]	R_1 = 0.0610, wR_2 = 0.1164
Largest diff. peak/hole / e $Å^{-3}$	0.99/-1.17

Appendix 14 Crystal data and structure refinement for [**5**-Br-**5**]PF_6

Identification code	[**5**-Br-**5**]PF_6
Empirical formula	$C_{12}H_{14}BrF_6N_2P$
Formula weight	411.13
Temperature/K	120.01(10)
Crystal system	triclinic
Space group	P-1
a/Å	6.7678(6)
b/Å	7.7861(8)
c/Å	7.8101(7)
α/°	81.889(8)
β/°	69.838(9)
γ/°	85.541(8)
Volume/$Å^3$	382.28(7)
Z	1
ρ_{calc}g/cm^3	1.786
μ/mm^{-1}	2.853
F(000)	204.0
Crystal size/mm^3	0.184 × 0.101 × 0.052
Radiation	MoKα (λ = 0.71073)
2Θ range for data collection/°	5.288 to 52.72
Index ranges	$-7 \leq h \leq 8$, $-9 \leq k \leq 9$, $-9 \leq l \leq 8$
Reflections collected	2577
Independent reflections	1568 [R_{int} = 0.0277, R_{sigma} = 0.0588]
Data/restraints/parameters	1568/0/104
Goodness-of-fit on F^2	1.026
Final R indexes [I>=2σ (I)]	R_1 = 0.0362, wR_2 = 0.0661
Final R indexes [all data]	R_1 = 0.0394, wR_2 = 0.0677
Largest diff. peak/hole / e $Å^{-3}$	0.48/-0.38

Appendix 15 Crystal data and structure refinement for [5-I-5]PF_6

Identification code	[**5**-I-**5**]PF_6
Empirical formula	$C_{12}H_{14}F_6IN_2P$
Formula weight	458.12
Temperature/K	120.01(10)
Crystal system	triclinic
Space group	P-1
a/Å	6.906(2)
b/Å	7.721(3)
c/Å	7.868(3)
α/°	82.82(3)
β/°	71.91(3)
γ/°	85.79(3)
Volume/$Å^3$	395.4(2)
Z	1
ρ_{calc}g/cm^3	1.924
μ/mm^{-1}	2.184
F(000)	222.0
Crystal size/mm^3	0.11 × 0.08 × 0.07
Radiation	MoKα (λ = 0.71073)
2Θ range for data collection/°	6.92 to 50.488
Index ranges	$-7 \leq h \leq 8$, $-9 \leq k \leq 9$, $-9 \leq l \leq 9$
Reflections collected	2511
Independent reflections	1431 [R_{int} = 0.0385, R_{sigma} = 0.0762]
Data/restraints/parameters	1431/0/104
Goodness-of-fit on F^2	1.091
Final R indexes [I>=2σ (I)]	R_1 = 0.0667, wR_2 = 0.1745
Final R indexes [all data]	R_1 = 0.0676, wR_2 = 0.1769
Largest diff. peak/hole / e $Å^{-3}$	3.62/-0.97

Appendix 16 Crystal data and structure refinement for [**7**-Ag-**7**]OTf

Identification code	[**7**-Ag-**7**]OTf
Empirical formula	$C_{11}H_6AgCl_4F_3N_2O_3S$
Formula weight	552.91
Temperature/K	170.0(1)
Crystal system	monoclinic
Space group	$P2_1/c$
a/Å	7.6468(15)
b/Å	16.640(3)
c/Å	14.189(3)
α/°	90
β/°	96.82(3)
γ/°	90
Volume/Å^3	1792.7(6)
Z	4
ρ_{calc}g/cm^3	2.049
μ/mm^{-1}	1.880
F(000)	1072.0
Crystal size/mm^3	0.12 × 0.092 × 0.071
Radiation	MoKα (λ = 0.71073)
2Θ range for data collection/°	3.788 to 50.484
Index ranges	$-9 \leq h \leq 8$, $-19 \leq k \leq 19$, $-17 \leq l \leq 17$
Reflections collected	18651
Independent reflections	3245 [R_{int} = 0.0623, R_{sigma} = 0.0546]
Data/restraints/parameters	3245/0/226
Goodness-of-fit on F^2	1.044
Final R indexes [I>=2σ (I)]	R_1 = 0.0396, wR_2 = 0.0611
Final R indexes [all data]	R_1 = 0.0700, wR_2 = 0.0683
Largest diff. peak/hole / e Å^{-3}	0.44/-0.46

Appendix 17 Crystal data and structure refinement for [8-Ag-8]BF_4

Identification code	[**8**-Ag-**8**]BF_4
Empirical formula	$C_{10}H_6AgBBr_4F_4N_2$
Formula weight	668.49
Temperature/K	120.01(10)
Crystal system	monoclinic
Space group	C2/c
a/Å	8.3835(3)
b/Å	14.2754(5)
c/Å	13.0402(6)
α/°	90
β/°	95.697(4)
γ/°	90
Volume/$Å^3$	1552.91(11)
Z	4
ρ_{calc}g/cm^3	2.859
μ/mm^{-1}	11.625
F(000)	1232.0
Crystal size/mm^3	0.148 × 0.086 × 0.059
Radiation	MoKα (λ = 0.71073)
2Θ range for data collection/°	5.656 to 52.734
Index ranges	$-10 \leq h \leq 5$, $-15 \leq k \leq 17$, $-15 \leq l \leq 16$
Reflections collected	3118
Independent reflections	1593 [R_{int} = 0.0230, R_{sigma} = 0.0420]
Data/restraints/parameters	1593/0/115
Goodness-of-fit on F^2	1.029
Final R indexes [I>=2σ (I)]	R_1 = 0.0277, wR_2 = 0.0453
Final R indexes [all data]	R_1 = 0.0353, wR_2 = 0.0479
Largest diff. peak/hole / e $Å^{-3}$	0.54/-0.54

Appendix 18 Crystal data and structure refinement for [8-Ag-8]OTf

Identification code	[**8**-Ag-**8**]OTf
Empirical formula	$C_{11}H_6AgBr_4F_3N_2O_3S$
Formula weight	730.75
Temperature/K	170.0(1)
Crystal system	monoclinic
Space group	C2/c
a/Å	30.730(6)
b/Å	8.8017(18)
c/Å	14.882(3)
α/°	90
β/°	111.52(3)
γ/°	90
Volume/Å^3	3744.5(15)
Z	8
ρ_{calc}g/cm^3	2.592
μ/mm^{-1}	9.767
F(000)	2720.0
Crystal size/mm^3	0.18 × 0.14 × 0.14
Radiation	MoKα (λ = 0.71073)
2Θ range for data collection/°	4.842 to 50.49
Index ranges	$-34 \leq h \leq 36$, $-10 \leq k \leq 10$, $-17 \leq l \leq 16$
Reflections collected	15262
Independent reflections	3381 [R_{int} = 0.0659, R_{sigma} = 0.0658]
Data/restraints/parameters	3381/0/226
Goodness-of-fit on F^2	1.074
Final R indexes [I>=2σ (I)]	R_1 = 0.0373, wR_2 = 0.0580
Final R indexes [all data]	R_1 = 0.0669, wR_2 = 0.0660
Largest diff. peak/hole / e Å^{-3}	0.65/-0.58

Appendix 19 Crystal data and structure refinement for [9-Ag-9]PF_6

Identification code	[**9**-Ag-**9**]PF_6
Empirical formula	$C_{10}H_6AgF_6I_4N_2P$
Formula weight	914.61
Temperature/K	120.01(10)
Crystal system	triclinic
Space group	P-1
a/Å	8.4754(3)
b/Å	8.9115(3)
c/Å	13.8263(4)
α/°	84.557(3)
β/°	88.153(3)
γ/°	63.176(4)
Volume/Å^3	927.64(6)
Z	2
ρ_{calc}g/cm^3	3.274
μ/mm^{-1}	62.334
F(000)	816.0
Crystal size/mm^3	0.224 × 0.159 × 0.095
Radiation	CuKα (λ = 1.54184)
2Θ range for data collection/°	6.422 to 144.22
Index ranges	$-7 \leq h \leq 10$, $-10 \leq k \leq 10$, $-17 \leq l \leq 17$
Reflections collected	10565
Independent reflections	3627 [R_{int} = 0.0493, R_{sigma} = 0.0431]
Data/restraints/parameters	3627/0/217
Goodness-of-fit on F^2	1.132
Final R indexes [I>=2σ (I)]	R_1 = 0.0389, wR_2 = 0.1013
Final R indexes [all data]	R_1 = 0.0401, wR_2 = 0.1022
Largest diff. peak/hole / e Å^{-3}	1.56/-2.05

Appendix 20 Crystal data and structure refinement for [**9**-Ag-**9**]OTf

Identification code	[**9**-Ag-**9**]OTf
Empirical formula	$C_{11}H_6AgF_3I_4N_2O_3S$
Formula weight	918.71
Temperature/K	170.0(1)
Crystal system	monoclinic
Space group	$P2_1/c$
a/Å	14.374(3)
b/Å	9.0631(18)
c/Å	15.175(3)
α/°	90
β/°	95.88(3)
γ/°	90
Volume/Å^3	1966.6(7)
Z	4
ρ_{calc}g/cm^3	3.103
μ/mm^{-1}	7.451
F(000)	1648.0
Crystal size/mm^3	0.08 × 0.07 × 0.07
Radiation	MoKα (λ = 0.71073)
2Θ range for data collection/°	2.848 to 50.5
Index ranges	$-17 \leq h \leq 17$, $-10 \leq k \leq 10$, $-17 \leq l \leq 18$
Reflections collected	14720
Independent reflections	3525 [R_{int} = 0.0461, R_{sigma} = 0.0477]
Data/restraints/parameters	3525/0/220
Goodness-of-fit on F^2	1.073
Final R indexes [I>=2σ (I)]	R_1 = 0.0429, wR_2 = 0.1059
Final R indexes [all data]	R_1 = 0.0582, wR_2 = 0.1210
Largest diff. peak/hole / e Å^{-3}	1.92/-1.91

Appendix 21 Crystal data and structure refinement for [10-Ag-10]OTf

Identification code	[**10**-Ag-**10**]OTf
Empirical formula	$C_{15}H_{18}AgF_3N_2O_3S$
Formula weight	471.24
Temperature/K	170.0(1)
Crystal system	triclinic
Space group	P-1
a/Å	8.1333(16)
b/Å	8.3549(17)
c/Å	15.279(3)
α/°	94.85(3)
β/°	100.01(3)
γ/°	117.16(3)
Volume/Å^3	893.7(4)
Z	2
ρ_{calc}g/cm^3	1.751
μ/mm^{-1}	1.291
F(000)	472.0
Crystal size/mm^3	0.25 × 0.25 × 0.25
Radiation	MoKα (λ = 0.71073)
2Θ range for data collection/°	5.512 to 50.496
Index ranges	$-9 \leq h \leq 9$, $-9 \leq k \leq 10$, $-18 \leq l \leq 18$
Reflections collected	6585
Independent reflections	3207 [R_{int} = 0.0200, R_{sigma} = 0.0295]
Data/restraints/parameters	3207/0/230
Goodness-of-fit on F^2	1.038
Final R indexes [I>=2σ (I)]	R_1 = 0.0222, wR_2 = 0.0527
Final R indexes [all data]	R_1 = 0.0243, wR_2 = 0.0537
Largest diff. peak/hole / e Å^{-3}	0.52/-0.33

Appendix 22 Crystal data and structure refinement for [10-Ag-10]PF_6

Identification code	[**10**-Ag-**10**]PF_6
Empirical formula	$C_{14}H_{18}AgF_6N_2P$
Formula weight	467.14
Temperature/K	120.00(10)
Crystal system	monoclinic
Space group	C2/c
a/Å	8.1428(6)
b/Å	15.1493(10)
c/Å	13.7391(10)
α/°	90
β/°	93.345(7)
γ/°	90
Volume/$Å^3$	1691.9(2)
Z	4
ρ_{calc}g/cm^3	1.834
μ/mm^{-1}	1.345
F(000)	928.0
Crystal size/mm^3	0.14 × 0.14 × 0.1
Radiation	MoKα (λ = 0.71073)
2Θ range for data collection/°	5.378 to 52.736
Index ranges	$-9 \leq h \leq 10$, $-17 \leq k \leq 18$, $-9 \leq l \leq 17$
Reflections collected	3281
Independent reflections	1730 [R_{int} = 0.0308, R_{sigma} = 0.0562]
Data/restraints/parameters	1730/33/130
Goodness-of-fit on F^2	1.056
Final R indexes [I>=2σ (I)]	R_1 = 0.0358, wR_2 = 0.0684
Final R indexes [all data]	R_1 = 0.0430, wR_2 = 0.0728
Largest diff. peak/hole / e $Å^{-3}$	0.64/-0.35

Appendix 23 Crystal data and structure refinement for [10-Br-10]Br_3

Identification code	[**10**-Br-**10**]Br_3
Empirical formula	$C_{14}H_{18}Br_4N_2$
Formula weight	533.94
Temperature/K	170.0(1)
Crystal system	triclinic
Space group	P-1
a/Å	7.3623(15)
b/Å	7.9949(16)
c/Å	8.6847(17)
α/°	63.11(3)
β/°	78.83(3)
γ/°	84.53(3)
Volume/$Å^3$	447.27(19)
Z	1
ρ_{calc}g/cm^3	1.982
μ/mm^{-1}	8.990
F(000)	256.0
Crystal size/mm^3	0.28 × 0.26 × 0.26
Radiation	MoKα (λ = 0.71073)
2Θ range for data collection/°	5.714 to 50.482
Index ranges	$-8 \leq h \leq 8$, $-9 \leq k \leq 9$, $-10 \leq l \leq 10$
Reflections collected	3367
Independent reflections	1587 [R_{int} = 0.0396, R_{sigma} = 0.0595]
Data/restraints/parameters	1587/0/96
Goodness-of-fit on F^2	1.054
Final R indexes [I>=2σ (I)]	R_1 = 0.0368, wR_2 = 0.0844
Final R indexes [all data]	R_1 = 0.0469, wR_2 = 0.0890
Largest diff. peak/hole / e $Å^{-3}$	0.75/-0.75

Appendix 24 Crystal data and structure refinement for [10-Br-10]OTf

Identification code	[**10**-Br-**10**]OTf
Empirical formula	$C_{15}H_{18}BrF_3N_2O_3S$
Formula weight	443.28
Temperature/K	170.0(1)
Crystal system	triclinic
Space group	P-1
a/Å	8.0390(16)
b/Å	8.2996(17)
c/Å	14.913(3)
α/°	80.32(3)
β/°	78.89(3)
γ/°	67.31(3)
Volume/Å^3	895.9(4)
Z	2
ρ_{calc}g/cm^3	1.643
μ/mm^{-1}	2.457
F(000)	448.0
Crystal size/mm^3	0.15 × 0.14 × 0.08
Radiation	MoKα (λ = 0.71073)
2Θ range for data collection/°	5.348 to 50.494
Index ranges	$-9 \leq h \leq 9$, $-9 \leq k \leq 9$, $-17 \leq l \leq 17$
Reflections collected	20693
Independent reflections	3218 [R_{int} = 0.0498, R_{sigma} = 0.0352]
Data/restraints/parameters	3218/0/231
Goodness-of-fit on F^2	1.117
Final R indexes [I>=2σ (I)]	R_1 = 0.0971, wR_2 = 0.2614
Final R indexes [all data]	R_1 = 0.1024, wR_2 = 0.2645
Largest diff. peak/hole / e Å^{-3}	3.12/-1.0

Appendix 25 Crystal data and structure refinement for [10-Br-10]PF_6

Identification code	[**10**-Br-**10**]PF_6
Empirical formula	$C_{14}H_{18}BrF_6N_2P$
Formula weight	439.18
Temperature/K	120.00(10)
Crystal system	triclinic
Space group	P-1
a/Å	7.1836(6)
b/Å	7.3568(5)
c/Å	8.6550(8)
α/°	87.286(7)
β/°	87.205(7)
γ/°	69.411(7)
Volume/$Å^3$	427.45(6)
Z	1
ρ_{calc}g/cm^3	1.706
μ/mm^{-1}	2.557
F(000)	220.0
Crystal size/mm^3	0.075 × 0.06 × 0.027
Radiation	MoKα (λ = 0.71073)
2Θ range for data collection/°	5.918 to 50.7
Index ranges	$-8 \leq h \leq 8$, $-8 \leq k \leq 8$, $-10 \leq l \leq 10$
Reflections collected	5394
Independent reflections	1491 [R_{int} = 0.0576, R_{sigma} = 0.1050]
Data/restraints/parameters	1491/0/114
Goodness-of-fit on F^2	1.031
Final R indexes [I>=2σ (I)]	R_1 = 0.0503, wR_2 = 0.1107
Final R indexes [all data]	R_1 = 0.0710, wR_2 = 0.1142
Largest diff. peak/hole / e $Å^{-3}$	1.56/-0.48

Appendix 26 Crystal data and structure refinement for [10-I-10]PF_6

Identification code	[**10**-I-**10**]PF_6
Empirical formula	$C_{14}H_{18}F_6IN_2P$
Formula weight	486.17
Temperature/K	170.0(1)
Crystal system	triclinic
Space group	P-1
a/Å	7.1617(14)
b/Å	7.6240(15)
c/Å	8.6720(17)
α/°	87.98(3)
β/°	88.62(3)
γ/°	69.04(3)
Volume/$Å^3$	441.86(15)
Z	1
ρ_{calc}g/cm^3	1.827
μ/mm^{-1}	1.960
F(000)	238.0
Crystal size/mm^3	0.1 × 0.08 × 0.07
Radiation	MoKα (λ = 0.71073)
2Θ range for data collection/°	4.7 to 50.5
Index ranges	$-8 \leq h \leq 8$, $-8 \leq k \leq 9$, $-10 \leq l \leq 9$
Reflections collected	3856
Independent reflections	1603 [R_{int} = 0.0547, R_{sigma} = 0.0744]
Data/restraints/parameters	1603/0/114
Goodness-of-fit on F^2	1.443
Final R indexes [I>=2σ (I)]	R_1 = 0.1088, wR_2 = 0.3147
Final R indexes [all data]	R_1 = 0.1128, wR_2 = 0.3196
Largest diff. peak/hole / e $Å^{-3}$	7.85/-1.19

Appendix 27 Crystal data and structure refinement for [11-Ag-11]PF_6

Identification code	[**11**-Ag-**11**]PF_6
Empirical formula	$C_6H_{10}AgF_6N_6P$
Formula weight	419.04
Temperature/K	170.0
Crystal system	trigonal
Space group	P-31c
a/Å	10.71600(10)
b/Å	10.71600(10)
c/Å	24.0554(5)
α/°	90
β/°	90
γ/°	120
Volume/$Å^3$	2392.26(7)
Z	6
ρ_{calc}g/cm^3	1.745
μ/mm^{-1}	1.423
F(000)	1224.0
Crystal size/mm^3	0.44 × 0.26 × 0.18
Radiation	MoKα (λ = 0.71073)
2Θ range for data collection/°	4.39 to 57.39
Index ranges	$-14 \leq h \leq 14$, $-12 \leq k \leq 11$, $-32 \leq l \leq 27$
Reflections collected	7316
Independent reflections	2079 [R_{int} = 0.0287, R_{sigma} = 0.0217]
Data/restraints/parameters	2079/63/117
Goodness-of-fit on F^2	1.167
Final R indexes [I>=2σ (I)]	R_1 = 0.0550, wR_2 = 0.1401
Final R indexes [all data]	R_1 = 0.0612, wR_2 = 0.1429
Largest diff. peak/hole / e $Å^{-3}$	1.01/-0.56

Appendix 28 Crystal data and structure refinement for [11-I-11]PF_6

Identification code	[**11**-I-**11**]PF_6
Empirical formula	$C_6H_{10}F_6IN_6P$
Formula weight	438.07
Temperature/K	119.99(10)
Crystal system	monoclinic
Space group	$P2_1/n$
a/Å	7.2322(3)
b/Å	9.9548(3)
c/Å	10.2131(4)
α/°	90
β/°	107.338(4)
γ/°	90
Volume/Å^3	701.88(5)
Z	2
ρ_{calc}g/cm^3	2.073
μ/mm^{-1}	2.462
F(000)	420.0
Crystal size/mm^3	0.235 × 0.158 × 0.097
Radiation	MoKα (λ = 0.71073)
2Θ range for data collection/°	5.848 to 58.094
Index ranges	$-9 \leq h \leq 9$, $-12 \leq k \leq 13$, $-13 \leq l \leq 13$
Reflections collected	7442
Independent reflections	1709 [R_{int} = 0.0503, R_{sigma} = 0.0396]
Data/restraints/parameters	1709/0/95
Goodness-of-fit on F^2	1.083
Final R indexes [I>=2σ (I)]	R_1 = 0.0261, wR_2 = 0.0585
Final R indexes [all data]	R_1 = 0.0375, wR_2 = 0.0675
Largest diff. peak/hole / e Å^{-3}	0.88/-0.52

Appendix 29 Crystal data and structure refinement for [15-Ag-15]PF_6

Identification code	[**15**-Ag-**15**]PF_6
Empirical formula	$C_{34}H_{42}AgF_6N_2P$
Formula weight	731.53
Temperature/K	119.98(10)
Crystal system	triclinic
Space group	P-1
a/Å	9.2658(6)
b/Å	9.5465(6)
c/Å	10.1388(8)
α/°	115.810(7)
β/°	90.926(6)
γ/°	96.772(6)
Volume/$Å^3$	799.45(11)
Z	1
ρ_{calc}g/cm^3	1.519
μ/mm^{-1}	0.742
F(000)	376.0
Crystal size/mm^3	0.34 × 0.19 × 0.11
Radiation	MoKα (λ = 0.71073)
2Θ range for data collection/°	4.44 to 56.562
Index ranges	$-12 \leq h \leq 9$, $-12 \leq k \leq 12$, $-13 \leq l \leq 13$
Reflections collected	6013
Independent reflections	3603 [R_{int} = 0.0212, R_{sigma} = 0.0440]
Data/restraints/parameters	3603/0/205
Goodness-of-fit on F^2	1.042
Final R indexes [I>=2σ (I)]	R_1 = 0.0295, wR_2 = 0.0589
Final R indexes [all data]	R_1 = 0.0318, wR_2 = 0.0607
Largest diff. peak/hole / e $Å^{-3}$	0.36/-0.46

Appendix 30 Crystal data and structure refinement for [17-Ag-17]PF_6

Identification code	[**17**-Ag-**17**]PF_6
Empirical formula	$C_{26}H_{42}AgF_6N_2P$
Formula weight	635.45
Temperature/K	120.01(10)
Crystal system	tetragonal
Space group	P4/ncc
a/Å	17.7545(2)
b/Å	17.7545(2)
c/Å	18.5167(5)
α/°	90
β/°	90
γ/°	90
Volume/$Å^3$	5836.9(2)
Z	8
ρ_{calc}g/cm^3	1.446
μ/mm^{-1}	0.801
F(000)	2624.0
Crystal size/mm^3	0.364 × 0.32 × 0.16
Radiation	MoKα (λ = 0.71073)
2Θ range for data collection/°	4.4 to 50.692
Index ranges	$-21 \leq h \leq 21$, $-21 \leq k \leq 19$, $-22 \leq l \leq 22$
Reflections collected	44226
Independent reflections	2686 [R_{int} = 0.0578, R_{sigma} = 0.0195]
Data/restraints/parameters	2686/18/198
Goodness-of-fit on F^2	1.121
Final R indexes [I>=2σ (I)]	R_1 = 0.0870, wR_2 = 0.2032
Final R indexes [all data]	R_1 = 0.1105, wR_2 = 0.2227
Largest diff. peak/hole / e $Å^{-3}$	1.11/-1.32

Appendix 31 Crystal data and structure refinement for [18-Ag-18]PF_6

Identification code	[**18**-Ag-**18**]PF_6
Empirical formula	$C_{24}H_{16}AgF_6N_4P$
Formula weight	613.25
Temperature/K	170
Crystal system	monoclinic
Space group	C2/c
a/Å	20.6911(16)
b/Å	15.0078(12)
c/Å	7.2126(6)
α/°	90
β/°	102.898(3)
γ/°	90
Volume/$Å^3$	2183.2(3)
Z	4
ρ_{calc}g/cm^3	1.866
μ/mm^{-1}	1.071
F(000)	1216.0
Crystal size/mm^3	0.48 × 0.1 × 0.06
Radiation	MoKα (λ = 0.71073)
2Θ range for data collection/°	3.382 to 56.66
Index ranges	$-27 \leq h \leq 27$, $-19 \leq k \leq 18$, $-9 \leq l \leq 9$
Reflections collected	4712
Independent reflections	2649 [R_{int} = 0.0530, R_{sigma} = 0.0539]
Data/restraints/parameters	2649/30/166
Goodness-of-fit on F^2	1.939
Final R indexes [I>=2σ (I)]	R_1 = 0.1684, wR_2 = 0.4268
Final R indexes [all data]	R_1 = 0.1825, wR_2 = 0.4400
Largest diff. peak/hole / e $Å^{-3}$	13.98/-2.10

Appendix 32 Crystal data and structure refinement for $[Ag_3\mathbf{19}_4][PF_6]_3 \cdot C_4H_8O$

Identification code	$[Ag_3\mathbf{19}_4][PF_6]_3 \cdot C_4H_8O$
Empirical formula	$C_{64}H_{48}Ag_3Cl_4F_{18}N_{12}OP_3$
Formula weight	1901.46
Temperature/K	119.9(3)
Crystal system	triclinic
Space group	P-1
a/Å	13.6327(5)
b/Å	15.2309(8)
c/Å	20.7777(12)
α/°	96.006(4)
β/°	101.521(4)
γ/°	116.542(4)
Volume/Å^3	3688.1(3)
Z	2
ρ_{calc}g/cm^3	1.712
μ/mm^{-1}	1.094
F(000)	1880.0
Crystal size/mm^3	0.492 × 0.441 × 0.263
Radiation	MoKα (λ = 0.71073)
2Θ range for data collection/°	3.476 to 58.03
Index ranges	$-17 \leq h \leq 18$, $-19 \leq k \leq 19$, $-25 \leq l \leq 26$
Reflections collected	30745
Independent reflections	16711 [R_{int} = 0.0560, R_{sigma} = 0.1020]
Data/restraints/parameters	16711/108/946
Goodness-of-fit on F^2	1.053
Final R indexes [I>=2σ (I)]	R_1 = 0.0970, wR_2 = 0.2290
Final R indexes [all data]	R_1 = 0.1217, wR_2 = 0.2448
Largest diff. peak/hole / e Å^{-3}	3.39/-3.00

Appendix 33 Crystal data and structure refinement for $[Ag_3\mathbf{19}_4][PF_6]_3$

Identification code	$[Ag_3\mathbf{19}_4][PF_6]_3$
Empirical formula	$C_{60}H_{40}Ag_3Cl_4F_{18}N_{12}P_3$
Formula weight	1829.36
Temperature/K	170.0
Crystal system	monoclinic
Space group	C2/c
a/Å	16.4837(4)
b/Å	26.2930(4)
c/Å	15.5078(3)
α/°	90
β/°	90.2500(10)
γ/°	90
Volume/Å^3	6721.1(2)
Z	4
ρ_{calc}g/cm^3	1.808
μ/mm^{-1}	1.196
F(000)	3600.0
Crystal size/mm^3	0.42 × 0.19 × 0.18
Radiation	MoKα (λ = 0.71073)
2Θ range for data collection/°	2.916 to 57.806
Index ranges	$-22 \leq h \leq 21$, $-35 \leq k \leq 34$, $-20 \leq l \leq 17$
Reflections collected	26707
Independent reflections	8744 [R_{int} = 0.0456, R_{sigma} = 0.0558]
Data/restraints/parameters	8744/0/452
Goodness-of-fit on F^2	1.059
Final R indexes [I>=2σ (I)]	R_1 = 0.0454, wR_2 = 0.1015
Final R indexes [all data]	R_1 = 0.0661, wR_2 = 0.1145
Largest diff. peak/hole / e Å^{-3}	0.47/-0.64

Appendix 34 Crystal data and structure refinement for $[Ag_2\mathbf{19}_2][OTf]_2 \cdot CH_2Cl_2$

Identification code	$[Ag_2\mathbf{19}_2][OTf]_2 \cdot CH_2Cl_2$
Empirical formula	$C_{33}H_{22}Ag_2Cl_4F_6N_6O_6S_2$
Formula weight	1134.22
Temperature/K	170
Crystal system	monoclinic
Space group	Cc
a/Å	17.9522(5)
b/Å	14.8705(3)
c/Å	16.2318(4)
α/°	90
β/°	116.4100(10)
γ/°	90
Volume/Å^3	3880.97(17)
Z	4
ρ_{calc}g/cm^3	1.941
μ/mm^{-1}	1.475
F(000)	2232.0
Crystal size/mm^3	0.44 × 0.44 × 0.24
Radiation	MoKα (λ = 0.71073)
2Θ range for data collection/°	3.73 to 61.01
Index ranges	$-25 \leq h \leq 25$, $-21 \leq k \leq 21$, $-23 \leq l \leq 23$
Reflections collected	10734
Independent reflections	10726 [R_{int} = 0.0151, R_{sigma} = 0.0347]
Data/restraints/parameters	10726/2/533
Goodness-of-fit on F^2	1.086
Final R indexes [I>=2σ (I)]	R_1 = 0.0382, wR_2 = 0.0787
Final R indexes [all data]	R_1 = 0.0426, wR_2 = 0.0816
Largest diff. peak/hole / e Å^{-3}	0.36/-0.68

Appendix 35 Crystal data and structure refinement for $[Ag_3\mathbf{19}_4][PF_6]_3 \cdot CH_2Cl_2$

Identification code	$[Ag_3\mathbf{19}_4][PF_6]_3 \cdot CH_2Cl_2$
Empirical formula	$C_{62}H_{44}Ag_3Cl_8F_{18}N_{12}P_3$
Formula weight	1999.21
Temperature/K	170
Crystal system	monoclinic
Space group	P2/n
a/Å	10.6061(2)
b/Å	14.8025(3)
c/Å	23.8230(3)
α/°	90
β/°	91.7890(10)
γ/°	90
Volume/Å^3	3738.31(11)
Z	2
ρ_{calc}g/cm^3	1.776
μ/mm^{-1}	1.222
F(000)	1968.0
Crystal size/mm^3	0.42 × 0.14 × 0.06
Radiation	MoKα (λ = 0.71073)
2Θ range for data collection/°	2.752 to 54.206
Index ranges	$-13 \leq h \leq 13$, $-14 \leq k \leq 18$, $-30 \leq l \leq 30$
Reflections collected	14631
Independent reflections	8236 [R_{int} = 0.0398, R_{sigma} = 0.0496]
Data/restraints/parameters	8236/81/479
Goodness-of-fit on F^2	1.065
Final R indexes [I>=2σ (I)]	R_1 = 0.0660, wR_2 = 0.1848
Final R indexes [all data]	R_1 = 0.0911, wR_2 = 0.2069
Largest diff. peak/hole / e Å^{-3}	1.22/-0.85

Appendix 36 Crystal data and structure refinement for $[\mathbf{19}AgI]_n[I_2]_n$

Identification code	$[\mathbf{19}AgI]_n[I_2]_n$
Empirical formula	$C_{15}H_{10}AgClI_9N_3$
Formula weight	1517.68
Temperature/K	170
Crystal system	monoclinic
Space group	Pn
a/Å	15.6707(18)
b/Å	4.3605(3)
c/Å	22.643(3)
α/°	90
β/°	107.653(4)
γ/°	90
Volume/Å^3	1474.4(3)
Z	2
ρ_{calc}g/cm^3	3.419
μ/mm^{-1}	10.207
F(000)	1324.0
Crystal size/mm^3	0.32 × 0.18 × 0.04
Radiation	MoKα (λ = 0.71073)
2Θ range for data collection/°	3.758 to 57.698
Index ranges	$-21 \leq h \leq 18$, $-5 \leq k \leq 5$, $-25 \leq l \leq 30$
Reflections collected	10922
Independent reflections	5351 [R_{int} = 0.0446, R_{sigma} = 0.0707]
Data/restraints/parameters	5351/149/263
Goodness-of-fit on F^2	1.113
Final R indexes [I>=2σ (I)]	R_1 = 0.0630, wR_2 = 0.1506
Final R indexes [all data]	R_1 = 0.0734, wR_2 = 0.1566
Largest diff. peak/hole / e Å^{-3}	4.09/-2.05
Flack parameter	-0.01(14)

Appendix 37 Crystal data and structure refinement for [**19**H_2][Br.Br_3]

Identification code	[**19**H_2][Br.Br_3]
Empirical formula	$C_{15}H_{12}Br_4ClN_3$
Formula weight	589.37
Temperature/K	170
Crystal system	monoclinic
Space group	$P2_1/c$
a/Å	6.5747(3)
b/Å	21.3827(8)
c/Å	13.6190(7)
α/°	90
β/°	103.581(2)
γ/°	90
Volume/$Å^3$	1861.09(15)
Z	4
ρ_{calc}g/cm^3	2.103
μ/mm^{-1}	8.794
F(000)	1120.0
Crystal size/mm^3	0.26 × 0.06 × 0.04
Radiation	MoKα (λ = 0.71073)
2Θ range for data collection/°	3.618 to 52.744
Index ranges	$-8 \leq h \leq 8$, $-26 \leq k \leq 26$, $-17 \leq l \leq 17$
Reflections collected	7211
Independent reflections	3803 [R_{int} = 0.0381, R_{sigma} = 0.0472]
Data/restraints/parameters	3803/0/208
Goodness-of-fit on F^2	1.086
Final R indexes [I>=2σ (I)]	R_1 = 0.0433, wR_2 = 0.0956
Final R indexes [all data]	R_1 = 0.0668, wR_2 = 0.1059
Largest diff. peak/hole / e $Å^{-3}$	0.68/-0.57

Appendix 38 Crystal data and structure refinement for [19H_2][Br.PF_6]

Identification code	[**19**H_2][Br.PF_6]
Empirical formula	$C_{15}H_{12}BrClF_6N_3P$
Formula weight	494.61
Temperature/K	120.01(10)
Crystal system	monoclinic
Space group	$P2_1/n$
a/Å	9.5935(2)
b/Å	17.0871(4)
c/Å	10.8529(3)
α/°	90
β/°	94.366(2)
γ/°	90
Volume/$Å^3$	1773.90(7)
Z	4
ρ_{calc}g/cm^3	1.852
μ/mm^{-1}	2.624
F(000)	976.0
Crystal size/mm^3	0.131 × 0.117 × 0.089
Radiation	MoKα (λ = 0.71073)
2Θ range for data collection/°	4.456 to 58.052
Index ranges	$-12 \leq h \leq 12$, $-23 \leq k \leq 22$, $-14 \leq l \leq 14$
Reflections collected	12680
Independent reflections	4187 [R_{int} = 0.0420, R_{sigma} = 0.0572]
Data/restraints/parameters	4187/0/250
Goodness-of-fit on F^2	1.056
Final R indexes [I>=2σ (I)]	R_1 = 0.0395, wR_2 = 0.0747
Final R indexes [all data]	R_1 = 0.0652, wR_2 = 0.0844
Largest diff. peak/hole / e $Å^{-3}$	0.48/-0.42

Appendix 39 Crystal data and structure refinement for [Ag**19**]OTf

Identification code	[Ag**19**]OTf
Empirical formula	$C_{34}H_{23}Ag_2Cl_2F_6N_7O_6S_2$
Formula weight	1090.35
Temperature/K	170
Crystal system	monoclinic
Space group	$P2_1/c$
a/Å	16.0598(5)
b/Å	15.7630(3)
c/Å	16.0505(5)
α/°	90
β/°	110.1650(10)
γ/°	90
Volume/Å^3	3814.13(18)
Z	4
ρ_{calc}g/cm^3	1.899
μ/mm^{-1}	1.362
F(000)	2152.0
Crystal size/mm^3	0.5 × 0.44 × 0.32
Radiation	MoKα (λ = 0.71073)
2Θ range for data collection/°	2.702 to 61.698
Index ranges	$-21 \leq h \leq 23$, $-22 \leq k \leq 22$, $-22 \leq l \leq 23$
Reflections collected	42411
Independent reflections	11895 [R_{int} = 0.0476, R_{sigma} = 0.0563]
Data/restraints/parameters	11895/0/532
Goodness-of-fit on F^2	1.040
Final R indexes [I>=2σ (I)]	R_1 = 0.0442, wR_2 = 0.0799
Final R indexes [all data]	R_1 = 0.0667, wR_2 = 0.0866
Largest diff. peak/hole / e Å^{-3}	0.47/-0.63

Appendix 40 Crystal data and structure refinement for [Ag**19**]NO_3

Identification code	[Ag**19**]NO_3
Empirical formula	$C_{15}H_{10}AgClN_4O_3$
Formula weight	437.59
Temperature/K	120.01(10)
Crystal system	monoclinic
Space group	$P2_1/n$
a/Å	7.5357(3)
b/Å	18.3027(9)
c/Å	10.5527(4)
α/°	90
β/°	98.896(4)
γ/°	90
Volume/Å^3	1437.96(11)
Z	4
ρ_{calc}g/cm^3	2.021
μ/mm^{-1}	13.185
F(000)	864.0
Crystal size/mm^3	0.291 × 0.182 × 0.022
Radiation	CuKα (λ = 1.54184)
2Θ range for data collection/°	9.764 to 144.258
Index ranges	$-9 \leq h \leq 8$, $-22 \leq k \leq 20$, $-7 \leq l \leq 12$
Reflections collected	5236
Independent reflections	2808 [R_{int} = 0.0331, R_{sigma} = 0.0415]
Data/restraints/parameters	2808/0/217
Goodness-of-fit on F^2	1.053
Final R indexes [I>=2σ (I)]	R_1 = 0.0361, wR_2 = 0.0942
Final R indexes [all data]	R_1 = 0.0406, wR_2 = 0.1004
Largest diff. peak/hole / e Å^{-3}	0.81/-1.18

Appendix 41 Crystal data and structure refinement for $[Ag_4\mathbf{19}_4]ClO_4$

Identification code	$[Ag_4\mathbf{19}_4]ClO_4$
Empirical formula	$C_{60}H_{40}Ag_4Cl_8N_{12}O_{16}$
Formula weight	1900.12
Temperature/K	120.01(10)
Crystal system	monoclinic
Space group	Cc
a/Å	25.0026(5)
b/Å	25.2085(4)
c/Å	11.4166(3)
α/°	90
β/°	97.311(2)
γ/°	90
Volume/Å^3	7137.1(3)
Z	4
ρ_{calc}g/cm^3	1.768
μ/mm^{-1}	12.054
F(000)	3744.0
Crystal size/mm^3	0.19 × 0.039 × 0.021
Radiation	CuKα (λ = 1.54184)
2Θ range for data collection/°	4.998 to 144.252
Index ranges	$-30 \leq h \leq 30$, $-21 \leq k \leq 31$, $-14 \leq l \leq 14$
Reflections collected	28909
Independent reflections	13553 [R_{int} = 0.0524, R_{sigma} = 0.0687]
Data/restraints/parameters	13553/20/901
Goodness-of-fit on F^2	1.010
Final R indexes [I>=2σ (I)]	R_1 = 0.0453, wR_2 = 0.1173
Final R indexes [all data]	R_1 = 0.0528, wR_2 = 0.1242
Largest diff. peak/hole / e Å^{-3}	0.82/-1.12
Flack parameter	-0.034(11)

REFERENCES

1. G.R. Desiraju, P.S. Ho, L. Kloo, A.C. Legon, R. Marquardt, P. Metrangolo, P. Politzer, G. Resnati, K. Rissanen, Pure Appl. Chem. **2013**, 85 (8), 1711–1713.
2. P. Politzer, J. S. Murray, T. Clark, *Phys. Chem. Chem. Phys.* **2013**, *15*, 11178–11189.
3. F. Guthrie, *J. Chem. Soc.* **1863**, *16*, 239–244.
4. P. Pelletier, J. Caventou, Sur Un Nouvel Alcali Végétal (la Strychine) Trouvé Dans La Fève de Saint-Ignace, La Noix Vomique Etc. Ann. Chim. Phys. **1819**, 10, 142–177.
5. R. S. Mulliken, *J. Am. Chem. Soc.* **1950**, *72*, 600–608.
6. O. Hassel, *Science* **1970**, *170*, 497–502.
7. I. Remsen, JF. Norris, Am. Chem. J. **1896**, 18, 90−95.
8. B. S. Ault, L. Andrews, Inorg. Chem. **1977**, 16, 2024−2028.
9. B. S. Ault, L. Andrews, J. Am. Chem. Soc. **1976**, 98, 1591−1593.
10. S. Riedel, T. Köchner, X. Wang, L. Andrews, Inorg. Chem. **2010**, 49, 7156−7164.
11. A. C. Legon, Angew. Chem., Int. Ed. **1999**, 38, 2686−2714.
12. R. S. Mulliken, J. Am. Chem. Soc. **1952**, 74, 811−824.
13. R. S. Mulliken, J. Phys. Chem. **1952**, 56, 801−822.
14. O. Hassel, J. Hvoslef, *Acta Chem. Scand.* **1954**, *8*, 873.
15. E. Gunnar, O. Hassel, *Acta Chem. Scand.* **1956**, *10*, 139–141.
16. O. Hassel, K. O. Stromme, *Acta Chem. Scand.* **1958**, *12*, 1146.
17. O. Hassel, K. O. Stromme, *Nature* **1958**, *182*, 1155–1156.
18. T. Bjorvatten, O. Hassel, *Acta Chem. Scand.* **1961**, *15*, 1429–1436.
19. O. Hassel, K. O. Stromme, Acta Chem. Scand. **1959**, 13, 1781−1786.
20. N. Ramasubbu, R. Parthasarathy, P. Murray-Rust, *J. Am. Chem. Soc.* **1986**, *108*, 4308–4314.
21. J. P. M. Lommerse, A. J. Stone, R. Taylor, F. H. Allen, *J. Am. Chem. Soc.* **1996**, *118*, 3108–3116.
22. H. Bent, Chem. Rev. **1968**, 68, 587–648.
23. J. M. Dumas, M. Gomel, M. Guerin, John Wiley & Sons, Ltd.: Chichester, U.K., **1983**, 985− 1020.
24. A. C. Legon, *Chem. Eur. J.* **1998**, *4*, 1890–1897.
25. V. Amico, S. V. Meille, E. Corradi, M. T. Messina, G. Resnati, *J. Am. Chem. Soc.* **1998**, *120*, 8261–8262.
26. E. Corradi, S. V. Meille, M. T. Messina, P. Metrangolo, G. Resnati, *Angew. Chem. Int. Ed.* **2000**, *39*, 1782–1786.
27. P. Metrangolo, G. Resnati, *Chem. Eur. J.* **2001**, *7*, 2511–2519.
28. P. Metrangolo, H. Neukirch, T. Pilati, G. Resnati, Acc. Chem. Res. **2005**, 38, 386−395.
29. T. Brinck, J. S. Murray, P. Politzer, Int. J. Quantum Chem. **1992**, 44, 57−64.
30. T. Brinck, J. S. Murray, P. Politzer, Int. J. Quantum Chem. **1993**, 48, 73−88.

31. J. S. Murray, K. Paulsen, P. Politzer, Proc. Indian Acad. Sci., Chem. Sci. **1994**, 106, 267−275.
32. M. Erdelyi, Nat. Chem. **2014**, 6, 762−764.
33. R. A. Zingaro, R. M. Hedges, *J. Phys. Chem.* **1961**, *65*, 1132–1138.
34. D. E. Martire, J. P. Sheridan, J. W. King, S. E. O'Donnell, J. Am. Chem. Soc. **1976**, 98, 3101−3106.
35. J.-M. Dumas, H. Peurichard, M. J. Gomel, *J. Chem. Res.* **1978**, *2*, 54.
36. S. C. Blackstock, J. P. Lorand, J. K. Kochi, *J. Org. Chem.* **1987**, *52*, 1451–1460.
37. L. Turunen, J.H. Hansen, M. Erdélyi, Chem. Rec. **2021**, 21, 1252–1257.
38. S.V. Rosokha, I.S. Neretin, T.Y. Rosokha, J. Hecht, J.K. Kochi, Heteroat. Chem. **2006**, 17, 449–459.
39. L.P. Wolters, F.M. Bickelhaupt, Chemistry Open, **2012**, 1, 96–105.
40. J. Thirman, E. Engelage, S.M. Huber, M. Head-Gordon, Phys. Chem. Chem. Phys. **2018**, 20, 905–915.
41. B. Inscoe, H. Rathnayake, Y. Mo, J. Phys. Chem. A, **2021**, 125, 2944–2953.
42. S.M. Huber, E. Jimenez-Izal, J.M. Ugalde, I. Infante, Chem. Commun. **2012**, 48, 7708–7710.
43. S.V. Rosokha, C.L. Stern, J.T. Ritzert, Chem. – A Eur. J. **2013**, 19, 8774–8788.
44. C. Wang, D. Danovich, Y. Mo, S. Shaik, J. Chem. Theory Comput. **2014**, 10, 3726–3737.
45. L.P. Wolters, P. Schyman, M.J. Pavan, W.L. Jorgensen, F.M. Bickelhaupt, S. Kozuch, WIREs Comput. Mol. Sci. **2014**, 4, 523–540.
46. L.P. Wolters, N.W.G. Smits, C.F. Guerra, Phys. Chem. Chem. Phys. **2015**, 17, 1585–1592.
47. S.W. Robinson, C.L. Mustoe, N.G. White, A. Brown, A.L. Thompson, P. Kennepohl, P.D. Beer, J. Am. Chem. Soc. **2015**, 137, 499–507.
48. V. Oliveira, E. Kraka, D. Cremer, Phys. Chem. Chem. Phys. **2016**, 18, 33031–33046.
49. V. Oliveira, E. Kraka, D. Cremer, Inorg. Chem. **2017**, 56, 488–502.
50. T. Clark, M. Hennemann, J. S. Murray, P. Politzer, *J. Mol. Model.* **2007**, *13*, 291–296.
51. S. V. Rosokha, M. K. Vinakos, Cryst. Growth Des. **2012**, 12, 4149−4156.
52. P. Murray-Rust, W. D. S. Motherwell, J. Am. Chem. Soc. **1979**, 101, 4374−4376.
53. P. Murray-Rust, W. C. Stallings, C. T. Monti, R. K. Preston, J. P. Glusker, J. Am. Chem. Soc. **1983**, 105, 3206−3214.
54. S. C. Nyburg, C. H. Faerman, Acta Crystallogr., Sect. B: Struct. Sci. **1985**, B41, 274−279.
55. P. Metrangolo, J. S. Murray, T. Pilati, P. Politzer, G. Resnati, G. Terraneo, Cryst. Growth Des. **2011**, 11, 4238−4246.
56. P. Metrangolo, J. S. Murray, T. Pilati, P. Politzer, G. Resnati, G. Terraneo, CrystEngComm **2011**, 13, 6593−6896.
57. V. R. Hathwar, D. Chopra, P. Panini, T. N. G. Row, Cryst. Growth Des. **2014**, 14, 5366−5369.

58. P. Politzer, J. S. Murray, T. Clark, *Phys. Chem. Chem. Phys.* **2010**, *12*, 7748-7757.
59. L. Turunen, M. Erdélyi, Chem. Soc. Rev. **2020**, 49, 2688–2700.
60. S.B. Hakkert, M. Erdélyi, J. Phys. Org. Chem. **2015**, 28, 226–233.
61. A.-C.C. Carlsson, M. Uhrbom, A. Karim, U. Brath, J. Gräfenstein, M. Erdélyi, Cryst. Eng. Comm. 2016, 15, 3087–3092.
62. I. Haque, J.L. Wood, J. Mol. Struct. **1968**, 2, 217–238.
63. G. Cavallo, P. Metrangolo, R. Milani, T. Pilati, A. Priimagi, G. Resnati, G. Terraneo, Chem. Rev. **2016**, 116, 2478–2601.
64. L.C. Gilday, S.W. Robinson, T.A. Barendt, M.J. Langton, B.R. Mullaney, P.D. Beer, Chem. Rev. **2015**, 115, 7118–7195.
65. M. Saccone, G. Cavallo, P. Metrangolo, A. Pace, I. Pibiri, T. Pilati, G. Resnati, G. Terraneo, CrystEngComm. **2013**, 15, 3102−3105.
66. A. Karim, M. Reitti, A.-C.C. Carlsson, J. Gräfenstein, M. Erdélyi, Chem. Sci. **2014**, 5, 3226–3233.
67. A. Vanderkooy, A.K. Gupta, T. Földes, S. Lindblad, A. Orthaber, I. Pápai, M. Erdélyi, Angew. Chem. Int. Ed. **2019**, 58, 9012–9016.
68. A.-C.C. Carlsson, J. Gräfenstein, J.L. Laurila, J. Bergquist, M. Erdélyi, Chem. Commun. **2012**, 48, 1458-1460
69. A.-C.C. Carlsson, A.X. Veiga, M. Erdélyi, Top. Curr. Chem. Springer International publishing., **2015**, 359, 49–76.
70. P. Metrangolo, T. Pilati, G. Terraneo, S. Biella, G. Resnati, *CrystEngComm* **2009**, *11*, 1187–1196.
71. A.C. Reiersølmoen, S. Battaglia, S. Øien-Ødegaard, A.K. Gupta, A. Fiksdahl, R. Lindh, M. Erdélyi, Chem. Sci. **2020**, 11, 7979–7990.
72. O. Hassel, H. Hope, Acta Chem. Scand. **1961**, 15, 407–416.
73. J.A. Creighton, I. Haque, J.L. Wood, Chem. Commun. **1966**, 8, 229.
74. J.A. Creighton, I. Haque, J.L. Wood, Chem. Commun. **1966**, 23, 892.
75. J. Barluenga, M. Trincado, E. Rubio, J.M. González, Angew. Chem. Int. Ed. **2003**, 42, 2406–2409.
76. J.M. Chalker, A.L. Thompson, B.G. Davis, N. Zaware, P. Wipf, Organic Syntheses. **2010**, 87, 288–298.
77. G. Espuña, G. Arsequell, G. Valencia, J. Barluenga, M. Pérez and J. M. González, Chemical Communications, **2000**, 1307–1308.
78. J. Barluenga, J. M. González, M. A. Garcia-Martin, P. J. Campos and G. Asensio, Journal of the Chemical Society, Chemical Communications, **1992**, 4, 1016–1017.
79. J. Barluenga, F. González-Bobes, M. C. Murguía, S. R. Ananthoju and J. M. González, Chemistry - A European Journal, **2004**, 10, 4206–4213.
80. J. Ezquerra, C. Pedregal, C. Lamas, J. Barluenga, M. Pérez, M. A. García Martín and J. M. González, Journal of Organic Chemistry, **1996**, 61, 5804–5812.
81. A. C. C. Carlsson, J. Gräfenstein, A. Budnjo, J. L. Laurila, J. Bergquist, A. Karim, R. Kleinmaier, U. Brath and M. Erdélyi, Journal of the American Chemical Society, **2012**, 134, 5706–5715.

82. D. von der Heiden, K. Rissanen and M. Erdélyi, Chemical Communications, **2020**, 56, 14431–14434.
83. A. C. C. Carlsson, K. Mehmeti, M. Uhrbom, A. Karim, M. Bedin, R. Puttreddy, R. Kleinmaier, A. A. Neverov, B. Nekoueishahraki, J. Gräfenstein, K. Rissanen and M. Erdélyi, Journal of the American Chemical Society, **2016**,138, 9853–9863.
84. M. Bedin, A. Karim, M. Reitti, A. C. C. Carlsson, F. Topić, M. Cetina, F. Pan, V. Havel, F. Al-Ameri, V. Sindelar, K. Rissanen, J. Gräfenstein and M. Erdélyi, Chemical Science, **2015**, 6, 3746–3756.
85. J. S. Ward, A. Frontera and K. Rissanen, Chemical Communications, **2021**, 57, 5094–5097.
86. J. S. Ward, A. Frontera and K. Rissanen, Inorganic Chemistry, **2021**, 60, 5383–5390.
87. J. S. Ward, A. Frontera and K. Rissanen, Dalton Transactions, **2021**, 50, 8297–8301.
88. S. Yu, J. S. Ward, K. Truong and K. Rissanen, Angewandte Chemie International Edition, **2021**, 60, 20739–20743.
89. J. S. Ward, G. Fiorini, A. Frontera and K. Rissanen, Chemical Communications, **2020**, 56, 8428–8431.
90. S. Yu, P. Kumar, J. S. Ward, A. Frontera and K. Rissanen, Chem, **2021**, 7, 948–958.
91. L. Turunen, U. Warzok, R. Puttreddy, N. K. Beyeh, C. A. Schalley and K. Rissanen, Angewandte Chemie - International Edition, **2016**, 55, 14033–14036.
92. L. Turunen, U. Warzok, C. A. Schalley and K. Rissanen, Chem, **2017**, 3, 861–869.
93. L. Turunen, A. Peuronen, S. Forsblom, E. Kalenius, M. Lahtinen and K. Rissanen, Chemistry - A European Journal, **2017**, 23, 11714–11718.
94. H. Pritzkow, Acta Cryst. **1975**, 20, 1505–1506.
95. N. W. Alcock, G. B. Robertson, J. Chem. Soc., Dalton Trans. **1975**, 2483–2486.
96. B. Y. G. D. Brayer, M. N. G. James, C. Tg, Acta Cryst. **1982**, B38, 654–657.
97. L. K. Blair, K. D. Parris, P. Sen Hii, C. P. Brock, H. Acta, J. Am. Chem. Soc. **1983**, 105, 3649–3653.
98. C. Pratt Brock, Y. Fu, Acta Cryst. **1988**, 30, 1582–1585.
99. A. A. Neverov, R. S. Brown, J. Org. Chem. **1998**, 63, 5977–5982.
100. A. A. Neverov, H. X. Feng, K. Hamilton, R. S. Brown, J. Org. Chem. **2003**, 68, 3802–3810.
101. M. J. Crawford, M. Göbel, K. Karaghiosoff, T. M. Klapötke, J. M. Welch, Inorg. Chem. **2009**, 48, 9983–9985.
102. L. Koskinen, P. Hirva, E. Kalenius, S. Jääskeläinen, K. Rissanen, M. Haukka, CrystEngComm **2015**, 17, 1231–1236.
103. C.R. Groom, I.J. Bruno, M.P. Lightfoot, S.C. Ward, Acta Crystallogr. Sect. B, **2016**, 72, 171–179.
104. E. Kukkonen, H. Malinen, M. Haukka, J. Konu, Cryst. Growth Des. **2019**, 19, 2434–2445.

105. L.C.F. Morgan, Y. Kim, J.N. Blandy, C.A. Murray, K.E. Christensen, A.L. Thompson, Chem. Commun. **2018**, 54, 9849–9852.
106. M. Eraković, D. Cinčić, K. Molčanov, V. Stilinović, Angew. Chem. Int. Ed. **2019**, 58, 15702–15706
107. Y. Kim, E.J. Mckinley, K.E. Christensen, N.H. Rees, A.L. Thompson, Cryst. Growth Des. **2014**, 14, 6294–6301.
108. Y.-M. Wang, J. Wu, C. Hoong, V. Rauniyar, F.D. Toste, J. Am. Chem. Soc. **2012**, 134, 12928–12931.
109. C. Weinberger, R. Hines, M. Zeller, S.V. Rosokha, Chem. Commun. **2018**, 54, 8060–8063.
110. G.A. Bowmaker, S.F. Hannan, Aust. J. Chem. **1971**, 24, 2237–2248.
111. U. Warzok, M. Marianski, W. Hoffmann, L. Turunen, K. Rissanen, K. Pagel, C.A. Schalley, Chem. Sci. **2018**, 9, 8343–8351.
112. B.H. Northrop, H.-B. Yang, P.J. Stang, Chem. Commun. **2008**, 5896–5908.
113. G. Gong, S. Lv, J. Han, F. Xie, Q. Li, N. Xia, W. Zeng, Y. Chen, L. Wang, J. Wang, S. Chen, Angew. Chem. Int. Ed. **2021**, 60, 14831–14835.
114. S. Lindblad, D. Sethio, O.B. Berryman, M. Erdélyi, Chem. Commun. **2021**, 57, 6261–6263.
115. L. Turunen, F.B. Németh, D.A. Decato, I. Pápai, O.B. Berryman, M. Erdélyi, Bull. Chem. Soc. Jpn. **2021**, 94, 191–196.
116. S. Lindblad, K. Mehmeti, A.X. Veiga, B. Nekoueishahraki, J. Gräfenstein, M. Erdélyi, J. Am. Chem. Soc. **2018**, 140, 13503–13513.
117. E. Taipale, M. Siepmann, K.-N. Truong and K. Rissanen, *Chem. Eur. J.* **2021**, 27, 17412 – 17419.
118. E. Taipale, J. S. Ward, G. Fiorini, L. D. Stares, A. C. Schalley, and K. Rissanen, Inorg. Chem. Front., **2022**, 9, 2231–2239.
119. S. B. Hakkert, J. Gräfenstein, M. Erdélyi, *Faraday Discuss*. **2017**, *203*, 333–346.
120. H. Wang, W. Wang, and W. J. Jin, Chem. Rev. **2016**, *116*, 5072–5104.
121. K. Rissanen, CrystEngComm, **2008**, *10*, 1107–1113.
122. N. K. Beyeh, F. Pan, and K. Rissanen, Angew. Chemie Int. Ed. **2015**, *54*, 7303–7307.
123. O. Dumele, N. Trapp, and F. Diederich, Angew. Chemie Int. Ed. **2015**, *54*, 12339–12344.
124. E. Arunan, G. R. Desiraju, R. A. Klein, J. Sadlej, S. Scheiner, I. Alkorta, D. C. Clary, R. H. Crabtree, J. J. Dannenberg, P. Hobza, et al. Pure Appl. Chem. **2011**, *83*, 1619–1636.
125. R. W. Troff, T. Mäkelä, F. Topić, A. Valkonen, K. Raatikainen, and K. Rissanen, European J. Org. Chem. **2013**, 1617–1637.
126. K. Raatikainen, and K. Rissanen, Chem. Sci. **2012**, *3*, 1235–1239.
127. M. Kurosu, S. S. Dey, and C. D. Crick, Tetrahedron Letters., **2006**, 47, 4871–4875.
128. T. Tanaka, N. Shirai, and Y. Sato, Chem. Pharma. Bull. **1992**, 40, 518-520.
129. S. Hanada, T. Ishida, Y. Motoyama, and H. Nagashima, J. Org. Chem., **2007**, 72, 7551-7559.

130. J. Schnekenburger, Arzneim. Forsch.**1975**,25, 185.
131. H. Fang, K. Xie, S. Kemper, and M. Oestreich, Angew. Chem. Int. Ed., **2021**,60, 8542–8546.
132. A. V. Semenov, O. Samultsev, Dmitry, and B. L. Krivdin, Magn.Reson.Chem., **2015**, 53, 433–441.
133. K. J. Sheehy, M. L. Bateman, T. N. Flosbach, M. Breugst, and A. P. Byrne, Eur. J. Org. Chem., **2020**, 3270–3281.
134. G. Berionni, B. P´egot, and R. Goumont, R.; Magn.Reson. Chem., **2010**, 48, 101 – 110.
135. WB. Cowden, and P. Waring, Australian Journal of Chemistry., **1981**, 34, 1539-1543.
136. Y. Tanaka, and A. Ono, Dalton Trans., **2008**, 4965–4974.
137. W. C. Vosburgh and S. A. Cogswell, J. Am. Chem. Soc. **1943**, 65, 12, 2412–2413.
138. J. D. Galloway, D. N. Mai, and R. D. Baxter, J. Org. Chem. **2019**, 84, 12131−12137.
139. U.S. Schubert, H. Hofmeier, G.R. Newkome, Wiley-VCH Verlag GmbH & Co, KgaA, Weinheim, **2006**, 69e130.
140. K. T. Potts, M. Keshavarzk, F. S. Tham, H. D. Abruna, and C. Arana, C., Inorg. Chem., **1993**, 32, 4450.
141. E. C. Constable, A. J. Edwards, M. J. Hannon, and P. R. J. Raithby, Polyhedron., **1998**, 17, 243 253.
142. E. C. Constable, T. Kulke, M. Neuburger, and M. Zehnder, Chem. Commun., **1997**, 489.
143. E. C. Constable, M. J. Hannon, A. Martin, P. R. Raithby, and D. A. Tocher, Polyhedron, **1992**, 11, 2967.
144. E. C. Constable, S. M. Elder, M. J. Hannon, A. Martin, P. R. Raithby, and D. A. Tocher, J. Chem. Soc., Dalton Trans., **1996**, 2423.
145. W. Su, M. Hong, J. Weng, Y. Liang, Y. Zhao, R. Cao, Z. Zhou, A. S. C. Chan, Inorg. Chim, Acta **2002**, 331, 8–15.
146. (a) R. P. Feazell, C. E. Carson, K. K. Klausmeyer, Inorg. Chem. **2006**, 45, 2627–2634. (b) M. Oh, C. L. Stern, C. A. Mirkin, Inorg. Chem. 2005, 44, 2647–2653. (c) M. A. Withersby, A. J. Blake, N. R. Champness, P. A. Cooke, P. Hubberstey, W. S. Li, Schröder, M. Inorg. Chem. **1999**, 38, 2259–2266. (d) I. G. Dance, J. Am. Chem. Soc. **1980**, 3445. (e) P. X. Yin, J. Zhang, Z. J. Li, Y. Y. Qin, J. K. Cheng, L. Zhang, Q. P. Lin, Y. G. Yao, Cryst. Growth Des. **2009**, 9, 4884–4896.
147. L. Pazderski, Annual reports on NMR Spectroscopy, **2013**, 80, 33–179.
148. M. Gil-Moles, M. C. Gimeno, J. M. López-de-Luzuriaga, M. Monge, M. E. Olmos, D. Pascual, Inorg. Chem. **2017**, 56, 9281–9290. (b) Z. Ma, Y. Hing, M. Yang, M. Hu, B. Liu, M. F. C. Guedes da Silva, A. J. L. Pombeiro, Inorg. Chim. Acta, **2009**, 362, 2921–2926.
149. CrysAlisPRO (Oxford Diffraction/Agilent Technologies UK Ltd, Yarnton, England, **2014**.

150. R. W. W. Hooft, COLLECT Data Collection Software, Nonius, B. V., Delft, The Netherlands, **1998**.
151. Z. Otwinowski, and W. Minor, Processing of X-ray diffraction data collected in oscillation mode, Methods in Enzymology (Academic Press, New York), 2009.
152. SADABS (Version 2008/2) (University of Göttingen, Germany), **1996**.
153. G. M. Sheldrick, SHELXT – Integrated space-group and crystal-structure determination. Acta Cryst. Sec. **2015,** A71, 3-8.
154. G. M. Sheldrick, Crystal structure refinement with SHELXL. Acta Cryst. Sec. **2015**, C71, 3-8.
155. O. V. Dolomanov, L. J. Bourhis, R. J. Gildea, J. A. K. Howard, and H. Puschmann, OLEX2: a complete structure solution, refinement and analysis program., J. Appl. Cryst. **2009**, 42, 339-341.

DEPARTMENT OF CHEMISTRY, UNIVERSITY OF JYVÄSKYLÄ
RESEARCH REPORT SERIES

1. Vuolle, Mikko: Electron paramagnetic resonance and molecular orbital study of radical ions generated from (2.2)metacyclophane, pyrene and its hydrogenated compounds by alkali metal reduction and by thallium(III)trifluoroacetate oxidation. (99 pp.) 1976
2. Pasanen, Kaija: Electron paramagnetic resonance study of cation radical generated from various chlorinated biphenyls. (66 pp.) 1977
3. Carbon-13 Workshop, September 6-8, 1977. (91 pp.) 1977
4. Laihia, Katri: On the structure determination of norbornane polyols by NMR spectroscopy. (111 pp.) 1979
5. Nyrönen, Timo: On the EPR, ENDOR and visible absorption spectra of some nitrogen containing heterocyclic compounds in liquid ammonia. (76 pp.) 1978
6. Talvitie, Antti: Structure determination of some sesquiterpenoids by shift reagent NMR. (54 pp.) 1979
7. Häkli, Harri: Structure analysis and molecular dynamics of cyclic compounds by shift reagent NMR. (48 pp.) 1979
8. Pitkänen, Ilkka: Thermodynamics of complexation of 1,2,4-triazole with divalent manganese, cobalt, nickel, copper, zinc, cadmium and lead ions in aqueous sodium perchlorate solutions. (89 pp.) 1980
9. Asunta, Tuula: Preparation and characterization of new organometallic compounds synthesized by using metal vapours. (91 pp.) 1980
10. Sattar, Mohammad Abdus: Analyses of MCPA and its metabolites in soil. (57 pp.) 1980
11. Bibliography 1980. (31 pp.) 1981
12. Knuuttila, Pekka: X-Ray structural studies on some divalent 3d metal compounds of picolinic and isonicotinic acid N-oxides. (77 pp.) 1981
13. Bibliography 1981. (33 pp.) 1982
14. 6th National NMR Symposium, September 9-10, 1982, Abstracts. (49 pp.) 1982
15. Bibliography 1982. (38 pp.) 1983
16. Knuuttila, Hilkka: X-Ray structural studies on some Cu(II), Co(II) and Ni(II) complexes with nicotinic and isonicotinic acid N-oxides. (54 pp.) 1983
17. Symposium on inorganic and analytical chemistry May 18, 1984, Program and Abstracts. (100 pp.) 1984
18. Knuutinen, Juha: On the synthesis, structure verification and gas chromatographic determination of chlorinated catechols and guaiacols occuring in spent bleach liquors of kraft pulp mill. (30 pp.) 1984
19. Bibliography 1983. (47 pp.) 1984
20. Pitkänen, Maija: Addition of BrCl, B_2 and Cl_2 to methyl esters of propenoic and 2-butenoic acid derivatives and ^{13}C NMR studies on methyl esters of saturated aliphatic mono- and dichlorocarboxylic acids. (56 pp.) 1985
21. Bibliography 1984. (39 pp.) 1985
22. Salo, Esa: EPR, ENDOR and TRIPLE spectroscopy of some nitrogen heteroaromatics in liquid ammonia. (111 pp.) 1985

23. Humppi, Tarmo: Synthesis, identification and analysis of dimeric impurities of chlorophenols. (39 pp.) 1985
24. Aho, Martti: The ion exchange and adsorption properties of sphagnum peat under acid conditions. (90 pp.) 1985
25. Bibliography 1985 (61 pp.) 1986
26. Bibliography 1986. (23 pp.) 1987
27. Bibliography 1987. (26 pp.) 1988
28. Paasivirta, Jaakko (Ed.): Structures of organic environmental chemicals. (67 pp.) 1988
29. Paasivirta, Jaakko (Ed.): Chemistry and ecology of organo-element compounds. (93 pp.) 1989
30. Sinkkonen, Seija: Determination of crude oil alkylated dibenzothiophenes in environment. (35 pp.) 1989
31. Kolehmainen, Erkki (Ed.): XII National NMR Symposium Program and Abstracts. (75 pp.) 1989
32. Kuokkanen, Tauno: Chlorocymenes and Chlorocymenenes: Persistent chlorocompounds in spent bleach liquors of kraft pulp mills. (40 pp.) 1989
33. Mäkelä, Reijo: ESR, ENDOR and TRIPLE resonance study on substituted 9,10-anthraquinone radicals in solution. (35 pp.) 1990
34. Veijanen, Anja: An integrated sensory and analytical method for identification of off-flavour compounds. (70 pp.) 1990
35. Kasa, Seppo: EPR, ENDOR and TRIPLE resonance and molecular orbital studies on a substitution reaction of anthracene induced by thallium(III) in two fluorinated carboxylic acids. (114 pp.) 1990
36. Herve, Sirpa: Mussel incubation method for monitoring organochlorine compounds in freshwater recipients of pulp and paper industry. (145 pp.) 1991
37. Pohjola, Pekka: The electron paramagnetic resonance method for characterization of Finnish peat types and iron (III) complexes in the process of peat decomposition. (77 pp.) 1991
38. Paasivirta, Jaakko (Ed.): Organochlorines from pulp mills and other sources. Research methodology studies 1988-91. (120 pp.) 1992
39. Veijanen, Anja (Ed.): VI National Symposium on Mass Spectrometry, May 13-15, 1992, Abstracts. (55 pp.) 1992
40. Rissanen, Kari (Ed.): The 7. National Symposium on Inorganic and Analytical Chemistry, May 22, 1992, Abstracts and Program. (153 pp.) 1992
41. Paasivirta, Jaakko (Ed.): CEOEC'92, Second Finnish-Russian Seminar: Chemistry and Ecology of Organo-Element Compounds. (93 pp.) 1992
42. Koistinen, Jaana: Persistent polychloroaromatic compounds in the environment: structure-specific analyses. (50 pp.) 1993
43. Virkki, Liisa: Structural characterization of chlorolignins by spectroscopic and liquid chromatographic methods and a comparison with humic substances. (62 pp.) 1993
44. Helenius, Vesa: Electronic and vibrational excitations in some

biologically relevant molecules. (30 pp.) 1993

45. Leppä-aho, Jaakko: Thermal behaviour, infrared spectra and x-ray structures of some new rare earth chromates(VI). (64 pp.) 1994
46. Kotila, Sirpa: Synthesis, structure and thermal behavior of solid copper(II) complexes of 2-amino-2- hydroxymethyl-1,3-propanediol. (111 pp.) 1994
47. Mikkonen, Anneli: Retention of molybdenum(VI), vanadium(V) and tungsten(VI) by kaolin and three Finnish mineral soils. (90 pp.) 1995
48. Suontamo, Reijo: Molecular orbital studies of small molecules containing sulfur and selenium. (42 pp.) 1995
49. Hämäläinen, Jouni: Effect of fuel composition on the conversion of fuel-N to nitrogen oxides in the combustion of small single particles. (50 pp.) 1995
50. Nevalainen, Tapio: Polychlorinated diphenyl ethers: synthesis, NMR spectroscopy, structural properties, and estimated toxicity. (76 pp.) 1995
51. Aittola, Jussi-Pekka: Organochloro compounds in the stack emission. (35 pp.) 1995
52. Harju, Timo: Ultrafast polar molecular photophysics of (dibenzylmethine)borondifluoride and 4-aminophthalimide in solution. (61 pp.) 1995
53. Maatela, Paula: Determination of organically bound chlorine in industrial and environmental samples. (83 pp.) 1995
54. Paasivirta, Jaakko (Ed.): CEOEC'95, Third Finnish-Russian Seminar: Chemistry and Ecology of Organo-Element Compounds. (109 pp.) 1995
55. Huuskonen, Juhani: Synthesis and structural studies of some supramolecular compounds. (54 pp.) 1995
56. Palm, Helena: Fate of chlorophenols and their derivatives in sawmill soil and pulp mill recipient environments. (52 pp.) 1995
57. Rantio, Tiina: Chlorohydrocarbons in pulp mill effluents and their fate in the environment. (89 pp.) 1997
58. Ratilainen, Jari: Covalent and non-covalent interactions in molecular recognition. (37 pp.) 1997
59. Kolehmainen, Erkki (Ed.): XIX National NMR Symposium, June 4-6, 1997, Abstracts. (89 pp.) 1997
60. Matilainen, Rose: Development of methods for fertilizer analysis by inductively coupled plasma atomic emission spectrometry. (41 pp.) 1997
61. Koistinen, Jari (Ed.): Spring Meeting on the Division of Synthetic Chemistry, May 15-16, 1997, Program and Abstracts. (36 pp.) 1997
62. Lappalainen, Kari: Monomeric and cyclic bile acid derivatives: syntheses, NMR spectroscopy and molecular recognition properties. (50 pp.) 1997
63. Laitinen, Eira: Molecular dynamics of cyanine dyes and phthalimides in solution: picosecond laser studies. (62 pp.) 1997
64. Eloranta, Jussi: Experimental and theoretical studies on some

quinone and quinol radicals. (40 pp.) 1997

65. Oksanen, Jari: Spectroscopic characterization of some monomeric and aggregated chlorophylls. (43 pp.) 1998
66. Häkkänen, Heikki: Development of a method based on laser-induced plasma spectrometry for rapid spatial analysis of material distributions in paper coatings. (60 pp.) 1998
67. Virtapohja, Janne: Fate of chelating agents used in the pulp and paper industries. (58 pp.) 1998
68. Airola, Karri: X-ray structural studies of supramolecular and organic compounds. (39 pp.) 1998
69. Hyötyläinen, Juha: Transport of lignin–type compounds in the receiving waters of pulp mills. (40 pp.) 1999
70. Ristolainen, Matti: Analysis of the organic material dissolved during totally chlorine-free bleaching. (40 pp.) 1999
71. Eklin, Tero: Development of analytical procedures with industrial samples for atomic emission and atomic absorption spectrometry. (43 pp.) 1999
72. Välisaari, Jouni: Hygiene properties of resol-type phenolic resin laminates. (129 pp.) 1999
73. Hu, Jiwei: Persistent polyhalogenated diphenyl ethers: model compounds syntheses, characterization and molecular orbital studies. (59 pp.) 1999
74. Malkavaara, Petteri: Chemometric adaptations in wood processing chemistry. (56 pp.) 2000
75. Kujala Elena, Laihia Katri, Nieminen Kari (Eds.): NBC 2000, Symposium on Nuclear, Biological and Chemical Threats in the 21st Century. (299 pp.) 2000
76. Rantalainen, Anna-Lea: Semipermeable membrane devices in monitoring persistent organic pollutants in the environment. (58 pp.) 2000
77. Lahtinen, Manu: *In situ* X-ray powder diffraction studies of Pt/C, CuCl/C and Cu_2O/C catalysts at elevated temperatures in various reaction conditions. (92 pp.) 2000
78. Tamminen, Jari: Syntheses, empirical and theoretical characterization, and metal cation complexation of bile acid-based monomers and open/closed dimers. (54 pp.) 2000
79. Vatanen, Virpi: Experimental studies by EPR and theoretical studies by DFT calculations of α-amino-9,10-anthraquinone radical anions and cations in solution. (37 pp.) 2000
80. Kotilainen, Risto: Chemical changes in wood during heating at 150-260 °C. (57 pp.) 2000
81. Nissinen, Maija: X-ray structural studies on weak, non-covalent interactions in supramolecular compounds. (69 pp.) 2001
82. Wegelius, Elina: X-ray structural studies on self-assembled hydrogen-bonded networks and metallosupramolecular complexes. (84 pp.) 2001
83. Paasivirta, Jaakko (Ed.): CEOEC’2001, Fifth Finnish-Russian Seminar: Chemistry and Ecology of Organo-Element Compounds. (163 pp.) 2001
84. Kiljunen, Toni: Theoretical studies on spectroscopy and

atomic dynamics in rare gas solids. (56 pp.) 2001

85. Du, Jin: Derivatives of dextran: synthesis and applications in oncology. (48 pp.) 2001
86. Koivisto, Jari: Structural analysis of selected polychlorinated persistent organic pollutants (POPs) and related compounds. (88 pp.) 2001
87. Feng, Zhinan: Alkaline pulping of non-wood feedstocks and characterization of black liquors. (54 pp.) 2001
88. Halonen, Markku: Lahon havupuun käyttö sulfaattiprosessin raaka-aineena sekä havupuun lahontorjunta. (90 pp.) 2002
89. Falábu, Dezsö: Synthesis, conformational analysis and complexation studies of resorcarene derivatives. (212 pp.) 2001
90. Lehtovuori, Pekka: EMR spectroscopic studies on radicals of ubiquinones Q-*n*, vitamin K_3 and vitamine E in liquid solution. (40 pp.) 2002
91. Perkkalainen, Paula: Polymorphism of sugar alcohols and effect of grinding on thermal behavior on binary sugar alcohol mixtures. (53 pp.) 2002
92. Ihalainen, Janne: Spectroscopic studies on light-harvesting complexes of green plants and purple bacteria. (42 pp.) 2002
93. Kunttu, Henrik, Kiljunen, Toni (Eds.): 4th International Conference on Low Temperature Chemistry. (159 pp.) 2002
94. Väisänen, Ari: Development of methods for toxic element analysis in samples with environmental concern by ICP-AES and ETAAS. (54 pp.) 2002
95. Luostarinen, Minna: Synthesis and characterisation of novel resorcarene derivatives. (200 pp.) 2002
96. Louhelainen, Jarmo: Changes in the chemical composition and physical properties of wood and nonwood black liquors during heating. (68 pp.) 2003
97. Lahtinen, Tanja: Concave hydrocarbon cyclophane π-prismands. (65 pp.) 2003
98. Laihia, Katri (Ed.): NBC 2003, Symposium on Nuclear, Biological and Chemical Threats – A Crisis Management Challenge. (245 pp.) 2003
99. Oasmaa, Anja: Fuel oil quality properties of wood-based pyrolysis liquids. (32 pp.) 2003
100. Virtanen, Elina: Syntheses, structural characterisation, and cation/anion recognition properties of nano-sized bile acid-based host molecules and their precursors. (123 pp.) 2003
101. Nättinen, Kalle: Synthesis and X-ray structural studies of organic and metallo-organic supramolecular systems. (79 pp.) 2003
102. Lampiselkä, Jarkko: Demonstraatio lukion kemian opetuksessa. (285 pp.) 2003
103. Kallioinen, Jani: Photoinduced dynamics of $Ru(dcbpy)_2(NCS)_2$ – in solution and on nanocrystalline titanium dioxide thin films. (47 pp.) 2004
104. Valkonen, Arto (Ed.): VII Synthetic Chemistry Meeting and XXVI Finnish NMR Symposium. (103 pp.) 2004

105. Vaskonen, Kari: Spectroscopic studies on atoms and small molecules isolated in low temperature rare gas matrices. (65 pp.) 2004
106. Lehtovuori, Viivi: Ultrafast light induced dissociation of $Ru(dcbpy)(CO)_2I_2$ in solution. (49 pp.) 2004
107. Saarenketo, Pauli: Structural studies of metal complexing Schiff bases, Schiff base derived *N*-glycosides and cyclophane π-prismands. (95 pp.) 2004
108. Paasivirta, Jaakko (Ed.): CEOEC'2004, Sixth Finnish-Russian Seminar: Chemistry and Ecology of Organo-Element Compounds. (147 pp.) 2004
109. Suontamo, Tuula: Development of a test method for evaluating the cleaning efficiency of hard-surface cleaning agents. (96 pp.) 2004
110. Güneş, Minna: Studies of thiocyanates of silver for nonlinear optics. (48 pp.) 2004
111. Ropponen, Jarmo: Aliphatic polyester dendrimers and dendrons. (81 pp.) 2004
112. Vu, Mân Thi Hong: Alkaline pulping and the subsequent elemental chlorine-free bleaching of bamboo (*Bambusa procera*). (69 pp.) 2004
113. Mansikkamäki, Heidi: Self-assembly of resorcinarenes. (77 pp.) 2006
114. Tuononen, Heikki M.: EPR spectroscopic and quantum chemical studies of some inorganic main group radicals. (79 pp.) 2005
115. Kaski, Saara: Development of methods and applications of laser-induced plasma spectroscopy in vacuum ultraviolet. (44 pp.) 2005
116. Mäkinen, Riika-Mari: Synthesis, crystal structure and thermal decomposition of certain metal thiocyanates and organic thiocyanates. (119 pp.) 2006
117. Ahokas, Jussi: Spectroscopic studies of atoms and small molecules isolated in rare gas solids: photodissociation and thermal reactions. (53 pp.) 2006
118. Busi, Sara: Synthesis, characterization and thermal properties of new quaternary ammonium compounds: new materials for electrolytes, ionic liquids and complexation studies. (102 pp.) 2006
119. Mäntykoski, Keijo: PCBs in processes, products and environment of paper mills using wastepaper as their raw material. (73 pp.) 2006
120. Laamanen, Pirkko-Leena: Simultaneous determination of industrially and environmentally relevant aminopolycarboxylic and hydroxycarboxylic acids by capillary zone electrophoresis. (54 pp.) 2007
121. Salmela, Maria: Description of oxygen-alkali delignification of kraft pulp using analysis of dissolved material. (71 pp.) 2007
122. Lehtovaara, Lauri: Theoretical studies of atomic scale impurities in superfluid ^4He. (87 pp.) 2007
123. Rautiainen, J. Mikko: Quantum chemical calculations of structures, bonding, and spectroscopic properties of some sulphur and selenium iodine cations. (71 pp.) 2007
124. Nummelin, Sami: Synthesis, characterization, structural and

retrostructural analysis of self-assembling pore forming dendrimers. (286 pp.) 2008

125. Sopo, Harri: Uranyl(VI) ion complexes of some organic aminobisphenolate ligands: syntheses, structures and extraction studies. (57 pp.) 2008
126. Valkonen, Arto: Structural characteristics and properties of substituted cholanoates and *N*-substituted cholanamides. (80 pp.) 2008
127. Lähde, Anna: Production and surface modification of pharmaceutical nano- and microparticles with the aerosol flow reactor. (43 pp.) 2008
128. Beyeh, Ngong Kodiah: Resorcinarenes and their derivatives: synthesis, characterization and complexation in gas phase and in solution. (75 pp.) 2008
129. Välisaari, Jouni, Lundell, Jan (Eds.): Kemian opetuksen päivät 2008: uusia oppimisympäristöjä ja ongelmalähtöistä opetusta. (118 pp.) 2008
130. Myllyperkiö, Pasi: Ultrafast electron transfer from potential organic and metal containing solar cell sensitizers. (69 pp.) 2009
131. Käkölä, Jaana: Fast chromatographic methods for determining aliphatic carboxylic acids in black liquors. (82 pp.) 2009
132. Koivukorpi, Juha: Bile acid-arene conjugates: from photoswitchability to cancer cell detection. (67 pp.) 2009
133. Tuuttila, Tero: Functional dendritic polyester compounds: synthesis and characterization of small bifunctional dendrimers and dyes. (74 pp.) 2009
134. Salorinne, Kirsi: Tetramethoxy resorcinarene based cation and anion receptors: synthesis, characterization and binding properties. (79 pp.) 2009
135. Rautiainen, Riikka: The use of first-thinning Scots pine (*Pinus sylvestris*) as fiber raw material for the kraft pulp and paper industry. (73 pp.) 2010
136. Ilander, Laura: Uranyl salophens: synthesis and use as ditopic receptors. (199 pp.) 2010
137. Kiviniemi, Tiina: Vibrational dynamics of iodine molecule and its complexes in solid krypton - Towards coherent control of bimolecular reactions? (73 pp.) 2010
138. Ikonen, Satu: Synthesis, characterization and structural properties of various covalent and non-covalent bile acid derivatives of N/O-heterocycles and their precursors. (105 pp.) 2010
139. Siitonen, Anni: Spectroscopic studies of semiconducting single-walled carbon nanotubes. (56 pp.) 2010
140. Raatikainen, Kari: Synthesis and structural studies of piperazine cyclophanes – Supramolecular systems through Halogen and Hydrogen bonding and metal ion coordination. (69 pp.) 2010
141. Leivo, Kimmo: Gelation and gel properties of two- and three-component Pyrene based low molecular weight organogelators. (116 pp.) 2011
142. Martiskainen, Jari: Electronic energy transfer in light-harvesting complexes isolated from *Spinacia oleracea* and from three

photosynthetic green bacteria *Chloroflexus aurantiacus*, *Chlorobium tepidum*, and *Prosthecochloris aestuarii*. (55 pp.) 2011

143. Wichmann, Oula: Syntheses, characterization and structural properties of [O,N,O,X´] aminobisphenolate metal complexes. (101 pp.) 2011
144. Ilander, Aki: Development of ultrasound-assisted digestion methods for the determination of toxic element concentrations in ash samples by ICP-OES. (58 pp.) 2011
145. The Combined XII Spring Meeting of the Division of Synthetic Chemistry and XXXIII Finnish NMR Symposium. Book of Abstracts. (90 pp.) 2011
146. Valto, Piia: Development of fast analysis methods for extractives in papermaking process waters. (73 pp.) 2011
147. Andersin, Jenni: Catalytic activity of palladium-based nanostructures in the conversion of simple olefinic hydro- and chlorohydrocarbons from first principles. (78 pp.) 2011
148. Aumanen, Jukka: Photophysical properties of dansylated poly(propylene amine) dendrimers. (55 pp.) 2011
149. Kärnä, Minna: Ether-functionalized quaternary ammonium ionic liquids – synthesis, characterization and physicochemical properties. (76 pp.) 2011
150. Jurček, Ondřej: Steroid conjugates for applications in pharmacology and biology. (57 pp.) 2011
151. Nauha, Elisa: Crystalline forms of selected Agrochemical actives: design and synthesis of cocrystals. (77 pp.) 2012
152. Ahkola, Heidi: Passive sampling in monitoring of nonylphenol ethoxylates and nonylphenol in aquatic environments. (92 pp.) 2012
153. Helttunen, Kaisa: Exploring the self-assembly of resorcinarenes: from molecular level interactions to mesoscopic structures. (78 pp.) 2012
154. Linnanto, Juha: Light excitation transfer in photosynthesis revealed by quantum chemical calculations and exiton theory. (179 pp.) 2012
155. Roiko-Jokela, Veikko: Digital imaging and infrared measurements of soil adhesion and cleanability of semihard and hard surfaces. (122 pp.) 2012
156. Noponen, Virpi: Amides of bile acids and biologically important small molecules: properties and applications. (85 pp.) 2012
157. Hulkko, Eero: Spectroscopic signatures as a probe of structure and dynamics in condensed-phase systems – studies of iodine and gold ranging from isolated molecules to nanoclusters. (69 pp.) 2012
158. Lappi, Hanna: Production of Hydrocarbon-rich biofuels from extractives-derived materials. (95 pp.) 2012
159. Nykänen, Lauri: Computational studies of Carbon chemistry on transition metal surfaces. (76 pp.) 2012
160. Ahonen, Kari: Solid state studies of pharmaceutically important molecules and their derivatives. (65 pp.) 2012

161. Pakkanen, Hannu: Characterization of organic material dissolved during alkaline pulping of wood and non-wood feedstocks. (76 pp.) 2012
162. Moilanen, Jani: Theoretical and experimental studies of some main group compounds: from closed shell interactions to singlet diradicals and stable radicals. (80 pp.) 2012
163. Himanen, Jatta: Stereoselective synthesis of Oligosaccharides by *De Novo* Saccharide welding. (133 pp.) 2012
164. Bunzen, Hana: Steroidal derivatives of nitrogen containing compounds as potential gelators. (76 pp.) 2013
165. Seppälä, Petri: Structural diversity of copper(II) amino alcohol complexes. Syntheses, structural and magnetic properties of bidentate amino alcohol copper(II) complexes. (67 pp.) 2013
166. Lindgren, Johan: Computational investigations on rotational and vibrational spectroscopies of some diatomics in solid environment. (77 pp.) 2013
167. Giri, Chandan: Sub-component self-assembly of linear and non-linear diamines and diacylhydrazines, formulpyridine and transition metal cations. (145 pp.) 2013
168. Riisiö, Antti: Synthesis, Characterization and Properties of Cu(II)-, Mo(VI)- and U(VI) Complexes With Diaminotetraphenolate Ligands. (51 pp.) 2013
169. Kiljunen, Toni (Ed.): Chemistry and Physics at Low Temperatures. Book of Abstracts. (103 pp.) 2013
170. Hänninen, Mikko: Experimental and Computational Studies of Transition Metal Complexes with Polydentate Amino- and Aminophenolate Ligands: Synthesis, Structure, Reactivity and Magnetic Properties. (66 pp.) 2013
171. Antila, Liisa: Spectroscopic studies of electron transfer reactions at the photoactive electrode of dye-sensitized solar cells. (53 pp.) 2013
172. Kemppainen, Eeva: Mukaiyama-Michael reactions with α-substituted acroleins – a useful tool for the synthesis of the pectenotoxins and other natural product targets. (190 pp.) 2013
173. Virtanen, Suvi: Structural Studies of Dielectric Polymer Nanocomposites. (49 pp.) 2013
174. Yliniemelä-Sipari, Sanna: Understanding The Structural Requirements for Optimal Hydrogen Bond Catalyzed Enolization – A Biomimetic Approach.(160 pp.) 2013
175. Leskinen, Mikko V: Remote β-functionalization of β'-keto esters. (105 pp.) 2014
176. 12th European Conference on Research in Chemistry Education (ECRICE2014). Book of Abstracts. (166 pp.) 2014
177. Peuronen, Anssi: N-Monoalkylated DABCO-Based N-Donors as Versatile Building Blocks in Crystal Engineering and Supramolecular Chemistry. (54 pp.) 2014
178. Perämäki, Siiri: Method development for determination and recovery of rare earth elements from industrial fly ash. (88 pp.) 2014

179. Chernyshev, Alexander, N.: Nitrogen-containing ligands and their platinum(IV) and gold(III) complexes: investigation and basicity and nucleophilicity, luminescence, and aurophilic interactions. (64 pp.) 2014
180. Lehto, Joni: Advanced Biorefinery Concepts Integrated to Chemical Pulping. (142 pp.) 2015
181. Tero, Tiia-Riikka: Tetramethoxy resorcinarenes as platforms for fluorescent and halogen bonding systems. (61 pp.) 2015
182. Löfman, Miika: Bile acid amides as components of microcrystalline organogels. (62 pp.) 2015
183. Selin, Jukka: Adsorption of softwood-derived organic material onto various fillers during papermaking. (169 pp.) 2015
184. Piisola, Antti: Challenges in the stereoselective synthesis of allylic alcohols. (210 pp.) 2015
185. Bonakdarzadeh, Pia: Supramolecular coordination polyhedra based on achiral and chiral pyridyl ligands: design, preparation, and characterization. (65 pp.) 2015
186. Vasko, Petra: Synthesis, characterization, and reactivity of heavier group 13 and 14 metallylenes and metalloid clusters: small molecule activation and more. (66 pp.) 2015
187. Topić, Filip: Structural Studies of Nano-sized Supramolecular Assemblies. (79 pp.) 2015
188. Mustalahti, Satu: Photodynamics Studies of Ligand-Protected Gold Nanoclusters by using Ultrafast Transient Infrared Spectroscopy. (58 pp.) 2015
189. Koivisto, Jaakko: Electronic and vibrational spectroscopic studies of gold-nanoclusters. (63 pp.) 2015
190. Suhonen, Aku: Solid state conformational behavior and interactions of series of aromatis oligoamide foldamers. (68 pp.) 2016
191. Soikkeli, Ville: Hydrometallurgical recovery and leaching studies for selected valuable metals from fly ash samples by ultrasound-assisted extraction followed by ICP-OES determination. (107 pp.) 2016
192. XXXVIII Finnish NMR Symposium. Book of Abstracts. (51 pp.) 2016
193. Mäkelä, Toni: Ion Pair Recognition by Ditopic Crown Ether Based bis-Urea and Uranyl Salophen Receptors. (75 pp.) 2016
194. Lindholm-Lehto, Petra: Occurrence of pharmaceuticals in municipal wastewater treatment plants and receiving surface waters in Central and Southern Finland. (98 pp.) 2016
195. Härkönen, Ville: Computational and Theoretical studies on Lattice Thermal conductivity and Thermal properties of Silicon Clathrates. (89 pp.) 2016
196. Tuokko, Sakari: Understanding selective reduction reactions with heterogeneous Pd and Pt: climbing out of the black box. (85 pp.) 2016
197. Nuora, Piia: Monitapaustutkimus LUMA-Toimintaan liittyvissä oppimisympäristöissä tapahtuvista kemian oppimiskokemuksista. (171 pp.) 2016

198. Kumar, Hemanathan: Novel Concepts on The Recovery of By-Products from Alkaline Pulping. (61 pp.) 2016
199. Arnedo-Sánchez, Leticia: Lanthanide and Transition Metal Complexes as Building Blocks for Supramolecular Functional Materials. (227 pp.) 2016
200. Gell, Lars: Theoretical Investigations of Ligand Protected Silver Nanoclusters. (134 pp.) 2016
201. Vaskuri, Juhani: Oppiennätyksistä opetussuunnitelman perusteisiin - lukion kemian kansallisen opetussuunnitelman kehittyminen Suomessa vuosina 1918-2016. (314 pp.) 2017
202. Lundell Jan, Kiljunen Toni (Eds.): 22nd Horizons in Hydrogen Bond Research. Book of Abstracts. 2017
203. Turunen, Lotta: Design and construction of halogen-bonded capsules and cages. (61 pp.) 2017
204. Hurmalainen, Juha: Experimental and computational studies of unconventional main group compounds: stable radicals and reactive intermediates. (88 pp.) 2017
205. Koivistoinen Juha: Non-linear interactions of femtosecond laser pulses with graphene: photo-oxidation, imaging and photodynamics. (68 pp.) 2017
206. Chen, Chengcong: Combustion behavior of black liquors: droplet swelling and influence of liquor composition. (39 pp.) 2017
207. Mansikkamäki, Akseli: Theoretical and Computational Studies of Magnetic Anisotropy and Exchange Coupling in Molecular Systems. (190 p. + included articles) 2018.
208. Tatikonda, Rajendhraprasad: Multivalent N-donor ligands for the construction of coordination polymers and coordination polymer gels. (62 pp.) 2018
209. Budhathoki, Roshan: Beneficiation, desilication and selective precipitation techniques for phosphorus refining from biomass derived fly ash. (64 pp.) 2018
210. Siitonen, Juha: Synthetic Studies on 1-azabicyclo[5.3.0]decane Alkaloids. (140 pp.) 2018
211. Ullah, Saleem: Advanced Biorefinery Concepts Related to Non-wood Feedstocks. (57 pp.) 2018
212. Ghalibaf, Maryam: Analytical Pyrolysis of Wood and Non-Wood Materials from Integrated Biorefinery Concepts. (106 pp.) 2018

DEPARTMENT OF CHEMISTRY, UNIVERSITY OF JYVÄSKYLÄ
DISSERTATIONS PUBLISHED IN THE JYU DISSERTATIONS RESEARCH SERIES

1. Bulatov, Evgeny: Synthetic and structural studies of covalent and non-covalent interactions of ligands and metal center in platinum(II) complexes containing 2,2′-dipyridylamine or oxime ligands. (58 pp.) 2019. JYU Dissertations 70.
2. Annala, Riia: Conformational Properties and Anion Complexes of Aromatic Oligoamide Foldamers. (80 pp.) 2019. JYU Dissertations 84.
3. Isoaho, Jukka Pekka: Dithionite Bleaching of Thermomechanical Pulp - Chemistry and Optimal Conditions. (73 pp.) 2019. JYU Dissertations 85.
4. Nygrén, Enni: Recovery of rubidium from power plant fly ash. (98 pp.) 2019. JYU Dissertations 136.
5. Kiesilä, Anniina: Supramolecular chemistry of anion-binding receptors based on concave macromolecules. (68 pp.) 2019. JYU Dissertations 137.
6. Sokolowska, Karolina: Study of water-soluble p-MBA-protected gold nanoclusters and their superstructures. (60 pp.) 2019. JYU Dissertations 167.
7. Lahtinen, Elmeri: Chemically Functional 3D Printing: Selective Laser Sintering of Customizable Metal Scavengers. (71 pp.) 2019. JYU Dissertations 175.
8. Larijani, Amir: Oxidative reactions of cellulose under alkaline conditions. (102 pp.) 2020. JYU Dissertations 217.
9. Kolari, Kalle: Metal-metal contacts in late transition metal polymers. (60 pp.) 2020. JYU Dissertations 220.
10. Kauppinen, Minttu: Multiscale computational investigation of catalytic properties of zirconia supported noble metals. (87 pp.) 2020. JYU Dissertations 231.
11. Ding, Xin: Halogen Bond in Crystal Engineering: Structural Studies on Crystals with Ruthenium Centered Complexes and 1-(4-Pyridyl)-4-thiopyridine Zwitterion as Halogen Bond Acceptors. (59 pp.) 2020. JYU Dissertations 323.
12. Neuvonen, Antti: Toward an Understanding of Hydrogen-Bonding Bifunctional Organocatalyst Conformations and Their Activity in Asymmetric Mannich Reactions. (77 pp.) 2020. JYU Dissertations 336.
13. Kortet, Sami: 2,5-Diarylpyrrolidines and Pyroglutamic-Acid-Derived 2-Diarylmethyl-5-Aryl-Pyrrolidines: Their Synthesis and Use in Asymmetric Synthesis. (221 pp.) 2020. JYU Dissertations 337.
14. Saarnio, Ville: Fluorescent probes, noble metal nanoparticles and their nanocomposites: detection of nucleic acids and other biological targets. (80 pp.) 2021. JYU Dissertations 361.
15. Chernysheva, Maria: σ-hole interactions: the effect of the donors and acceptors nature in selenoureas, thioureas, halogenated species, substituted benzenes, and their adducts. (72 pp.) 2021. JYU Dissertations 370.
16. Bulatova, Margarita: Noncovalent interactions as a tool for supramolecular self-assembly of metallopolymers. (62 pp.) 2021. JYU Dissertations 377.

17. Romppanen, Sari: Laser-spectroscopic studies of rare earth element- and lithium-bearing minerals and rocks. (66 pp.) 2021. JYU Dissertations 393.
18. Kukkonen, Esa: Nonlinear optical materials through weak interactions and their application in 3D printing. (58 pp.) 2021. JYU Dissertations 441.
19. Kuosmanen, Riikka: The Effect of Structure on the Gel Formation Ability and the Properties of Bile Acid Based Supramolecular Organogels. (68 pp.) 2021. JYU Dissertations 465.
20. Reuna, Sini: Development of a Method for Phosphorus Recovery from Wastewaters. (67 pp.) 2022. JYU Dissertations 486.
21. Taipale, Essi: Synthetic and Structural Studies on the Effect of Non-Covalent Interactions on N(*sp2*)-Heterocyclic Molecules. (67 pp.) 2022. JYU Dissertations 496.
22. Järvinen, Teemu: Molecular Dynamics View on Matrix Isolation. (143 pp.) 2022. JYU Dissertations 544.